Twenty Fifth Edition

Photovoltaics International

THE TECHNOLOGY RESOURCE FOR PV PROFESSIONALS

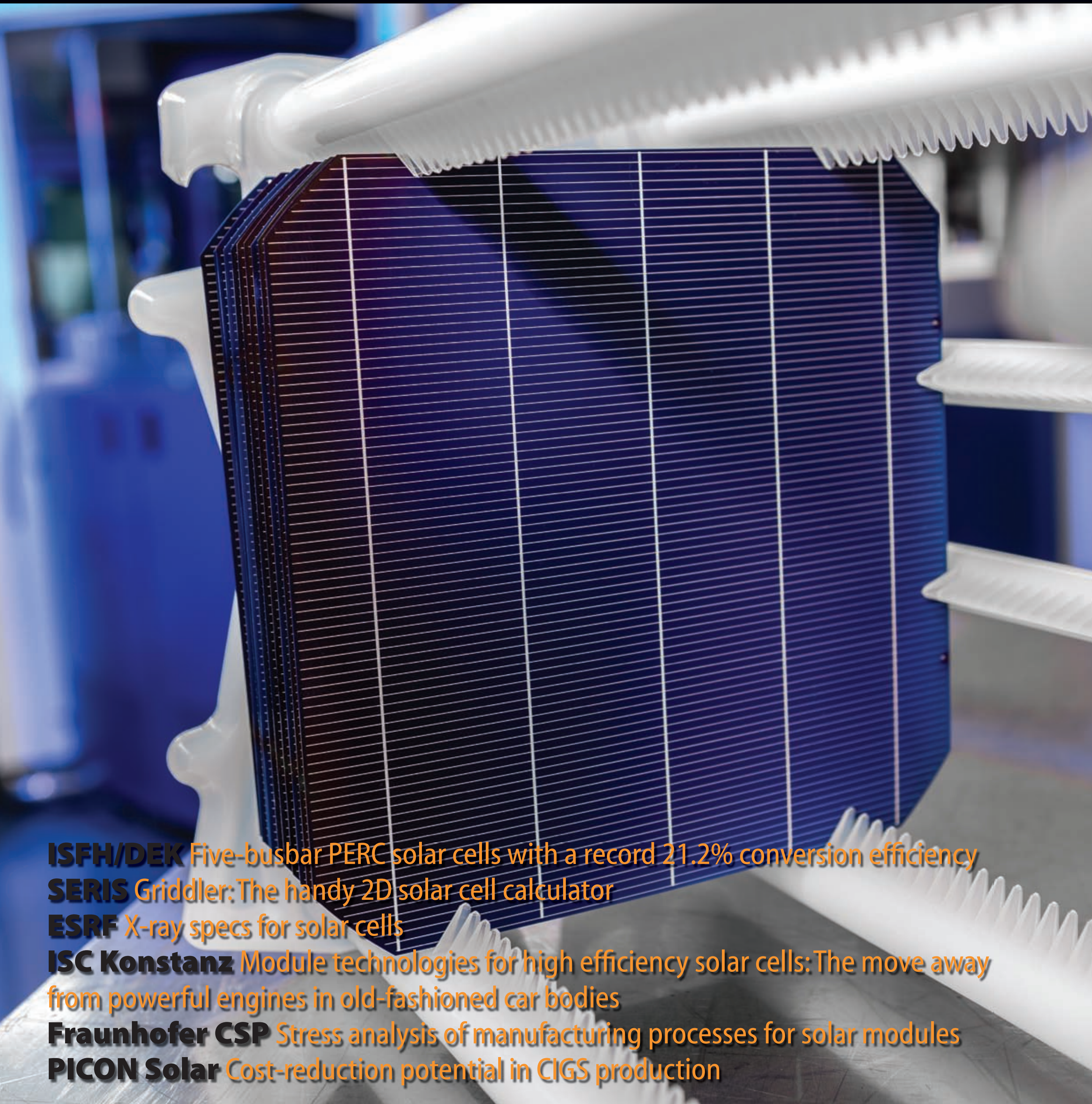

ISFH/DEK Five-busbar PERC solar cells with a record 21.2% conversion efficiency

SERIS Griddler: The handy 2D solar cell calculator

ESRF X-ray specs for solar cells

ISC Konstanz Module technologies for high efficiency solar cells: The move away from powerful engines in old-fashioned car bodies

Fraunhofer CSP Stress analysis of manufacturing processes for solar modules

PICON Solar Cost-reduction potential in CIGS production

Third Quarter, September 2014 www.pv-tech.org

Photovoltaics International

Published by:
Solar Media Ltd.,
5 Prescot Street,
London E1 8PA, UK
Tel: +44 (0) 207 871 0122
Fax: +44 (0) 207 871 0101
E-mail: info@pv-tech.org
Web: www.pv-tech.org

Publisher: David Owen

Head of Content: Ben Willis
Deputy Head of Content: John Parnell
Commissioning Editor: Adam Morrison
Sub-Editor: Steve D. Brierley
Senior News Editor: Mark Osborne
Reporters: Andy Colthorpe, Lucy Woods
Design: Tina Davidian
Production: Daniel H Brown, Sarah-Jane Lee

Sales Director: David Evans
Account Managers: Adam Morrison,
Graham Davie, Lili Zhu

Cover image: The cover image shows a 21.2% efficient PERC solar cell with 5 busbars processed at the ISFH SolarTeC. Image provided by ISFH, Hamelin, Germany.

Photographer Ulf Salzmann

Printed by Buxton Press
Photovoltaics International
Twenty Fifth Edition
Third Quarter 2014
Photovoltaics International is a quarterly journal published in February, May, August and November.

Distributed in the USA by Mail Right International, 1637 Stelton Road B4, Piscataway, NJ 08854.

ISSN: 1757-1197

USPS Information
USPS Periodical Code: 025 313

Periodicals Postage Paid at
New Brunswick, NJ
Postmaster: Send changes to:
Photovoltaics International,
Solar Media Ltd., C/o 1637 Stelton
Road, B-4, Piscataway, NJ 08854, USA

Foreword

In the last issue of Photovoltaics International we presented evidence pointing definitively to the start of the upturn the industry has been so desperately craving after two brutal years. Our analysis charted how all the big-name module manufacturers are now looking to invest again in manufacturing capacity expansions.

In this issue we offer some insights into what the next wave of photovoltaic technologies may look like as that upturn gathers pace. Industry observers have been in broad agreement that the major next-gen PV technology innovations won't happen straight away. But there's also little doubt that the search is now on in earnest for the breakthroughs that will come to define the state of the art in the industry in the years to come.

Most notable is the research described by the team at **ISFH** in Germany, along with colleagues at **DEK Solar** in the UK, into record-breaking PERC cell technology. Their paper on p.35 outlines how they combined the best of PERC and multi-busbar technologies to set a new conversion efficiency record – 21.2% – in an industrially produced cell of this kind. By comparison, the best conversion rate achieved previously in a three-busbar cell was 20.6%.

That may not sound a lot, but in an industry that moves forward by increments, this is a significant milestone, and demonstrates how small advances such as this in cell technology will be crucial in propelling the industry onwards.

But while improvements in cell efficiencies have understandably been attracting significant interest, not to be forgotten in the general quest to improve the performance of solar technology are the modules themselves.

On p.98 scientists from **ISC Konstanz** take up this theme in a paper exploring the current trends and future developments in module technology. Their analogy is that "powerful engines" – high-efficiency cells – have come to be housed in "old-fashioned car bodies" – dated module architecture. The recent downturn, they argue, stifled any significant innovation in this area, but with that now in the past, manufacturers are turning their attention to the design of modules to maintain their competitive edge.

Also in this issue of Photovoltaics International, we feature the second part of **PICON Solar's** analysis of the future of CIGS thin-film technology. Having in the previous issue asked whether CIGS modules could ever compete with c-Si, PICON's paper on p.72 analyzes the cost-reduction potential in CIGS technology that could allow that to happen.

All this and much more can be found in the 25th issue of Photovoltaics International. We will be at EU PVSEC in Amsterdam in September. Be sure to catch our team there at booth D10 and look out for our live reporting from the event on www.pv-tech.org. I hope you enjoy this issue.

Ben Willis
Head of Content
Solar Media Ltd

Photovoltaics International

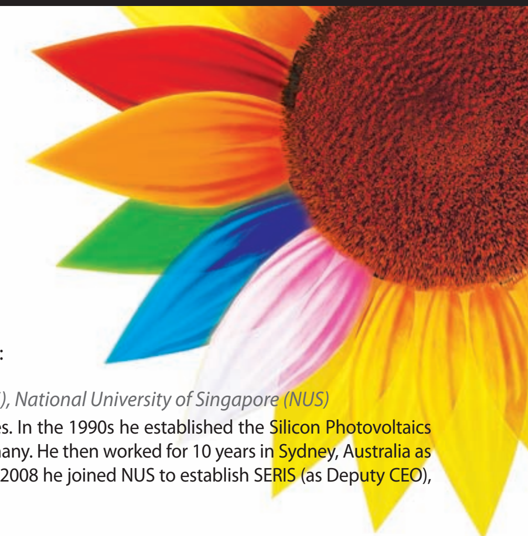

Photovoltaics International's primary focus is on assessing existing and new technologies for "real-world" supply chain solutions. The aim is to help engineers, managers and investors to understand the potential of equipment, materials, processes and services that can help the PV industry achieve grid parity. The Photovoltaics International advisory board has been selected to help guide the editorial direction of the technical journal so that it remains relevant to manufacturers and utility-grade installers of photovoltaic technology. The advisory board is made up of leading personnel currently working first-hand in the PV industry.

Editorial Advisory Board

Our editorial advisory board is made up of senior engineers from PV manufacturers worldwide. Meet some of our board members below:

Prof Armin Aberle, CEO, Solar Energy Research Institute of Singapore (SERIS), National University of Singapore (NUS)

Prof Aberle's research focus is on photovoltaic materials, devices and modules. In the 1990s he established the Silicon Photovoltaics Department at the Institute for Solar Energy Research (ISFH) in Hamelin, Germany. He then worked for 10 years in Sydney, Australia as a professor of photovoltaics at the University of New South Wales (UNSW). In 2008 he joined NUS to establish SERIS (as Deputy CEO), with particular responsibility for the creation of a Silicon PV Department.

Dr. Markus Fischer, Director R&D Processes, Hanwha Q Cells

Dr. Fischer has more than 15 years' experience in the semiconductor and crystalline silicon photovoltaic industry. He joined Q Cells in 2007 after working in different engineering and management positions with Siemens, Infineon, Philips, and NXP. As Director R&D Processes he is responsible for the process and production equipment development of current and future c-Si solar cell concepts. Dr. Fischer received his Ph.D. in Electrical Engineering in 1997 from the University of Stuttgart. Since 2010 he has been a co-chairman of the SEMI International Technology Roadmap for Photovoltaic.

Dr. Thorsten Dullweber, R&D Group Leader at the Institute for Solar Energy Research Hamelin (ISFH)

Dr. Dullweber's research focuses on high efficiency industrial-type PERC silicon solar cells and ultra-fineline screen-printed Ag front contacts. His group has contributed many journal and conference publications as well as industry-wide recognized research results. Before joining ISFH in 2009, Dr. Dullweber worked for nine years in the microelectronics industry at Siemens AG and later Infineon Technologies AG. He received his Ph. D. in 2002 for research on Cu(In,Ga)Se2 thin-film solar cells.

Julia Hamm, president and CEO, Solar Electric Power Association (SEPA)

SEPA is an educational non-profit organization dedicated to helping utilities integrate solar power into their energy portfolios. Prior to leading SEPA, Julia Hamm worked as a senior associate at ICF International where she supported the US Environmental Protection Agency with implementation of its ENERGY STAR programme. She holds a Bachelors of Science in Business Management from Cornell University.

Yong Liu, Chief Operating Officer and Chief Technology Officer, JA Solar

Yong Lui has more than 15 years of operation management experience at semiconductor wafer and solar cell manufacturing facilities. Prior to joining JA Solar, he served as fab director at Semiconductor Manufacturing International Corporation (SMIC), responsible for running three 12-inch wafer foundry fabs, which were the most advanced wafer fabs in China. Mr. Liu received his master's degree in solid state chemistry and bachelor's degree in solid state physics from the University of Science and Technology of China in 1992 and 1990, respectively.

Florian Clement, Head of Group, MWT solar cells/printing technology, Fraunhofer ISE

Dr. Clement received his Ph.D in 2009 from the University of Freiburg. He studied physics at the Ludwigs-Maximilian-University of Munich and the University of Freiburg and obtained his diploma degree in 2005. His research is focused on the development, analysis and characterization of highly efficient, industrially feasible MWT solar cells with rear side passivation, so called HIP-MWT devices, and on new printing technologies for silicon solar cell processing.

Sam Hong, Chief Executive, Neo Solar Power

Dr. Hong has more than 30 years' experience in solar photovoltaic energy. He has served as the Research Division Director of Photovoltaic Solar Energy Division at the Industry Technology Research Institute (ITRI), and Vice President and Plant Director of Sinonar Amorphous Silicon Solar Cell Co., the first amorphous silicon manufacturer in Taiwan. Dr. Hong has published three books and 38 journal and international conference papers, and is a holder of seven patents. In 2011 he took office as Chairman of Taiwan Photovoltaic Industry Association.

Matt Campbell, Senior Director, Power Plant Products, SunPower

Matt Campbell has held a variety of business development and product management roles since joining the SunPower, including the development of the 1.5MW AC Oasis power plant platform, organized SunPower's power plant LCOE reduction programmes, and the acquisition of three power plant technology companies. Campbell helped form a joint venture in Inner Mongolia, China for power plant project development and manufacturing. He holds an MBA from the University of California at Berkeley and a BBA in Marketing, Finance, and Real Estate from the University of Wisconsin at Madison.

Ru Zhong Hou, Director of Product Center, ReneSola

Ru Zhong Hou joined ReneSola as R&D Senior Manager in 2010 before being appointed Director of R&D in 2012. Before joining ReneSola he was a researcher for Microvast Power Systems, a battery manufacturer. His work has been published in numerous scientific journals. He has a Ph.D. from the Institute of Materials Physics & Microstructures, Zhejiang University, China.

Contents


8


19


32

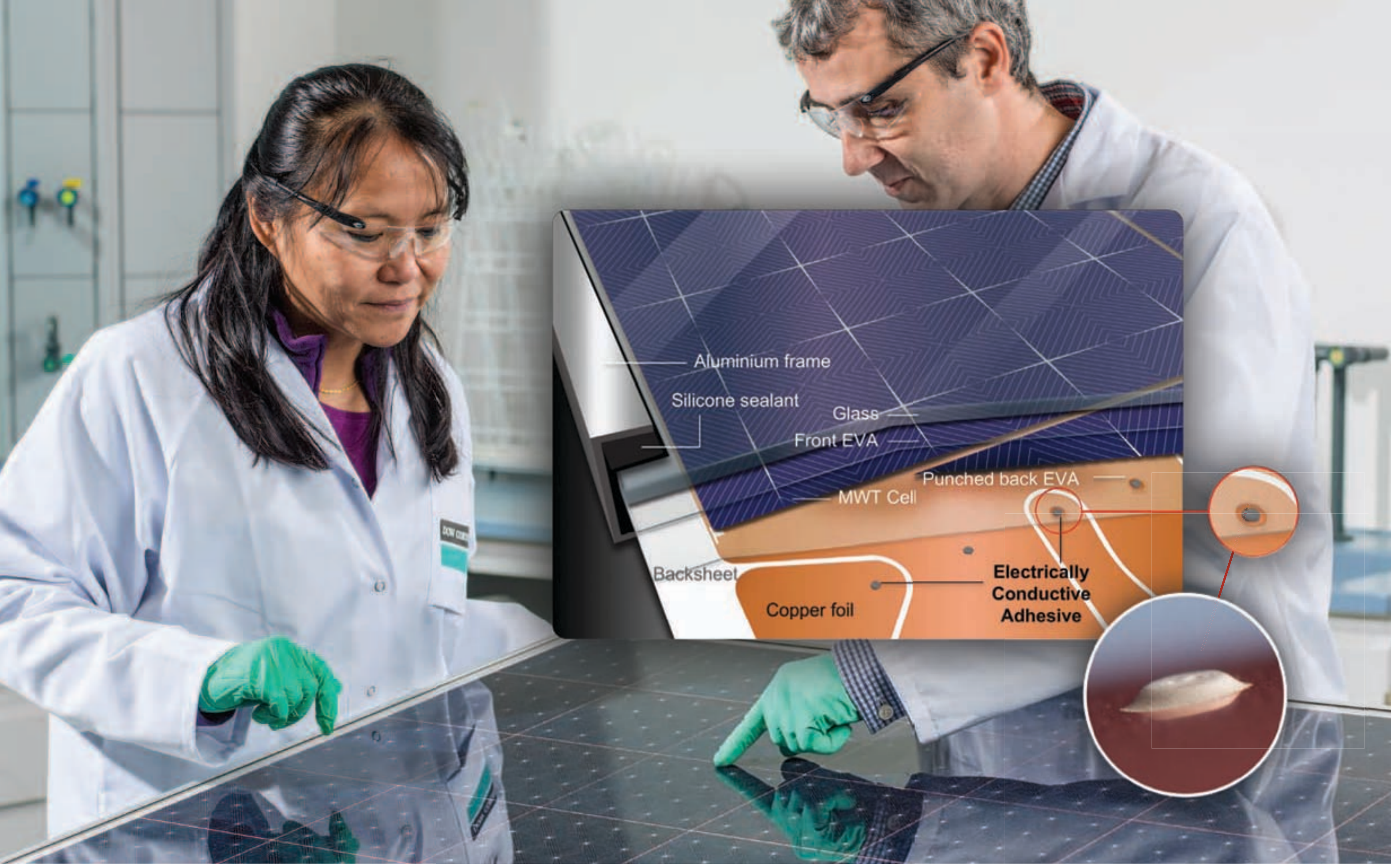

Aluminium frame
Silicone sealant
Glass
Front EVA
Punched back EVA
MWT Cell
Backsheet
Electrically Conductive Adhesive
Copper foil

Contents

Fab & Facilities

News

SolarCity expects Silevo 1GW fab to cost up to US$450 million


Source: SolarCity

SolarCity hopes to secure its module supply with Silevo.

SolarCity's plans to build a 1GW integrated PV manufacturing plant based on the technology it has recently acquired with the purchase of Silevo are expected to require capital expenditures of US$400 million to US$450 million, according to Deutsche Bank analyst, Vishal Shah after attending a SolarCity investor event.

Shah said in a research note to investors that SolarCity's plans to bring online the largest PV manufacturing plant in the US remained on track for 2016, with negotiations with NY State on the right incentive packages, ongoing.

SolarCity expects its own capital expenditure contribution for the new facility to be in the several hundred million range, according to Deutsche Bank, which suggested the company would need to make a secondary public offering of shares by the end of the year to support the expenditure requirements.

The Deutsche Bank analyst also noted that it expected SolarCity to continue to experience "strong near-term bookings momentum", which could result in the company raising its 2015 deployed guidance above the 900MW to 1,000MW current guidance range.

Tier One China Goes Overseas

Trina Solar looking at sites for first overseas manufacturing base

Major PV manufacturer Trina Solar is planning to better serve its growing US customer base on the back of increased demand through establishing its first PV module manufacturing operations outside China. Management noted in its second quarter earnings call that module demand from the US had increased significantly in the second quarter of 2014 and projected similar strong demand through the rest of the year. Management expects demand to remain strong in 2015 based on preliminary customer requirements. Indicating that the US market was a key market for Trina Solar in the future, the company said it was undertaking site selection analysis for a manufacturing plant but did not say what countries' assessments were being made in. Recent reports have identified Mexico and Malaysia as prime candidates, though the US should not yet be ruled out.

JA Solar's next manufacturing expansion in US or Southeast Asia

China-based tier one integrated PV manufacturer, JA Solar expects the next phase of its manufacturing expansions to be in 2015 and to include new facilities in either the US or South East Asia. JA Solar management said during its second quarter earnings call that no further capacity expansions would be made in China in 2014. Although not ruling out further capacity expansions in China next year, management noted that it was planning overseas expansions in 2015, which could include the US or Southeast Asia. Management noted that it had increased PV module shipments to the US in the second quarter ahead of the anti-dumping decision, yet the extra 50MW or so of shipments would not last long. Module shipments to the US in the first quarter of 2014 accounted for only 4.1% of total shipments, while shipments to the country accounted for 11.2% in the second quarter.


Source: JA Solar

JA Solar will look overseas for the site of its next new fab.

Jinko Solar set to open 120MW Cape Town factory, South African minister claims

Jinko Solar opened a 120MW PV module factory in Cape Town, according to South Africa's minister for trade and industry Rob Davies. A statement on the Department of Trade and Industry (DTI) website claimed that the 80 million Rand (US$7.5 million) facility was opening in response to the demand generated by the country's Renewable Energy Independent Power Producers Programme (REIPPP). The DTI claims to have helped secure Jinko's commitment through a number of measures including "reduction of red tape, facilitation and support on local content requirements". According to the DTI, Jinko Solar has 30% market share in South Africa. News of the factory's opening was later confirmed by Jinko Solar.

More Fabs for South America

S4 Solar do Brasil establishing 100MW PV module plant

New firm S4 Solar do Brasil has teamed with equipment suppliers, Meyer Burger, Confirmware and Jinchen Machinery Co to provide a 100MW automated c-Si PV module assembly plant at a cost of around R$30 million (US$13.2 million).

S4 Solar said that it had already signed module supply contracts with agricultural companies in the Mato Grosso and Goiás regions of Brazil totalling 45MW, expected to be its key initial markets. S4 Solar noted that it would be able to fabricate conventional c-Si PV modules as well as glass/glass modules once the line was commissioned. The company expects production to start ramping at around 2MW per month in January 2015, increasing to 7-8MW per month in the first year of production. S4 Solar has also teamed with Chinese producer Linuo Solar for solar cell technology, which is planned to be added to the plant in 2017. The company plans on obtaining all necessary international certifications to export modules in the future.

Uruguay set for 50MW module factory

Uruguayan developer, Tecnova Renovables and global renewable energy developer, Sky Solar are to build a 50MW factory in Paysandú, western Uruguay.

The factory will manufacture crystalline silicon PV modules for national projects, but also to market for demand in other Latin America countries. The factory will employ 60-100 people and cost US$2.3 million in investment. Of that, US$1 million is being invested in machinery and equipment and US$1.35 million

Source: wikimedia

Uruguay joins manufacturing set.

in infrastructure. The factory will be commissioned by the end of this year and developed on 1.44 hectares of land. It will have a single production line initially, with the possibility of expansion. The average price of the modules will be US$0.60 per watt, depending on demand and market fluctuation. The modules manufactured are to be used for Sky Solar and Tecnova solar projects currently under development and also to meet utility and residential market demand, depending on government policies and stimulus of the national solar industry.

China's BYD to set up solar fab in Sao Paulo

Chinese manufacturer BYD has chosen Sao Paulo in Brazil for a new manufacturing campus, including a solar panel factory. Located in the city of Campinas, the new campus is expected to create 450 jobs, and will build solar panels and energy storage systems. Set to open in 2015 the facility will also manufacture electric buses with accompanying battery packs. The two manufacturing facilities are to be built on the same campus, one 30,000 square metres in size, the other 20,000 square metres, and will be accompanied with a solar research and development (R&D) centre, to focus on PV, LEDs and smart grids.

Capacity Flux

Kyocera planning 1.4GW of PV module production

Kyocera Corporation is targeting annual PV module production of 1.4GW in the current fiscal year, up from approximately 1.2GW in the previous fiscal year.

Source: Kyocera

Kyocera will up its output.

Kyocera noted that increased demand was due to the booming Japanese market as well as buoyant demand across other key markets served, such as the US. The company said that its total accumulated production of modules (since 1975) had passed the 5GW milestone. However, should the recently announced 430MW solar power project on the island of Ukujima become reality, Kyocera noted that it would ramp production further to support the need for an extra 1,720,000 multicrystalline modules. Kyocera has steadily added module manufacturing capacity over the last six years.

SunPower to remain capacity constrained through 2015

SunPower will remain capacity constrained through 2015 and rely on only a 350MW new fab in the Philippines through 2016, before starting the construction of a giga-fab in 2017. Despite running at full capacity, SunPower is limiting capital expenditures to its Fab 4 facility in the Philippines through 2016, with expectations of only having 50MW of module production from the fab next year, compared to previous guidance of production being between 50MW and 100MW. The main ramp of the new facility is planned for 2016 with an expected production capacity of 250MW. A key reason for the slow ramp of Fab 4 may be due to it being SunPower's pilot volume production plant for its Gen 3 solar cell technology.

Hanwha Q CELLS to expand production off buoyant shipments

Germany headquartered Hanwha Q CELLS has revealed plans to expand production capacity to over 1.5GW by the end of the year. The company said it hoped to boost capacity of around 1.1GW through a combination of a new production line and efficiency measures at existing plants. The company said it was close to completing its new 204MW production line in Malaysia and is also looking to implement 'manufacturing excellence initiatives' to increase throughput at both its Malaysian and smaller German plants, boosting their productivity by 200MW and 30MW respectively.

Start-Ups

Smartenergy ramping dual-glass c-Si modules for utility markets

Germany-based PV manufacturing start-up Smartenergy Renewables said that recent success with its glass/glass utility market crystalline modules would lead to ramping production higher and that it had strengthened its management team to further exploit downstream business opportunities. Having acquired the former CIGS thin-film production line of failed US-based NanoSolar and converting the facility to conventional crystalline module production for glass/glass modules, Smartenergy reiterated its nameplate capacity was 120MW and was producing modules of 295Wp. The company did not provide details concerning current utilization rates or expected ramp targets.

Source: Smartenergy

Smartenergy to ramp production.

Canadian start-up gains funding for low-cost mono polysilicon

Canada-based start-up Ubiquity Solar Inc has received CA$3.1 million (US$2.85 million) in funding to further develop its low-cost hyper-pure polysilicon and monocrystalline ingot/wafer technology, ahead of plans to commercialise the technology. Funding was secured via a not-for-profit foundation funded by the government of Canada, Sustainable Development Technology Canada (SDTC), and will be used by Ubiquity Solar to support its US$10.9 million demonstration pilot plant project. Ubiquity Solar has gathered a consortium of research institutes and universities to support the development of low-cost polysilicon and high-performance N-type and P-type monocrystalline ingots and wafers.

Other Fab News

Meyer Burger confirms SmartWire deal with Polish start-up Hanplast

Major PV equipment supplier, Meyer Burger, has officially confirmed the recent deal, exclusively revealed by PV Tech, to supply plastic mouldings engineering firm, Hanplast with a complete turnkey 'SmartWire' module assembly line. Financial details were not disclosed. Meyer Burger noted that it had successfully concluded a strategic 'Preferred Supplier' contract for the delivery and installation of the 'SmartWire' module assembly line to the Polish firm which has built a dedicated production plant at the Bydgoszcz Technology Park in Poland. Meyer Burger said the module assembly line would have an annual production capacity of 80MW, with delivery of the systems as well as the start of production by Hanplast in the first half of 2015.

Solar-Fabrik expands capacity with Centrosolar fab acquisition

German PV module manufacturer Solar-Fabrik has acquired the module manufacturing facility of insolvent firm Centrosolar, Sonnenstromfabrik, in Wismar, Germany, securing 143 jobs. The deal was organized through the insolvency administrator. Solar-Fabrik had been operating its own three-line production plant at around 150MW in 2013 with a nameplate capacity of 210MW. The acquisition of the Sonnenstromfabrik plant was said to increase its capacity to around 300MW. Solar-Fabrik has established a new subsidiary company to operate Sonnenstromfabrik with a capital injection of €25 million (US$32.8 million), headed by Joern Wirth, VP finance at Solar-Fabrik, and Ralf Hennigs, the long-term managing director of Sonnenstromfabrik. The company noted that it expected a smooth transition for the production plant from insolvency back to normal operation, including processing of outstanding orders. Solar-Fabrik has also acquired as part of the deal current inventory valued at around €300,000 (US$394,000) and will also have the rights to produce Centrosolar's module range.

Suniva starts work on its second PV module plant in US

US-based PV module manufacturer, Suniva, is to build its second production plant in Saginaw Township, Michigan, providing an additional 200MW of annual nameplate capacity. The company said that construction of the plant would be underway in August this year, with production expected to start in the fourth quarter of 2014. When fully ramped the plant is expected to create around 350 jobs, Suniva said. The company noted that it currently produced its Optimus monocrystalline module line with power ratings up to 280W (60-cell format) and 330W (72-cell format) at its Norcross, Georgia plant.

PV trade barriers: Strategies for Chinese and Taiwanese producers

Matthias Grossmann, Viridis.iQ GmbH, Konstanz, Germany

ABSTRACT
The latest rounds of formal complaints against alleged breaches of trade agreements, the initiation of circumvention investigations, and preliminary announcements and rulings in various countries and trading zones all demonstrate that the multidimensional trade conflict in global PV markets is far from being resolved and is still simmering. The trade dispute is largely focused on the import of downstream products (c-Si wafer, cell and module) in current and prospective high-volume markets, such as the EU, the USA and potentially India. These nations or trading zones have implemented, or have proposed to implement, anti-dumping and countervailing duties, predominantly targeted against Chinese downstream producers. New rounds of investigations might lead to existing tariffs being extended to Taiwanese manufacturers that directly or indirectly import into the USA, while the EU might scrap a previous quota and minimum price system and revert to tariffs. This paper gives a brief historical review of the global PV trade dispute, and analyses the formal and legal grounding of anti-circumvention actions, which in general increase the complexities of business planning. Because more than 70% of the global downstream manufacturing capacity is located in China and Taiwan, the manufacturers in these regions have no choice but to embrace an internationalization strategy that consists of production offshoring. The paper concludes with the introduction of potential strategies and recommendations which take account of increased complexities and uncertainties in business planning that arise from shifting trade barriers.

Overview of PV trade dispute

The global PV market has been troubled with trade litigations in various national jurisdictions and trading zones ever since the Coalition for American Solar Manufacturing filed a complaint in October 2011 with the U.S. Department of Commerce against unfair trade practices of China-based cell and module manufacturers.

This section gives a high-level overview of the chronology and current status of the various multinational anti-dumping (AD) and anti-subsidy (AS) investigations and rulings. Apart from the retaliatory actions taken by the Chinese Ministry of Commerce against polysilicon imports from the USA, Korea and the EU, the dispute can largely be characterized as a downstream phenomenon.

From the perspective of China- and Taiwan-based c-Si wafer, cell and module producers the downstream centricity of the trade conflict is particularly worrisome, as more than 70% of the global solar manufacturing capacity is located in these regions (estimate based on internal bottom-up capacity-tracking for estimated end-of-year capacities in 2014e). The last section of this paper will analyse strategic offshoring options for manufacturers that have so far clustered their production facilities in regions that are subject to continuous investigations by trade bodies in high-volume export markets.

The listed investigations comply with the General Agreement on Tariffs and Trade (GATT), Article 6, which allows members to investigate and take action against alleged dumping and subsidies that distort competition. (For a review of anti-dumping, subsidies and safeguard provisions set forth in World Trade Organization (WTO) agreements, see WTO [1].) Further, regular process rules grant nations or trading blocs that are subject to anti-dumping and anti-subsidy (AD/AS) tariffs the right to contest unilateral decisions through the multilateral WTO Dispute Settlement Body.

> "The trade conflict between the EU and the USA versus China is escalating."

The timeline of key events in the global PV trade dispute reveals that the trade conflict between the EU and the USA versus China is escalating, with second-round investigations and formal compliance assessments fuelling tensions between the trading blocs (Fig. 1).

While the conflict's centre stage has so far been occupied by the three aforementioned regions, the new round of investigations in the USA might lead to an extension of AD/AS tariffs to products from Taiwan. Further, other volume markets with promising growth prospects have begun investigations into PV imports and might therefore soon start contributing to global PV trade frictions. For example, in India an AD/AS ruling is pending which basically means that imports of c-Si PV products would be limited to producers based in Europe, while Australia has initiated a formal investigation into PV module imports from China.

The intensification of the PV trade dispute, with second-round proceedings and the spreading to other prospective volume and growth regions, demonstrates the necessity of incorporating in business plans some contingency plans that take into account erratic shifts in the institutional trade environment for PV components.

Drifting trade barriers: expect the unexpected

The brief chronological description of major events in the global PV trade dispute illustrates the tremendous tit-for-tat-like dynamic and ambiguity of discretionary rulings by regional trade-enforcement bodies. In particular, the new round of 'anti-circumvention' investigations in the USA and the EU leaves discretionary power to the regional trade bodies, as these proceedings are usually grounded in unilateral and local laws. A diligent and insightful comparative analysis of anti-circumvention rules in the EU and the USA, with a thorough analysis of the extent to which these regional codes might be in conflict with WTO agreements, has been provided by Ostoni [2].

It is clear that such an environment increases investment uncertainty and as a consequence suppresses offshoring

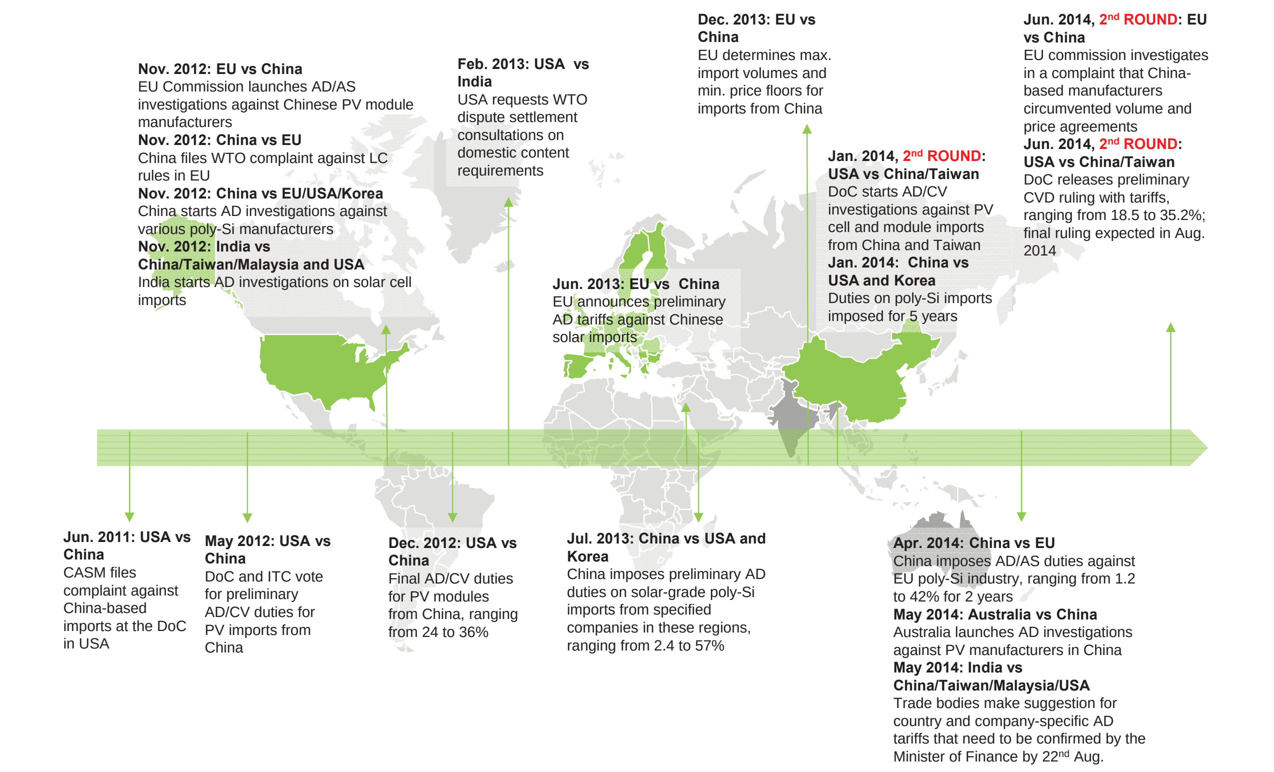

Source: Viridis.iQ GmbH

Figure 1. Timeline of global PV trade conflict.

decisions. The regional composition of a diversified production base is no longer 'just' a function of regional market growth rates and institutional frameworks, as well as of procurement and distribution network design, but also of low predictability events, such as continued trade litigations.

Increased complexity arises from the reopening of trade cases through anti-circumvention investigations. Depending on the scope and final ruling of such renewed litigations, previous investments that were made to satisfy trade requirements in target export markets could turn out, in the worst case, to be useless and lead to extraordinary depreciation of otherwise irreversible sunk costs.

> "Increased complexity arises from the reopening of trade cases through anti-circumvention investigations."

The investigations by EU and USA trade bodies that followed formal complaints by Solar World AG are good examples of increased investment risks caused by dynamically shifting trade barriers. In order to evaluate location decisions in the light of their resilience against future changes to trade agreements and existing tariffs, a basic understanding of the premises that could trigger renewed investigations is needed.

Since the main concern of the following analysis is the risk associated with irreversible sunk costs once an investment decision has been made for an offshore location, the subsequent discussion focuses on the interpretation and implementation of international trading rules as they relate to anti-circumvention procedures by the EU and the USA. These high-volume PV markets are of particular interest to any PV manufacturer and are therefore also referred to in the last section of this paper, which covers incumbent expansion strategies. That review is based on common-sense deductions applied to existing rules and procedures as set forth in publicly available information from the WTO and the EU. Any strategic investment decision that is intended to satisfy minimum local content requirements within the international target/export market(s) should also be reviewed by a law firm specializing in international trade.

As highlighted in the previous section, various jurisdictions or trading blocs have already utilized instruments such as import volume quotas, minimum prices, and AD and AS tariffs for PV products. (AS tariffs are also commonly referred to as countervailing duties – CVDs.) In addition, follow-up investigations into the trade practices of Chinese and Taiwanese PV downstream producers (ingot to module) have been launched by local trade authorities as a result of formal complaints against alleged breaches and/or circumvention actions ('loopholes').

As the EU and the USA are dominating and influential members of the WTO, their respective interpretations of anti-dumping and anti-circumvention agreements in conjunction with Article VI of GATT are regarded as influential in international arbitration case law. Further, the two regions encompass a significant demand share of the current and future PV installation market and therefore cannot be disregarded in any Tier 1 downstream manufacturer's mid- to long-term business strategy.

The WTO members have so far not officially determined whether circumvention of anti-dumping as well as anti-subsidy tariffs constitutes an offence against GATT. In the absence of general and binding WTO rules on trade circumvention and implementation procedures for counter-protective measures, the general interpretation is that members can implement protective anti-circumvention policies independently, as long as these are not in conflict with

other WTO agreements. For the EU see Paragraph 22 of Council Regulation (EC) No. 1225/2009 [3] and p. 4 of Vermulst [4].

The absence of a multilateral legislation with coherent and generally accepted procedural rules demonstrates that countervailing anti-circumvention actions exhibit a high degree of administrative discretion within the boundaries of nations or trading zones. This leaves room for subjective and politically motivated rulings which increase the uncertainty of investment decisions that are concerned with the internationalization of the production capacity base. This statement holds true regardless of the underlying motivation, whether or not the international diversification of the production base is a consequence of trade barriers.

The definition of 'circumvention' rests on five cumulative conditions in accordance with the Directorate General for Trade in the EU Commission (Article 13, Paragraph 1 of Council Regulation (EC) No. 1225/2009 [3]). (The cumulative definition for AS countervailing measures is similar: see p. 12 of Vermulst [4].) The five conditions are:

(a) a change in trade pattern after or slightly before AD/AS tariffs have been implemented

(b) as a result of a practice, process or work,

(c) for which there is insufficient due cause or economic justification other than the tariff or duty, and

(d) with evidence of injury to domestic manufacturers as a consequence of duties being undermined, and

(e) dumping investigations have been positively concluded in an original investigation for a like product.

The widely interpretable and construable definitions of circumvention strategies as employed by trade authorities show that their application in formal investigations rulings exhibit again a relatively high degree of discretion. The following circumvention strategies are commonly cited (Ostoni [2], p. 409; Vermulst [4], p. 6):

1. Third-party circumvention: exporting individual key parts and assembly in a third country that is not subject to AD, AS or CV duties.

2. Importing country circumvention: assembly of imported key components into the country that enacted trade tariffs.

3. Part of or the entire production moves to a third country or the importing country.

4. Minor product modification circumvention: the end product is altered such that it can be distinguished from the product that is subject to the AD/AS order while not discouraging consumers from purchasing.

5. Lower duty rate country/company circumvention.

It is hardly disputable that strategies 4 and 5 constitute straightforward and blunt circumvention actions under any imaginable circumstance, as they are intended to confuse the customs service in the importing country as regards the origin or product specification. However, this is not necessarily the case for strategies 1 and 2, and certainly not for 3, as these go together with alterations to the value chain.

The U.S. Department of Commerce (DOC) applies a similar definition for anti-circumvention and also implements a similar set of indicators to determine whether a company engages in circumvention. These are set forth in the Tariff Act §781, 19 U.S.C. §1677j (Ostoni [2], pp. 422–425). In principle, the definition by the trade authorities in the USA also refers to product alteration and component assembly in a third country or the importing country. Likewise, in order to prove circumvention, changes in trade statistics of the subject product and its key components are analysed, as well as affiliations of assembling plants with companies that are subject to AD and/or AS tariffs.

Because international expansions or the relocation of existing production capacities of *selected parts* of the value chain can be challenged in formal petitions to trade authorities as circumvention actions, it is necessary to analyse the underlying formal rules that are applied in such second-round investigations and determinations. Here again, as will be shown, there is ample room for interpretation, which increases the complexities in business planning and the general investment risk associated with the establishment of offshore production bases in response to trade tariffs.

Article 13, Paragraph 2 of the EU Council Regulation No. 1225/2009 [3] gives the following definition of the circumstances under which an assembling plant based in a third country or the importing country itself will be regarded as a circumvention operation:

1. There is a chronological interdependence between the beginning of AD/AS investigations and the ramp of the assembly plant.

2. Parts used in the assembly come from the subject country.

3. Parts make up at least 60% of the total value of all utilized components/materials of the final product.

4. In cases where the local value add exceeds 25% of the manufacturing costs, circumvention will be ruled out.

5. The remedial effects from a tariff established in a previous AD investigation are being undermined by the third- or importing-country operation.

In terms of setting up an offshore manufacturing operation that is shielded against existing AD/AS duties and safeguarded against potential second-round circumvention investigations by the EU, points 2–4 of the assembly circumvention definition deserve particular attention. It is worthwhile here to analyse how the local value add is determined. If the 25% threshold is reached, the import of components from the country that is subject to AD/AS tariffs may exceed the 60% cap. In other words, as long as the value creation of the third- or import-country 'assembling' operation exceeds the 25% value creation criterion, the manufacturers have almost unlimited freedom in the design of their individual supply chain composition. This statement holds as long as the individual components are not separately subject to AD and AS (CVD) tariffs. For example, the final EU ruling that levied AD rates of 0.4 to 36.1% and AS rates ranging from 3.2 to 17.1% on solar glass imports from China impairs free component choice and thereby alters the otherwise optimal supply-chain structure under a tariff-free regime.

The commission's definition of the manufacturing costs includes the value of all parts and materials purchased at arm's length plus labour costs and factory overheads, while it excludes operating expenses such as SG&A and R&D. The interpretation of the 25% criterion is not unambiguous and different approaches have been implemented. While one strict approach just takes direct labour, depreciation and indirect fabrication overhead into consideration, a more liberal approach also takes account of the value of domestically procured parts [4, p. 29].

The criteria set forth by the U.S. Department of Commerce to determine whether merchandise assembled in

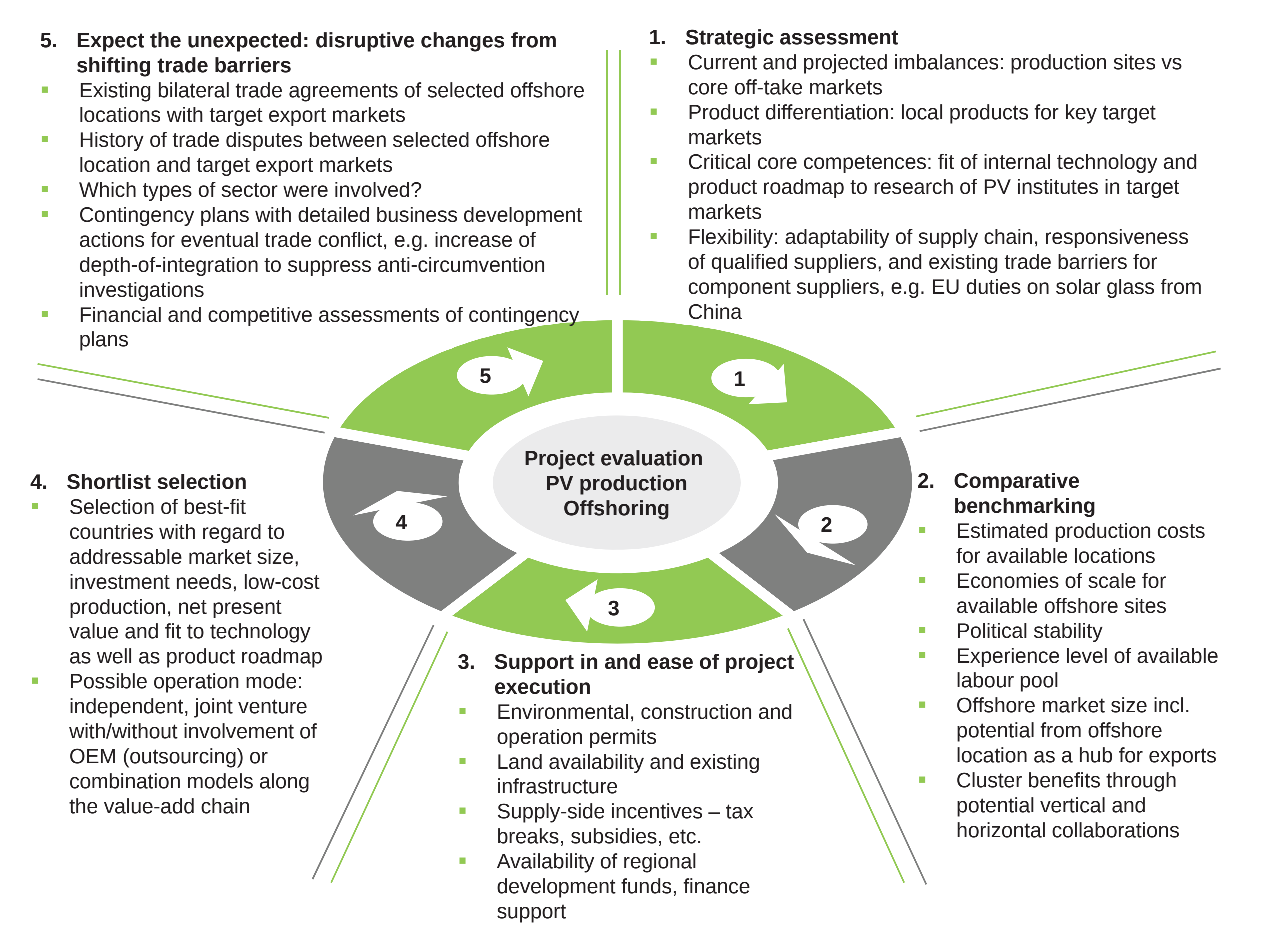

Source: Viridis.iQ GmbH

Figure 2. PV offshoring evaluation.

the USA or a third country constitutes circumvention are similar, but lack commitment to definitive quantities as regards the value of imported components from the subject country and the value creation within the third-country or domestic assembly plant. An affirmative circumvention ruling can be made when the components utilized in the assembly of a product come from an AD/CVD subject country and comprise "a significant portion of the total value of merchandise" and/or the "process of assembly or completion ... is minor or insignificant" (Chapter 26, Section IV of U.S. Department of Commerce [5]). The level of discretion that results from such unspecific definitions is intended by Congress. The argument of the legislator is that the DOC needs this freedom to account for industry-specific circumstances.

While the general definition of circumvention and the interpretation of deployed strategies are similar in the EU and the USA, the rules under which an import- or third-country operation will be classified as a circumvention assembly show some divergence. The EU sets forth quantifiable thresholds with regard to the local value creation that need to be exceeded in order to be classified as a regular local operation. The USA trade legislation leaves a greater degree of freedom to trade bodies and thereby increases the uncertainty for offshoring investment decisions.

Incumbent expansion strategies

The resumption of previously concluded investigations and the possible erection of new trade barriers in attractive growth markets pose tremendous threats to existing PV cell and module manufacturers with production bases in China or Taiwan. Historically, the producers in these regions follow a domestic manufacturing approach that is predominantly oriented towards economies of scale. The obvious strategic response, to embrace internationalization and offshoring of production to markets that have enacted tariffs, needs to be reviewed in a diligent manner from various angles.

The scrutiny should involve the typical working packages – such as strategic assessment and comparative benchmarking, as well as a project execution appraisal – that help to arrive at a shortlist of preferable sites (Fig. 2). However, as the PV market is riddled by multidimensional trade differences, the analysis should also include a package that focuses on the examination of potential later-stage trade litigations against and second-round investigations into products produced from the new offshoring location.

Despite the first modest signs that a negotiated settlement might happen between major trading blocs and nations sparring over PV-related trade imbalances, Chinese and Taiwanese producers should not be distracted from investigating available options for a regional diversification of their production base. This reasoning is based on the presumption that a negotiated settlement will most likely not be reached before the end of 2015 [6], while investigations by various trade bodies are ongoing and will probably be concluded before a multinational negotiated settlement can be reached. (The extent to which a negotiated political settlement can overturn existing AD/AS rulings that are usually valid for a duration of five years is a question for the individual national legislations. However, such a process is in general believed to be complex, as it would inflict damage on the integrity of national trade bodies and also impair the predictability of legal decisions, and could therefore be appealed by local manufacturers that benefited from trade barriers.)

"Chinese and Taiwanese producers should not be distracted from investigating available options for a regional diversification of their production base."

In addition, many of the high-volume markets (HVMs) to which manufacturers from China or Taiwan have only limited access exhibit some favourable characteristics, such as high internal demand, decent growth rates and lower bilateral trade barriers. In the case of Europe, AD/AS-free access to the Indian market would still be possible, even if the Indian Minister of Finance decides to enact the pending AD/AS tariff scheme.

The markets that have or might implement AD/AS duties against PV imports from China or Taiwan – namely Australia, the EU, India and the USA – comprised roughly 45% of the global PV market in 2013 (Fig. 3). These markets are expected to continue to be a significant demand driver over the short to medium term, with a relative contribution to global installations in the range of 41–48% for the period running up to 2017e. The compounded average growth rate for these markets is expected to be approximately 8% for the period 2013–17e. Hence, the markets in question are simply too important for a passive business strategy to be followed that relies on an uncertain negotiated settlement by the end of 2015.

Markets with local content requirements for modules or systems have purposely been omitted in the previous analysis, as this category needs to be tackled using a slightly different go-to-market strategy.

Once the potential and attractiveness of internal demand for prospective offshore locations have been determined, a search for suitable sites needs to follow. As highlighted in Fig. 2, site selection touches the strategic, operational and project execution planning spheres as well as the later trade-barrier contingency planning stage. From a strategic standpoint the adaptability of the existing supply chain must be assessed in the light of the internal technology and product roadmap. The fit to internal development projects should ideally take into consideration possible product modifications that are tailored not only to the offshore location itself but also to possible export markets that could be served from the new site. In this context possible collaborations with local research institutes could lead to a new impetus for internal research activities. Finally, a rigorous review of existing trade restrictions for key components concludes the strategic supply-chain assessment.

From an operational perspective the comparative benchmarking should review, among other things, potential future scaling benefits for the different offshore locations. These arise from internal demand and accessible export markets from the international production hub. Further, cluster benefits from a local PV industry and experienced personnel can have a significant positive impact on the success of the offshoring endeavour.

The familiarity with the industry of the local bureaucracy and public administration bodies usually eases project execution. If such an administrative environment is coupled with supply-side incentive packages, the project economics are likely to be influenced positively through a shorter development time, a faster time to market, and potential direct or indirect impacts on free cash-flow over the short to medium term.

In some instances the authorization of incentive packages or low-interest development funds might influence the operation mode through certain requirements – minimum job creation, stricter environmental or social controls, participation of local partners, etc.

The testing for resilience of the envisioned business concept(s) to potential new or second-round trade litigations, along with the development of potential contingency plan(s), can help in the selection and determination of the optimal offshore hub and lead to further optimization rounds of the operation and business model.

The big question is: how can an

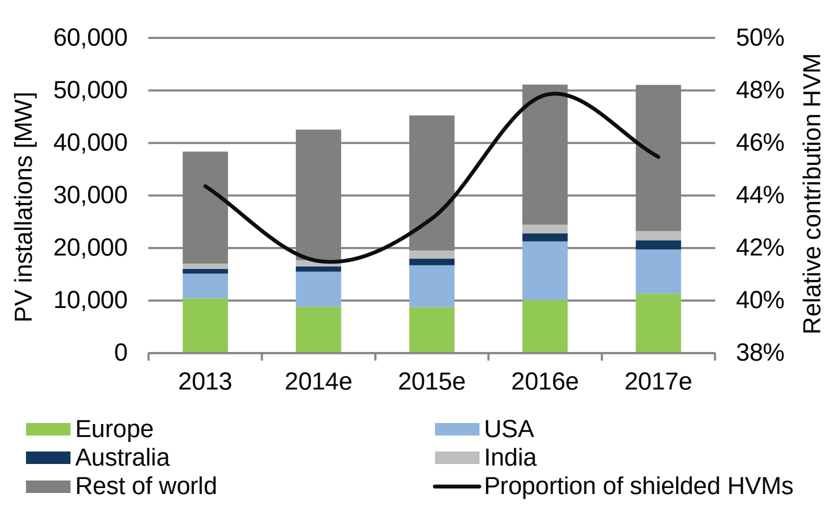

Source: Viridis.iQ GmbH

Figure 3. PV installation volumes in HVMs.

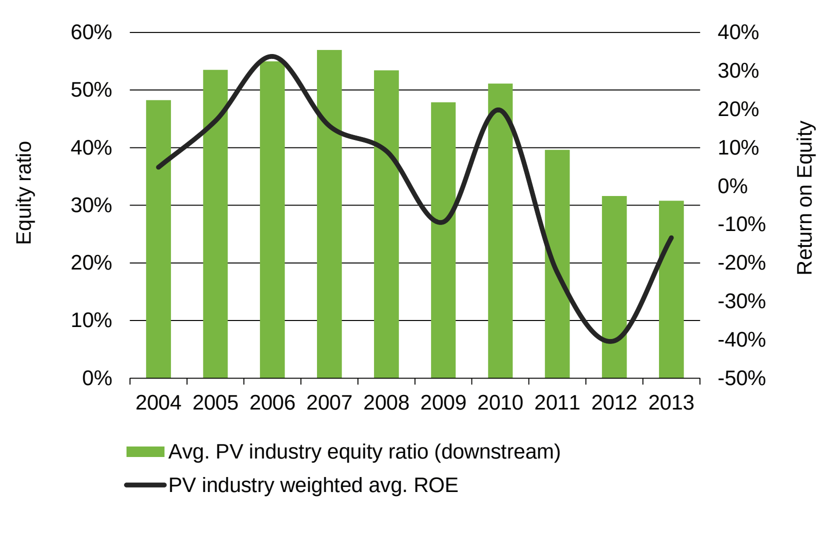

Source: Viridis.iQ GmbH

Figure 4. Equity ratio and return on equity (ROE) – PV downstream.

industry, that has been racked by havoc through overcapacity-induced marginal cost pricing for an extended period of more than three years, raise the necessary capital to adopt an expansion strategy in offshore locations, especially since this might prolong the process of market clearance in the eyes of potential capital providers? As Fig. 4 shows, the average equity ratio declined by 20% from approximately 50% in 2010 to just above 30% in 2013, while the average return on equity remained negative in 2013. Such figures hardly make for a compelling investment case.

If one looks through the aggregated figures on a company-specific level, however, there are several Tier 1 producers in Taiwan and China that have decent balance sheet ratios, good brand names and global distribution channels on which a diversification and internationalization undertaking could be successfully shouldered.

Besides, Tier 1 producers in these regions hardly have a choice if they want to avoid being trapped in a passive state in which their medium-term business prospects rely on negotiated political deals on which they have no direct influence. In addition, individual companies can still gain a first-mover advantage if they relocate production to locations that are being shielded by trade barriers.

On the basis of the general criteria listed above, Europe seems to be the ideal candidate for consideration as an offshore location for the following reasons:

- Available production sites that have been closed in the midst of the PV market crisis at which operating permissions should be readily available at short notice.

- Extensive knowledge base from a research standpoint and also from the perspective of the available human-resource pool at virtually all needed skill levels.

- Cluster benefits in the c-Si PV segment, with a diverse and industry-leading base of equipment manufacturers and access to feedstock from Tier 1 producers.

- Huge accessible market size in that all markets that have trade barriers, or are in the process to enact such, could be served from Europe. Since Europe and the USA are in negotiation of the "Transatlantic Trade and Investment Partnership" it seems unlikely that the USA would attack PV imports with the same rigour as has been the case with China- and now Taiwan-based producers.

- Even though European trade legislation leaves ample room for interpretation, this is not so much the case when it comes to the definition of circumvention, especially in comparison to trade legislation in the USA. The EU legislation is clear in that no operation shall be classified as circumvention if the local value creation exceeds 25% of the total cost. This threshold should generally be reached if the operation starts with the cell production, and definitely achieved if European-sourced feedstock is utilized.

The offshore operation could start with a large-scale cell-manufacturing nucleus from which different module production plants (satellites) could be served. The satellites could be placed in different countries within Europe and also in the target export locations that are to be served from this hub. The advantage of such a web-based strategy is that it could be utilized in a highly flexible and adaptable 'Made in xyz' marketing campaign and also support the production of specialized local modules. Eventually this leads to shorter feedback loops and faster innovation cycles for regionally specialized module concepts.

For specialized Taiwanese c-Si cell producers the move to an offshore location could also be coupled with a continuation of vertical integration efforts, which would decrease the dependence on integrated producers from China.

> "The EU offers a compelling mix of industrial and research experience in the c-Si PV segment."

Conclusion

Any China- or Taiwan-based Tier 1 producer would be ill-advised to abandon a proactive strategy in response to pending trade decisions in high-volume PV markets.

The author does not concur with the oft-repeated claim that the ideal offshore production hub is limited to locations in Malaysia, Mexico or Singapore. As demonstrated in this paper, the EU offers a compelling mix of industrial and research experience in the c-Si PV segment. This includes a highly experienced workforce, existing industrial PV sites, a long-term track record in c-Si PV manufacturing, globally renowned research institutes, industry-leading feedstock providers, accessibility to regional development funds, and, last but not least, a clear and precisely quantifiable definition of circumvention operations.

References

[1] WTO 2014, "Anti-dumping, subsidies, safeguards: contingencies, etc" [http://www.wto.org/english/thewto_e/whatis_e/tif_e/agrm8_e.htm].

[2] Ostoni, L. 2005, "Anti-dumping circumvention in the EU and US: Is there a future for multilateral provisions under the WTO?", *Fordham J. Corp. Law & Fin. Law*, Vol. 10, No. 2, pp. 406–438.

[3] Council Regulation (EC) No. 1225/2009 (2009), *Official Journal of the European Union*, L343/51 [http://trade.ec.europa.eu/doclib/press/index.cfm?id=829].

[4] Vermulst, E. 2012, "EU anti-circumvention rules & practice", Presentation at Seminar on Trade Defense Measures, Bangkok, Thailand [http://eeas.europa.eu/delegations/thailand/documents/thailande_eu_coop/eu_anti_circumvention_rules_and_practice_by_mr_edwin_vermulst_en.pdf].

[5] U.S. Department of Commerce 2009, *2009 Antidumping Manual* [http://enforcement.trade.gov/admanual/].

[6] Parnell, J. 2014, "China, EU and US open talks to end solar trade spats", News Report (8th July) [http://www.pv-tech.org/news/china_eu_and_us_open_talks_to_end_solar_trade_spats].

About the Author

Matthias Grossmann studied business administration and economics at Georg-August-Universität Göttingen. He works as a business development manager at Viridis.iQ GmbH, a specialized PV advisory boutique. Prior to this he worked at centrotherm photovoltaics AG and in the investment banking industry, with a focus on high-tech companies.

Enquiries

Dipl.-Kfm. Matthias Grossmann, CFA, FRM
Director Business Development & Strategy
Viridis.iQ GmbH
Moltkestr. 2–4
78467 Konstanz
Germany

Email: matthias.grossmann@viridis-iq.de
Website: www.viridis-iq.de

Materials

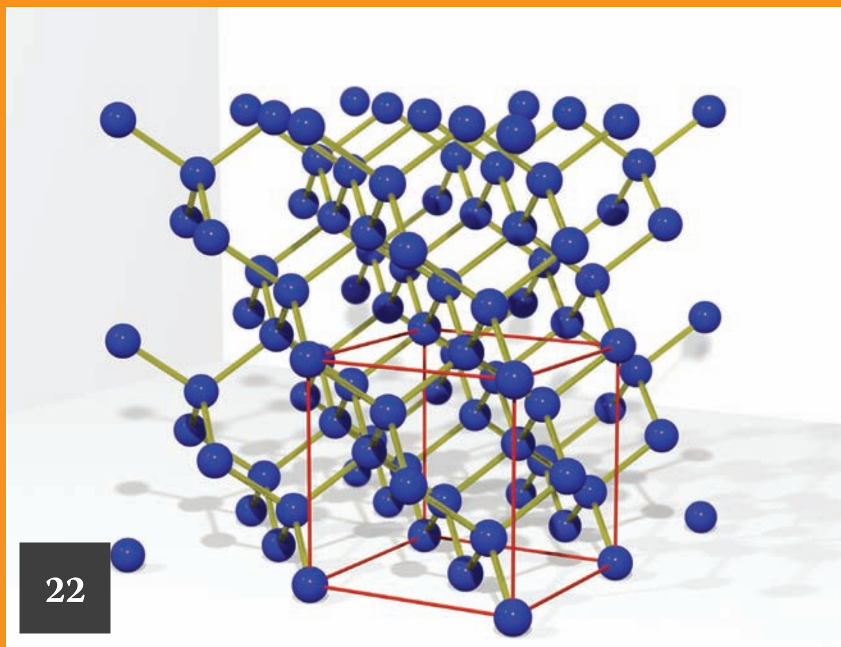

News

'Eteris' new name for merged Applied Materials and Tokyo Electron

Two of the most iconic names in the semiconductor equipment market, Applied Materials and Tokyo Electron have been dropped as part of the merger between the companies. The yet-to-be merged companies have a new name in the form of 'Eteris,' said to be derived from the concept of eternal innovation for society and not to be confused with other equipment suppliers to the sector such as Entegris and Axelis, or a Lithuanian television channel, Eteris TV. Tetsuro Higashi, chairman, president and CEO of TEL and Gary Dickerson, president and CEO of Applied Materials unveiled the rebrand to press at the Applied Materials annual analyst day in San Francisco. The financial costs of the name-change and rebranding were not disclosed. The companies expect the merger to be officially completed in the second-half of the year. Both companies have PV related equipment segments.

Source: Eteris

Applied Materials CEO Gary Dickerson and Tokyo Electron CEO Tetsuro Higashi.

Market Watch

Polysilicon prices to peak at around US$23/kg, says Bernreuter Research

The recovery in polysilicon prices to above US$20/kg since the beginning of the year is set to peak soon at around the US$23/kg mark, according to specialist polysilicon market research firm, Bernreuter Research. Citing delays in the ramp of new polysilicon plants in 2014, coupled to increased demand from China, the polysilicon spot price will rise for a short period but as new plant expansions begin later in the year, pricing is set to fall and could decline to around US$18/kg range, depending on end market demand. Johannes Bernreuter, head of Bernreuter Research said: "We assume that only 10,000 to 15,000MT of the new capacities will become effective by the end of 2014. Hence, oversupply will not be an issue this year, but return in 2015."

Scalable solar a good match for South America, says DuPont

Falling technology costs and scalability make solar highly suitable for the South American market, according to PV materials manufacturer DuPont. Hydroelectric dominates deployed renewables in South America with wind making progress in recent years. Falling solar costs have opened up a new opportunity, with Chile the first market to deploy in significant volumes. Small-scale solar projects have also opened the door to decentralised off-grid options for more remote parts of the continent. DuPont's interest in the market could be linked to the growing number of confirmed – and speculated – manufacturing capacity additions in Latin America.

Big Deals

Kazatomprom inks polysilicon deal with Qatar Solar Energy

In a strategic deal encompassing polysilicon supply and possible downstream PV project collaboration, Qatar Solar Energy (QSE) has secured a long-term polysilicon supply with Kazakhstan state-owned industrial firm, Kazatomprom. QSE, the first vertically integrated PV manufacturer in the MENA region, recently opened a 300MW PV module production plant in Qatar with future plans to expand operations to 2.5GW. Industry sector sources familiar with the polysilicon supply agreement, said metallurgical-grade silicon producer, KazSilicon, a subsidiary of Kazatomprom, would be the supplier, although further refining was expected to be supplied by a third party. Volume polysilicon supply shipments were said by sources to be set to start in 2016 at 500MT.

RENA to provide Shaanxi Youser with wet processing kit

As part of its PV manufacturing expansion plans to 1GW, Shaanxi Non-ferrous Photovoltaic Technology Co., Ltd, a subsidiary of state-owned Shaanxi Youser Group, has also placed equipment orders with RENA. Following on from orders placed with Schmid and centrotherm, Shaanxi Youser has selected RENA's 'BatchTex' processing tools and 'monoTEX' additive for solvent-free texturing of

Source: Qatar Solar Energy

Qatar Solar Energy has a signed wide-reaching deal with Kazatomprom.

monocrystalline wafers. Shaanxi Youser is building a 120MW monocrystalline cell line as part of its expansion plans. The specialist equipment supplier is also supplying its ‘InOxSide’ Inline systems for solar cell junction isolation processes for Shaanxi Youser’s 380MW multicrystalline solar cell line expansion. Financial details were not disclosed.

Cost Reduction and Pricing

Yingli expects to slash costs with new ingot process

Leading Chinese module manufacturer Yingli Solar has completed trials on a new technology for pulling monocrystalline silicon ingots it claims could reduce production costs by US$0.01/W. The process uses crucibles made from a carbon-carbon composite, rather than the traditional graphite, which Yingli said are prone to cracking during heating and leaking silicon. It said the new material was not as vulnerable to this problem as its structure is more resistant to thermal shock due to its high thermal conductivity. The new process could increase the utilisation rate of monocrystalline silicon ingots by around 3%, Yingli said.

PV Crystalox squeezed by lower wafer and stable poly pricing

UK-based merchant solar wafer producer PV Crystalox Solar reported increased shipments and revenue. However margins declined due to lower wafer selling prices, and stable polysilicon purchase pricing led to a loss in the first half of 2014. The company reported wafer shipments of 99MW for the reporting period, up slightly from 84MW in the prior year period as sales to PV manufacturers in Europe and Taiwan increased. The wafer producer is currently operating at 30% utilization rates with a nameplate capacity of 750MW.

R&D News

China Sunergy adds 48th Research Institute to R&D collaborators

Mid-sized tier one PV manufacturer, China Sunergy (CSUN), has teamed with state-owned 48th Research Institute of China Electronics Technology Group Corporation on materials and equipment research as well as to “co-develop solar projects”. Dr. Jianhua Zhao, chief technology officer of China Sunergy said: "For this strategic collaboration, we mainly aim to co-declare scientific research, co-research photovoltaic materials and equipment, and co-develop solar projects."

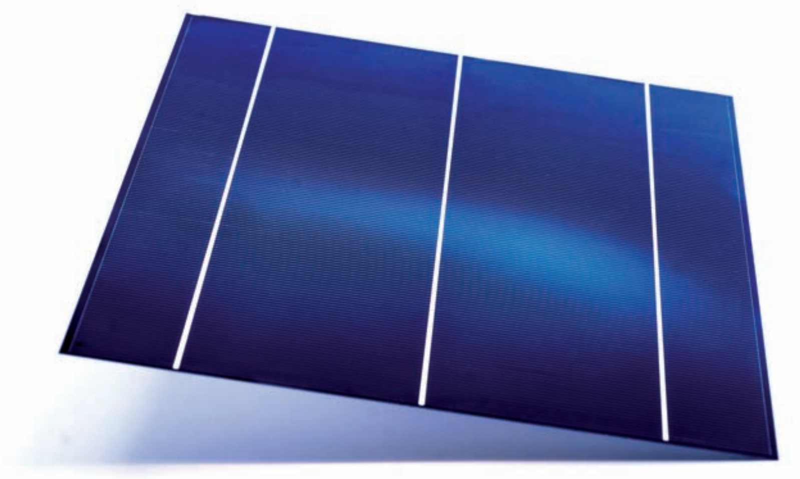

Source: SoLayTec

SoLayTec's ALD process was used in imec's record breaking cell.

Zhao said he believed the collaboration would “accelerate the development and monetisation of innovations”. CSUN is not alone in having a network of strategic R&D collaborations and currently has its R&D centre located at Nanjing University and also works with Hebei University of Technology. The company also teamed with New South Innovations Pty Ltd., a wholly owned subsidiary of the University of New South Wales, to improve wafer material quality in a five-year collaborative research agreement.

SoLayTec and Meco technology used in imec’s record 21.5% N-type PERT solar cell

Researchers at imec have achieved a new record conversion efficiency for N-type PERT (passivated emitter, rear totally diffused) solar cells using Ni/Cu/Ag plating (3 bus bars grid) technology from Meco and Atomic Layer Deposited (ALD) Al2O3 process from SoLayTec. Imec said that the large area wafer (156mm x 156mm) N-type PERT solar cell had calibrated at Fraunhofer ISE CalLab. The cell was said to have achieved an open circuit voltage (Voc) of 677mV, a short circuit current (Jsc) of 39.1 mA/cm2, and 81.3% fill factor, demonstrating the potential for improved conversion efficiencies with two side contacted crystalline silicon solar cells for volume commercial production.

Company News

GCL Poly secures US$490 million credit line

GCL Poly has secured two new credit lines worth a total of US$490 million. Downstream subsidiary GCL New Energy also confirmed it had secured a 95% interest in a project in Jiangsu Province. Both facilities have a three-year term. The bank was not named in the filing to the Hong Kong Stock Exchange detailing the new finance. It does say that it is the same organization that provided the company with credit lines in 2011 and 2013, suggesting that the lender is the China Development Bank. The company said the first US$240 million credit line would be used to fund one of its subsidiaries.

Solid Q2 for Daqo as capacity expansion progresses

Polysilicon firm Daqo New Energy posted solid Q2 results and confirmed its capacity expansion plans are progressing on schedule. The company confirmed its profit margin had climbed compared to the previous quarter while revenue hit US$43.7 million compared to US$27.8 million in the same period last year. Production cost per kg fell from US$14.49 in the first quarter to US$14.13 in the second. "In May, we successfully raised US$54.6 million through a follow-on offering in the public market. We will use the net proceeds mainly for the expansion and technology improvement at our Xinjiang polysilicon facility," said Dr. Gongda Yao, CEO, Daqo New Energy.

DuPont targets SunEdison in Te paste patent infringement

PV materials firm DuPont filed a patent infringement lawsuit against SunEdison and its affiliate NVT LLC in the US District Court for the District of Delaware over the use of its tellurium paste technology. The claim may target SunEdison but the company claims that Cheil Industries, now part of Korea-based Samsung SDI, was the paste supplier to Neo Solar Power (NSP), which supplied cells to SunEdison module assembly sub-contractor, Flextronics. DuPont said installers and module makers, including SunEdison, were responsible for ensuring that their products did not use infringing components.

Product Reviews

Lamer

Lamers High Tech Systems chemical storage and distribution system offers greater operator safety

Product Outline: Lamers High Tech Systems (LHTS) storage and distribution systems for corrosive and toxic chemicals offer increased safety within PV manufacturing facilities. The IBC (intermediate bulk container) handler is a system of LHTS in which reusable containers can be emptied automatically. The equipment is engineered and constructed in a modular manner to customer specifications.

Problem: Larger-scale PV production facilities have led to the need for improved efficiency and utmost safety when handling a range of chemicals used in high-volume production. Handling a lot of chemicals which are delivered in IBCs or by tankers means that the persons handling them are constantly in a dangerous situation and have to protect themselves.

Solution: The patented IBC handler ensures the safe draining of IBCs into storage tanks for the distribution of chemicals to the PV production process area, which is said to result in greater efficiency and significantly better operator safety, negating the need for special protection. The IBC is put in a closed cabinet foreseen with a leakage pan. Then the IBC is connected from outside the closed cabinet in one operation without any direct contact with the chemicals. The chemical handling and distribution can only be started after a safety check by the integrated control system.

Applications: Handling typical process chemicals used in the PV industry such as hydrofluoric acid (HF), nitric acid (HNO3), hydrochloric acid (HCL) and sulphuric acid (H2SO4).

Platform: The IBC Handler is part of the chemical distribution system, which consists of a valve manifold box, a pump section and a vessel. The patented system makes it possible to connect it to the chemical distribution system by means of a single plug and play action. This ensures the safe draining of IBCs into storage tanks and the distribution of chemicals to the production process.

Availability: Currently available.

SiTec

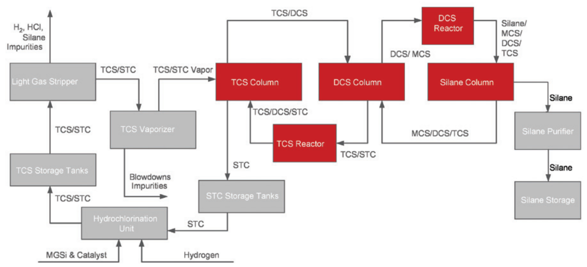

SiTec's monosilane process technology offers retrofit capability for lower production costs

Product Outline: SiTec has developed an innovative monosilane process technology that is expected to provide substantial energy savings compared to legacy processes. Marketed under the name 'STAR' the technology is applicable to both new and existing monosilane plants.

Problem: Continuous cost reductions are required to make overall polysilicon production as cost effective as possible. Providing lower energy consumption, while boosting overall productivity from existing monosilane production plants is required.

Solution: The STAR technology begins with metallurgic silicon and produces electronic-grade quality monosilane for polysilicon production and VSLI (very large-scale integration) quality monosilane for sale. Improvements have been developed for the reduction in equipment and process contamination as well as improved STC vaporization that eliminates plugging issues to boost uptime. STAR's novel attributes are claimed to significantly reduce both electrical and thermal energy requirement while debottlenecking the monosilane distillation train. A high conversion single train hydrochlorination reactor provides 10,000MTA to 15,000MTA of silane per train. New plants are said to experience best-in-class on-stream time and reduced costs, and up to 20% greater productivity from similarly sized equipment, compared to traditional plant designs. STAR is also claimed to provide up to 10% to 15% lower cash cost depending on geographic-dependent energy pricing.

Applications: SiTec offers monosilane plant designs exceeding 10,000 MTA (metric tonnes per annum) capacities.

Platform: The technology is applicable to both new and existing monosilane plants. Retrofitted plants will benefit by 20% greater capacity from existing redistribution and refining train equipment, reduced energy costs, and a two to six-month payback period on retrofit investment. STAR's unique drop-in technology enables uninterrupted production during the retrofit process.

Availability: Currently available.

X-ray specs for solar cells

Tamzin Lafford, European Synchrotron Radiation Facility, Grenoble, France, & **Richard Bytheway** & **Daniel Bright**, Jordan Valley Semiconductors UK Ltd., Durham, UK

ABSTRACT
Solar cell performance depends on material quality, as well as on the architecture of the cell. In the search for higher-performing cells, an ability to visualize the bulk and surface quality of the material is an advantage; to do this non-destructively, even in-line, is even better. It would be good to have X-ray vision to look inside, would it not? X-ray diffraction imaging (XRDI) does just that. Images are obtained of the distortions caused by crystal defects, and quantitative measures of the lattice deformation are available. In this paper the results obtained on a commercially available XRDI tool are compared with those from a large-scale public research facility.

Introduction

Consider, for example, p-type homojunction solar cells. When fabricated with electronics-grade Czochralski-grown silicon (Cz-Si), cells achieve typical PV conversion efficiencies of 19%. The same architecture made with multicrystalline silicon (mc-Si) yields ~15–17%. An advancing competitor to Cz-Si is 'mono-like' silicon (also known as *quasi-monocrystalline silicon*), grown on industrial scales by directional solidification on a bed of high-quality seed crystals. Mono-like Si is faster and cheaper to manufacture than Cz-Si, and PV conversion efficiencies are now reaching ~18% in industrial processes.

It is fairly easy to identify a multicrystalline Si wafer or solar cell just by looking at it – the way the different crystalline orientations reflect the light (with or without surface treatments) reveals the different centimetric grains, even if one cannot classify all of them. Distinguishing a mono-like sample from a Czochralski sample is less obvious – and in either case, the outside appearance cannot tell you what the internal structure is like. Yet what is inside makes a significant difference to the performance of the finished cell, and localized defects may even be catastrophic, causing electrical breakdown or leading to wafer breakage during module construction.

> "The diffraction image of a sample indicates the crystal defects that are present and where they are located."

This is where X-ray vision has an advantage over visible light microscopy or even electron microscopy. While conventional inspection techniques can reveal defects on the surface following

Bragg's Law: $n\lambda = 2d\sin\theta$

where n is an integer, λ is the wavelength of the X-rays, d is the spacing between lattice planes of a given orientation, and θ is the angle of diffraction.

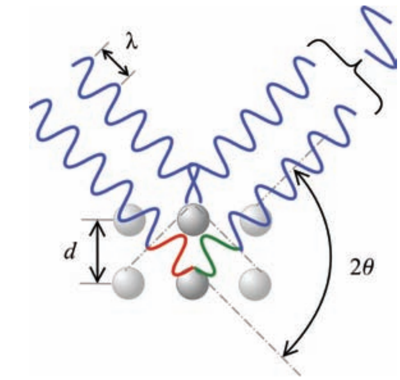

Credit: Image from Wikimedia Commons.

Figure 1. Derivation of Bragg's Law, for which W.H. and W.L. Bragg won the Nobel prize for physics in 1915, and illustration of X-ray diffraction from atomic planes. Constructive interference takes place when the path difference of the waves reflected from atomic planes differs by a whole number of wavelengths.

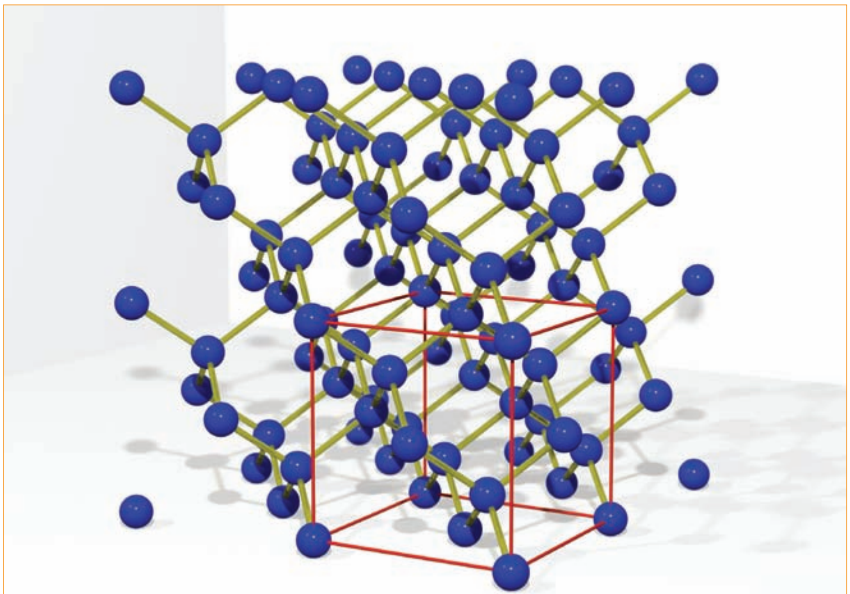

Figure 2. Crystal structure of silicon. The blue balls represent the positions of the Si atoms, and the yellow sticks the chemical bonds between them. The red outline represents a unit cell (face-centred cube).

particular surface treatment of small samples, X-rays can pass through the silicon; straightforward radiography (the same technique as used in hospitals for looking at broken bones inside the body) can be applied to the inspection of mechanical parts and electronic components.

But X-rays have an additional talent. Catch them at the right angle, and the planes of atoms in the silicon cause the X-ray beam to *diffract* according to Bragg's Law (see Figs. 1 and 2). This opens up a different type of imaging for crystalline samples, on a much finer scale and with the ability to look beyond the surface, with no special requirements as regards sample preparation. Where the 3D organization of the atoms in the crystal is near perfect, the resultant diffracted beam shows a uniform distribution of intensity. Defects such as dislocations, grain boundaries and precipitates deform the crystal locally and give *contrast* in the image, with different defects having characteristic 'signatures'. Thus the diffraction image of a sample indicates the crystal defects that are present and where they are located. Many types of defect can be highly detrimental to final PV performance, as can be demonstrated by light beam induced current (LBIC) or microwave photoconductance decay (μ-PCD) mapping, for example.

X-ray diffraction imaging (XRDI, also known as *X-ray [diffraction] topography*) was developed in the 1950s and 1960s using standard laboratory X-ray tubes, and was, somewhat belatedly, key in the development of the growth of high-quality single crystals for the microelectronics industry. The advent of synchrotrons – special large facilities producing extremely high-intensity, quasi-coherent X-ray beams with very low divergence – extended the range of possibilities, in particular with regard to the exposure time, the accessible spatial resolution, and the scope for detailed quantitative analysis. However, for a wide variety of inspection-type applications, commercially available, simple-to-operate lab-based tools provide practical solutions.

Both approaches have their advantages. In this paper, XRDI images of samples of silicon wafers and solar cell structures (fabricated by the CEA-INES) obtained using the Jordan Valley (JV) QC-TT, fitted with a sealed tube X-ray source, are compared with images taken using beamline BM05 at the European Synchrotron Radiation Facility (ESRF). XRDI has only recently been applied to mono-like silicon and solar cells. Rocking curve imaging is a further refinement, leading to quantitative maps of crystal deformation, as described below.

How X-rays are generated by a synchrotron and in a sealed tube source

Synchrotron facilities are large and are usually operated at a national or international level for the benefit of academic and industrial users in the communities which finance them. There are many such facilities around the world. Access is typically open via competitive proposal processes or by purchasing beam time (with or without scientific support) or a measurement service.

The spectrum from a 'bending magnet' source, such as BM05 at the ESRF, is several orders of magnitude more intense than that from a sealed tube and is smooth and continuous – a skewed bell shape extending from a few eV up to hundreds of keV. BM05's spectrum peaks at 17keV. Synchrotrons also offer 'wiggler' and 'undulator' beamlines, which are yet

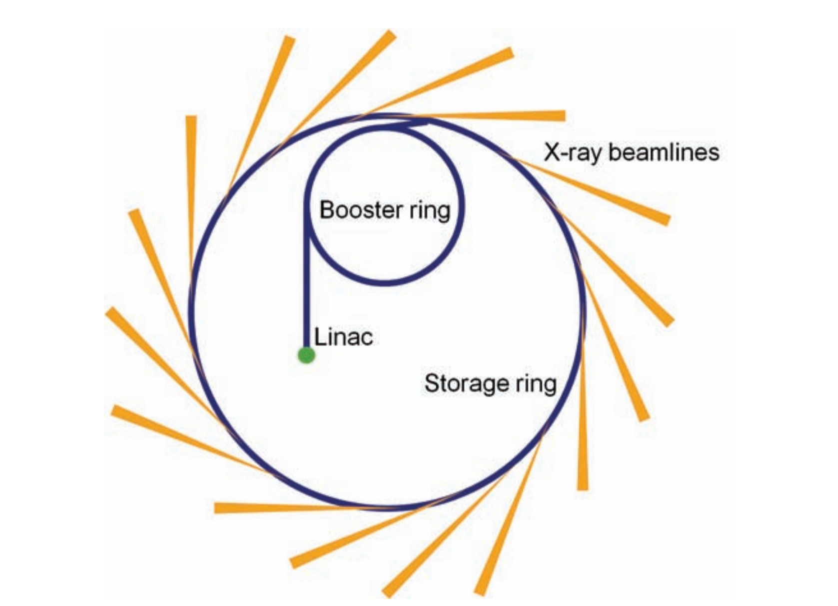

Figure 3. Schematic layout of a synchrotron. Electrons are generated at the start of the linear accelerator (Linac) and accelerated into the booster ring, where they are further accelerated before being injected into the storage ring at nearly the speed of light. When the electron trajectory is made to change direction (by magnetic fields), highly intense X-ray beams are generated in a forward direction. The ESRF has about 30 operational beamlines around a storage ring 844m in circumference.

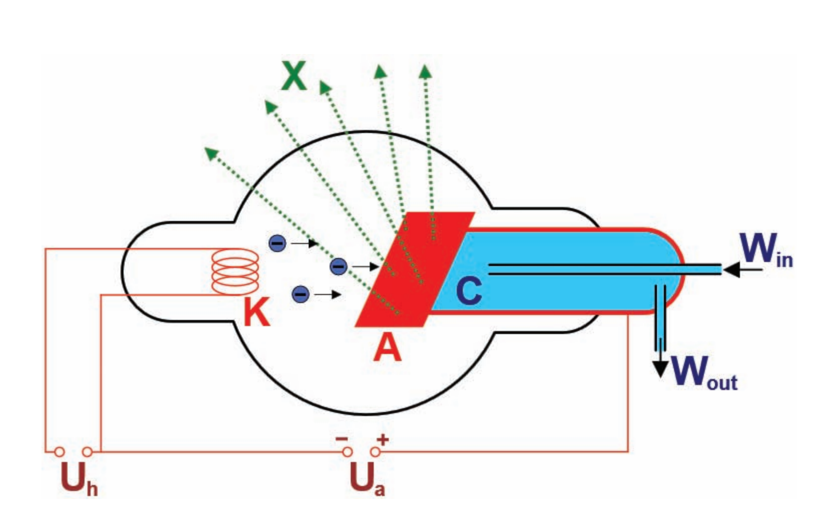

Credit: Image by Hmilch via Wikimedia Commons.

Figure 4. Diagram of a typical sealed tube X-ray source. Electrons are emitted by the heated cathode (K) and accelerated by a high voltage (U_a, typically ~40kV) to the anode (A), where they impinge, leading to the emission of X-rays (X). The anode is water cooled (W, C).

more intense, and give spectra with many peaks. Monochromation of a synchrotron beam thus offers a choice of beam energy over a wide range. The schematic layout of a synchrotron is shown in Fig. 3.

Compare this with a sealed tube X-ray source (Fig. 4). Electrons are generated in the same way, and accelerated to typically 30–50keV by an anode, which also serves as a target. The impinging electrons ionize atoms of the target material, leaving electrons at other energy levels to fall into the gaps, generating 'characteristic X-rays' at specific energies as they do so. Other impinging electrons are decelerated, giving rise to the broad continuum 'Bremßtrahlung' radiation at much lower intensity. The X-rays are emitted in all directions, and slits and windows are used to define the view of the source and its apparent divergence. The X-ray tube with its shielding assembly is less than 40cm in length and can be conveniently powered on or off as required by the user.

How does XRDI work?

XRDI at the synchrotron in white beam

BM05 allows a large, polychromatic ('white') beam to impinge on the sample. The different sets of atomic planes in the crystal select appropriate energies at appropriate diffraction angles (see Fig. 5) according to Bragg's Law (Fig. 1). With the use of a 2D detector, information on the quality of the crystal can be obtained from the detail within each spot. A perfect, strain-free crystal yields a uniformly illuminated, undistorted diffraction spot. Defects in or on the crystal – such as dislocations, inclusions and precipitates, stacking faults and surface scratches – locally distort the crystal lattice and give rise to *contrast* in the diffraction spot. The pattern of the contrast is a 'signature' of the type of defect. An overall stress causes the sample to curve and distorts the shape of the diffraction spot. In transmission geometry (the beam passing through the sample rather than diffracting from the incident surface), the image originates from the entire examined volume of the sample. In reflection geometry, the resulting images are dominated by diffraction from the material in a region of several microns (typically ~5–50µm) near the surface.

XRDI with a sealed tube

When imaging is performed with a sealed tube X-ray source, the near-monochromatic characteristic emission line is used, requiring appropriate orientation of the sample in order to produce a single diffraction spot. Only a line region diffracts at a given angular and spatial position, so the sample is moved through the beam and either the image is integrated on photographic film or a series of digital images is stitched together afterwards to produce the complete topograph.

A comparison of white beam synchrotron XRDI and lab XRDI is presented in Table 1.

What do we see with X-ray vision?

XRDI shows the distortions in a crystal lattice, and these traces can be linked back to the defect which caused them. Fig. 6 shows close-ups of synchrotron topographs of a Czochralski silicon (Cz-Si) wafer and a mono-like wafer. The Cz-Si wafer is practically defect free; in contrast, the mono-like wafer exhibits images of tangles of randomly oriented

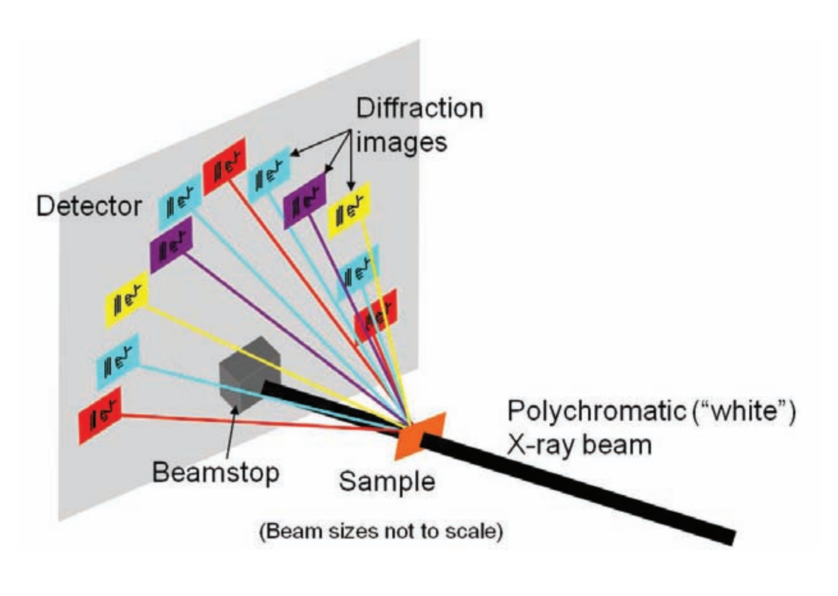

Figure 5. Illustration of white beam XRDI (topography) in transmission geometry.

	White beam synchrotron XRDI (BM05, ESRF)	Lab XRDI (Jordan Valley QC-TT)
Maximum topograph size	~100mm (H) × ~10mm (V) may be imaged in a single exposure; up to ~150mm (H) × ~100mm (V) by displacing the sample and stitching the images together	Samples up to 450mm diameter may be mounted and fully imaged with no edge loss
Incident beam	White beam (polychromatic): a few keV to more than 200keV; very low divergence (quasi-parallel)*	X-ray tube (predominantly monochromatic) – typically 8keV or 17keV, divergent
Sample planes imaged	Many, in different directions	One set of planes imaged per measurement
Image collection	Film for large area collection	Digital X-ray sensor with software image integration
Experimental geometric resolution	1µm	6µm
Image resolution	~5µm (film)	75µm in survey mode, 10µm in review mode
Typical measurement time	~0.1s exposure + a few minutes for film development	A few minutes for scanning + image stitching

* The synchrotron beam may also be highly monochromated using appropriate beam optics. This is necessary for rocking curve imaging, discussed later, where high-resolution optics and camera systems are used for data collection, with sub-micron image pixel sizes attainable.

Table 1. Comparison of synchrotron and lab XRDI systems.

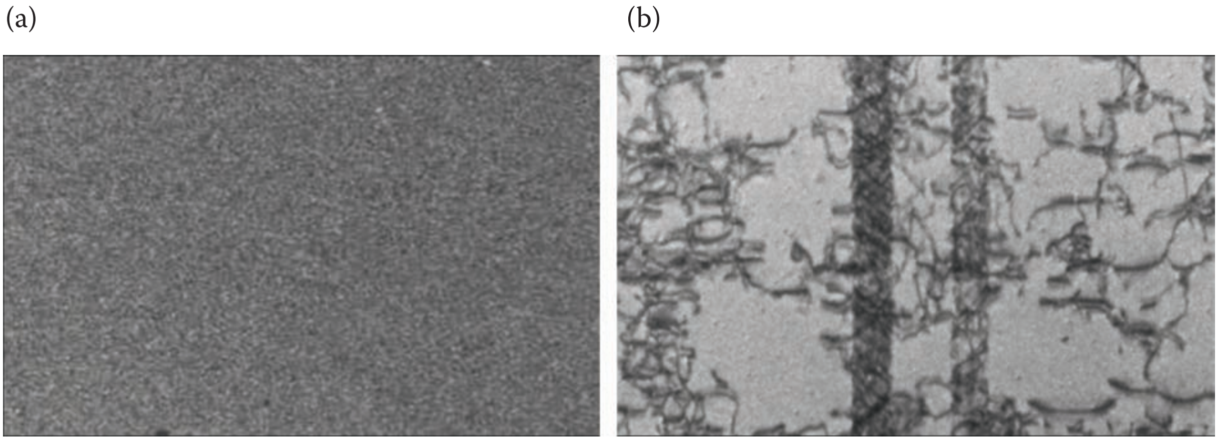

Figure 6. Topographs recorded by BM05: (a) close-up of XRDI of a Cz-Si sample, which is practically free of defects (graininess in the image is caused by the film emulsion); (b) the same type of image for a mono-like silicon sample. The observation of tangled dislocations is fairly typical, but it is unusual to see the bands of parallel dislocations. (Height of images ~1mm.)

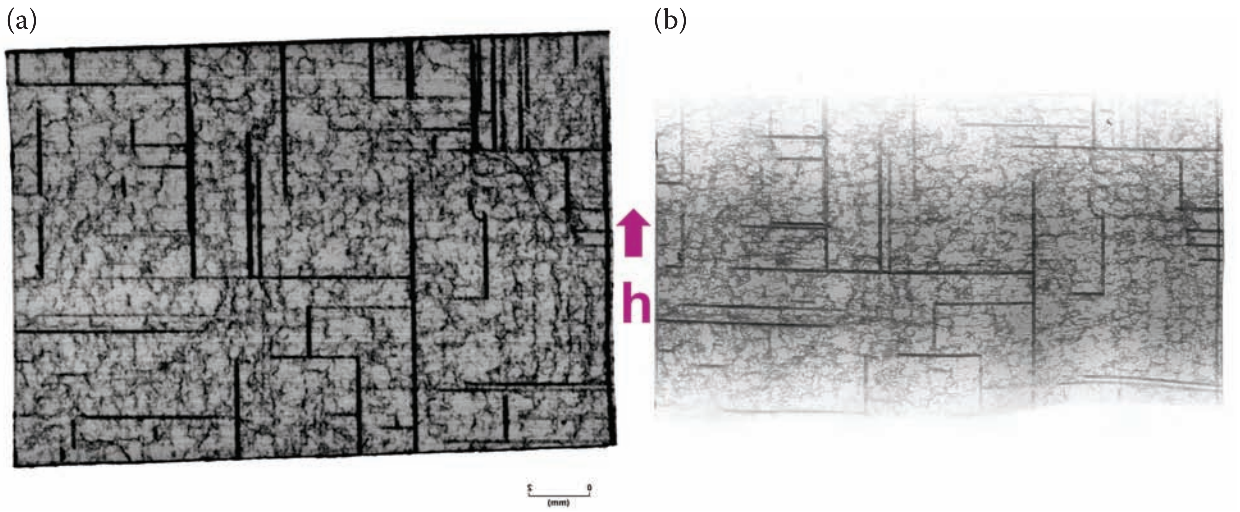

Figure 7. (a) Digital transmission topograph of the 220 planes of a mono-like silicon wafer sample, collected with the QC-TT; (b) the same measurement taken by BM05 using film, subsequently digitized using an optical microscope. (The scale bar is 2mm long, and h is the projection of the diffraction vector on the plane of the images.)

dislocations, as well as straight bands consisting of parallel dislocations running through the thickness of the sample, lying on particular crystallographic planes. These bands were observed to run through neighbouring wafers, and are unusual in mono-like samples – in the vast majority of cases, only tangles of dislocations are observed. There is no evidence of precipitates in this sample. Precipitates sometimes get caught at grain boundaries, and may be sources of dislocations. Control of growth conditions to minimize or control the generation and multiplication of dislocations, grain boundaries and precipitates is the subject of much study in the PV R&D community, as these can all reduce PV performance (e.g. [1–3]).

"XRDI shows the distortions in a crystal lattice."

Fig. 7 compares XRDI images of a mono-like Si sample 20mm × 15mm, taken by the QC-TT and at the synchrotron. The main features are evident in the images from both methods – straight lines of dislocations, as well as tangles. There are some differences to note, however:

- Slight misorientations notwithstanding, the two images are not the same shape. This is because:
  - In the QC-TT, diffraction is obtained from the whole width of the sample, then the sample is scanned and the image stitched together. This image therefore more faithfully represents the physical dimensions of the sample.
  - The synchrotron image is a single exposure. The beam covers the width of the sample but not the full height, so not all of the sample is imaged in a single shot. However, multiple exposures may be collected and stitched together after digital scanning, if required.
  - Curvature of the sample effectively focuses or defocuses the diffracted synchrotron beam in the direction of the diffraction vector. The dimensions of the diffraction spot compared with the area of the sample illuminated can be used to calculate the sample curvature
  - In addition, the equipment used at BM05 holds the sample in a clamp at the bottom. This

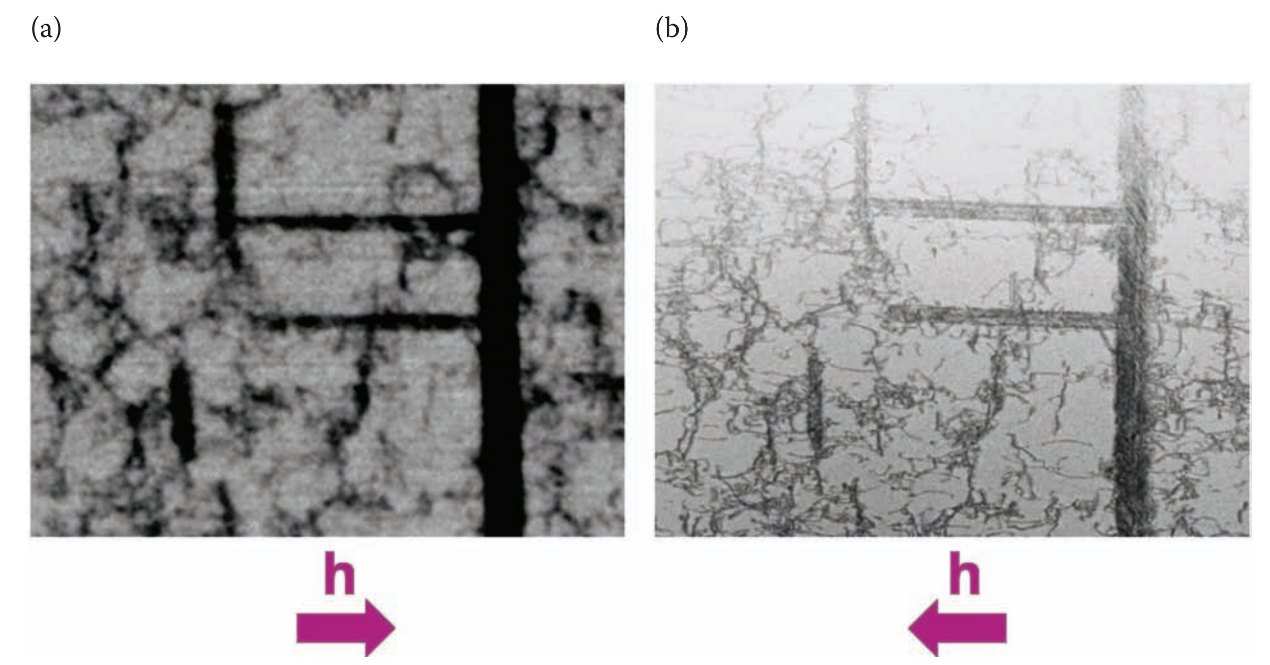

Figure 8. Zoom-in on other topographs of the mono-like Si sample shown in Fig. 7: (a) QC-TT image; (b) synchrotron image, showing sharper dislocation images and resolving the straight bands into groups of parallel dislocations running through the thickness of the sample. (Each image is approximately 4mm across, and h is the projection of the diffraction vector on the plane of the image.)

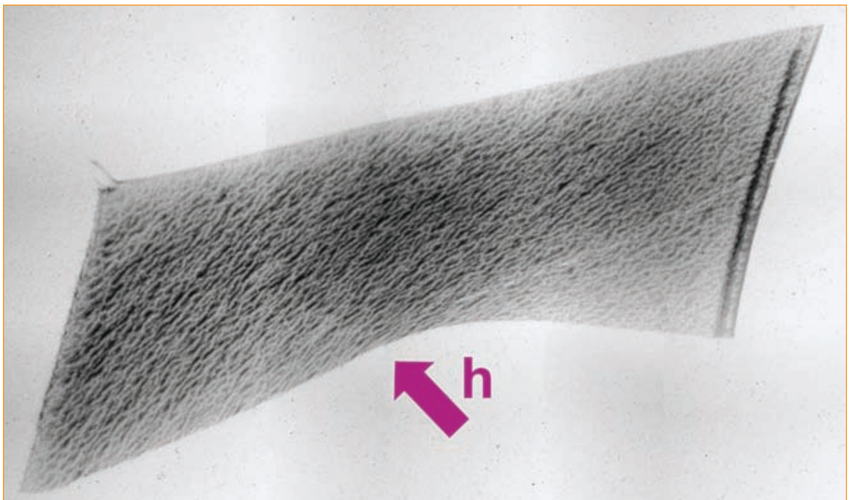

Figure 9. Synchrotron white beam topograph of a mono-like silicon sample with aluminium back-plane but no silver contact lines. The image is dominated by the 'orange-peel' effect of inhomogeneous distortions induced in the silicon by the back-plane.

shadows that part of the sample and, if the clamping is a little tight, also introduces strain, which locally distorts the image.

- The illumination is more uniform in the QC-TT image, owing to a more uniform diffraction line (which is then scanned) and to subsequent image processing. No image processing has been applied to the synchrotron data here, and the beam intensity profile in the vertical direction shows through.

The advantages of the synchrotron are evident in the finer details (Fig. 8). The lines of dislocations are revealed to consist of 'walls' of parallel dislocations passing from one surface of the sample to the other. The inherent geometric resolution of the BM05 experiment is around 1µm in the white beam case, decreasing to 0.1µm or lower when configured for a monochromatic beam. For the QC-TT, the resolution is 6µm, coupled here with a 10µm pixel camera. That said, the widths of features in the images are often tens or hundreds of micrometres, which is determined by the width of the strained crystal regions around the defects and by the measurement configuration.

In addition to taking measurements on bare wafers, XRDI can be applied at any stage of the processing, through to the final solar cell structure. In the case of conventional-architecture p-type silicon solar cells, the images are dominated by an 'orange-peel' effect arising from the inhomogeneous strain induced in the silicon by the screen-printed aluminium back-plane contact, which is co-fired along with the silver contact lines on the front face. Details of defects in the wafer itself are obscured. In addition, the Al back-plane induces bow in the silicon wafer, and the synchrotron white beam topographs are distorted in the direction of the diffraction vector – perpendicular to this, the images are not sensitive to distortion (Fig. 9). The distortion can be exploited to extract the sample curvature and stress.

Quantitative detail via monochromatic beam XRDI and rocking curve imaging

The extremely high intensity of the synchrotron beam, and the ability to monochromate it finely at the energy of choice using a crystal monochromator, gives access to a quantitative imaging technique called *rocking curve imaging* (RCI) [4,5]. With a single-energy X-ray beam incident on the sample, the sample angle must be set precisely if the diffraction condition is to be met. The sample can then be scanned around this angle. The 'rocking curve' is the plot of diffracted intensity vs. angle.

Instead of measuring a single value of intensity and integrating while the sample angle is scanned, individual images are collected at different angular positions across the rocking curve using an optics and charge-coupled device (CCD) system. Considering all the images as if superposed in a stack, each pixel, looking through the stack, contains a local rocking curve. The integrated intensity, the full width at half-maximum (FWHM) and the angular position of the diffraction peak can be extracted for each pixel, generating quantitative maps of the local sample crystalline quality (Fig. 10).

In addition, a comparison of images from diffraction from different planes of atoms can identify the type of dislocations (screw, edge or mixed) and the planes affected by them – useful information, since not all dislocations are necessarily electrically active. If the sample is not too distorted, individual pixels map directly to physical locations on the sample.

> "To obtain depth resolution, section topography is employed."

However, there is no information in such an image about where in the thickness of the examined sample lies the defect; to obtain depth resolution, section topography is employed (Fig. 11). With BM05, multiple beams – each 10μm wide – facilitate multiple sections in a single data collection. The QC-TT offers a single beam, typically

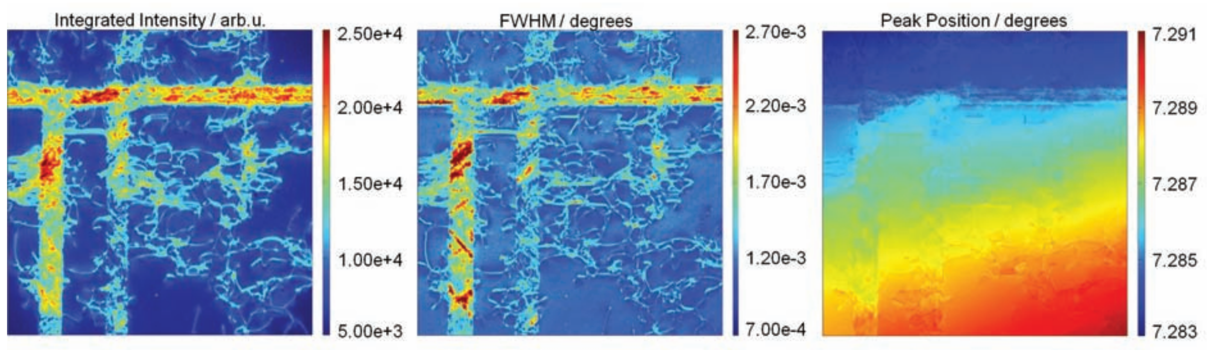

Figure 10. Maps of three rocking curve parameters, indicators of sample quality, showing defect behaviour and extracted from an RCI data set. (Images 1.5mm across; image pixel size 0.75μm; mono-like silicon; diffraction vector vertical upwards.)

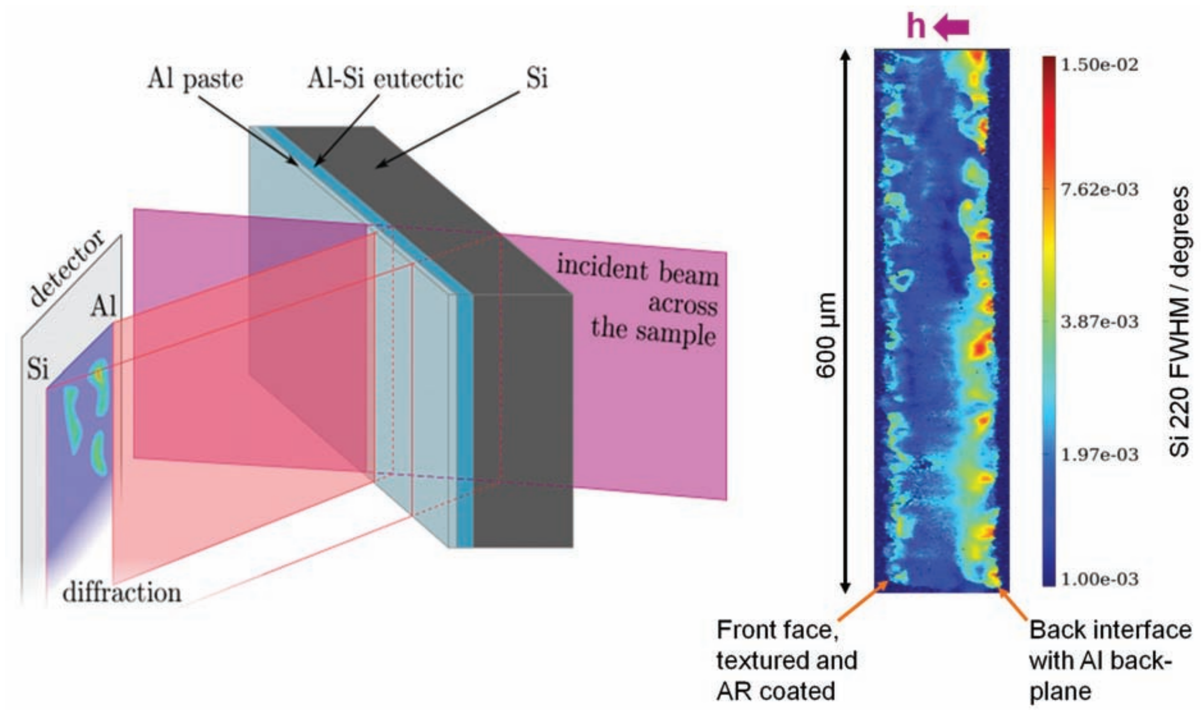

Figure 11. (a) Schematic of section topography; (b) close-up of a synchrotron section topograph of a mono-like Si sample with an Al back-plane. Only the silicon diffracts, so just the effects on the silicon of the back-plane and of the front-surface texturing, doping and anti-reflective coating are seen – not the effect on the actual back-plane or texturing. Greater distortion gradients show up in the larger diffraction peak FWHM values. (The image width corresponds to the silicon thickness of ~200μm.)

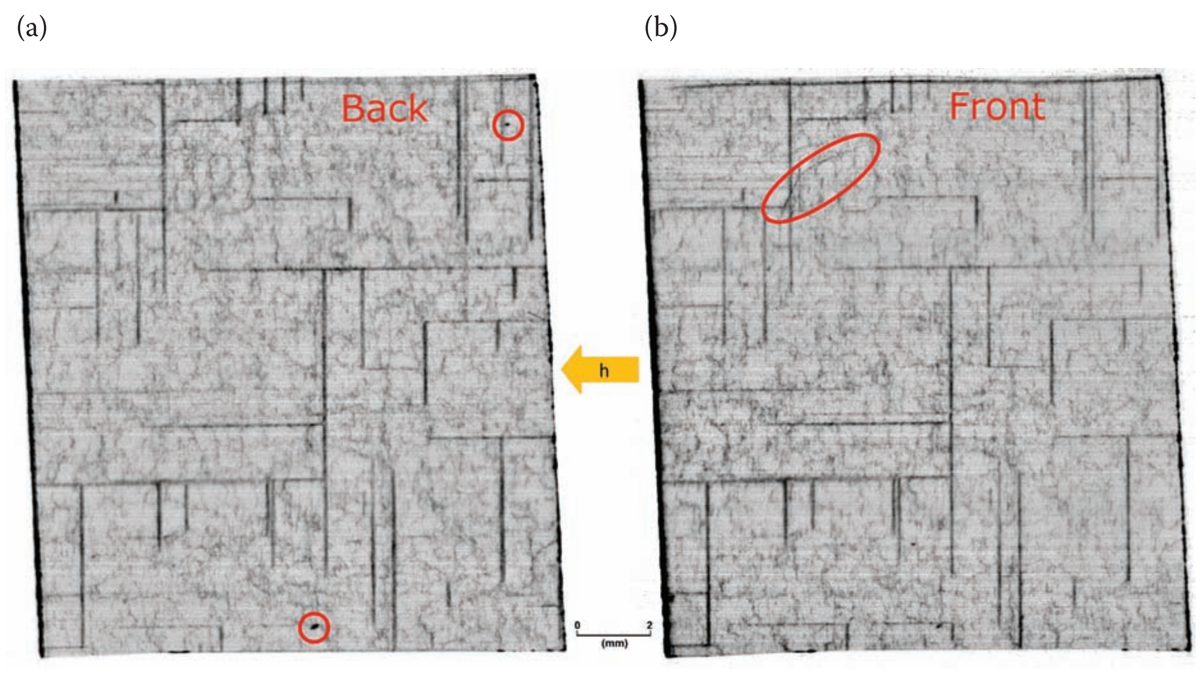

Figure 12. Depth-selective images from the QC-TT, generated from the same measurement data set: (a) back of a mono-like Si sample; (b) front of the sample. The red ellipses indicate some features which are not common to the two images and therefore arise from defects located at or near the respective surfaces.

50µm wide, via an adjustable slit system. The narrow region of the sample intersected by the X-ray beam diffracts, giving a virtual, non-destructive, slice view through the sample and thus of the distribution of defects through its thickness. This also enables meaningful measurements to be performed on full solar cell structures, getting around the 'orange-peel' effect induced by metallic back-planes, which dominates projection images [6,7].

In the example shown in Fig. 11, the combination of surface texturing, anti-reflective coating and local doping causes distortion gradients at the front side of the silicon. In the centre of the wafer, the silicon quality is near perfect in places (the FWHM approaches the instrumental limit for the configuration used), while much higher, further-reaching distortions are induced by the Al back-plane, which, on annealing, has generated a p^+ Al-doped layer and an Al-Si eutectic layer as well as the inhomogeneous Al back contact.

Alternatively, thanks to the digital imaging technique used in the QC-TT, some depth information can be accessed via the way the original images are processed. Scanning topography collects a series of adjacent cross sections across the area of the sample. Rather than stitch the entirety of every cross-section image together, a region of interest (RoI) can be selected corresponding to a particular depth range through the sample. Stitching these RoIs together creates a top-down view of the sample area at a given depth, in contrast to the section topograph, which gives a virtual slice through the thickness at a given position.

Fig. 12(a) shows the back and Fig. 12(b) the front of a mono-like Si sample. Many features are common between the two images, which means that these features exist throughout the whole sample thickness; however, some are clearly stronger in one image or the other, indicating that they are at the front or back surface (examples marked with ellipses). On the image of the back of the sample (Fig. 12(a)), there are two dark spots (possibly arising from inclusions, precipitates or surface damage) that do not show up on the front image (Fig. 12(b)); moreover, on the front surface there is a scratch that is not on the back.

That is not all that X-ray vision can reveal

Other X-ray techniques are also useful for examining material for solar cells, from bare wafers through to full cell structures. Nano-X-ray diffraction (n-XRD) enables additional quantitative detail of the crystal distortion to be probed [7]. Also, the fact that X-rays (like sunlight) are photons means that they too provoke a PV response in a cell; this allows the simultaneous measurement of local defects and their effect on PV performance, as in the case of nano-X-ray fluorescence studies (e.g. [2,3,8]), which correlate local impurities with pre-breakdown sites and non-uniformity of the PV response.

"XRDI gives unique insights into crystalline structure and its defects in a non-destructive way."

Conclusions

XRDI gives unique insights into crystalline structure and its defects in a non-destructive way. It is applicable to samples ranging from bare material (and not restricted to silicon) to full cell structures, requiring only that the sample be predominantly monocrystalline in the area investigated. Information can be obtained by using either a lab system or a synchrotron, with each having benefits. The lab system can be applied in the production line, as clean-room compatible equipment is commercially available, and could be used to screen and select samples for measurement at a synchrotron facility, where higher spatial resolution XRDI or rocking curve analysis can be performed for more in-depth investigations.

Materials

Acknowledgements

Thanks to S. Dubois of the CEA-INES for the samples (under a collaboration between the CEA-INES and the ESRF), and to T.N. Tran Thi for the images in Figs. 9 and 11.

References

[1] Tsoutsouva, M.G. et al. 2014, "Segregation, precipitation and dislocation generation between seeds in directionally solidified mono-like silicon for photovoltaic applications", *J. Cryst. Growth*, pp. 397–403 (doi: 10.1016/j.jcrysgro.2013.12.022).

[2] Kwapil, W. et al. 2009, "Observation of metal precipitates at prebreakdown sites in multicrystalline silicon solar cells", *Appl. Phys. Lett.*, Vol. 95, pp. 232113-1–232113-3.

[3] Buonassi, T. et al. 2005, "Quantifying the effect of metal-rich precipitates on minority carrier diffusion length in multicrystalline silicon using synchrotron-based spectrally resolved x-ray beam-induced current", *Appl. Phys. Lett.*, Vol. 87, pp. 044101-1–044101-3

[4] Lübbert, D. et al. 2000, "µm-resolved high resolution X-ray diffraction imaging for semiconductor quality control", *Nucl. Instr. Meth. Phys. Res. B*, Vol. 160, pp. 521–527.

[5] Lübbert, D. et al. 2005, "Distribution and Burgers vectors of dislocations in semiconductor wafers investigated by rocking-curve imaging", *J. Appl. Cryst.*, Vol. 38, pp. 91–96.

[6] Lafford, T.A. et al. 2013, "Synchrotron X-ray imaging applied to solar photovoltaic silicon", *J. Phys.: Conf. Series*, Vol. 425, pp. 192019-1–192019-4 (doi:10.1088/1742-6596/425/19/192019).

[7] Tran Thi, T.N. et al. 2014, "Czochralski and mono-like p-type and n-type silicon solar cells: Relationship between strain and stress induced by the back contact, and photovoltaic performance", *Solar Energy Mater. & Solar Cells* [submitted for publication].

[8] Villanova, J. et al. 2012, "Synchrotron microanalysis techniques applied to potential photovoltaic materials", *J. Synchrotron Rad.*, Vol. 19, pp. 521–524.

About the Authors

Tamzin Lafford is a beamline scientist/industrial liaison scientist for BM05 at the ESRF, having previously spent several years working in industry on X-ray characterization. Her research interests centre on XRDI applied to silicon for solar cells, from bare wafers to full structures. This has been carried out in collaboration with the CEA-INES (Institut National pour l'Énergie Solaire), where, together with industrial partners, cutting-edge and applied research is combined with innovation.

Richard Bytheway is a technologist at Jordan Valley Semiconductors UK Ltd., where he has spent 13 years developing X-ray metrology instruments. He previously worked in the fields of laser diffraction and geotechnical metrology, and is currently involved in applications development of the XRDI tools.

Daniel Bright is an applications engineer at Jordan Valley Semiconductors UK Ltd., specializing in X-ray topography. He has been developing XRDI methods and instruments for two years, as well as working on applications development of the XRDI tools.

Enquiries

Tamzin Lafford
ESRF
71 Avenue des Martyrs
CS 40220
38043 Grenoble Cedex 9
France
Email: tamzin.lafford@esrf.fr
Website: www.esrf.eu

Richard Bytheway
Jordan Valley Semiconductors UK Ltd.
Belmont Business Park
Durham DH1 1TW, UK
Email: richard.bytheway@jvsemi.co.uk
Website: www.jvsemi.com

Cell Processing

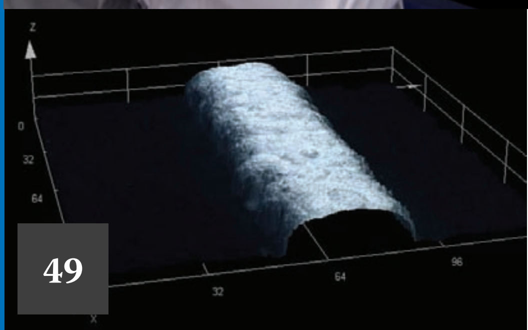

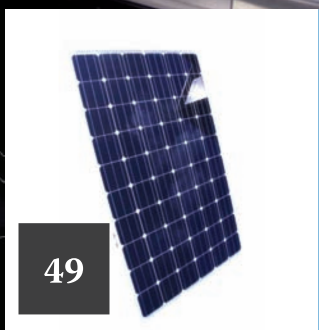

News

News

Taiwanese PV producers mulling options after US imposed anti-dumping duties

The latest anti-dumping duties (ADD) set by the US Department of Commerce (DoC) has left Taiwanese producers of PV modules and solar cells considering their options. It is the first time Taiwan-based producers have been affected by such proceedings and at least one has said it will consider establishing a manufacturing base outside of Taiwan. The petitioner in the case, SolarWorld, has repeatedly said that a "loophole" had existed since the first ADD case that allowed Chinese module producers to use Taiwanese solar cells in modules destined for the US market to avoid duties. However, the original ADD case put forward by SolarWorld did not include solar cells made in Taiwan. Despite announcements from many of the Taiwanese producers attempting to profile limited impact of the DoC judgement, Taiwan-based market research firm, EnergyTrend, said that producers face serious business challenges.

Anti-Dumping Hits Taiwan

Taiwan government to intervene in US trade row

The Taiwanese government is to intervene on behalf of solar manufacturers hit by the US government's latest solar trade duties. A preliminary decision in August on Chinese modules included new levies on Taiwanese cell makers including Gintech and Motech. It was alleged that cheap Taiwanese cells were being used by Chinese manufacturers to circumvent duties announced on them in 2012. The minister of economic affairs, Chang Chia-juch, has reportedly confirmed with local media that he will be taking up the issue with the US Department of Commerce (DoC). The Taiwanese authorities were approached by the industry to represent them in future talks in Washington.

E-Ton Solar sales continue decline on US trade decision

Taiwan-based solar cell producer, E-Ton Solar Tech reported a second severe sequential decline in revenue for July, 2014. E-Ton Solar reported revenue of NT$355.2 million in July, down from NT$422.1 million (US$14.03 million) in the previous quarter. The fall in revenue was expected, due to US anti-dumping preliminary findings and customers holding off from orders awaiting the decision. E-Ton Solar received a preliminary US dumping duty of 35.89% that was later revised down due to administrative errors, to 24.23%.

Innovations and New Technologies

Manufacturers innovating their way toward record cell efficiencies

Cell manufacturers are increasing their research efforts to push for greater cell efficiencies, according to a new report by NPD Solarbuzz. With over-capacity wracking the industry in the past and trade uncertainties continuing to make their mark, cell manufacturers are taking more aggressive steps to cut costs and boost the efficiency of their products. According to the research firm's PV equipment Quarterly, during the next 12 months, a standard 60-cell silicon-based module will reach 275W. Overcapacity created by new capacity additions in 2011, stalled the development of plants in subsequent years. New advances since then are now available to be taken advantage of by firms looking to upgrade existing lines.

Source: Wikimedia

New trade difficulties in the US look set to impact some Taiwanese firms.

Roll-out of GT's Merlin tech nears with certifications

The commercial roll-out of GT Advanced Technologies' Merlin metallization and interconnection technology has moved a step closer with the securing of three key certifications. GTAT said Merlin now conformed to the various performance, safety and quality standards enshrined in the IEC 61215, IEC 61730-1 and -2 and UL1703 standards, which determine the long-term reliability of silicon-based modules. Certification testing was carried out by the Renewable Energy Test Center and verified by the Canadian Standards Association and TUV-Sud.

Shin-Etsu Chemical wants to license bifacial mono solar cell technology

Japanese electronics materials firm, Shin-Etsu Chemical, is offering to license its production-ready bifacial monocrystalline solar cell technology that is claimed to have the highest conversion efficiency of 21% for conventional screen-printing processes. Shin-Etsu Chemical said it had around 10 patents related to its commercial 156x156mm cell processing technology, which it claimed offers a relatively easy manufacturing process, applicable to the existing mass production processes that are based on conventional screen-printing technology. Shin-Etsu Chemical could potentially also benefit from supplying high-purity P-type and N-type mono wafers.

Trina Solar to supply new anti-PID modules to China project

Solar module manufacturer, Trina Solar is to supply 82MW of its anti-degradation modules to a project in China. The 'anti potential-induced degradation' or anti-PID modules are to be shipped to developer, Tianganghu PV Power Generation. The agreement will see 320,000 of Trina Solar's

Source: Fraunhofer

Anti-PID modules are gaining momentum.

TSM-PC05A modules, with power outputs of 245W, 250W and 255W shipped to the eastern province of Jiangsu in China for a solar power plant currently under construction. The shipment is scheduled to be complete by the end of 2014. Trina Solar announced in March this year, that by optimiszng its manufacturing, all of its modules are to be anti-PID.

DEK adds Suzhou Sunshine Laser to licensed stencil suppliers

PV screen printing specialist, DEK, has licensed its 'VectorGuard' stencil technology to China-based Suzhou Sunshine Laser and Electronics Technology Company. Suzhou Sunshine Laser was said to have 19 facilities located in China, all of which will be offering VectorGuard laser cut stencil foils. DEK provides stencils as well as screen printers for solar cell metallization steps.

AkzoNobel and SERIS work on lower cost ALD and PECVD precursors

Materials specialist, AkzoNobel, is collaborating with the Solar Energy Research Institute of Singapore (SERIS) at the National University of Singapore in a bid to offer lower-cost ALD and PECVD precursors for aluminium oxide passivation layer processing. Backside c-Si solar cell passivation is seen as a key technology step being deployed by PV manufacturers to improve cell efficiencies along with PERC and MWT technologies. AkzoNobel's High Purity Metalorganics (HPMO) business unit has already developed a new technology for the production of high purity trimethylaluminum (TMAl), known as 'TMAL Solar.' However, the work at SERIS will focus on more cost-efficient metal organic precursor grades that also need to be robust for the long-term performance of high-efficiency solar cells.

SERIS opens PV testing lab in Singapore

Research and Development (R&D) centre, Solar Energy Research Institute of Singapore (SERIS) has officially opened its module development and testing laboratory, the 'CleanTech Park' in Singapore. The new 1,700 square metre facility comprises an R&D pilot production line for PV modules and a fully-equipped testing and certification centre, said to be the first in Southeast Asia.

Latest Production Lines

Helios founder buys firm's cells lines for new venture

The founder of Helios Technology has bought two cell production lines from the company for his new firm Megacell. Franco Traverso has paid €3 million (US$4 million) as part of a €10 million (US$13.5 million) investment to establish bifacial cell production in Italy. It is hoped the new facility in Padua will begin operation before the end of the year and will reach a capacity of 80MW by January 2015. Traverso claimed that Megacell would be the first large-scale bifacial cell manufacturer worldwide with cells in excess of 20% efficiency.

BTU International books PV pilot line orders in Q2

Thermal processing equipment specialist, BTU International reported second quarter sales of US$16.4 million, a 40.7% increase from the previous quarter, while the company booked several PV pilot line equipment orders in the quarter. Net sales for the first half of 2014 were US$28.1 million, compared to US$24.7 million, in the same period of 2013, driven primarily by sales in the electronics sector. The company reported a net loss for H1 2014 of US$1.2 million, compared to a net loss of US$3.4 million in the same period last year. The company ended the second quarter with cash of US$10 million.

Mission Solar Energy targeting N-type mono c-Si solar cell production in Q3

Mission Solar Energy, formerly known as Nexolon America, a joint venture with Korean-owned OCI Solar Power and partner of Texas-based CPS Energy, has started PV module production in June and expects N-type monocrystalline solar cell production to start in the early part of the third quarter of 2014. The San Antonio-based start-up is planning an initial first phase 100MW ramp as part of its PV power plant projects, primarily in Texas. The company has been working on UL certification for the modules since the beginning of the year, while cell processing equipment also began being installed at the same time. Updated production plans were disclosed in Korean firm OCI's recent quarterly results.

Expanding Markets

JA Solar ups module guidance on stronger China market

Major tier-one PV manufacturer JA Solar reported second quarter financial results within guidance but raised full-year shipment guidance on the back of stronger than expected demand in China. The company reported total shipments of 681.8MW, 6.8% up from the previous quarter and 47% higher, year-on-year. Modules and module tolling in the quarter was said to have reached 445.8MW, up 14.9% from the prior quarter and up 75.6% year-on-year. Solar cell and cell tolling were 236.0MW, up 12.5% year-on-year.

Shunfeng posts profit and plans overseas project expansion

China-based PV Energy Provider, Shunfeng Photovoltaic International (SF-PV) said it expected to report a profit for the first six months of 2014, primarily due to the increased solar cell sales coming from its manufacturing subsidiary, Wuxi Suntech Power Co. According to a financial statement, SF-PV "experienced significant improvement in its financial performance for the six months ended 30 June 2014", due to "increased shipment volume of solar cells" during the period".

Product Reviews

Applied Materials

Applied Materials' 'Vericell' system fully automates production wafer inspection

Product Outline: The 'Vericell' system is designed to fully automate in-line solar wafer inspection to address the quality limitations of manual review. It has the capability to automatically predict wafer cell efficiency through photoluminescence (PL) technology.

Problem: Wafer manufacturers must deliver high-quality wafers at a competitive price to cell producers, who in turn must produce high-efficiency cells in volume while maintaining high production yields. Wafer quality needs to be cost-effectively tracked and manufacturing processes adjusted to improve yield and binning to remove low-efficiency wafers and subsequently identify those that require process modifications.

Solution: The Vericell system's multiple integrated inspection modules automatically evaluate each wafer to find and eliminate defective wafers from production, as well as detecting defects. Employing PL technology combined with multiple sensing capability and advanced software algorithms, the Vericell system can predict final cell efficiency from bare wafer material with a mean average prediction error of less than 0.15% on multicrystalline silicon wafers.

Applications: c-Si wafer inspection and predictive final solar cell efficiency mapping.

Platform: The Vericell system is available with Applied's proprietary yield management software that can be used to collect, consolidate and analyze real-time data. The plug-and-play architecture supports customization and easy module expansion to include higher levels of inspection. The automation capabilities of the tool enable easy integration into existing production lines.

Availability: Currently available.

centrotherm

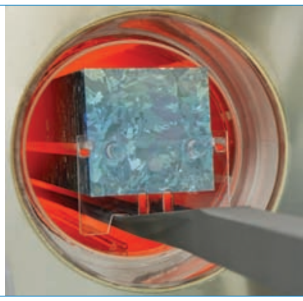

centrotherm's low-pressure diffusion technology offers up to 40% cost saving

Product Outline: centrotherm's low-pressure diffusion technology can offer up to 40% cost saving per wafer for solar cell emitter formation as a result of almost a doubling of the system's wafer throughput, to more than 140MW per year, and overall lower media consumption.

Problem: Achieving both cost savings and efficiency improvements is the main challenge in the mass production of c-Si solar cells. Among other things, this demands homogeneous high-quality emitters as well as high emitter sheet resistances (>100Ω/sq.) – fundamental to exploiting the efficiency potentials of commonly used metallization pastes.

Solution: The low-pressure diffusion process enables high homogeneity even at emitter sheet resistances of up to 150Ω/sq., and can further exploit the efficiency potentials of both conventional and new metallization pastes (emitter resistances >100Ω/sq.). Furthermore, the centrotherm technology opens up a broad range of options to solar cell manufacturers for diffusion processes, especially through the fast and changing deployment of gases in the process tube. Because of low-pressure processing there is a high cost-saving potential regarding materials and media consumption.

Applications: Low-pressure diffusion.

Platform: The low-pressure diffusion system is based on the modular design of the standard diffusion furnace, allowing fast installation and start-up. Available in various configurations regarding process capability, capacity and automation level, the equipment can process 5000 wafers simultaneously at 2.38mm back-to-back loading and 6000 wafers at 2mm back-to-back loading.

Availability: Currently available.

SCANLAB

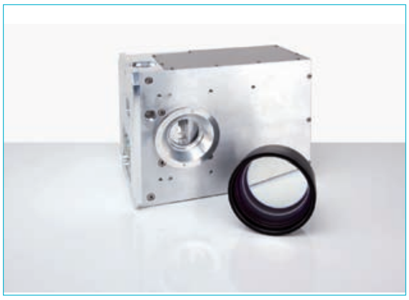

SCANLAB's hybrid scanner system provides high-speed back-side wafer processing

Product Outline: SCANLAB has introduced an integrated hybrid polygon laser scan system that can provide high-volume solar cell production of electrical busbars, arranged as alternating strips of emitter and base regions, on the backs of cells. The new hybrid system combines the dynamic superiority of polygon scanners with the high precision of galvanometers to drastically reduce wafer processing times.

Problem: Ultra-short-pulse (USP) lasers are ideal for high-precision microprocessing of components, but to achieve industry-suitable productivity, the USP laser must team up with an ultra-swift scanner capable of positioning the individual laser pulses onto a work piece without pulse overlaps, even at high pulse rates. In principle, the high speed of polygon scanners makes them well-suited for separating such high-frequency pulses, but they have limitations in accuracy and flexibility and have been difficult to integrate into USP processing systems.

Solution: The new scanning system drastically reduces process times. Full-surface back-side structuring of a 6-inch wafer previously required nearly a minute, whereas SCANLAB's system can cut the process time to less than 5 seconds – with any pattern and at the highest resolution.

Applications: Line-by-line laser processing of surfaces, e.g. silicon wafers, via high-repetition USP lasers.

Platform: Galvanometer scanners are high-performance rotary motors for optical applications. The primary area of application is the fast and precise positioning of mirrors for the deflection of laser beams.

Availability: Currently available.

Five-busbar PERC solar cells with a record 21.2% conversion efficiency

Thorsten Dullweber[1], **Helge Hannebauer**[1], **Ulrike Baumann**[1], **Tom Falcon**[2] & **Rolf Brendel**[1]

[1]Institute for Solar Energy Research Hamelin (ISFH), Emmerthal, Germany; [2]DEK Solar, Weymouth, UK

ABSTRACT

The PV industry is intensively evaluating technologies for further increasing conversion efficiency while maintaining, or even further reducing, production costs. Two promising technologies that meet these objectives are 1) the passivated emitter and rear cell (PERC), which reduces optical and recombination losses of the solar cell's rear side; and 2) multi-busbar/multi-wire module interconnection, which reduces optical and resistive losses of the front grid. This paper evaluates a combination of these two technologies, in particular industrial PERC solar cells with printed metal contacts employing a five-busbar (5BB) front grid instead of the typical three-busbar (3BB) design. The resulting 5BB PERC solar cells demonstrate an independently confirmed conversion efficiency of 21.2%, compared with the 20.6% efficiency for 3BB PERC cells. To the authors' knowledge, a value of 21.2% is the highest reported so far for typical industrial silicon solar cells with printed metal front and rear contacts. The higher conversion efficiency is primarily due to an increased short-circuit current, resulting from the reduced shadowing loss of the 5BB front-grid design, in combination with stencil-printed finger widths of only 46µm.

Introduction

Passivated emitter and rear cells (PERCs) are considered by many solar cell manufacturers and R&D institutes to be the next technology generation for industrial production. Fig. 1 shows the evolution of record conversion efficiencies obtained with industrial PERC solar cells (large area > 148cm^2 p-type monocrystalline silicon wafers, printed metal front and rear contacts) [1–11]. Starting with an efficiency of 19.2% [1] reported by Centrotherm in 2010, the benchmark for almost two years now has been 21.0% [6,7], demonstrated by Schott Solar in 2012.

According to the information available, many of the record PERC cells in Fig. 1 utilize AlO_x/SiN_y as the rear-surface passivation layer stack [3,4,7,9,11], in addition to laser contact opening (LCO) to form local Al rear contacts [1,2,4,7,8,9,11]. Only two papers report laser-fired contacts as the rear-contact formation method [3,5].

Regarding the emitter technology, several record efficiencies were obtained using a homogeneously diffused emitter instead of a selective emitter. The record 21.0%-efficiency PERC cell of Schott Solar [7] used a homogeneously diffused emitter as well, which was optimized by etching back the dead layer of the front surface and subsequently oxidizing the emitter, thereby reducing emitter recombination and increasing voltage and efficiency. In comparison, the PERC solar cells reported in this paper employ an AlO_x/SiN_y rear-surface passivation, LCO and a homogeneously diffused 70Ω/sq. emitter [11].

Besides PERC, another attractive technology is to increase the number of busbars (BB), as implemented, for example, in multi-wire module interconnection technologies [12–14] or multi-busbar approaches [15]. The printed Ag finger-line resistance contribution to the series resistance depends on the finger length between two busbars [16]: a greater number of BBs, therefore, reduces the finger length and hence the series resistance losses of the front finger grid. At the same time, in order to reduce the shadowing loss and Ag paste consumption, a larger finger pitch or a reduced finger width can be utilized without significantly increasing the series resistance [16].

In the work presented in this paper, a 5BB Ag-printed front-grid layout is applied to state-of-the-art

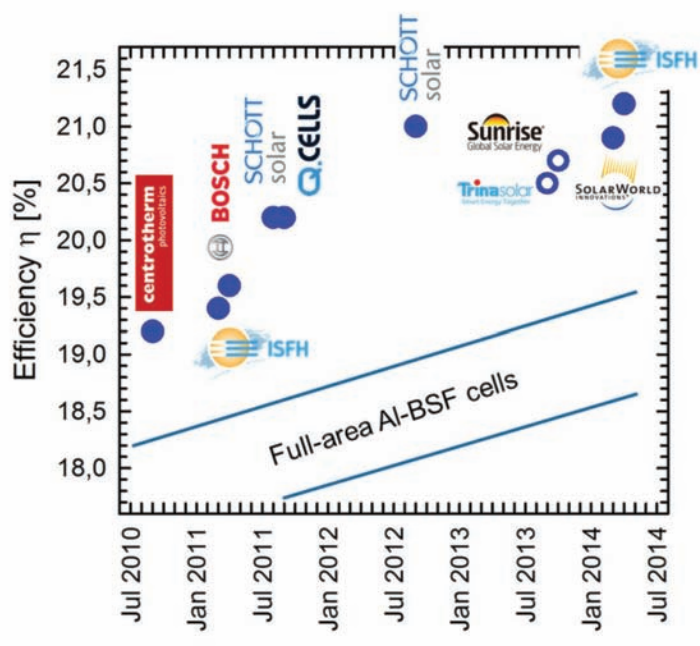

Figure 1. Record conversion efficiencies of PERC solar cells with printed metal contacts, using monocrystalline large-area p-type silicon wafers [1–11]. Solid blue circles refer to independently confirmed efficiencies, and open blue circles to in-house measurements. Typical efficiencies of full-area Al-BSF solar cells are also indicated.

industrial PERC solar cells, resulting in a record conversion efficiency of 21.2% [11]. Print-on-print (PoP) and stencil print (dual print) methods are evaluated for the fine-line Ag finger print. Each BB has a width of 0.5mm, which is very challenging for today's module interconnection technology. Nevertheless, Cu ribbons with a width of only 0.8mm are already under development [15], and, in combination with other technological advances, a 0.5mm-thick 5BB design is quite likely to be industrially feasible within the next few years.

"A 0.5mm-thick 5BB design is quite likely to be industrially feasible within the next few years."

Fine-line printed fingers with 5BB front grid

Three different split groups are evaluated for the silver front-side grid: the groups differ in the number of busbars (BB) and the printing process, as shown in Table 1. In the conventional 3BB design, each BB has a width of 1.3mm, which equates to a total BB width of 3.9mm. The 5BB design has a width of 0.5mm per BB, and therefore a 2.5mm BB width in total. The finger grid spacing has been optimized for each BB design and print process.

PoP means the fingers are printed twice in two consecutive printing steps, with 40 and 50µm screen openings; in the second print, the busbars are also printed. Both prints use the same Ag paste. *Dual print* means that first the busbars are screen printed with a non-firing-through Ag paste; in a second print step the fingers are printed using a stencil with a 40µm finger opening. For the finger stencil print, the same Ag paste as for PoP is used.

Table 1 summarizes several properties of the resulting front grids. The BB width of 1.3mm of the conventional 3BB design corresponds to a metal fraction (shadowing loss) of 2.5%. The 5BB design, with a BB width of just 0.5mm, leads to a lower BB metal fraction of 1.6%. The finger width on the final solar cells is measured using an optical light microscope: the images are shown in Fig. 2(a) and (b), and the resulting average values are given in Table 1. While the PoP process results in finger widths between 62 and 66µm, the stencil print leads to a smaller finger width of 46µm, which significantly decreases the finger metal fraction to 2.4%. In total, the metal fraction of busbars and fingers has been reduced from 5.8% for the conventional 3BB layout using PoP, to 4.0% for the 5BB layout using dual print.

Five-busbar PERC solar cells

For this study 156mm × 156mm, 2–3Ωcm, boron-doped Cz silicon wafers were used. The process flow is described in detail in Hannebauer et al. [11] and Dullweber et al. [17], but only the most important process steps will be highlighted here. After cleaning, the rear side is coated with a protection layer which acts as an etching and diffusion barrier in the subsequent alkaline texturing and $POCl_3$ diffusion, with a resulting emitter sheet resistance of 70Ω/sq. Following the texturing and diffusion, the protection layer is removed by wet chemistry, and the rear side is passivated using a stack of ALD Al_2O_3 and PECVD SiN_x, whereas the front side is passivated with PECVD SiN_x. Line-shaped LCOs are formed on the rear side using a picosecond laser; the width and pitch of the line-shaped rear contacts has been optimized in

(a) (b)

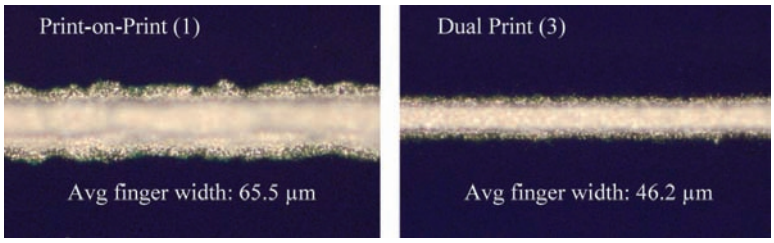

Figure 2. Optical light microscope images of fine-line printed Ag fingers, taken after firing on fully processed PERC solar cells in Tables 1 and 2: (a) PoP (group 1); (b) dual print (group 3). The extracted finger widths based on these measurements are summarized in Table 1.

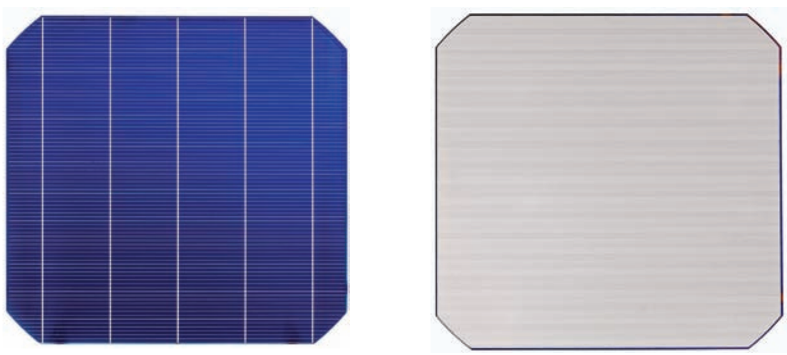

Figure 3. Photographs of the front and rear sides of the 5BB PERC solar cell.

Group	No. of BBs	Print technology	BB width [mm]	BB metal fraction [%]	Finger width [µm]	Finger metal fraction [%]
1	3	PoP	1.3	2.5	66	3.3
2	5	PoP	0.5	1.6	62	2.9
3	5	Dual print	0.5	1.6	46	2.4

Table 1. Summary of front-grid parameters for the three split groups. Whereas the conventional 3BB design (group 1) has a total (BB + fingers) metal fraction of 5.8%, for the best 5BB front grid (group 3) the total metal fraction is significantly reduced, to 4.0%.

order to obtain the best compromise between recombination losses and resistive losses.

After printing the front grid using the fine-line printing techniques and busbar designs as described in the previous section, the rear side of the PERC cell is full-area screen printed with an Al paste that has been specifically developed for PERC cell applications. The front and rear contacts are fired in a conventional belt furnace; during this process the Al paste locally alloys with the silicon wafer in areas where the rear passivation has been removed by laser ablation. Photographs of the front and rear sides of the resulting 5BB PERC solar cell are presented in Fig. 3.

The results of the best PERC solar cells for each BB design and front-grid printing process are summarized in Table 2. The 5BB PERC cells demonstrate an independently confirmed conversion efficiency of 21.2%, which to the authors' knowledge is the highest reported so far for a silicon solar cell with printed metal contacts. In comparison, the conventional 3BB PERC cell metallized with PoP achieves an independently confirmed efficiency of 20.6% – a typical value for the ISFH PERC baseline process. The efficiency increase of 0.6% abs. for the best 5BB PERC cells versus the conventional 3BB PERC cells is mainly due to the large increase in short-circuit current density J_{sc}, from 38.9mA/cm^2 to 39.8mA/cm^2.

> "The efficiency increase for the best 5BB PERC cells is mainly due to the large increase in short-circuit current density J_{sc}."

Fig. 4 shows the measured short-circuit current densities of the 3BB and 5BB PERC cells as a function of the calculated total shadowing loss of the front grid (BB and finger metallization fractions in Table 1). The J_{sc} error bars have been chosen in accordance with ISE CalLab specifications. The dashed line models the J_{sc} dependence on the shadowing loss.

The J_{sc} improvement for the 5BB PERC cells originates from the reduced shadowing loss of 1.8%, where 0.9% is due to the reduced BB width, and the other 0.9% to the reduced finger width (see Table 1). The open-circuit voltage V_{oc}, as shown in Table 2, increases from 658mV for the 3BB design to 662mV for the 5BB design because of the reduced front-contact area. In addition, because of the non-firing-through BB Ag paste, the front-contact area is further reduced for the dual-print group, leading to the highest V_{oc} value of 662mV.

The 5BB design yields an increase in *FF* from 80.5% to 80.9% as a result of reduced resistive losses. However, the root cause of the slightly lower fill factor *FF* of the dual-printed 5BB PERC cells still needs to be analysed.

Conclusions and outlook

This paper demonstrates a record high efficiency of 21.2% for industrial PERC solar cells which implement a 5BB front-grid design using either PoP or dual print as fine-line metallization processes. With the dual-print process, the finger width is reduced to 46µm, in contrast with 62–66µm when PoP is employed; the decreased finger width leads to a lower finger metal fraction of 2.4% for dual print. The front-grid metal fraction is further reduced by decreasing the width of each busbar from 1.3mm (3BB design) to 0.5mm (5BB design). Hence, the 5BB front grid with the best dual-print process reduces the total shadowing loss of the front grid to 4.0%, in contrast with 5.8% for a conventional 3BB front grid printed using PoP.

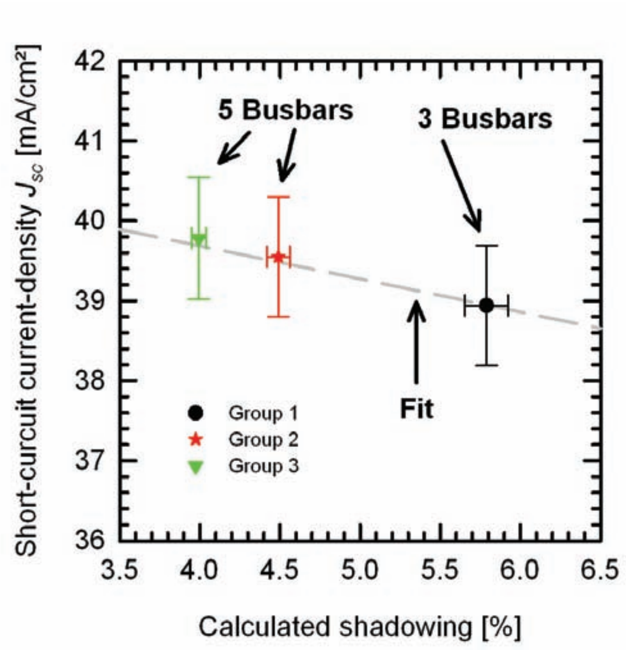

Figure 4. Measured short-circuit current density J_{sc} for the 3BB and 5BB PERC solar cells in Table 2 as a function of the calculated shadowing loss based on the front-grid layout and the measured finger widths in Table 1. The dashed line models the expected J_{sc} vs. shadowing loss dependence. The 5BB design with dual print (group 3) yields the lowest shadowing loss of 4.0% and the highest J_{sc} value of 39.8mA/cm^2.

Group	No. of BBs	Print technology	Efficiency [%]	J_{sc} [mA/cm^2]	V_{oc} [mV]	*FF* [%]
1	3	PoP	20.6*	38.9	658	80.5
2	5	PoP	21.2*	39.6	661	80.9
3	5	Dual print	21.2*	39.8	662	80.6

* Independently confirmed by Fraunhofer ISE CalLab.

Table 2. Solar cell parameters for the best PERC solar cells for each of the front-grid layout and printing processes, obtained from *I–V* measurements performed at standard testing conditions (25°C, AM1.5G spectrum).

> "The resulting 5BB PERC solar cells demonstrate an independently confirmed conversion efficiency of 21.2%, compared with 20.6% efficiency for the 3BB PERC cells."

The resulting 5BB PERC solar cells demonstrate an independently confirmed conversion efficiency of 21.2%, compared with 20.6% efficiency for the 3BB PERC cells. The increased conversion efficiency is primarily due to an increase of $0.9mA/cm^2$ in short-circuit current resulting from the reduced shadowing loss. Additionally, the 5BB PERC cells yield the highest V_{oc} values of up to 662mV because of the reduced metal contact area, as well as the highest *FF* of up to 80.9% because of lower resistance losses of the finger grid. Even though the 5BB design used in this work is quite challenging with today's module interconnection technology, it is expected that 5BB designs with a BB width of only 0.5mm will be manufacturable using advanced interconnection technologies within the next few years.

Acknowledgements

We thank our colleagues at ISFH for their support in the processing of the solar cells. This work was funded by the German Federal Ministry for the Environment, Nature Conservation and Nuclear Safety within the HighScreen R&D project, and by our industry partners SolarWorld, Heraeus, Singulus Technologies and Rena.

References

[1] Münzer, K.A. et al. 2010, "Advanced rear side technology for industrial high efficiency solar cells", *Proc. 25th EU PVSEC*, Valencia, Spain, p. 2314.

[2] Gatz, S. et al. 2011, "19.4%-efficient large-area fully screen-printed silicon solar cells, *physica status solidi (RRL)*, Vol. 5, pp. 147–149.

[3] Bosch Solar Energy AG 2011, Press release (April).

[4] Schott Solar AG 2011, Press release (August).

[5] Engelhart, P. et al. 2011, "Q.antum – Q-Cells next generation high-power silicon cell & module concept", *Proc. 26th EU PVSEC*, Hamburg, Germany, p. 821.

[6] Lachowicz, A. et al. 2012, "NO_x-free solution for emitter etch-back", *Proc. 27th EU PVSEC*, Frankfurt, Germany, p. 1846.

[7] Metz, A. et al. 2014, "Industrial high performance crystalline silicon solar cells and modules based on rear surface passivation technology", *Solar Energy Mater. & Solar Cells*, Vol. 120, pp. 417–425.

[8] Chen, D. et al. 2013, "Preventing the formation of voids in the rear local contact areas for industrial-type PERC solar cells", *Proc. 28th EU PVSEC*, Paris, France, p. 770.

[9] Tjahjono, B. et al. 2013, "Optimizing CELCO cell technology in one year of mass production", *Proc. 28th EU PVSEC*, Paris, France, p. 775.

[10] Fischer, G. et al. 2014, "Simulation based development of industrial PERC cell production beyond 20.5% efficiency", *Proc. 4th SiliconPV Conf.*, 's-Hertogenbosch, The Netherlands [in press].

[11] Hannebauer, H. et al. 2014, "21.2%-efficient fineline-printed PERC solar cell with 5 busbar front grid", *physica status solidi (RRL)*, DOI 10.1002/pssr.201409190.

[12] Schneider, A. et al. 2006, "Solar cell efficiency improvement by new metallization techniques – the Day4™ electrode concept", *Proc. 4th WCPEC*, Waikoloa, Hawaii, USA, pp. 1095–1098.

[13] Braun, S. et al. 2012, "Solar cell improvement by using a multi busbar design as front electrode", *Energy Procedia*, Vol. 27, pp. 227–233.

[14] Braun, S. et al. 2013, "Multi-busbar solar cells and modules: High efficiencies and low silver consumption", *Energy Procedia*, Vol. 38, pp. 334–339.

[15] PHOTON International 2013 (September), "The buzz on busbars", pp. 84–87.

[16] Mette, A. 2007, "New concepts for front side metallization of industrial silicon solar cells", Ph.D. dissertation, University of Freiburg, Germany, p. 27.

[17] Dullweber, T. et al. 2012, "Towards 20% efficient large-area screen-printed rear-passivated silicon solar cells", *Prog. Photovolt.: Res. Appl.*, Vol. 20, pp. 630–638.

About the Authors

Thorsten Dullweber received his Ph.D. from the University of Stuttgart in 2002. From 2001 to 2009 he worked as a microelectronics project leader at Siemens, Infineon and Qimonda. Since 2009 he has led the ISFH R&D solar cell production processes group, focusing on process and efficiency improvements in industrial-type screen-printed silicon solar cells.

Helge Hannebauer studied technical physics at the Leibniz University of Hanover from 2005 to 2009. For his diploma thesis at ISFH he investigated the optimization of screen-printed solar cells. He started his Ph.D. degree in 2010, also at ISFH, with a focus on advanced screen printing and selective emitters.

Ulrike Baumann graduated in 2011 as a laboratory technical assistant in chemistry. She then joined the solar cell production processes R&D group at ISFH, where she is in charge of processing industrial PERC solar cells. She is also responsible for the optimization and maintenance of a production-type wet chemical batch processing tool.

Tom Falcon has been with DEK since 2001, initially specializing in process development for DEK's semiconductor packaging technologies team, before moving to DEK Solar in 2008. He is currently responsible for developing metallization processes for silicon solar cells. Prior to joining DEK he held senior engineering positions with IBM, Nortel and Cookson Electronics.

Rolf Brendel is the scientific director of ISFH. He received his Ph.D. in materials science from the University of Erlangen, for which he researched infrared spectroscopy. In 2004 he joined the Institute of Solid State Physics of the Leibniz University of Hanover as a full professor. His main research focuses on the physics and technology of crystalline silicon solar cells.

Enquiries

Thorsten Dullweber
Institute for Solar Energy Research Hamelin (ISFH)
Am Ohrberg 1
31860 Emmerthal
Germany

Tom Falcon
DEK Solar
11 Albany Road
Weymouth DT4 9TH
UK

Griddler: The handy 2D solar cell calculator

Johnson Wong & **Ranjani Sridharan**, Solar Energy Research Institute of Singapore, National University of Singapore, Singapore

ABSTRACT

Actual solar cells are large-area, two-dimensional (2D) devices with lateral variations in internal voltage, but most of the time they are represented by simplistic equivalent circuits consisting of a few lumped elements. Griddler© is a finite-element-method (FEM) simulator that constructs and solves the full 2D distributed network representation of a metallized solar cell. Not only is this approach far more versatile and adaptable to real-world problems, accurate in predicting subtle device characteristics, and compatible with mapping data, but it can also be implemented in a way that is as easy and quick to use as a handy calculator. This paper covers a broad range of applications related to full-area 2D modelling and introduces Griddler 1.0 – a compact freeware computer program that places much of that power at the fingertips of any solar cell engineer with a PC.

Introduction

Photovoltaic engineers are no doubt familiar with the H-pattern metallization on the front side of silicon wafer solar cells. The simplicity and elegance of the H pattern lends itself to analytical determination of the power losses due to shading and series resistance, enabling one to derive equivalent circuit parameters to predict the cell performance with reasonable accuracy. But in the manufacturing environment, where every 0.1% absolute efficiency gain is worth fighting for, the simple equivalent circuit model has some severe limitations in terms of resolution. For example, the model is unable to provide the answer to the question of how much ohmic power loss originates from the rear side of the aluminium back-surface field (Al-BSF) cell, which features blanket metal rather than an H pattern. Moreover, it cannot assess the impact of metal finger breaks or striations, or of local shunts and highly recombinative regions across the wafer, created by process or wafer non-uniformity. The equivalent circuit approach becomes rather unwieldy at evaluating segmented busbars, and is not amenable to the design of metallization patterns with even a slight deviation from an H pattern, let alone more complex patterns such as those in metal-wrap-through (MWT) solar cells.

> "The simple equivalent circuit model has some severe limitations in terms of resolution."

It is obviously advantageous to tackle the innately two-dimensional problem of the solar cell with a wide net that is adaptable to all metallization patterns and spatial distributions of diode characteristics. To this end, SERIS has developed Griddler©, a two-dimensional (2D) finite-element-method (FEM) mesh generator and solver optimized for steady-state solar cell problems [1]. The following discussion will cover some examples of real-world problems that a 2D solver such as Griddler is designed to handle. While some of the more sophisticated features are still being optimized in-house, the core mesh-builder and solver for the 2D voltage distribution in solar cells is now freely available as Griddler 1.0, which will be introduced later in this paper.

Example 1: H-pattern solar cell

Griddler is equally effective as a solution for solar cells of all kinds of metallization geometry, including simple ones like the H pattern. Since Griddler simulates an I–V curve reasonably quickly for an FEM solver (typically within 40s on a laptop PC), it can still be the calculation tool of choice for analysing the H-pattern solar cell. There are two advantages in choosing Griddler over the equivalent circuit model in this case: 1) the simulated I–V curves take on a more accurate shape; and 2) Griddler enables an impact analysis on cell performance to be carried out for a wide range of scenarios. Fig. 1 shows a multicrystalline silicon wafer solar cell and its Griddler-simulated voltage distribution near the 1-sun maximum power point (MPP), in the case of current extraction from the bottom ends of ribbons soldered to the three busbars.

Fig. 2 compares the current density–voltage (J–V) as well as aggregate series resistance–voltage (R_s–V) curves derived using the double-light

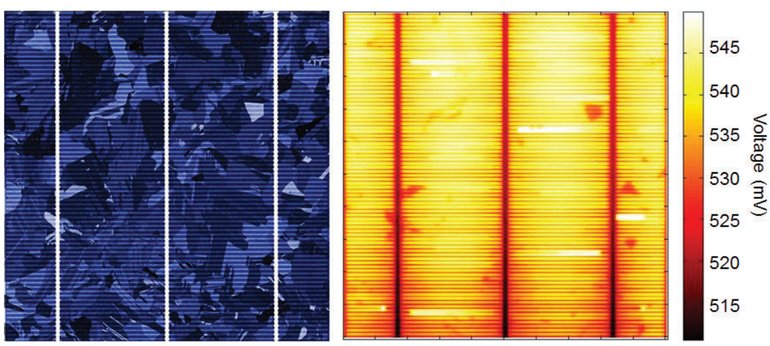

Figure 1. An example of a multicrystalline silicon wafer solar cell and its simulated voltage distribution near the maximum power point (MPP), showing underlying features such as grain quality, metal shading and recombination, edge recombination, and finger breaks. Current is extracted by soldered ribbons at the busbar ends.

method [2], generated by an equivalent circuit model and by Griddler. For the J–V curves, it is only upon close examination that differences can be found in the MPP and V_{oc} points predicted by the two models (discussed in more detail below), and the curves appear more or less similar in shape.

In contrast, the R_s–V characteristics generated from the J–V curves for Griddler and the equivalent circuit model diverge sharply. Griddler is able to capture the nuances one finds in a distributed network of diodes and resistors that are far more representative of a solar cell; as a result, the derived R_s–V is highly voltage dependent, as would be observed in reality. By comparison, the equivalent circuit model generates an R_s–V curve that is flat, thus revealing its over-simplified treatment of the device characteristics. This highlights a fundamental limitation of the equivalent circuit model: while it may suffice for predicting the MPP of an H-pattern solar cell with reasonable accuracy, it does not model the voltage or light intensity dependence well enough to predict R_s–V, Suns–V_{oc}, ideality factor and other in-depth characteristics that shed light on the inner workings of the solar cell.

“Griddler is able to capture the nuances one finds in a distributed network of diodes and resistors that are far more representative of a solar cell.”

A 2D simulator, such as Griddler, is a far more accurate tool for finding the causal link between the solar cell structure and device output characteristics. The resolution at which structural details are fed into a simulator to predict output, and at which measurement data is exhaustively examined to pinpoint power loss mechanisms in the solar cell, must be raised by taking into account the 2D nature of the solar cell device plane. This cannot be more true today, when all sorts of mapping data – such as photoluminescence (PL)/electroluminescence (EL) imaging, light-beam-induced current (LBIC), sheet resistance, and microwave photoconductance decay (μ-PCD) – have become commonplace or even routine.

Next, to illustrate how Griddler facilitates a quick analysis of cell performance for a wide range of real-world scenarios, Table 1 chronicles the evolution of the open-circuit voltage (V_{oc}), short-circuit current density (J_{sc}), fill factor (FF), and efficiency (η), as different recombinative elements and other imperfections are progressively incorporated in the 2D model. The current density J_{sc} is held constant in the simulation in order to focus on V_{oc}, FF and η.

In scenario 1, the J_{01} and J_{02} values across the wafer are taken to be averages and spatially uniform, whereas in scenario 2 they take on local values as would be found in mapping data. The difference is not trivial: in scenario 2, where the low-quality regions are highly concentrated and localized, both the V_{oc} and η improve, because the low-quality regions are now connected to the rest of the solar cell via a metallization network of finite conductance that reduces the diode current sunk into these regions.

Next, in scenario 3, edge recombination at the wafer edges is added to the solar cell model, in the form of a second diode (ideality factor $n = 2$). Obviously, this leads to significant reductions in FF and η, but again the impact of the edge recombination is to some extent dampened by the spatially localized nature of this diode current sink, compared with the case if it were evenly distributed across the wafer. This scenario is also simulated using the equivalent circuit model, which simply uses as inputs the average values of J_{01} and J_{02} across the wafer; R_s is subsequently derived using standard formulae applicable to the H pattern. The equivalent circuit model is observed to fare reasonably well compared with Griddler, but neglects

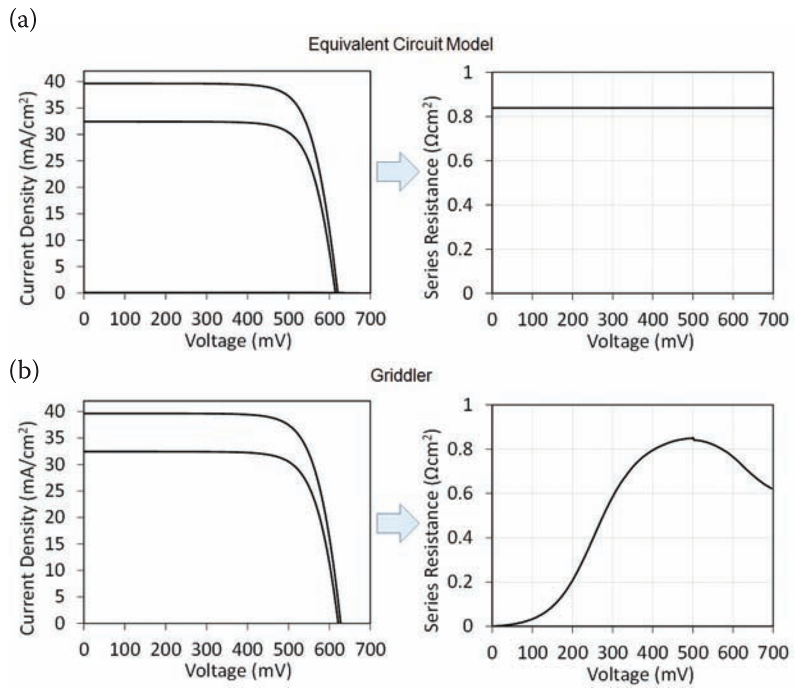

Figure 2. Current density–voltage (J–V) curves and series resistance–voltage (R_s–V) curves simulated by (a) the equivalent circuit model, and (b) Griddler.

	V_{oc} [mV]	J_{sc} [mA/cm^2]	FF [%]	η [%]
Griddler scenario 1	617.5	36.04	76.50	17.03
Griddler scenario 2	625.4	36.04	76.09	17.15
Griddler scenario 3	624.8	36.04	75.82	17.07
Equivalent circuit model for scenario 3	617.6	36.04	76.05	16.93
Griddler scenario 4	624.7	36.04	75.65	17.03

Table 1. Griddler-simulated J–V parameters of the multicrystalline silicon solar cell for the different scenarios discussed. The parameters predicted by the equivalent circuit model for scenario 3 are also shown for comparison.

a few subtle effects, namely 1) the localized nature of the low-quality regions and edge recombination, and 2) the localized metal recombination and metal shading. As already discussed, the first effect impacts V_{oc} and η less than the case of uniform recombination across the wafer; in contrast, the second effect impacts these parameters more than would a uniform distribution, because the local dips in voltage under the metal regions influence the terminal voltage. Overall, for this particular simulation, the equivalent circuit model underestimates V_{oc} and η, and overestimates *FF*, both by significant degrees.

Not only is Griddler more accurate in finding the MPP, V_{oc} and the overall shape of the *J–V* curve, but it can also simulate situations that are completely beyond the reach of the equivalent circuit model. For example, scenario 4 simulates the same solar cell with striations in the metal finger height throughout the wafer plane, which introduces a number of finger breaks, as can be seen in the voltage map of Fig. 2. These metallization imperfections are fairly commonplace in practice, and Table 1 shows that they have a subtle impact on device performance. With 2D simulation, it becomes quick and easy to explore a myriad of situations that occur in solar cells – including partial shading, local shunts and wafer breaks – thus opening up a world of possibilities in the assessment of device performance to aid cell design and optimization.

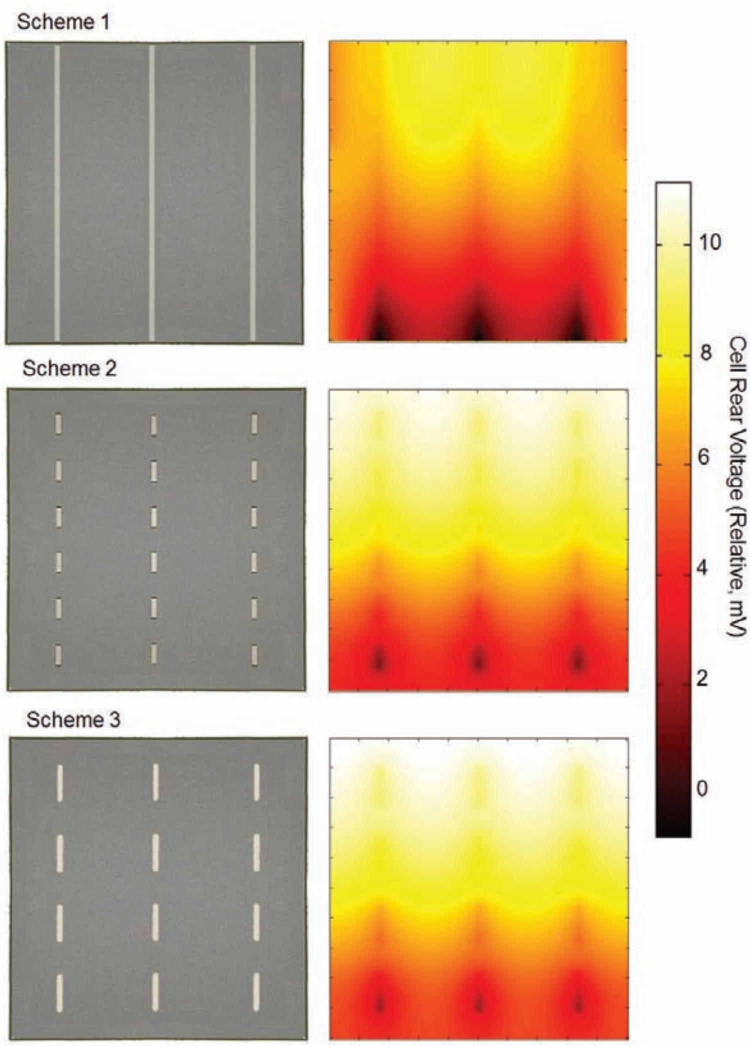

Figure 3. Simulated rear-cell voltage distribution (relative), for three different rear solder pad layout schemes.

Example 2: Solar cell rear metallization

While the solar cell H pattern is relatively carefully optimized and analysed in research and industry, the rear-side metallization is often more of an afterthought. This is partly because there is no routine way of calculating the influence of series resistance in the rear Al metal plane of a standard Al-BSF solar cell, since the current flow pattern is highly two-dimensional rather than strictly parallel to the wafer sides as in the case of the H pattern. The problem is further compounded by a fair degree of arbitrariness in the rear-contacting scheme during cell measurement: many lab *I–V* testers place the rear of the solar cell in intimate contact with a large-area metal chuck, thus rendering the cell-rear ohmic loss practically zero.

The lack of measurement and calculation standards obscures the understanding of the contribution of rear metallization to cell series-resistance losses. Indeed, the H-pattern solar cell in the previous section is itself a story half told: the Griddler simulations thus far have assumed an infinitely conductive rear metal, corresponding to the case of measurement in the lab. In order to gain a comprehensive picture of how the cell performs after interconnection in the module, Griddler is used to assess the impact of cell rear ohmic losses on performance.

Fig. 3 shows a few Al-BSF solar cell rear schemes with different solder pad layouts and the corresponding relative voltage distributions across the cell rear near the MPP. For quickness, a non-rigorous approach is adopted for predicting the overall interconnected solar cell *J–V* parameters. First, Griddler simulations are redone for the front H pattern, still assuming an infinitely conductive rear, but taking into account the higher recombination regions introduced by the rear solder pads. Next, Griddler simulations are carried out for the rear-metallization schemes, assuming an infinitely conductive front, to determine the *FF* drop relative to the case of negligible series resistance. Finally, the relative *FF* drop in each case is subtracted from the *FF* of the front H-pattern simulation. Admittedly, this method is not as ideal as a full bifacial simulation, which is still in the developmental stages, but nevertheless it yields sufficiently accurate insight into the impact of the rear metallization.

Table 2 shows the estimated *J–V* parameters of the solar cell after interconnection with front and rear ribbons. The message is clear that the rear metallization makes a significant difference to the performance of the final device. Relative to the case of the simulation of the front H pattern only while assuming an infinitely conductive rear (which produced the parameters of scenario 4 in Table 1), the additional series resistance on the cell rear induced a further 0.6–1.0% (absolute) drop in *FF* and up to 0.2% (absolute) drop in efficiency. Evidently, V_{oc} is also slightly reduced when the high-recombination regions introduced by the rear solder pads

	V_{oc} [mV]	J_{sc} [mA/cm^2]	FF [%]	η [%]
Rear scheme 1	623.9	36.04	75.03	16.87
Rear scheme 2	624.4	36.04	74.76	16.82
Rear scheme 3	624.3	36.04	74.72	16.81

Table 2. Estimates of the final solar cell *J–V* parameters, with ribbons connected to both the front and rear sides of the cell, and current extracted from the ends of the cell. The rear solder pad schemes correspond to the ones illustrated in Fig. 3.

are accounted for, but in this case the impact is negligible. This may not be the case, however, for solar cells with higher V_{oc}s, which are more sensitive to additional recombination sources.

Example 3: The fine-line screen-printed grid

Screen printing is the industry standard for solar cell metallization. As manufacturers push for finer and finer silver fingers using this technology, it also becomes increasingly challenging to print uniformly conductive silver fingers. At a certain point, the non-uniformity of fingers – in the form of striations, bottlenecks and finger breaks – begins to erode cell performance in a measurable way. Fig. 4 shows 3D microscopy data of different silver fingers, printed using three different screens that produce fingers with respective nominal widths of 80, 70 and 60µm. The same figure also shows 2D simulations of the ohmic losses in these fingers. Clearly, the narrower the nominal width, the greater the rates of striations and bottlenecks.

With the use of the microscopy data, combined with line resistance and busbar-to-busbar (B2B) resistance measurements, it is possible to build up adequate statistics about the distribution of finger segment conductance. This statistical model can then be fed into Griddler to simulate a realistic fine-line-printed solar cell with an uneven distribution of silver. As an example, four sets of statistics – starting with zero variations in line conductance in case A, then with increasing variations as one progresses from cases B to D – are input into Griddler for the simulation of a monocrystalline silicon wafer solar cell. In all cases the fingers have a width of 70µm and a nominal metal sheet resistance of approximately 3.3mΩ/sq. Fig. 5 maps the cell voltages near MPP, and Table 3 shows the corresponding *J–V* parameters. It is apparent that, even between cases A and B (which is in a way comparing perfect metallization to a level of imperfection that resembles what is found in industrial cells), there can be significant differences in *FF* and efficiency. Obviously, at the

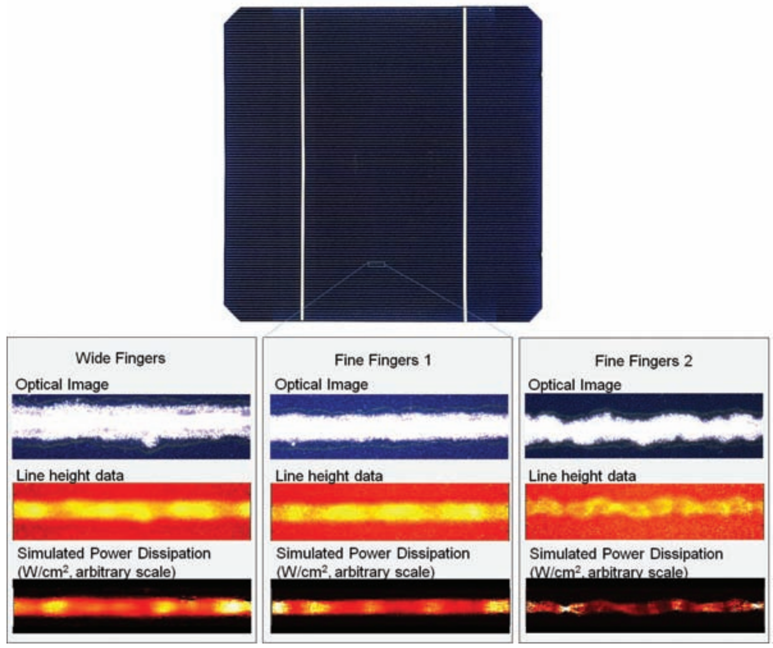

Figure 4. 3D microscope data of different screen-printed metal fingers, and for each case the simulated power dissipation during current flow.

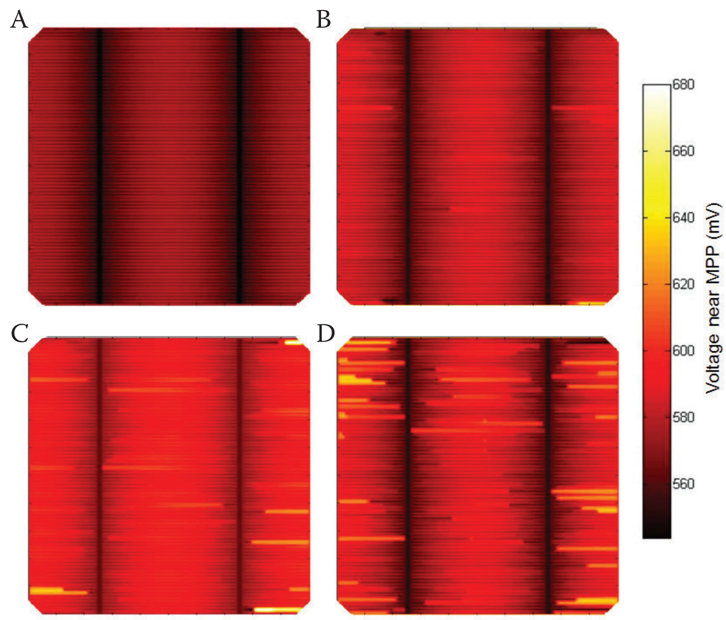

Figure 5. Simulation of the voltage distribution near MPP for a monocrystalline silicon wafer solar cell, with increasing severity of conductance variations in the metal finger segments. Case A represents the perfect cell with no variations in the metal conductance.

	V_{oc} [mV]	J_{sc} [mA/cm^2]	*FF* [%]	η [%]
Case A	640.7	37.92	80.40	19.53
Case B	640.5	37.92	79.89	19.40
Case C	640.3	37.92	79.53	19.31
Case D	640.2	37.92	78.27	19.00

Table 3. Simulated *J–V* parameters for the four cases of metal finger striations severity, corresponding to Fig. 5.

rates of defects found in cases C and D, the erosion of efficiency reaches an unacceptable level. In practice, to alleviate the impact of uneven metal line conductance, industry takes several measures, such as the joining of finger ends near the wafer edges to produce redundant current paths, and adopting three-busbar and even four-busbar designs. More advanced interconnection schemes, such as the use of numerous parallel wires in place of ribbons, are yet more tolerant of finger striations and breaks. All of these scenarios are quite straightforward to simulate using Griddler.

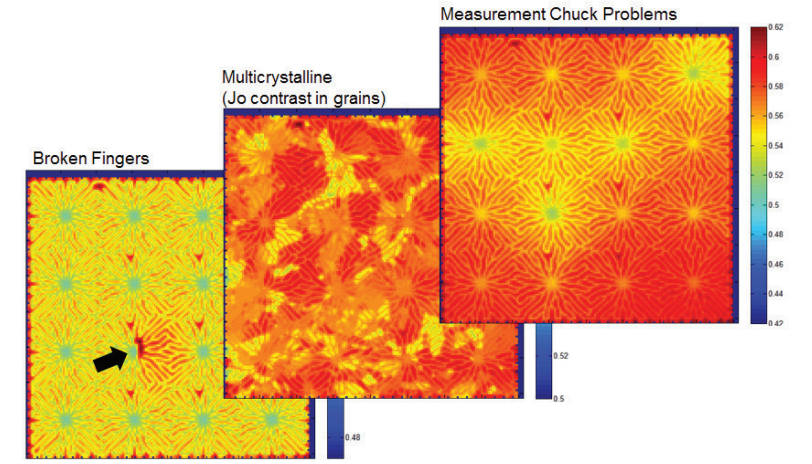

Figure 6. Simulated voltage distributions of a solar cell with the SunWeb metal-wrap-through (MWT) metallization pattern, for different scenarios.

Example 4: Alternative metallization schemes

As its name suggests, Griddler is designed to calculate metallization grids of all kinds. Being a FEM mesh builder and solver, it is undaunted by complex metallization patterns, making it the ideal tool for the study of cell types or metal structures that inherently feature irregular grids. As an illustration, Fig. 6 shows Griddler-simulated voltage distributions on the elegant Solland SunWeb metal-wrap-through (MWT) solar cell [3,4], for three scenarios: 1) the cases of broken fingers; 2) a multicrystalline wafer with different recombination regions under the metal pattern; and 3) the interesting situation where the voltages at the current extraction points are unequal. The last case is actually quite commonly encountered during the measurements of MWT and other rear-contact solar cells, because the test jigs for these cells must rely on suction force to hold the cell down against the probe pins, and the relatively weak pin spring-force can lead to significant and uneven contact resistance. The resultant uneven voltages at the current extraction points may lead to non-repeatable measured fill factors that tend to be underestimations. By simulating this effect, Griddler can be a useful tool for error analysis in the test lab.

Griddler is equally adept at calculating the conductance of complex metal networks, such as the one shown in Fig. 7. This is a nanoparticle

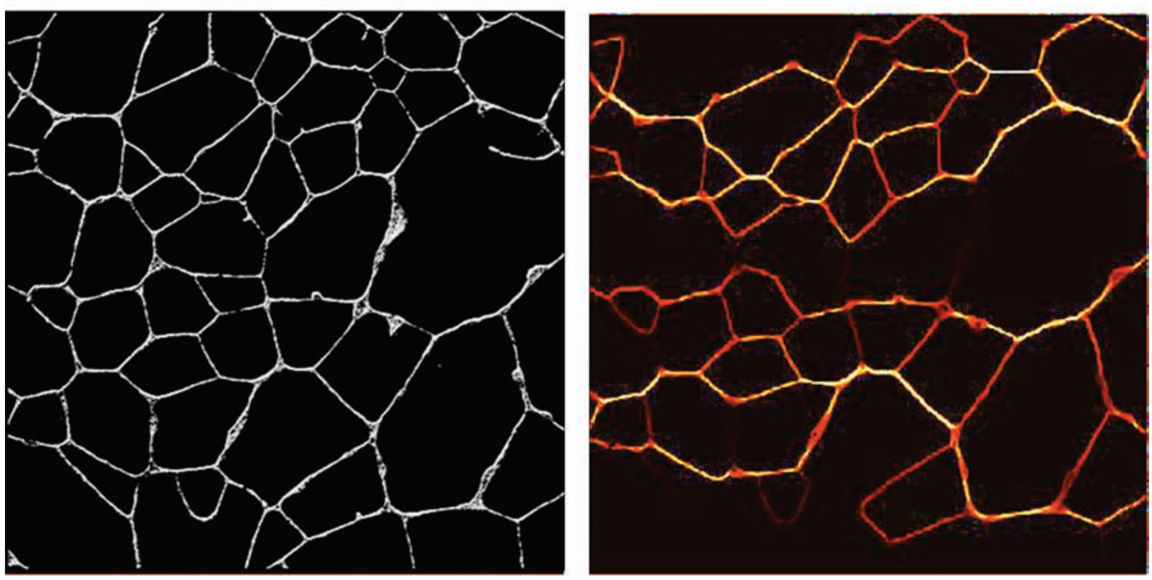

Figure 7. Metallization that consists of a random mesh-like network: (a) SEM image; (b) simulated current density, when a voltage difference is set up between the left and right edges of the image.

conductive coating that self-assembles into a random mesh-like network when coated onto a substrate, and is currently in the research phase for solar cell applications. Fig. 7(a) shows a scanning electron microscope (SEM) image of the network, and Fig. 7(b) shows the simulated current density through the network when a voltage difference is set up between points on the left and right edges of the picture. The simulation of the network conductance versus the network mesh properties enables better solar cell metallization schemes to be designed that can incorporate the nanoparticle conductive coating in place of the traditional transparent conductive oxides (TCOs).

Griddler 1.0: Two-dimensional power for everyone

The software for implementing the concept of a sophisticated simulation does not necessarily have to be difficult to use. The visualization of the solar cell as a 2D plane is a very intuitive idea for anyone to grasp, and the high degree of automation provided by FEM meshing should make it simpler and more flexible for the user to define the geometry of the solar cell problem compared with, say, keying in parameters in a spreadsheet to perform an equivalent circuit model simulation.

> "Griddler 1.0 is designed to be used by an untrained user having just a basic understanding of solar cells."

In this spirit, Griddler 1.0 was designed as compact freeware that runs on 32- or 64-bit Microsoft Windows machines. Although it does not include some of the more sophisticated features such as the incorporation of mapping data, it incorporates the essential features of mesh building and determination of the 2D voltage distribution across a solar cell with arbitrary metallization patterns. Griddler 1.0 is designed to be used, without any instructions, by an untrained user having just a basic understanding of solar cells, and is built to be very tolerant of faults. The program includes the following key features:

1. Arbitrary grid geometries can be imported from common file types, such as images and CAD files.

2. The user can alternatively design an H-pattern front grid on wafers of any size and format.

3. To study the robustness of the metallization design, finger breaks can be created by clicking on the metal pattern.

4. Visualization of the voltage distribution on the solar cell is possible.

5. The *J–V* curve can be quickly simulated by inputting some common metallization-related parameters, such as metal sheet resistance, metal contact resistance and semiconductor sheet resistance.

6. The ohmic losses of the solar cell at the MPP are broken down into separate components.

Fig. 8(a) shows the Griddler 1.0 interface after loading a particular solar cell design that features wire-connection (an example file that comes with the installation). Fig. 8(b) shows the voltage map near the MPP as current is extracted from the ends of the wires at the bottom edge of the cell. Fig. 8(c) shows the simulated *J–V* curve and the breakdown of ohmic losses as percentages of the cell pseudo-maximum power. Running on a 32-bit 2.67GHz laptop, Griddler takes 10s to generate the mesh

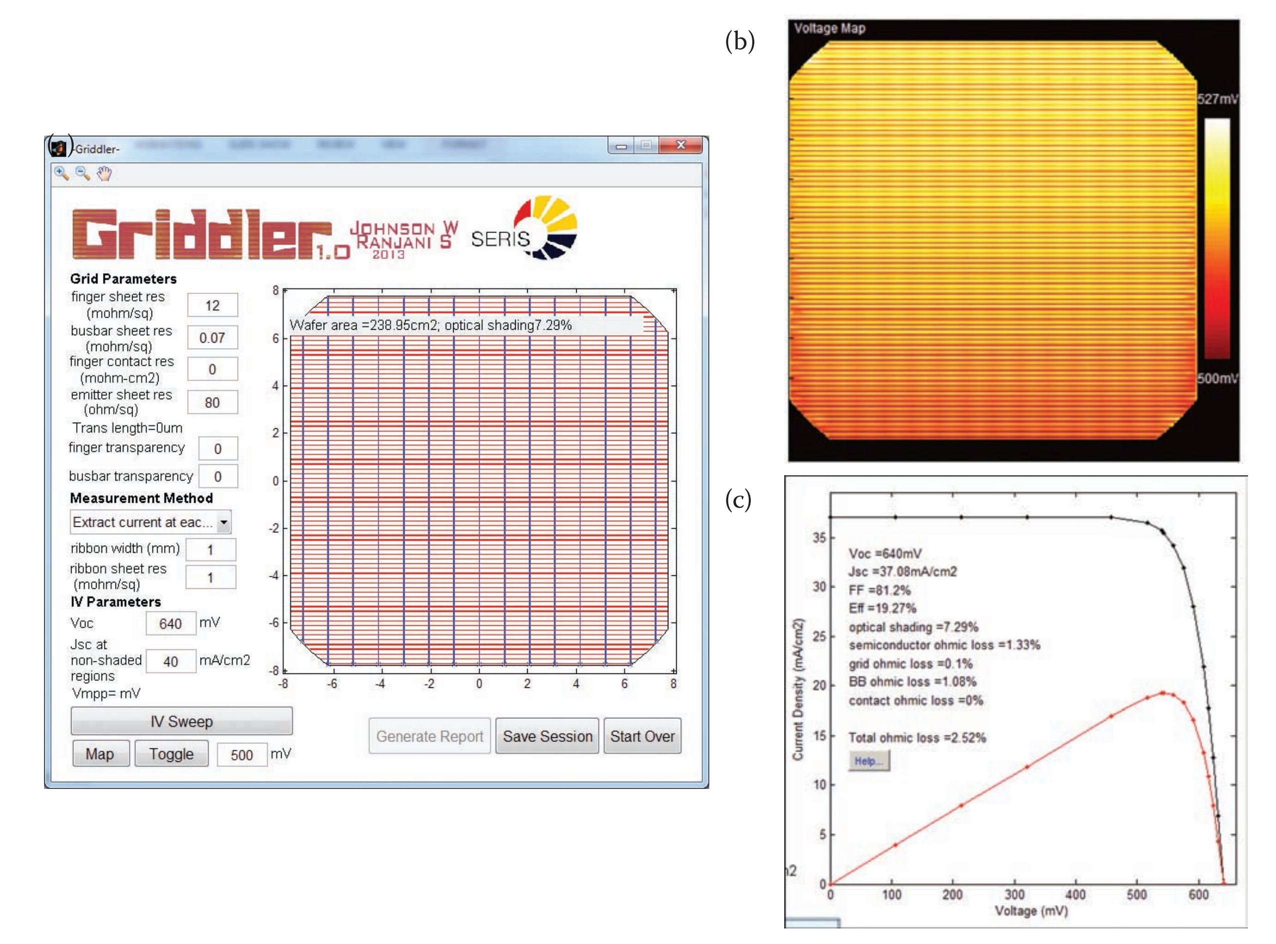

Figure 8. Griddler 1.0 interface: (a) after loading a solar cell example; (b) simulation of the voltage distribution near MPP; (c) simulation of the *J–V* curve and ohmic losses.

for this solar cell design, and completes the *J–V* curve in 30s.

Be it for a simple H pattern or the most complex of metallization problems, it is hoped that Griddler 1.0 (available as a free download [5]) will become the handy calculator that universally comes to mind.

Acknowledgements

SERIS, a research institute at the National University of Singapore (NUS), is sponsored by NUS and Singapore's National Research Foundation (NRF) through the Singapore Economic Development Board (EDB).

References

[1] Wong, J. 2013, "Griddler: Intelligent computer aided design of complex solar cell metallization patterns", *Proc. 39th IEEE PVSC*, Tampa, Florida, USA, pp. 0933–0938.

[2] Fong, K.C., McIntosh, K.R. & Blakers, A.W. 2013, "Accurate series resistance measurement of solar cells", *Prog. Photovolt.: Res. Appl.*, pp. 490–499.

[3] Solland Solar Cells [http://www.sollandsolar.com/].

[4] Weeber, A.W. et al. 2006, "How to achieve 17% cell efficiencies on large back-contacted mc-Si solar cells", *Proc. 4th IEEE WCPEC*, Waikoloa, Hawaii, USA, pp. 1048–1051.

[5] SERIS 2014, Griddler FEM simulator freeware [http://www.seris.sg/OurServices/Griddler.html].

About the Authors

Johnson Wong is the head of PV characterization at SERIS. After receiving his Ph.D. in photovoltaic engineering at UNSW in the area of thin-film silicon on glass solar cells, he joined SERIS as a scientist, engaging in various research topics such as screen-printed and evaporated-metal all-back-contact solar cells, and a-Si:H/uc-Si:H c-Si heterojunction solar cells. His current work includes the development of photoluminescence and electroluminescence detection and analysis methods, the application of solar cell reciprocity relations, and the study of the impacts of solar cell lateral non-uniformity and distributed resistances on device performance. Johnson also heads the effort to set up an ISO17025 test and calibration lab at SERIS.

Ranjani Sridharan began her career in the field of metallization at imec Leuven, where she focused on screen printing and characterization of solar cells. She has been working at SERIS since 2011 as a research engineer, and has extensive experience in lithography, screen printing and other advanced metallization techniques related to the fabrication of silicon-wafer-based solar cells. As well as her involvement in the Griddler project, she currently works on the development of hybrid solar cells, which combine deposited heterojunctions and silicon-doped layers.

Enquiries

Johnson Wong
Solar Energy Research Institute of Singapore (SERIS)National University of Singapore (NUS)7 Engineering Drive 1Building E3A, #06-01Singapore 117574

Tel: +65 9625 1242
Email: Johnson.wong@nus.edu.sg

Simple and reliable processes for creating fully plated nickel–copper contacts

Jonas Bartsch, **Andreas Brand**, **Dirk Eberlein**, **Andrew Mondon**, **Carola Völker**, **Marco Tranitz**, **Martin Graf**, **Jan Nekarda**, **Ulrich Eitner**, **Daniel Philipp** & **Markus Glatthaar**, Fraunhofer Institute for Solar Energy Systems ISE, Freiburg, Germany

ABSTRACT

This paper presents the first 60-cell module results from a very simple process scheme for creating fully plated nickel–copper contacts on crystalline silicon solar cells. Standard Cz back-surface field (BSF) cells are processed in a completely analogous way to the standard process sequence up to and including rear-side screen printing. After a firing step for BSF formation, the front-grid positions are defined by picosecond pulse laser ablation and plated with nickel, copper and silver; this is followed by a short thermal anneal. Cell classification produces a very neat efficiency distribution of 19.6±0.1%. Solder and peel testing shows this approach to be competitive with standard screen-printed contacts in terms of adhesion. A batch of 60-cell modules were fabricated from the cells in a standard automated tabber–stringer system and subjected to thermal cycling and damp heat testing as part of the IEC 61215 reliability test sequence. The modules passed the test sequence without showing any signs of electrical degradation caused by, for example, copper diffusion.

Introduction

The silver paste conductor grid on a traditional silicon PV cell contributes approximately 18% to the cell's cost. For this reason, industry roadmaps call for the use of an alternative to silver paste by 2018 in order to render PV the most economical choice for electricity production [1].

Direct nickel–silicon contacts offer many advantages and prospects for the metallization of current and future solar cell concepts. The nickel–silicon contact resistance is lower than that of printed silver contacts; moreover, nickel allows the use of copper as a conducting layer, since it effectively hinders the diffusion of copper into the silicon bulk. The cost of raw materials is considerably lower for plated metallization (even at the currently low price of silver), and process costs can be expected to decrease even more as this technology enters the market. An example of the resulting contact system is shown in Fig. 1.

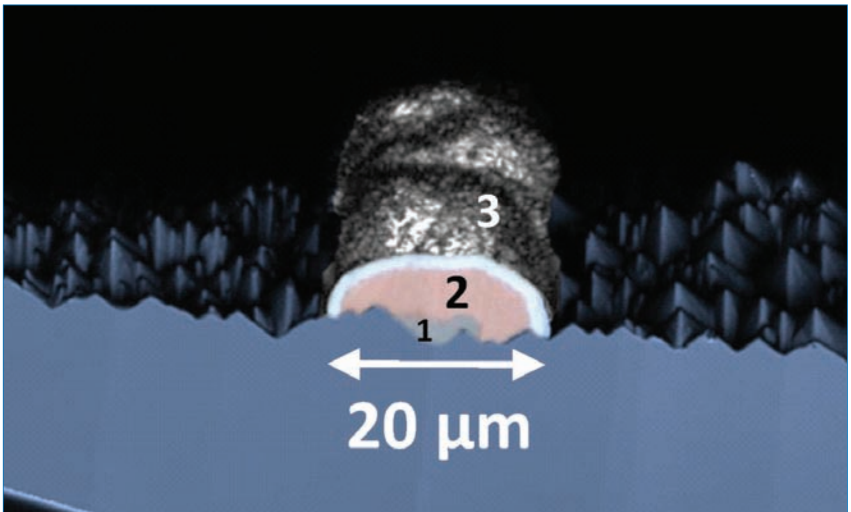

Figure 1. Microscopic image of the cross section of a directly plated nickel–copper contact; in this case the seed layer is ~5µm wide, resulting in a total contact width of 20µm. Nickel (1) is directly deposited onto silicon in regions removed by laser scribing. Copper (2) is plated on top of the nickel, producing a dense layer with very high conductivity. Silver (3) (or tin) is used to protect the contact against corrosion and to promote solderability. Adjacent to the nickel diffusion barrier layer, direct copper–silicon contact is prevented by the SiN_x ARC.

"Direct nickel–silicon contacts offer many advantages and prospects for the metallization of current and future solar cell concepts."

The plating process is also very attractive for future cell designs. In cell concepts where the rear side is no longer the limiting factor (e.g. PERC solar cells), it has been shown that plated metallization approaches allow considerable efficiency advantages [2,3]. This is supported by new innovations in laser structuring techniques [4] that may allow feature sizes of as little as 5µm in the future, resulting in a geometrical finger width of ~15–20µm and an optical finger width less than 10µm [5] (cf. 40µm in Fig. 2). PERC cell concepts will approach 22% efficiency, or even surpass this mark, using a plated metallization. The first promising steps in this direction have already been made using standard rear passivation schemes with Al_2O_3 and SiN_x [2,3], or using p-type PassDop [6]. With the use of plated NiCu metallization (H-pattern cells) on 156mm × 156mm PERC cells provided by Roth & Rau, the latest results at Fraunhofer ISE have demonstrated up to 21.1% efficiency. In addition to low-cost front copper contacts, these cells featured a low-cost rear Al foil metallization [7].

A further development step in PV with the aim of achieving higher efficiencies may well be the transition to n-type base material. Here the task of contacting boron emitters is accomplished very well with the use of nickel [8], whereas silver–aluminium pastes still suffer from V_{oc} losses due to Al-induced spiking [9,10].

With n-type material, there is some industrial focus on very advanced cell concepts that are easily scalable in principle, but have very high requirements in terms of metallization (e.g. n-type PassDop [11] or TopCon [12]). The n-type PassDop cell concept has already demonstrated cell efficiencies of above 23% [13], while the TopCon design recently demonstrated 24.4% efficiency [14], with the potential of reaching over 25%. Even though the passivation layers that yield the highest efficiency can be deposited using simple 1D processes, their temperature stability is critical, which prohibits the use of standard screen printing as the metallization technique.

Such cell concepts profit immensely from a plated metallization that is technologically close to an evaporated metallization approach, as used in CMOS technology and for the highest-efficiency achieving laboratory solar cells. However, in contrast to the clean-room model process, costly structuring and vacuum metal deposition processes can be replaced by simple and cheap laser and plating processes, making the approach suitable for industrial solar cell manufacturing.

Historically, nickel plating for solar cell metallization has been employed by several groups and industrial players, the most prominent being BP Solar (Saturn cell) [15] and SunTech (PLUTO cell) [16]. While the former uses a process sequence that, although expensive, works well, the latter uses cheap and simple techniques. However, despite excellent cell results, large-scale implementation has not yet been realized. One possible explanation for this is the low contact adhesion that has been observed for plated contacts in the past.

Accordingly, both process complexity and metal–silicon contact adhesion need to be considered in current developments to enable chances for industrial success. The work reported in this paper demonstrates that a simple process route can fulfil the requirements in terms of both adhesion and electrical cell parameters.

Experimental

In this study more than 600 precursor cells without front-side metallization provided by an industrial partner were contacted with a plated front-side metallization. It must be stressed that the cells were entirely pre-processed on an automated production line that was fully optimized with regard to the requirements of a screen-printed front-side metallization. This shows that the process is more or less directly implementable in accordance with a given production standard. The state of the precursors before plating was: diffused $POCl_3$ emitter, random pyramid texture, SiN_x ARC and printed and fired rear-side metallization (Al BSF and silver pads). The 65Ω/sq. emitter selected for this demonstration

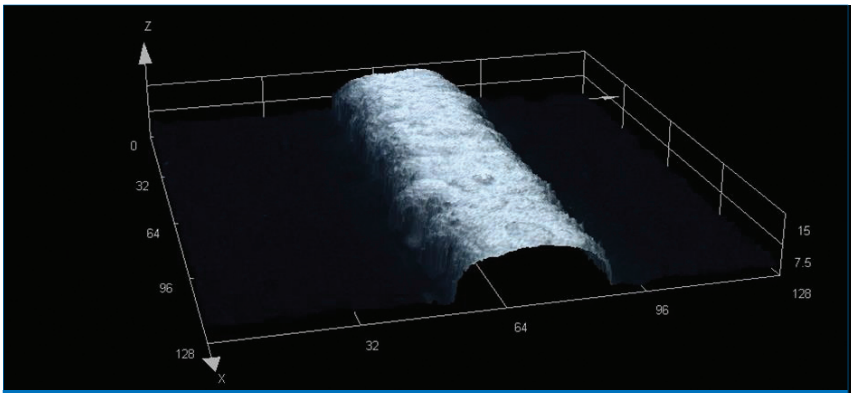

Figure 2. 3D microscope image of the contact fingers achieved for this batch using a non-optimized laser process.

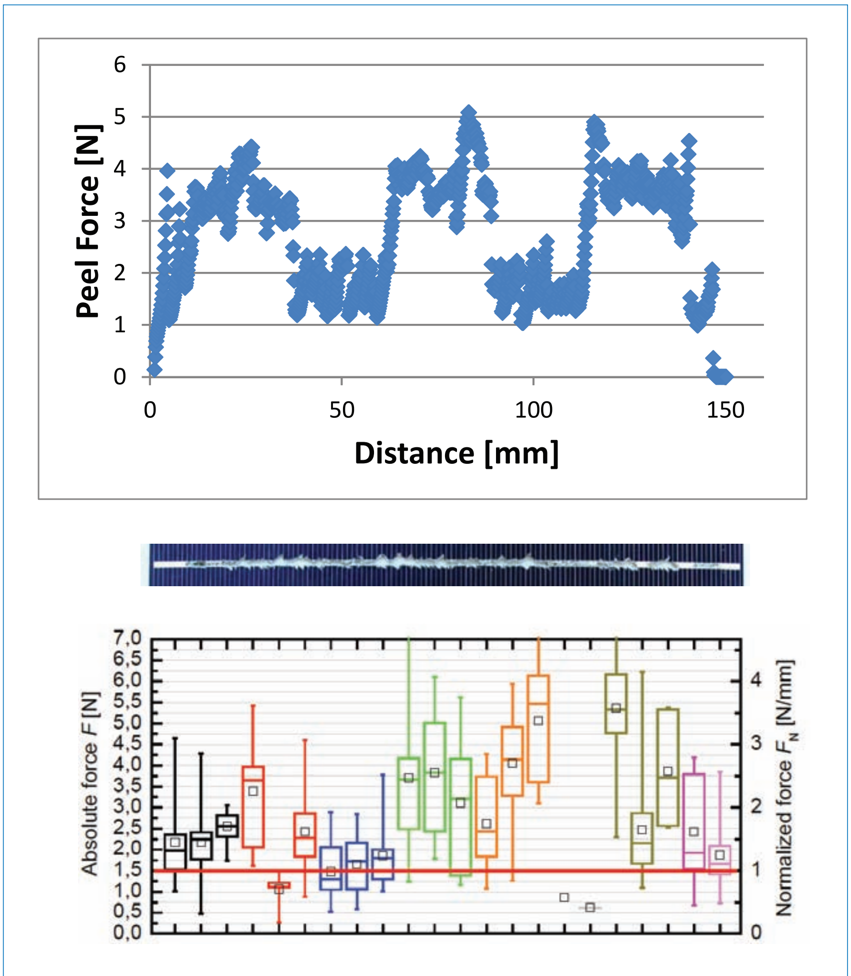

Figure 3. Top: typical peel force diagram obtained for plated cells. Middle: the corresponding failure mode is cell breakage at high forces. Bottom: statistical evaluation of peel forces for different soldering processes (represented by different colours), with simultaneous soldering of the front and rear sides. Highest peak values of peel forces are greater than 7N. Note: low adhesion values relate to the adhesion of the ribbon between soldered attachment points.

A Better Conductor,
A Lower Cost

The Copper Solution.

Copper Grid for Silicon Cells

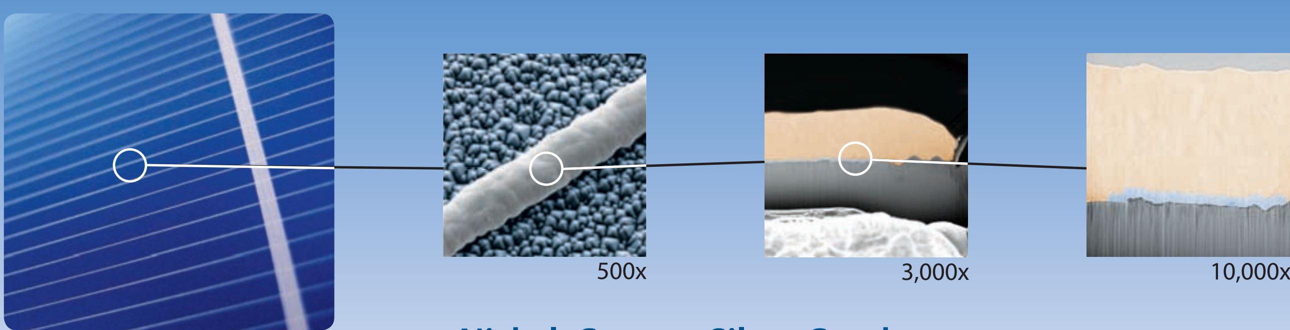

Nickel, Copper, Silver Conductor

- Electroplated or LIP
- 30 µm finger width
- 1.7 µΩ·cm resistivity
- Efficiency gain 0.3% = $0.03/cell
- Conductor savings $0.07/cell
- ROI = 12 months
- Proven IEC-61215 reliability
- ***Eliminate Silver Paste!***

MacDermid
Photovoltaics Solutions

245 Freight Street, Waterbury, CT 06702 USA • Telephone +1 203.575.5700 • **electronics.macdermid.com**

represents a typical diffusion for large-volume production during late 2013, when the cells were procured.

The front ARC was then structured using a picosecond (ps) laser installed in a high-throughput industrial tool (Innolas), and the plating of nickel and copper and a very thin silver capping was realized in an industrially applicable inline plating tool system (RENA) using commercially available plating solutions (MacDermid). The cells were subjected to a short thermal anneal step using an industrially suitable inline furnace (BTU).

The resulting contact fingers have a semi-roundish appearance and are ~40µm wide (Fig. 2); this result was obtained without intensive optimization. The silver finish has a very bright appearance that reflects incoming light onto a large portion of the wafer surface. Through optimization of the laser process, the effective shading of the very narrow fingers can be reduced to virtually zero in the future (see the outlook discussion later).

In order to adapt the inspection system of the automated tabber–stringer system (Somont) to the very bright appearance of the plated capping layer, it was necessary to make slight adjustments to optimize the stringing process. Standard contact soldering was employed, where almost no alterations were necessary compared with a standard process.

> "While adhesion has been an issue for plated contacts in the past, the selection of a suitable laser process solves this problem."

Solder and peel test results show that adhesion is comparable to that with standard screen-printed contacts (Fig. 3). Peel testing was carried out at a 90-degree angle to eliminate any doubt as to the actual adhesive fracture energies [17] in comparison with those for screen-printed contacts. While adhesion has been an issue for plated contacts in the past, the selection of a suitable laser process solves this problem. On removing the ARC, the laser process creates a rough surface, which is likely to improve mechanical adhesion (Fig. 4). Thermal annealing improves adhesion and contact resistance so that even a very demanding emitter with reduced surface dopant concentration can be contacted [18]. Further optimizations of the laser

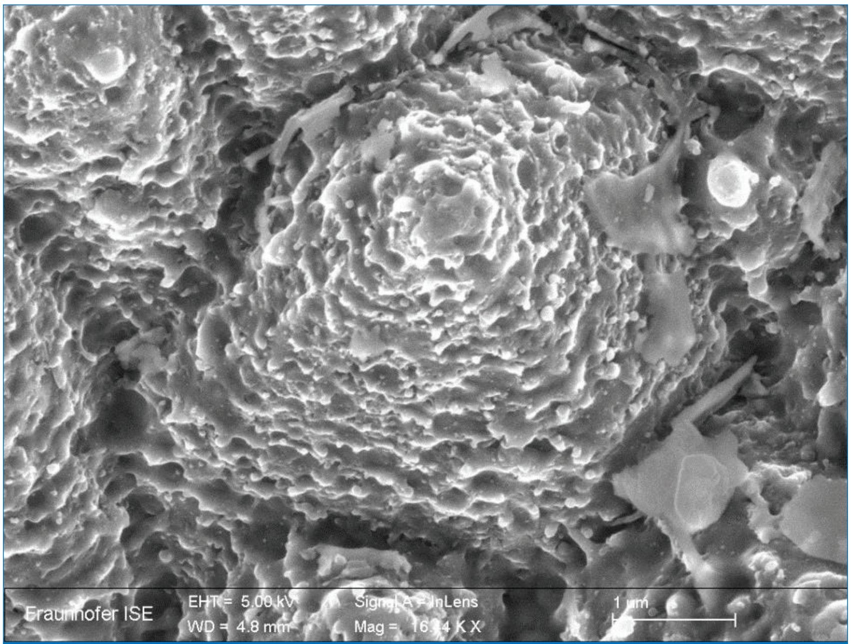

Figure 4. SEM image of the solar cell surface area with the ARC removed by ps laser ablation. The random pyramid texture shows considerable surface roughness. The space charge region remains undamaged because of the very small optical laser penetration depth (~10nm).

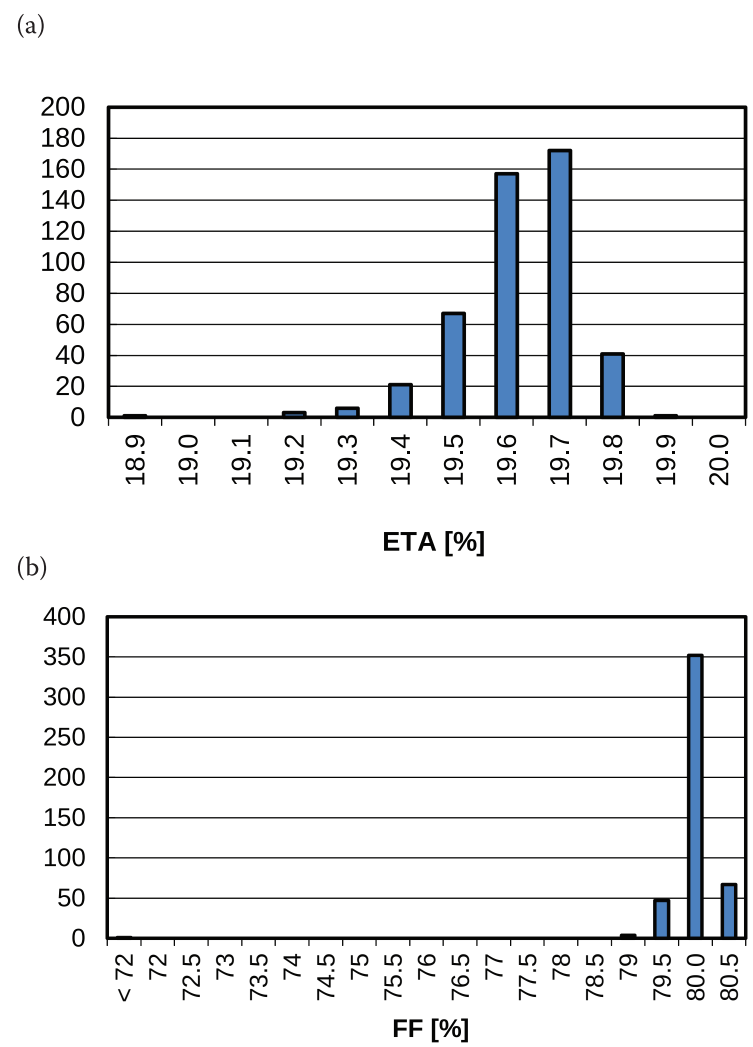

Figure 5. Cell efficiency (a) and fill factor (b) distributions achieved for several hundred Al-BSF cells featuring ps laser ablation, a nickel, copper and silver plating, and a subsequent anneal.

processing might even allow the thermal step to be eliminated altogether, thereby offering a greater savings potential.

I–V measurements of the finished cells yielded a median efficiency of 19.6±0.1%, with a very neat efficiency distribution, as shown in Fig. 5(a). With respect to the metallization quality, the fill factor (*FF*) is a key parameter. Here, an even better distribution was obtained, resulting in a high average value of 80.3% and a standard deviation of 0.2% (Fig. 5(b)). The narrow distribution in electrical performance is especially noteworthy. Whereas printed cells have matured in production over many years, plated cells have yet to reach their full optimization potential in high-volume production.

From these cells, four 60-cell modules were constructed (Fig. 6) using standard module materials. After an initial characterization, the modules were subjected to climate chamber testing: thermal cycling (TC) tests (–40°C to +80°C, 200 cycles) and damp heat (DH) tests (85°C, 85% relative humidity, 1000h) were chosen in accordance with the IEC 61215 reliability testing procedure. These tests affect the metallization and are suitable for demonstrating the difficulties that plated metallization could engender at the module level.

> "Reliability testing showed no critical degradation of the modules after 1000h DH and 200-cycle TC tests."

Reliability testing showed no critical degradation of the modules after 1000h DH and 200-cycle TC (TC 200) tests. Fig. 7 summarizes the development of the electrical parameters of two 60-cell modules for each test procedure, relative to the initial values. All modules remained well above the 95% efficiency criterion. The TC 200 test led to a slight (though not unusual) decrease in *FF*, which can most probably be fixed by optimization of the soldering process. It should be noted that, even though a few cells featured cracks (see discussion below), copper does not seem to affect module performance and reliability.

As a result of manual handling in between the automated processing steps, cracks were observed in a few cells through an electroluminescence (EL) characterization of the modules (Fig. 8). Cracking was especially evident with thermal cycling, and most likely due to crack propagation as a consequence of repeated thermal compression and expansion.

If the cracks on cells with printed and plated metallizations are compared, it becomes apparent that, despite cell cracking, separated parts of the plated cells still contribute to power generation. It has been previously reported [19,20] that a plated metallization is less sensitive to cell cracks, as the ductile plated material can compensate for slight height differences and thus all parts of the cell and module remain electrically interconnected.

Conclusion and outlook

In the experiment discussed in this paper, industrial-type solar cells were produced with a plated front-side metallization using industrial equipment and on a relatively large scale (~700 solar cells). Despite the non-optimized cell architecture, excellent cell efficiency and module stability were achieved, while front silver consumption was drastically reduced, from 120mg to 8mg per cell, resulting in as much as a $0.08/

Figure 6. Photograph of a 60-cell module incorporating nickel/copper-plated solar cells.

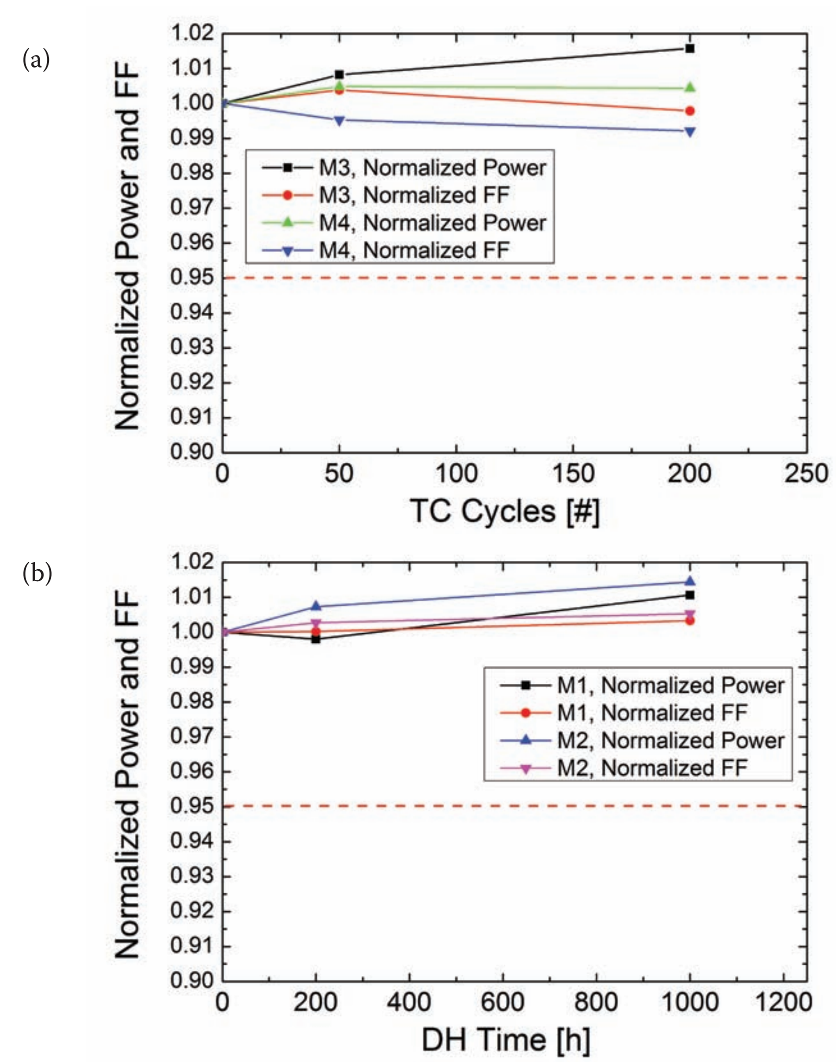

Figure 7. Results of reliability testing: (a) TC (–40°C to +80°C, 200 cycles); (b) damp heat (85°C, 85% relative humidity, 1000h). Relative power and fill factor degradation remain well above the 95% criterion (red dashed line) for all modules tested.

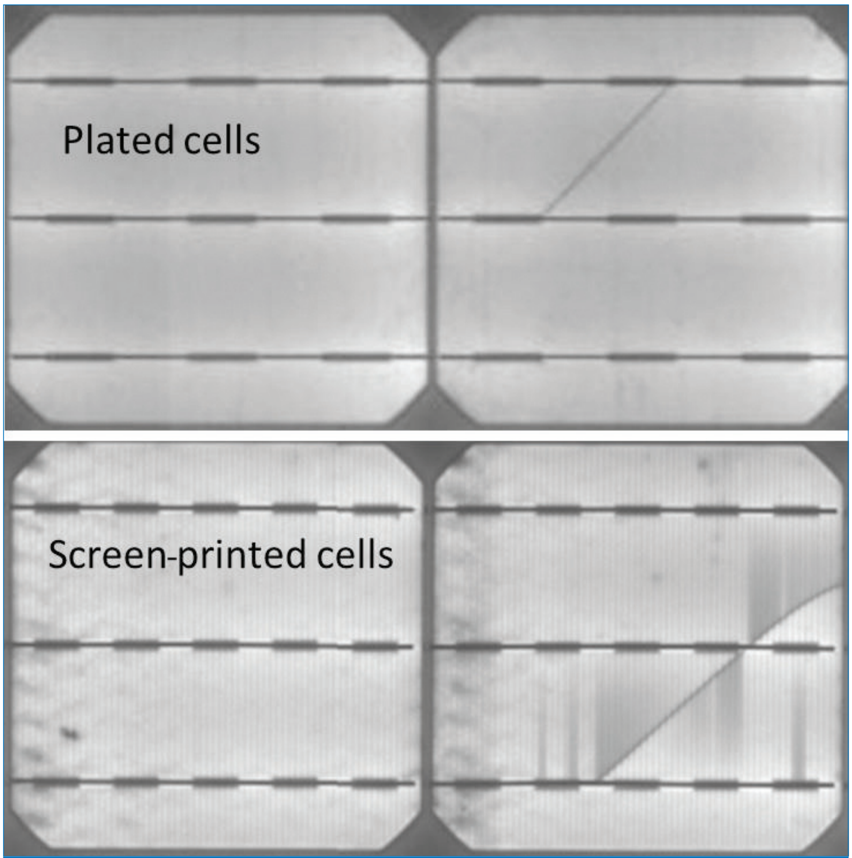

Figure 8. EL images of two cells with cracks from 60-cell modules after 200 thermal cycles. Top: plated cell metallization (this study). Bottom: typical image for screen-printed cell metallization (earlier study). The plated cells show no degradation effects (e.g. caused by copper migration or by finger interruptions). The crack in the screen-printed metallization results in breakage of the brittle finger metal and induces power loss.

cell reduction in cost. Excellent contact adhesion was obtained by employing ps laser ablation, which yielded ~20μm-wide contact finger openings with no optimization of the process.

> "Excellent cell efficiency and module stability were achieved, while front silver consumption was drastically reduced."

In a subsequent cell run, finger widths down to 20μm were achieved, reducing finger shading to virtually zero. The construction of more modules is planned in order to improve the performance of modules with plated metallization even further by applying the knowledge gained from the present experiment. Additionally, experimental work for plated contacts on PERC-type solar cells is ongoing, and work on advanced PassDop and TopCon approaches is progressing. The benefit of a plated metallization on such high-efficiency solar cells will be even greater, having already been demonstrated in the latest PERC cell run, which yielded 21.1% efficiency.

Because of the savings in material consumption, the process is cost efficient, especially if it is kept lean. Plated conductors can ideally be complemented by physical vapour deposition (PVD) or foil metallization (using laser-fired contacts – LFC) in high-efficiency concepts. This will make large firing furnaces unnecessary and opens the path to low-temperature backend processing, which is required for advanced passivation layers. While optimization of these more advanced constructions continues, the simple process described herein is ready for production as presented, with only one process alteration – the replacement of the screen-printed conductor by plated Ni, Cu and Ag. For the first time, reliability data in large-module format demonstrates state-of-the-art adhesion and electrical performance with the lowest cost for the bill of materials.

Acknowledgements

The authors would like to thank the contributors from Fraunhofer ISE PVTEC, EtaLab and ModuleTech for their constant support, H. Ambrosi for taking care of the reliability measurements, and Fraunhofer ISE CalLab PVModules for the *I–V* testing.

References

[1] SEMI PV Group Europe 2014, "International technology roadmap for photovoltaic (ITRVP): Results 2013", 5th edn (March) [http://www.itrpv.net/Reports/Downloads/].

[2] Metz, A. et al. 2014, "Industrial high performance crystalline silicon solar cells and modules based on rear surface passivation technology", *Solar Energy Mater. & Solar Cells*, Vol. 120, Part A, pp. 417–425.

[3] Lee, K. et al. 2014, "Copper metallization of silicon PERL solar cells: 21% cell efficiency and module assembly using conductive film", *Proc. 40th IEEE PVSC*, Denver, Colorado, USA.

[4] Brand, A.A. et al. 2014, "Reduction of picosecond laser ablation threshold and damage via nanosecond pre-pulse for removal of dielectric layers on silicon solar cells", *Appl. Phys. A*. [http://dx.doi.org/10.1007/s00339-014-8444-x].

[5] Woehl, R., Hoerteis, M. & Glunz, S.W. 2008, "Analysis of the optical properties of screen-printed and aerosol-printed and plated fingers of silicon solar cells", *Adv. in Optoelectron.*, Vol. 2008.

[6] Steinhauser, B. et al. 2014, "PassDop rear side passivation based on Al_2O_3/a-SiCx:B stacks for p-type PERL solar cells", *Proc. 4th SiliconPV*, 's-Hertogenbosch, The Netherlands.

[7] Nekarda, J. et al. 2013, "Laser-based foil metallization for industrial PERC solar cells", *Proc. 28th EU PVSEC*, Paris, France.

[8] Bartsch, J. et al. 2014, "21.8 % efficient n-type solar cells with industrially feasible plated metallization", *Proc. 4th SiliconPV*, 's-Hertogenbosch, The Netherlands.

[9] Edler, A. et al. 2012, "On the metallization losses of bifacial n-type silicon solar cells", *Proc. 27th EU PVSEC*, Frankfurt, Germany.

[10] Heinz, F. et al. 2014, "Microscopic origin of the aluminium spiking problematique in n-type silicon solar cells", *Proc. 4th SiliconPV*, 's-Hertogenbosch, The Netherlands.

[11] Suwito, D. et al. 2010, "Industrially feasible rear passivation and contacting scheme for high-efficiency n-type solar cells yielding a V_{oc} of 700 mV", *IEEE Trans. Electron Dev.*, Vol. 57, No. 8, pp. 2032–2036.

[12] Feldmann, F. et al. 2013, "A passivated rear contact for high-efficiency n-type silicon solar cells

enabling high V_{oc}s and *FF*>82%", *Proc. 28th EU PVSEC*, Paris, France.
[13] Benick, J. et al. 2014, "High efficiency n-type PERT and PERL solar cells", *Proc. 40th IEEE PVSC*, Denver, Colorado, USA.
[14] Feldmann, F. et al. 2014, "Efficient carrier-selective n- and p-contacts using semiconductor-insulator-semiconductor structures", *Proc. 4th SiliconPV*, 's-Hertogenbosch, The Netherlands.
[15] Mason, N., Jordan, D. & Summers, J. 1991, "A high efficiency silicon solar cell production technology", *Proc. 10th EU PVSEC*, Lisbon, Portugal.
[16] Shi, Z., Wenham, S. & Ji, J. 2009, "Mass production of the innovative PLUTO solar cell technology", *Proc. 34th IEEE PVSC*, Philadelphia, Pennsylvania, USA.
[17] Eitner, U. & Rendler, L.C. 2014, "The mechanical theory behind the peel test", *Proc. 4th SiliconPV*, 's-Hertogenbosch, The Netherlands.
[18] Bartsch, J. 2011, "Advanced front side metallization for crystalline silicon solar cells with electrochemical techniques", Ph.D. dissertation, University of Freiburg, Germany.
[19] Koentges, M., Jung, V. & Eitner, U. 2010, "Requirements on metallization schemes on solar cells with focus on photovoltaic modules", 2nd Worksh. Si. Sol. Cell Metalliz., Konstanz, Germany. [http://www.secondmetal.eu/fileadmin/secondmetal/docs/Session8/3_K_ntges.pdf].
[20] Käsewieter, J. et al. 2014, "Cracks in solar cell metallization leading to module power loss under mechanical loads", *Proc. 4th SiliconPV*, 's-Hertogenbosch, The Netherlands.

About the Authors

Jonas Bartsch studied chemical engineering at the University of Karlsruhe and received his diploma in 2007. He then joined Fraunhofer ISE to pursue a Ph.D. in the field of advanced front contacts for silicon solar cells with plating technology. After receiving his Ph.D. from the Albert Ludwig University of Freiburg in 2011, he remained at ISE as head of the plating process technology team.

Andreas Brand studied physics and laser technology at RWTH Aachen, Germany, and at the University of Western Australia in Perth. He gained many years' experience with ultrashort pulse lasers and their applications while studying for his master's at the Fraunhofer Institute for Laser Technology in Aachen. In 2011 he joined the production technology and quality assurance department at Fraunhofer ISE, where he is currently working towards his Ph.D.

Dirk Eberlein received a diploma (FH) in mechanical engineering, specializing in renewable energy, from the Cologne University of Applied Science. The work for his diploma thesis was carried out at Fraunhofer ISE and concerned the development of a supersonic soldering technology for solar cells. Since 2009 Dirk has been working as a project engineer at Fraunhofer ISE in the photovoltaic modules group.

Andrew Mondon studied materials science in Freiburg, Germany, and graduated in 2010. He began working on electrochemical solar cell metallization at Fraunhofer ISE in 2009, and has been studying for his Ph.D. since June 2012, with a focus on nickel silicide formation.

Carola Völker works in the TestLab PV Modules facility at Fraunhofer ISE. She received her diploma in 2010 in mechanical engineering, with a focus on energy systems, from the University of Applied Sciences Aachen. Carola is in charge of project coordination for testing services, R&D projects and the implementation of new test facilities.

Marco Tranitz obtained his diploma degree in environmental technology at the University of Applied Sciences Jena and joined Fraunhofer ISE in 2002, where his research focuses on interconnection and solar module technology. In 2012 he completed a master's in electrical and information engineering at the University of Hagen, with a thesis topic of the series connection of solar cells by direct contact with the finger metallization.

Martin Graf received his diploma degree in physics in 2011 from the University of Augsburg in Germany. Since autumn 2011 he has been working towards a Ph.D. degree with Fraunhofer ISE in Freiburg, Germany, where his research focuses on laser-fired contacts for the foil-based rear-side metallization of silicon solar cells.

Jan Nekarda studied physics at the Ludwig Maximilian University of Munich and the Albert Ludwig University of Freiburg. He received a Ph.D. from the University of Konstanz in 2012 for his work on laser-fired contacts for crystalline silicon solar cells. Since 2011 he has been leading the laser process technology group at Fraunhofer ISE.

Ulrich Eitner studied technical mathematics at the University of Karlsruhe (TH), Germany. From 2006 to 2011 he worked in the field of thermomechanics of PV modules at the Institute for Solar Energy Research Hamelin (ISFH) and obtained his Ph.D. from the University of Halle-Wittenberg in 2011. Dr. Eitner has been managing the photovoltaic modules group at Fraunhofer ISE since 2011.

Daniel Philipp is head of the module testing group at Fraunhofer ISE, where he is responsible for reliability and certification testing of PV modules. He has been working in the field of service life analysis of modules and materials since receiving his diploma in environmental engineering and renewable energies from the FHTW Berlin in 2005.

Markus Glatthaar studied physics at the Eberhard Karls University, Tübingen, Germany, and received his Ph.D. in 2007 from the Albert Ludwig University of Freiburg in the field of organic solar cells. From 2008 to 2010 he carried out postdoctoral work at Fraunhofer ISE on the characterization of silicon solar cells, mainly on photoluminescence imaging methods. In 2011 he was a senior solar cell technologist at RENA GmbH. Since 2012 he has been head of the novel processes department within the solar cell development and characterization division at ISE.

Enquiries

Dr. Jonas Bartsch
Fraunhofer ISE
Heidenhofstr. 2
79110 Freiburg
Germany

Tel: +49 761 4588 5737

Email: jonas.bartsch@ise.fraunhofer.de
Website: www.ise.fraunhofer.de

Improvements in advanced industrial n-type solar cells and modules

Ingrid Romijn, **Bas van Aken**, **John Anker**, **Ian Bennet**, **Bart Geerligs**, **Nicolas Guillevin**, **Astrid Gutjahr**, **Eric Kossen**, **Martien Koppes** & **Kees Tool**, ECN Solar Energy, Petten, **Marten Renes** & **Peter Venema**, Tempress Systems BV, Vaassen, & **Nico van Ommen** & **Jan Bakker**, Eurotron BV, Bleskensgraaf, The Netherlands

ABSTRACT

This paper reports on the progress of R&D in two n-type cell and module concepts: the n-Pasha solar cell and bifacial module, and the n-MWT (metal wrap-through) cell and module. Both are part of ECN's technology platform, acting as a roadmap for research in n-type Cz cells and modules. The technology platform also encompasses low-cost IBC solar cells. In the case of n-Pasha, recent developments involve improved stencil-printed metallization, resulting in an increased I_{sc} and V_{oc} and efficiencies of up to 20.5%. For the bifacial module aspect, research has been done on the effect of different albedo on the module output. A gain of 20%$_{rel}$ in module output power was obtained with an optimized background, increasing the module power from 314W to 376W. As regards n-MWT cells, the front-side metallization pattern has been changed significantly. The number of vias for conducting the emitter current to the rear has been increased from 16 to 36, resulting in reduced lengths of busbars and fingers and consequently an increase in FF. At the same time, the metal coverage on the front side has been reduced from 5% to 3% of the total area, leading to a gain in I_{sc} and V_{oc} and a significant reduction in Ag consumption. All these factors will result in a lower cost/Wp. For the improved n-MWT design, average efficiencies of 20.8% over a large batch (134) of cells have been obtained, with the highest recorded efficiencies being 21.0%.

Introduction: n-type cell concepts

High efficiency, ease of industrialization and reliability are the main drivers towards low-cost (€/Wp) silicon PV. The March 2014 edition of the International Technology Roadmap for PV (ITRPV) envisages the share of n-type solar cells and modules becoming close to 40% in the next 10 years [1]. Compared with p-type material, n-type Cz material is known for its stable high carrier lifetimes because of the absence of light-induced degradation (LID) [2] and its higher tolerance to the most common metallic impurities such as Fe [3]. These longer lifetimes are consequently reflected in

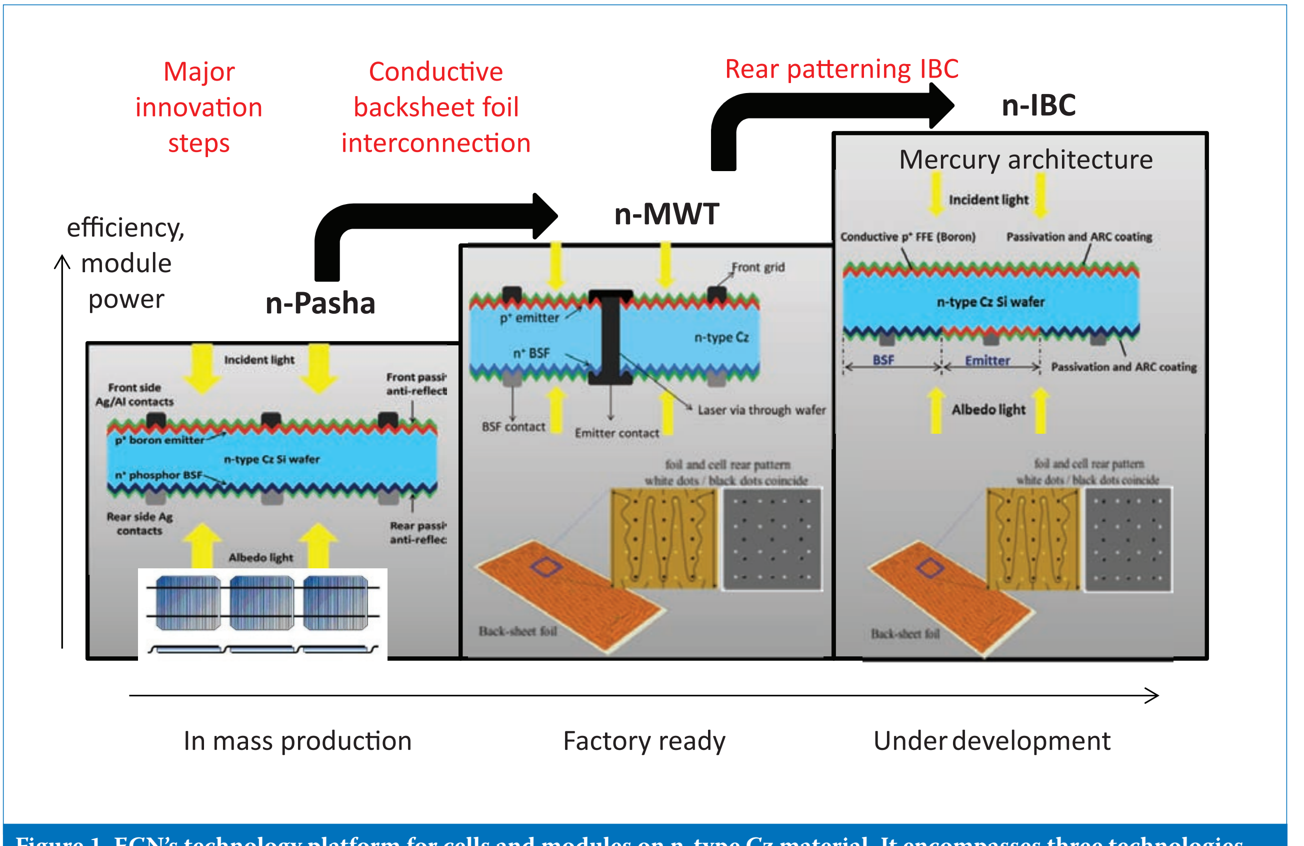

Figure 1. ECN's technology platform for cells and modules on n-type Cz material. It encompasses three technologies that are logical steps on the efficiency and development ladder.

higher efficiencies; indeed, the highest efficiency crystalline silicon modules currently on the market are based on the SunPower Maxeon technology, which uses n-type Cz material for manufacturing interdigitated back-contact (IBC) solar cells with efficiencies above 24%, and module efficiencies above 21% [4]. Very high efficiencies on n-Cz material can also be obtained with the heterojunction (HIT) technique used by Panasonic; Panasonic recently reported cell efficiencies of 25.6%, made possible by combining heterojunction and back-contact (IBC) technologies [5].

> "The March 2014 edition of the ITRPV envisages the share of n-type solar cells and modules becoming close to 40% in the next 10 years."

Many institutes and companies have started to adopt simpler structures on n-type Cz material that still enable efficiencies above 20% to be realised. Yingli Solar began mass production of their PANDA cell line in 2010, and in 2012 was already reporting efficiencies of 20% [6]. Other companies, such as PVGS [7] and Motech [8], are now also reporting efficiencies of 20–20.5% for bifacial n-type cells from their R&D or pilot production using boron emitter diffusion. Others, like Bosch [9] and CEA/INES [10], adopt ion implantation for the back-surface field (BSF) and emitter formation, which yields efficiencies higher than 20.5%. Recently, FhG ISE has taken a different approach to obtaining higher efficiencies by using (on a laboratory scale) passivated rear contacts and a selective emitter in their TopCon process, enabling an efficiency of 24.4% to be achieved [11].

ECN's n-type technology platform

ECN's aim is to develop highly efficient, low-cost and reliable solar cell and module concepts that can be easily adopted in mainstream industrial production. On the basis of over 10 years of research, ECN has established a technology platform on n-type Cz material that encompasses three different cell–module concepts (see Fig. 1). The basis of the technology platform is the relatively simple n-Pasha cell [12] – a bifacial solar cell with H-patterned metallization on both front and rear. ECN, Tempress and Yingli introduced this cell to the market in 2010 as a novel bifacial cell concept called PANDA [13], while in 2013 Nexolon America selected this cell concept for their new production line, enabling the production of bifacial modules.

The next step up in performance on the technology platform is the back-contact n-MWT (metal wrap-through) integrated cell and module concept, which combines two of ECN's cell concepts that are already proven both in the laboratory and on a large scale in industry: 1) ECN's p-type MWT cell and module concept [14], based on foil interconnection; and 2) the n-Pasha n-type cell concept, as described above. The n-MWT cell process is very close to that of the n-Pasha cell, while yielding a higher short-circuit current and corresponding efficiency because of the reduction in front-side metal coverage [15]. The modules are produced using a conducting backsheet foil, on which the cells are assembled with conductive adhesive. The back-contact foil technology enables higher module power as a result of the reduction in cell-to-module losses, because relatively wide metal grids in the conducting foil can be used and connected to many contact spots on the rear side of the cells. The n-MWT modules are ready to be produced on an industrial scale, as Yingli announced recently in a press release [16].

Apart from being a cost-effective high-efficiency PV technology, n-MWT technology is also a bridge or a step in the roadmap from n-Pasha to n-type IBC technology. In an IBC cell, the p-n junction and all metallization is moved to the rear. Recently ECN presented n-type IBC Mercury cells [17], which employ a relatively conductive front floating emitter to avoid electrical shading issues present in conventional front-surface field (FSF) IBC cells, resulting in relaxed demands on the geometrical resolution in the processing. This allows the processing of highly efficient solar cells (no metal on the front side) with a process complexity similar to that for n-pasha and n-MWT cells. The IBC Mercury design can be combined with

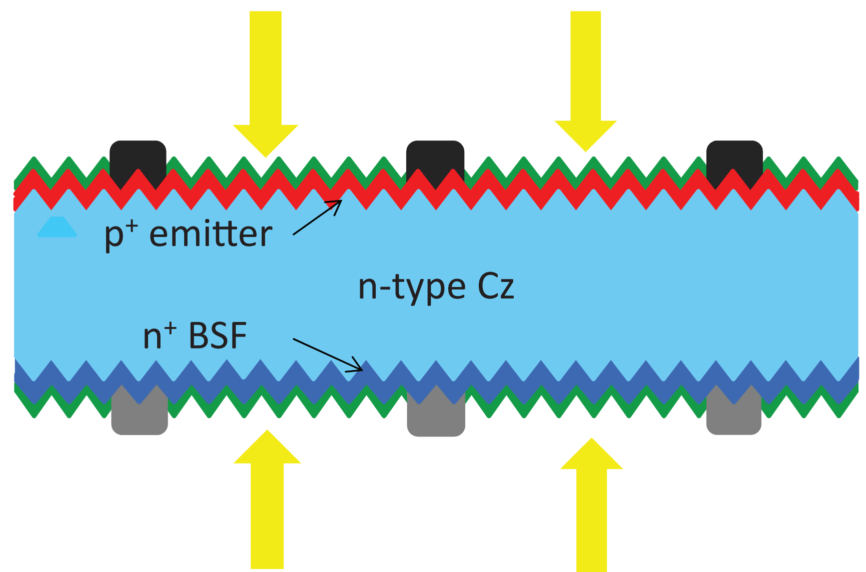

Figure 2. Cross section of the ECN n-Pasha cell, featuring an n-type Cz Si wafer with a boron p$^+$ emitter and a phosphorus n$^+$ BSF. Yingli's PANDA cells are also based on this structure.

back-contact module technology in a very similar way to n-MWT modules.

This paper will focus on the first two concepts of the technology platform: the n-Pasha cell and bifacial module, and the n-MWT cell and foil-interconnection module.

The n-Pasha cell

The basic configuration of the n-Pasha solar cell is shown in Fig. 2. The n-Pasha cells are fabricated on 6-inch n-type Cz wafers, and all processing steps used are compatible with an industrial-scale production. The texturing and cleaning steps are performed by wet chemical processes, while both the p^+ (boron) and n^+ (phosphorus) doped layers are created by tube furnace diffusion processes. Passivation and anti-reflection coatings are deposited using plasma-enhanced chemical vapour deposition (PECVD) tools. The metal grids are printed, and the contacts on the emitter and BSF are formed during a single co-firing step. Both front and rear metallization can be directly soldered, so no additional metallization step is necessary to enable cell interconnection into a module. The n-Pasha solar cells fabricated using the ECN 'baseline' process now typically achieve average efficiencies above 20% on a wide range of materials. The consistent performance of n-Pasha processing for different materials and a wide range of base resistivities was extensively tested and published in 2013 [18]. More details regarding n-Pasha cell processing can be found in previous publications [12,13,18].

If the n-Pasha cells are assembled in a standard monofacial module, maximum light trapping can be obtained by the rear dielectric layers in combination with a reflecting backsheet foil. On the other hand, the open rear-side H-patterned metallization makes the n-Pasha concept very suitable for bifacial cell and module technology, in which case an even higher module output power and an increased annual energy yield can be obtained when the modules are appropriately placed in the field.

Bifacial n-Pasha modules

Because of the transparent rear side and the absorbent background, bifacial modules demonstrate lower efficiency or power output per unit area when measured under standard test conditions (STC) than monofacial modules. However, the annual output of bifacial modules can be significantly higher, depending on albedo, orientation and tilt angle [19–21]. At ECN, 72-cell bifacial modules were manufactured using six 12-cell strings made of (relatively old) n-Pasha solar cells with efficiencies of 19.0%. A resulting peak power of 314W was measured for the bifacial module under STC of 1000W/m^2 irradiation, 25°C and a black background and environment. With another batch of n-Pasha cells of 19.6% efficiency, a monofacial 72-cell module was made that produced 334W. Average cell and corresponding module I–V data are summarized in Table 1, together with the cell-to-module (CtM) ratios for the bifacial and monofacial modules. The modules were measured under STC, which includes an absorbent black background.

The CtM ratios for V_{oc} (above 100%) and FF (above 96%) are very similar for both modules. The I_{sc} CtM ratio for the bifacial modules, however, is 2.7% lower (99.7% compared with 102.4%): this difference can be directly related to the loss of transmitted light that is not reflected at the white backsheet but absorbed in the black background.

To simulate the effect of albedo on the power output of bifacial modules, and evaluate the potential gain for

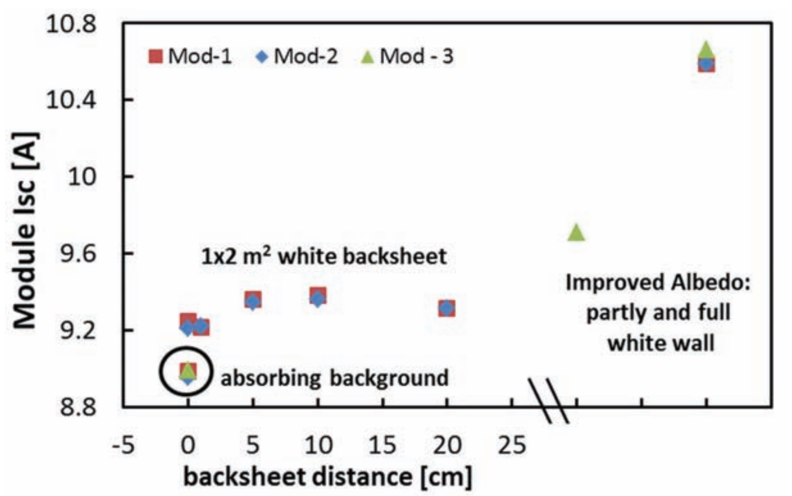

Figure 3. Increase in module I_{sc} for bifacial modules when the albedo is changed. Under STC with an absorbent background, the I_{sc} for all modules is under 9A; with a full white wall behind the module, the I_{sc} becomes 10.6A, with a corresponding module output of 376W.

Module		I_{sc} [A]	V_{oc} [V]	FF [-]	Eta [%]	P_{max} [W]
Bifacial with ARC	Avg cell	9.14	0.638	78.0	19.05	4.55
	72-cell module	9.12	45.98	75.0	18.3 (per cell)	314.3
	CtM ratio	99.7%	100.1%	96.2%	96.0%	
	Full white wall	10.59				376
Monofacial with ARC	Avg cell	9.25	0.650	77.9	19.6	4.69
	72-cell module	9.47	47.16	74.9	19.5 (per cell)	334.4
	CtM ratio	102.4%	100.7%	96.1%	99.1%	

Table 1. Cell and module data for bifacial and monofacial modules manufactured from n-Pasha cells, measured under STC (and also with a full white wall behind the bifacial module).

Finger width [µm]	I_{sc} [A]	J_{sc} [mA/cm^2]	V_{oc} [V]	FF [-]	Eta [%]
55 avg	9.29	38.87	0.649	78.89	19.9
45 avg	9.44	39.49	0.651	78.15	20.1
40 avg	9.45	39.54	0.654	78.49	20.3 (20.5 max)

Table 2. Average *I–V* data for n-Pasha cells with different front metallization: the finger width of the stencilled fingers is decreased while the number of fingers stays the same.

the bifacial modules when they are placed in a proper environment, two bifacial modules were measured with a white backsheet (same material as for the monofacial module) at various distances behind the module (see Fig. 3). With a white backsheet directly against the transparent backsheet, the I_{sc} of the bifacial module increased to the value expected for the same module in a monofacial layout, namely 9.2A. When the white backsheet was placed further away from the module (5 to 20cm), the I_{sc} output increased even more. A full white back wall (approximately 3m × 2m, behind the module) yielded 10.6A and 376W; more than 90% of the gain is due to rear illumination.

In summary, when bifacial n-Pasha modules are placed in an environment with sufficient albedo (for instance crushed shells or specially coated roofs, so-called *cool roofs*), a gain in module output power of up to 20% (314W to 376W) is observed.

> "When bifacial n-Pasha modules are placed in an environment with sufficient albedo, a gain in module output power of up to 20% is observed"

Improvements in n-Pasha cell and module: metallization

To reduce Ag consumption, increase the active area of the cell, and decrease recombination losses due to the metallization grid, stencil printing of narrow high-aspect-ratio lines was investigated. An added advantage of stencil printing is the uniformity of the print cross section, improving the efficiency of the Ag usage. The results are presented here for three different stencil designs with nominally 40-, 45- and 55µm-wide fingers. All other processing, including the number of grid fingers, was kept constant. The resulting average cell parameters are shown in Table 2. For the best cell group, average efficiencies of 20.3% and a highest efficiency of 20.5% were obtained. The gain in I_{sc} for the 45- and 40µm-wide fingers is even larger than expected for the decreased finger width: this may be due to the change of metal paste for these two groups, which enabled fingers with very high aspect ratios of almost 1, and is currently under investigation.

These cells were subsequently laminated in single-cell test laminates using a white backsheet similar to the monofacial module in Table 1. The module I_{sc} increases in all cases, as compared with the cell I_{sc}. The CtM ratio gain in I_{sc} is somewhat lower for the narrow-finger cells, as can be expected from the reduced benefit from the internal reflection of light scattered off the fingers inside the module. Very high currents of up to 9.6A were measured for the best single-cell laminates, as shown in Fig. 4.

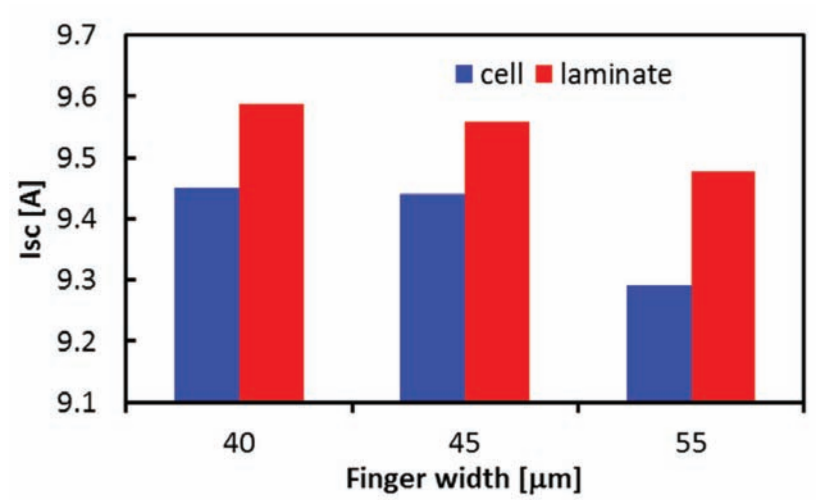

Figure 4. Improvement in I_{sc} for mini-modules made from four cells, for different front-finger widths.

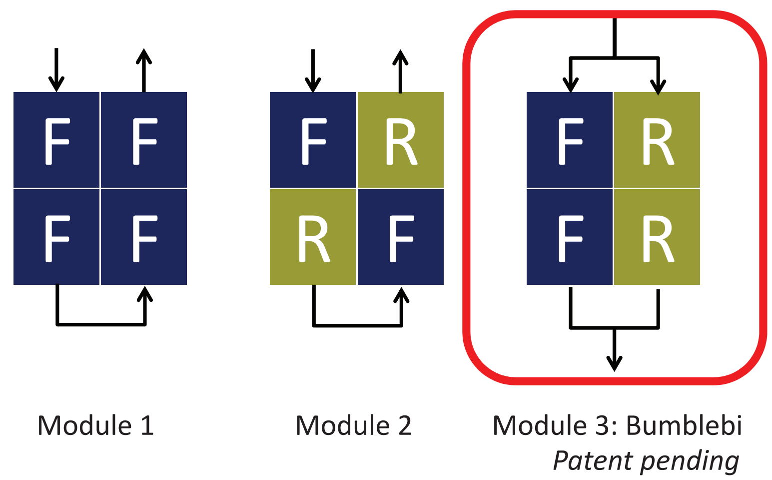

Figure 5. Schematic view of a normal bifacial, a mixed-cell bifacial and a Bumblebi bifacial mini-module. F and R indicate the front and rear sides of the bifacial n-Pasha cells. Module 1 has no mismatch but is asymmetric in terms of front and rear illumination. The second module has mismatch in I_{sc} because of the mixing of F and R cells, but is symmetric in front and rear illumination. Module 3, the Bumblebi, has a very small voltage mismatch because of F and R strings, but is also symmetric.

Improvements in bifacial module: Bumblebi

Typical bifacial modules do not have an equal power (or appearance) on both sides of the module, mainly because of the lower I_{sc} when the modules are illuminated from the rear. A new approach in which the front and rear response (and appearance) of the modules is equalized is currently under investigation at ECN and will be briefly described in this section. An equal front and rear response of a module will be especially useful if the bifacial modules are used in an east–west orientation, because in this case the harvested power will be more evenly distributed over the whole day.

In this new approach, named Bumblebi, 50% of the cells in a module are turned around: thus each side of the module has 50% of the cells with the positive contact(s) and 50% of the cells with the negative contacts on that side. To avoid the current mismatch between turned cells, the forward- and backward-facing cells are connected in series in separate strings, which are subsequently connected in parallel (ECN patent pending). The idea is shown in Fig. 5 for small 2×2 modules, but this can easily be extrapolated to larger strings, e.g. 60- or 72-cell modules. The first results from these mini-modules indicate that the Bumblebi module outperforms by ~3%$_{rel}$ the regular bifacial geometry under bifacial circumstances (diffuse light and addition of white panels as a back wall in the Pasan flash tester). The improved performance is confirmed by modelling and further experimental investigation is currently under way.

n-MWT cells

The n-MWT cell processing in general remains very close to the conventional front-to-back contact n-Pasha cell processing. Additional laser processing is used to form via holes by means of which the front-side metal grid is wrapped through the wafer. Like the n-Pasha cells, the cell structure comprises a front-side boron emitter, a phosphorus BSF and an open rear-side metallization suitable for thin wafers (Fig. 6). Metal contacts can be deposited by an industrial screen-printing process with no further requirements regarding alignment compared with the screen-printing process used in the industrial n-Pasha process. The front- and rear-side metal grid patterns can be based on a H-pattern lookalike grid design, or on a modular (front) grid design, combined with the unit cell concept.

To compare the performance of n-MWT with n-Pasha cells, both cell types were prepared from adjacent n-type Cz wafers (239cm^2, 200µm

	J_{sc} [mA/cm^2]	V_{oc} [V]	FF [-]	Eta [%]	R_{series} [mΩ]
n-Pasha avg	38.90	652	78.4	19.89	4.9
n-Pasha best	38.97	653	78.5	19.98	4.8
n-MWT avg	39.95	652	76.8	20.04	5.7
n-MWT best	40.01	653	77.0	20.10	5.6

Table 3. I–V characteristics of n-Pasha and n-MWT cells with comparable J_0 and metallization parameters. (R_{series} was obtained from the fit to a two-diode model.)

thickness, approximately 1.7Ω·cm resistivity). Both groups were processed in parallel and received comparable processing, with the exception of the steps specific to n-MWT, such as via drilling and via metallization. The I–V data are presented in Table 3: average efficiencies of 20.04 and 19.89% respectively were obtained for n-MWT and n-Pasha, equating to a 0.15%$_{abs}$ efficiency gain for n-MWT over n-Pasha [15].

The J_{sc} gain of 2.6% for the n-MWT cells is related to the reduced front metal-shading losses thanks to the narrow and tapered front busbars. Because the n-Pasha process used non-contacting front busbar paste [18], there is no additional V_{oc} gain realized by the n-MWT cells from the reduction of busbar area (reduced metal recombination). In this experiment the cell efficiency benefit of the MWT structure is therefore ~0.15%$_{abs}$, compared with ~0.25%$_{abs}$ previously reported [22]. The n-MWT cells exhibit a lower FF than the n-Pasha cells, which stems from a higher series resistance. The major contributions to series resistance and FF losses are summarized in Table 4.

Source of R_{series} in MWT cell	R_{series}	FF loss
Metal via resistance	0.2mΩ	0.3%$_{abs}$
Front- and rear-side busbars	0.7mΩ	1.1%$_{abs}$
Increase in I_{sc}		0.1%$_{abs}$
Total	0.9mΩ	1.5%$_{abs}$

Table 4. Calculated contributions to series resistance and FF losses of n-MWT cells compared with n-Pasha cells.

As can be seen in Table 4, the largest factor contributing to series resistance in n-MWT cells is the busbars, which deviate from the n-Pasha situation in that no tab is soldered to the busbar to enhance conductance. Resistive losses therefore occur in transport through the busbar to the vias. Several options exist for reducing the resistive losses and consequently the FF loss of n-MWT cells. A straightforward option is to increase the number of vias, which shortens both the busbars and the metal fingers at the same time; however, a drawback of this could be the increased chance of recombination and thus V_{oc} loss as a result of the numerous contact points.

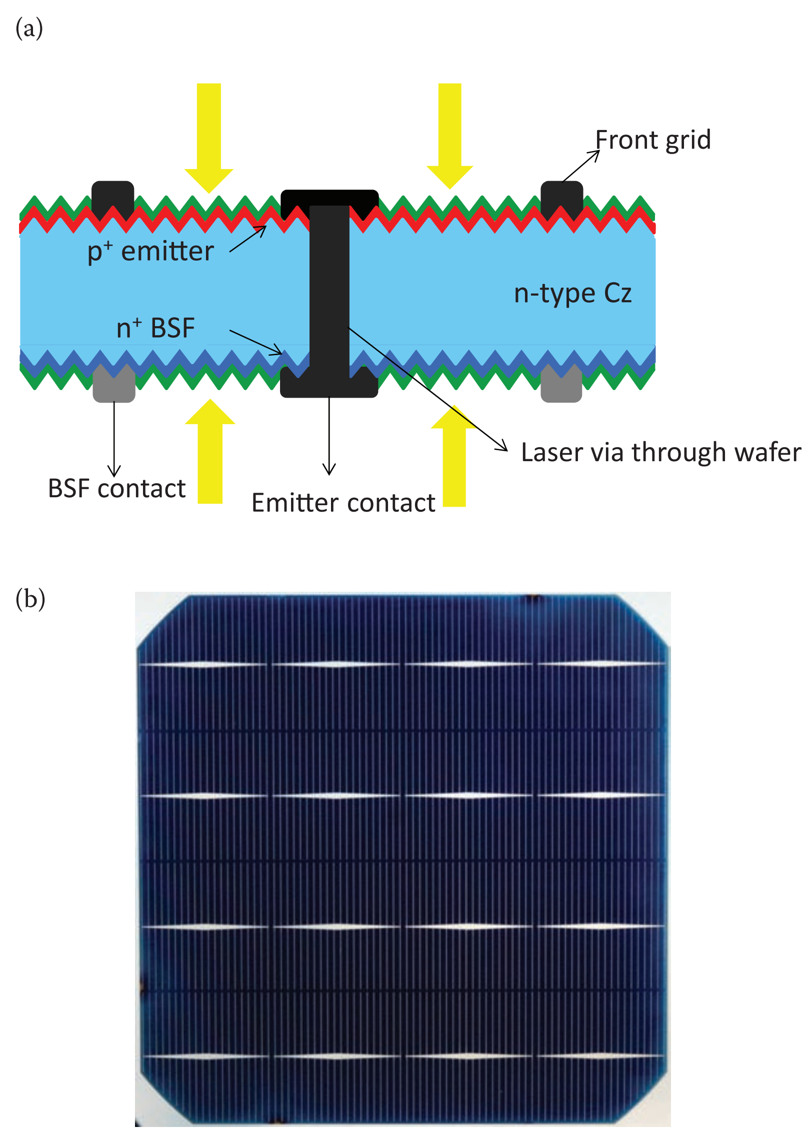

Figure 6. (a) Schematic cross section of an n-MWT cell; (b) a 4×4 n-MWT front-grid design, with tapered busbars. The 16 vias are located in the thicker parts of the busbars. The metal fraction of the front-side metallization is around 5% of the total area.

n-MWT cells with new front-side patterns

To improve n-MWT performance, new MWT patterns with 36 vias (six rows, each with six vias) were designed. The simplest new n-MWT design was based on six thin busbars connecting the rows of vias. The rear pattern also consists of thin busbars, connecting 7×7 (–4, because of semi-square wafer format) base contact points (Figs. 7(a) and (b)). Alternatively, different front-side patterns can be designed for improved aesthetics. Two examples were tested: the so-called 'starship' pattern and a circles pattern (Figs. 7(c) and 7(d)). All three 6×6 front-side configurations were combined with the rear-side metal pattern shown in Fig. 7(b) and compared with the 4×4 pattern in a cell experiment consisting of four groups.

The I_{sc} and V_{oc} data of the four groups are shown in Fig. 8; these two parameters were both found to depend mainly on the metal fraction. The increased number of vias did not seem to have a negative effect on the passivation (V_{oc}) at this stage. The 'old' 4×4 n-MWT pattern has the largest metal fraction of around 5% including the busbars, resulting in the lowest currents and voltages. The 'new' n-MWT pattern, with busbars and 36 vias, has the smallest metal fraction of 3.1%, which resulted in cells with an average high current of 9.63A, and an average V_{oc} of 654mV.

"To improve n-MWT performance, new MWT patterns with 36 vias were designed."

As expected, the FF for the 6×6 busbar pattern is clearly better than for the 4×4 busbar pattern, but the highest FFs are obtained for the 6×6 starship pattern, which is specially modelled and designed to limit resistance losses (Fig. 9). The highest average efficiency of 20.3%, however, is obtained for the 6×6 busbar pattern because of its superior J_{sc} and V_{oc}.

Another important benefit of the 6×6 busbar pattern is that the paste consumption for both the front and the rear metallization is significantly reduced compared with that for the 4×4 pattern. The paste consumption for the latter is similar to that for three-busbar n-Pasha cells. In this experiment the reduction for the 6×6 pattern is already over 20%, and it is expected that in a (cost-)optimized situation a reduction of 50% should be possible, with only minor FF and

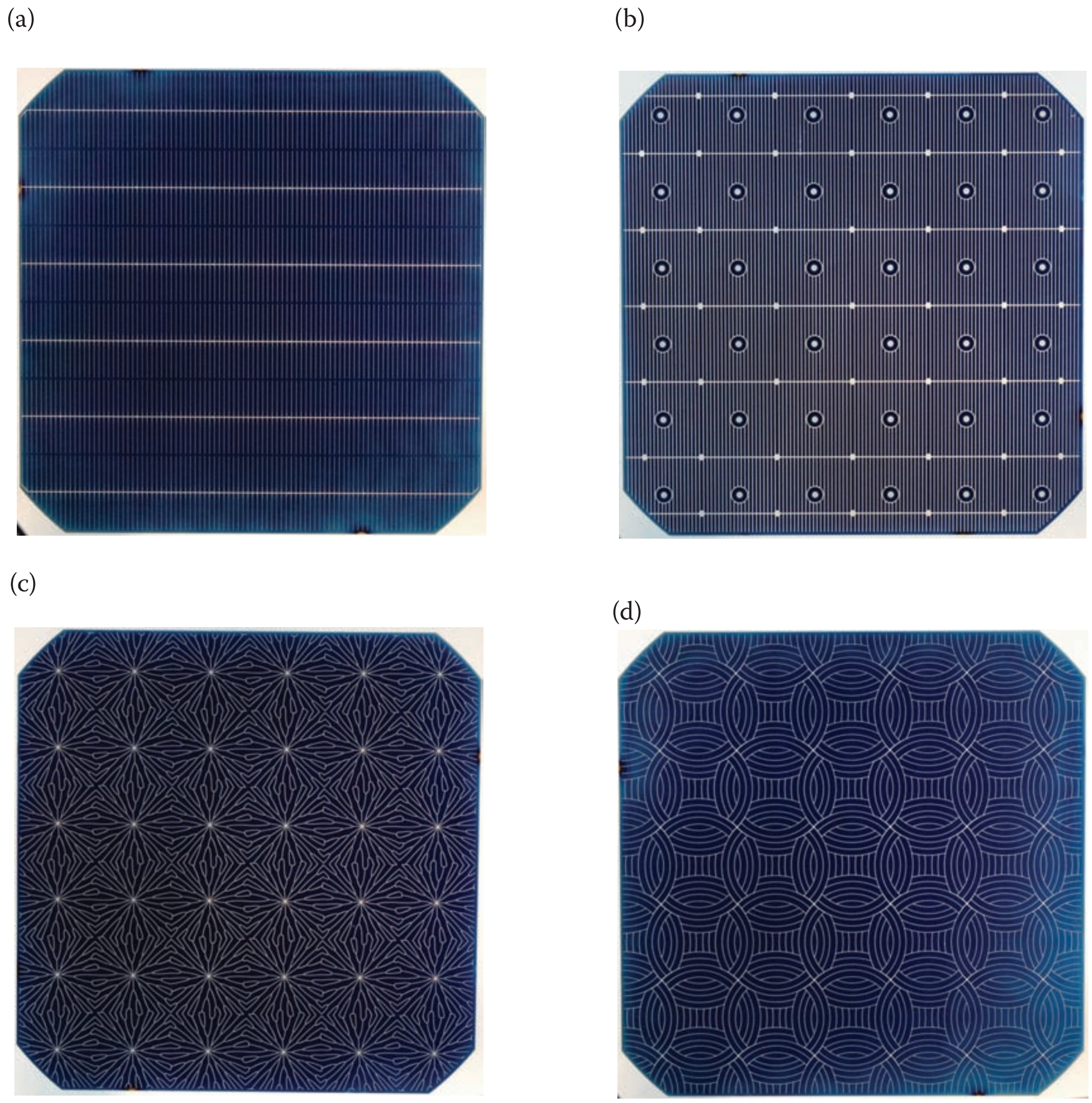

Figure 7. (a) Front-side 'new' n-MWT: 6×6 vias with thin busbars; metal fraction ~3.1% of total cell area. (b) Rear-side 'new' n-MWT: 6×6 emitter contacts and (7×7)–4 base contacts (corners are excluded because of the semi-square wafer). (c) Starship pattern; metal fraction ~4.7% of total cell area. (d) Circles pattern; metal fraction ~4.4% of total cell area.

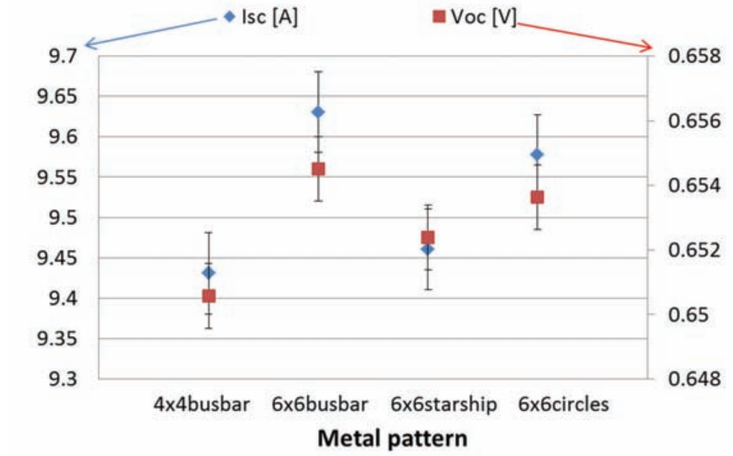

Figure 8. I_{sc} and V_{oc} of n-MWT cells with different numbers of vias (16 and 36) and different front metal patterns.

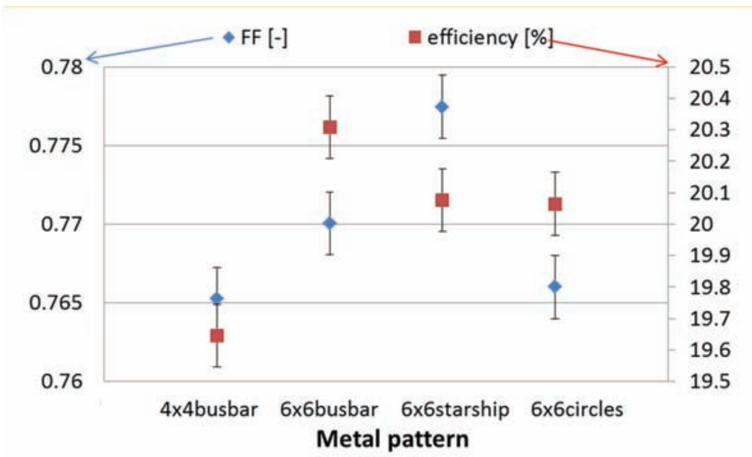

Figure 9. FF and efficiency of n-MWT cells with different numbers of vias (16 and 36) and different front metal patterns.

efficiency penalties.

n-MWT modules

In two recent large n-MWT runs, high-quality n-Cz material and process improvements adopted from recent n-Pasha cell optimizations were used [23,24]. In the first run, the old via pattern with 4×4 vias was employed (see Fig. 6(b)). A best cell efficiency of 20.5% (certification pending) and average efficiencies over 60 cells of 20.3% were obtained. These cells were assembled in a 60-cell module using commercially available equipment from Eurotron to pick and place the cells onto the copper backsheet foil [14]. The module has been tested using an A-class multi-flash solar simulator to demonstrate a power of 291Wp under STC, as can be seen in Fig. 10. The average cell data and module I–V are shown in Table 5.

In the second run, the best 6×6 via pattern was used (see Fig. 7(a)); in addition, recent improvements from n-Pasha cells were transferred to the n-MWT cells. The results obtained from this run were a best cell efficiency of 21.0% (measured on a reflecting chuck) and an average efficiency of 20.8% over more than 100 cells. The efficiency distribution of the full batch of 134 cells (shown in Fig. 11) was quite narrow, indicating a very stable process. The best 60 cells yielded an average 20.9% efficiency and will be assembled into a module in September 2014. With a CtM ratio similar to that for the 4×4 via module, a module power output of over 300W is expected.

Summary and conclusions

Two n-type solar cell and module concepts have been discussed: the n-Pasha solar cell and bifacial module, and the n-MWT cell and module. In the case of n-Pasha cells, recent developments involve improved stencil-printed metallization, resulting in an increased I_{sc} and V_{oc} and efficiencies of up to 20.5%. For the bifacial module aspect, research has been done on improving the module output power by changing the albedo. A gain of 20%$_{rel}$ in module output power was obtained with optimized background, increasing the module power from 314W to 376W. Furthermore, a new bifacial module concept called Bumblebi was introduced, in which the front and rear response (and appearance) of the modules are equalized. Equal front and rear responses will be especially useful if the bifacial modules are used in an east–west orientation, because in this case the harvested power will be more evenly distributed over the whole day.

> "A module under construction using sixty n-MWT cells with an average efficiency of 20.9% is expected to deliver a power output of over 300W."

For n-MWT cells, the front-side metallization pattern has been changed significantly by adopting 36 (6×6) vias instead of the 16 (4×4) that have traditionally been used up to now. This results in reduced lengths of busbars and fingers and consequently an increase in FF. The metal coverage on the front side was reduced from 5% to 3% of the total area, resulting in a gain in I_{sc} and V_{oc}, and at the same time a significant reduction in Ag consumption. All these factors will result in a (much) lower cost/Wp. For the improved n-MWT design, average efficiencies of 20.8% over a large batch (134) of cells have been obtained, with the highest recorded efficiencies being 21% (before mismatch correction). The pattern of the backsheet for the modules was adjusted accordingly. A module under construction (September 2014) using sixty n-MWT cells with an average efficiency of 20.9% is expected to deliver a power output of over 300W.

Acknowledgements

The authors are grateful for the collaboration with our research partners from the TKI [25] projects NChanted and Pamplona, and in particular to the companies Tempress and Eurotron for their help in manufacturing the n-MWT cells and modules.

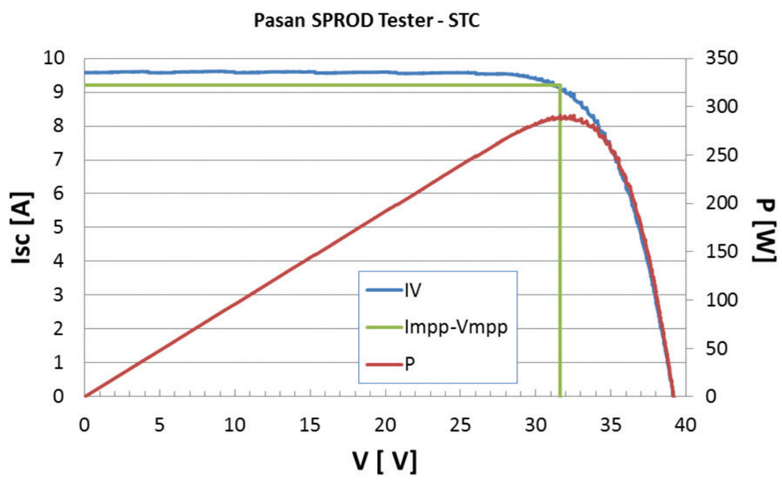

Figure 10. ***I–V*** **data for a 60-cell module made with n-MWT cells with 4×4 vias. A resulting power of 291Wp was demonstrated.**

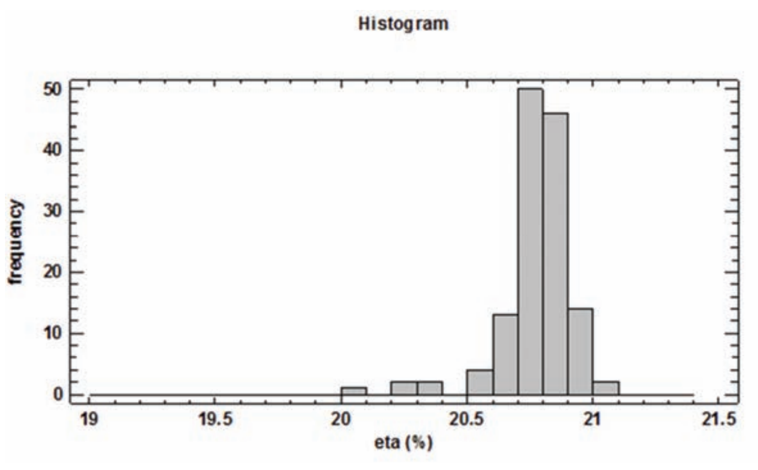

Figure 11. Efficiency distribution of 134 n-MWT cells fabricated with the optimized 6×6 via pattern and including recent n-Pasha improvements. The highest efficiency obtained was 21%.

References

[1] SEMI PV Group Europe 2014, "International technology roadmap for photovoltaic (ITRVP): Results 2013", 5th edn (March) [available online at http://www.itrpv.net/Reports/Downloads/].

[2] Glunz, S. et al. 1998, *Proc. 2nd WCPEC*, Vienna, Austria, p. 1343.

[3] Macdonald, D. & Geerligs, L.J. 2008, *Appl. Phys. Lett.*, Vol. 92, p. 4061.

[4] SunPower [http://us.sunpower.com/].

[5] Panasonic 2014, "Panasonic HIT® solar cell achieves world's highest energy conversion efficiency of 25.6% at research level", Press Release (April) [http://eu-solar.panasonic.net/fileadmin/user_upload/News_PDFs/140410_Panasonic_HIT_E.pdf].

[6] Song, D. et al. 2012, *Proc. 38th IEEE PVSC*, Austin, Texas, USA.

[7] Gonsui, S. et al. 2013, *Proc. 28th EU PVSEC*, Paris, France.

[8] Hsieh, P. et al. 2013, *Proc. 28th EU PVSEC*, Paris, France.

[9] Boescke, T.S. et al. 2012, *Proc. 38th IEEE PVSC*, Austin, Texas, USA.

[10] Lanterne, A. et al. 2014, *Proc. 4th SiliconPV*, 's-Hertogenbosch, The Netherlands.

[11] Fraunhofer ISE 2013, "24 percent efficient n-type silicon solar cell – Top-notch European research raises potential for cost reductions in photovoltaics", Press Release (November) [http://www.ise.fraunhofer.de/en/press-and-media/press-releases/presseinformationen-2013/24-prozent-siliciumsolarzelle-auf-n-typ-material].

[12] Romijn, I.G., Fang, L. & Vlooswijk, A. 2012, *Photovoltaics International*, 15th edn, p. 81.

[13] Burgers, A.R. et al. 2011, *Proc. 26th EU PVSEC*, Hamburg, Germany.

[14] Bennet, I.J. et al. 2009, *Proc. 24th*

	T_m [°C]	Irr [W/m^2]	I_{sc}[A]	V_{oc} [V]	P_m [W]	FF [%]	Cell eff [%]
Cell average			9.51	38.927	290.79	78.50	20.28
B392 (8 flashes)	26.2	1000	9.59	39.196	290.99	77.42	20.29
Rel. CtM ratio change			+0.81%	+0.69%	+0.07%	–1.41%	

Table 5. Average cell and module ***I–V*** **data for a 60-cell module made with n-MWT cells with 4×4 vias.**

EU PVSEC, Hamburg, Germany.
[15] Guillevin, N. et al. 2014, *Proc. 8th SNEC Intl. PV Power Gen. Conf.*, Shanghai, China.
[16] Energy Matters 2014, "Yingli Solar trialing n-MWT manufacturing technology", News Report [http://www.energymatters.com.au/index.php?main_page=news_article&article_id=4315].
[17] Cesar, I. et al. 2014, *Proc. 4th SiliconPV*, 's-Hertogenbosch, The Netherlands.
[18] Romijn, I.G. et al. 2013, *Photovoltaics International*, 20th edn, p. 44.
[19] Mishima, T. et al. 2011, *Solar Energy Mater. & Solar Cells*, Vol. 95, pp. 18–21.
[20] Kreinin, L. et al. 2011, *Proc. 26th EU PVSEC*, Hamburg, Germany.
[21] van Aken, B. & Carr, A. 2014, *Proc. 40th IEEE PVSC*, Denver, Colorado, USA.
[22] Guillevin, N. et al. 2011, *Proc. 26th EU PVSEC*, Hamburg, Germany.
[23] Romijn, I.G. et al. 2014, *Proc. 8th SNEC Intl. PV Power Gen. Conf.*, Shanghai, China.
[24] van de Loo, B. et al. 2014, *Photovoltaics International*, 24th edn, p. 43.
[25] TKI Solar Energy [http://www.tkisolarenergy.nl/]

About the Authors

Ingrid Romijn joined ECN Solar Energy in 2004, where she started working as a researcher and later on (2006) as a project leader in the crystalline silicon group. Research topics included passivating layers, optimization of SiN_x deposition systems and (advanced) p-type solar cell concepts. During 2011 the focus of her work shifted towards the development and industrialization of n-type cell concepts. In 2012 Ingrid became the topic coordinator for industrial n-type cells and modules at ECN Solar Energy.

Bas van Aken studied materials science at Delft University of Technology, after which he studied for his Ph.D. at the University of Groningen. Following that he worked as a postdoctoral researcher at Cambridge University and at the Max Born Institute for Nonlinear and Ultrafast Optics in Berlin. After around five years in the thin-film Si group at ECN Solar Energy, he is now with the PV modules and application group, where he focuses on the fabrication and reliability of n-type PV modules – both conventional H-pattern modules and more advanced concepts, such as back-contact technology and bifacial modules.

Ian Bennet is a researcher at ECN Solar Energy and received a Ph.D. in materials science from the University of Bath. He has worked for several research institutes, investigating high-temperature processing of ceramic materials. Ian has been with ECN since 2006 as a member of the module technology and application group, where he has been involved in the development of module technology for back-contact cells and the application of new and novel module materials and module concepts.

LJ (Bart) Geerligs has been at ECN Solar Energy since 2000, where he has set up several research fields. From 2004 he led a number of projects in which n-type cell technology at ECN was developed. From 2009 to 2010 he was project leader at ECN for the development and successful transfer to industrial pilot production of n-Pasha cell technology (subsequently transferred to mass production), and from 2010 to 2012 for the development and successful transfer to industrial pilot production of n-MWT cell technology. Since 2012 he has been the coordinator of R&D at ECN for high-efficiency silicon cells and applications of nanotechnology, and the coordinator of a European project on reducing the environmental footprint of silicon PV, including design for recycling.

Nicolas Guillevin is a researcher in the device architecture and integration group at ECN Solar Energy. He joined ECN in 2007, where he started his research activities in the development of n-type-based silicon solar cells, focusing mainly on back-contact cell architectures (EWT, MWT and IBC). Nicolas studied at the National Engineering School of Industrial Ceramics in Limoges (France), where he obtained a master's in the field of materials science and processes.

Astrid Gutjahr studied mineralogy at the University of Bonn and was a postdoctoral researcher in the liquid phase epitaxy group at Max Planck Institute for Solid State Research in Stuttgart. In 1999 she joined ECN, where she has worked on the development of RGS, a crystalline Si ribbon growth technology. Astrid's current research focuses on the characterization and cell processing of n-type silicon wafer material.

Eric Kossen has been working in the solar department at ECN Solar Energy as a senior process engineer for 17 years. He specializes in different metallization concepts for n- and p-type solar cells, especially in fine-line stencil printing. Eric also has wide experience in delivering training on the subject of metallization to engineers and operators in industry.

Martien Koppes began working as a chemist in the molten carbonate fuel cell group at ECN Solar Energy 23 years ago. For the last 14 years he has been a researcher in solar energy. Martien's main work concerns the chemical aspect of solar cells, with a focus on etching and cleaning.

Kees Tool has been working in the solar energy field for almost 20 years. After an education in chemistry, he embarked on a career in solar energy as a researcher. For around seven years his main work has involved transferring both n-type and p-type ECN technology to industry. He also carries out troubleshooting and tuning of industrial crystalline silicon solar cell production lines.

Enquiries

Ingrid Romijn
ECN Solar Energy
P.O. Box 1
NL-1755 ZG Petten
The Netherlands

Tel: +31 224 56 4959
Fax: +31 224 56 8214
Email: romijn@ecn.nl

Thin Film

Hanergy changes name and acquires wearable tech firm

In August, a special meeting of Hanergy shareholders voted to change the name of the company to Hanergy Thin Film Power Group Limited. All the shares represented in the vote were in favour of the proposed change. The company has made a number of project announcements in 2014 and added downstream partnerships in Japan and the US to add to high profile deals with Tesla and IKEA. Earlier in August the company acquired Alta Devices in a move that opens up the Internet of Things market for the company. Alta Devices develops single crystalline thin-film (Gallium arsenide, or GaAs) solar cells, including its AnyLight technology, which it claims can work well under low light conditions. In addition to Hanergy expanding Alta Devices' range of products, the new relationship will see the two companies collaborate on research and development, especially with regards to mobile power and 'wearable tech' applications. As well as representing the company's downstream ambitions, a rebrand will also help its consumer facing image.

Hanergy is to change its name.

Source: Hanergy Solibro

Space-age Solar

Ascent Solar teams with NASA on large space-based solar array programme

Flexible CIGS thin-film producer, Ascent Solar, is collaborating with NASA through its Small Business Innovative Research (SBIR) initiative to develop low-cost lightweight large area solar arrays for a range of space applications in the future. Ascent will be working with Vanguard Space Technologies, which has proprietary space environment protection technology as well automated manufacturing approaches to produce the large-area arrays.

EMCORE Corporation enters into long-term space solar-cell supply contract with SSL

Component and subsystem provider EMCORE Corporation has agreed to a long-term supply deal with Space Systems/Loral, LLC (SSL) that will see EMCORE construct and deliver solar cells for SSL's satellite programmes. EMCORE has supplied SSL with solar cells for 15 years, delivering its one-millionth solar cell to the satellite provider in 2013 – representing 1MW of power delivered into space. The solar cells will be designed and constructed at EMCORE's manufacturing plan in Albuquerque, New Mexico. EMCORE solar cells or panels have helped supply energy to 130 space missions since 2001.

Efficiencies In R&D and in Practice

First Solar hits 21.0% thin-film PV record

First Solar has achieved a 21.0% conversion rate in a cadmium-telluride (CdTe) PV cell, a new record. Certified at the Newport Corporation's Technology and Applications Center PV Lab, the cell beats First Solar's own previous CdTe record set in February 2014 of 20.4% and surpasses the 20.9% CIGS thin-film record held by Japan's Solar Frontier (see below). The milestone also sets an all-time record for single-junction thin-film technologies, and has already been incorporated into the US National Renewable Energy Laboratory's 'Best Research Cell Efficiencies' chart.

First Solar set a new CdTe record.

Source: First Solar

First Solar said the cell had been built at its factory and R&D centre in Perrysburg, Ohio using processes and materials designed for commercial-scale manufacturing, suggesting the company is looking for a rapid incorporation of the new technology into its production lines.

CIGS cell efficiency of 15% targeted at Solar Frontier's 'blueprint' module factory

Solar Frontier will target a cell efficiency of 15% on the production lines of its new 150MW module factory. The company is currently building a module production facility in the north-eastern Tohoku region of Japan with a nameplate capacity of 150MW. Construction of the facility was announced late last year and began in March. The new factory will not only serve to meet existing demand for modules, but, the company claims, it will also serve as a "blueprint for future production facilities". The main idea is that by building a relatively small facility such as the 150MW Tohoku plant the company will gain knowledge and experience of building facilities as geographically close to the markets it is intended to serve as possible. In late July, Solar Frontier announced three senior management changes, including the promotion of vice president Atsuhiko Hirano to the position of president and

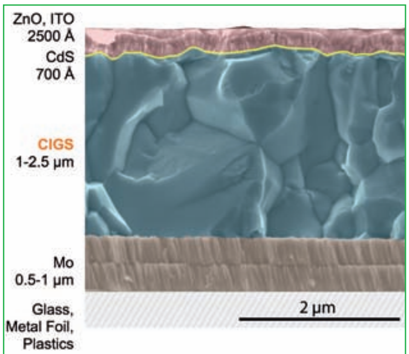

Cross section of a Siva cell.

Source: Siva Power

chief executive officer. Additionally, Solar Frontier has now been split from its parent company, Showa Shell and is now a separate entity.

Siva Power touts new CIGS low-cost roadmap Image

Start-up Siva Power has touted a revised low-cost roadmap for CIGS thin-film modules that would generate US$0.28/W on a single 300MW, fully-automated production line. Siva Power, formerly Solexant, had reported a lab-based CIGS cell efficiency of 18.8%, verified by NREL in December, 2013 as well as recruiting former head of Applied Materials PV operations and a former NREL director, Charlie Gay to its Technical Advisory Board. Currently Siva Power is only in the process of building a small mini-module pilot line, yet is claiming its modelled US$0.28/W cost is geographically agnostic, due to the use of commercially proven FPD (Flat Panel Display) equipment and technology. The 300MW production line was also said to have been modelled as the best scale for module production.

Solyndra Makes Low Key Return

Bankrupted Solyndra's modules make comeback in post-subsidy Europe

Some of the distinctive cylindrical photovoltaic modules produced by bankrupted US thin-film manufacturer Solyndra are being resold in Europe through Photon Energy, a PV solutions company headquartered in The Netherlands. Photon Energy said that despite the lack of warranties available, customers are happy to purchase the modules due to their low price, an increasingly decisive factor in the context of dwindling subsidies in some European countries. Solyndra developed proprietary technology for its unique modules, which were designed to be lightweight and durable while being of comparable efficiency to other copper indium gallium selenide (CIGS) thin-film modules. Solyndra specifically targeted the commercial rooftop segment of the market. The company's failure to compete on costs as crystalline prices plummeted in 2011 and 2012 was cited as the reason it eventually went bankrupt.

Funding News

Ascent Solar secures US$32 million in deal with investors

Thin-film PV module developer and manufacturer Ascent Solar Technologies, Inc. has reached an agreement with investors that will see the company secure US$32 million in senior secured notes and warrants in order to buy shares of its common stock in a private placement. The deal was expected to close by late July, 2014. WestPark Capital, Inc. served as the only placement agent. Ascent Solar will receive US$7 million at the closing of the transaction and will gain the remaining US$25 million over an 18-month period through instalments. The notes will carry an 8% annual interest rate and will also mature on the fifth anniversary of closing. The notes can also be converted, in whole or in part, onto shares of Ascent Solar's common stock at the value of US$0.5246 per share.

Rollable solar system beats crowd-funding target

A flexible, transportable solar array that can be easily deployed or stored has taken one step closer to launching after raising £263,000 (US$435,000) through an online crowdfunding campaign. UK cleantech start-up, Renovagen has developed a rollable solar array that uses flexible thin-film solar cells attached to a tensile fabric – allowing the system to be stored on an electric spool. The 'Roll Array' product is aiming to compete with diesel generators. The company believes that the rollable solar array will be especially useful for military applications, disaster relief, mining and events. Renovagen estimates that a standard 20-foot shipping container could house a 100kWp Roll-Array. In addition, multiple systems can be used to generate multi-megawatts of transportable energy. Renovagen will continue to field test its prototype with an eye towards a full product launch in 2015.

Thin-Film Fab News

Masdar PV a-Si thin-film plant in Germany to close

One of the last remaining a-Si thin-film manufacturing plants in production globally and the last in Germany is to close with the loss of 160 jobs at Masdar PV in Ichterhausen. Owned by Mubadala Development Company of the UAE, Masdar PV had been a turnkey client of Applied Materials and had occasionally supplied various sizes of a-Si modules to both ground-mount and BIPV projects over the last five-years since production started in late 2009. The company cited the significant collapse in conventional c-Si modules due to massive overcapacity for its inability to be competitive. However, overcapacity has eased significantly as global end market demand is expected to reach almost 50GW in 2014, yet a-Si thin-film costs and efficiencies have lagged the mainstream market, causing the vast majority of a-Si module producers to close down operations in the last few years.

Hevel Solar starts tandem-junction a-Si thin-film production in Russia

Russian thin-film module manufacturing start-up Hevel Solar has started trial production of its Oerlikon Solar-supplied turnkey tandem-junction 'Micromorph' a-Si plant. The company, which is said to have a nameplate capacity of 120MW, is a joint venture with Russian technology firm Rusnano expects to ramp production in the second half of 2014 to meet previously planned supply of modules for PV projects with financing from Rusnano and partnerships with state-run construction firm Avelar. Hevel Solar said that 200,000 modules would be produced by the end of the year for the construction of PV power plants with an installed capacity of 25MW. The production plant was said to employ around 230 workers, which currently included 45 employees from TEL Solar, which previously acquired Oerlikon Solar, yet decided to stop a-Si thin-film equipment development and sales but continue to support its customer base.

Project News

Hanergy plans PV projects in Japan through partnership with Sojitz Machinery Corporation

Hanergy Global Solar Power & Applications Group, a subsidiary of Hanergy Solar Group Limited, has signed a strategic partnership framework with Sojitz Machinery Corporation – one of the largest trading corporations in Japan. As a result of the agreement, both companies plan to construct a multitude of PV projects, including a 10MW thin-film electricity generation plant in Japan, which is scheduled to begin construction in March 2015.

First Solar to develop first project in India with 45MW plant in Telangana

US thin-film manufacturer, First Solar is to build its first solar development in India, a 45MW solar power plant in the state of Telangana. The project is to be constructed in the Mahabubnagar district, in the former southern half of Andhra Pradesh, the new Indian state of Telangana. Electricity from the plant is to be sold to the Southern Power Distribution Company of Telangana (TSSPDCL) with a tariff of INR6.49/kWh (US$0.107), agreed in a 20-year power purchase agreement (PPA). The plant is scheduled for completion by May 2015. First Solar enjoyed early success in India but struggled in a recent solar capacity auction.

Fab & Facilities

Materials

Cell Processing

Thin Film

PV Modules

Power Generation

Competitiveness of CIGS technology in the light of recent PV developments – Part II: Cost-reduction potential in CIGS production

Ilka Luck, PICON Solar GmbH, Berlin, Germany

ABSTRACT

A detailed analysis of state-of-the-art CIGS technology has resulted in a direct cost of ownership (CoO) of €0.44/Wp for this PV module type. However, the reduction in production costs, although impressive, is not sufficient for CIGS to become competitive with today's c-Si technology. In order to answer the question as to whether CIGS will ever be able to challenge c-Si, the cost-reduction potential of CIGS is investigated. The impact of savings is evaluated in respect of the material segment, production equipment, energy and labour, production yield, device efficiency and absorber thickness. A total cost-reduction potential of around €0.21/Wp is identified, which would be enough to put CIGS back into the game (the direct CoO will continue to be dominated by material and equipment depreciation, adding up to 68%). These cost reductions, however, cannot be realized immediately: within the next two years, €0.03/Wp is expected to be feasible, while it will take two to four years for the next €0.107/Wp. For the final €0.073/Wp, a time frame of at least five years is predicted, with corresponding costs for the technology developments. Provided that someone is willing to spend the necessary amount of time and money, the second part of the answer regarding CIGS' competitiveness will depend on how c-Si evolves within this time period.

Introduction

In the previous edition of *Photovoltaics International* the current status of $CuIn_{1-x}Ga_x(Se_{1-y}S_y)_2$ (CIGS) production was analysed [1]. The cost of ownership (CoO) for CIGS module production, according to the author's calculations, is today around €0.44/Wp – and this is only under best-case assumptions. Fig. 1 reveals that around 70% of this cost has to be allotted to materials and depreciation. The €0.44/Wp figure signifies great progress with regard to CIGS production costs, but is still clearly above the best-in-class results of the US$0.50–0.55/Wp cost reported for c-Si module production. However, when talking about production costs, it must be borne in mind that the discussion here is about *direct* production costs. One example of all-in costs for PV module production can be taken from REC Solar ASA's first-quarter results released on April 25th 2014: US$0.67/Wp including SG&A and special items.

For CIGS to become competitive, further reductions in production costs are essential; the potential for accomplishing this will therefore be evaluated in this second paper. The main cost drivers identified in the current status analysis will be examined: materials, equipment depreciation, energy and labour, and production yield. Technology improvements – such as higher device efficiencies and thinner CIGS absorber layers – will also be looked at. The discussion will focus on how potential cost reduction could be achieved, the calculation of how it would influence the direct production costs, and the probability of its being realized.

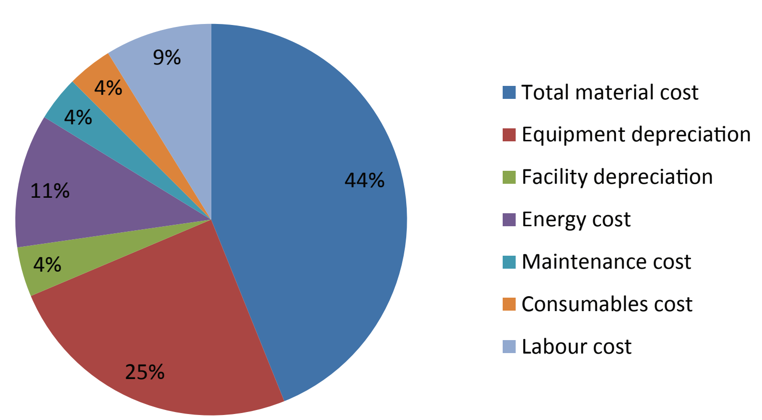

Figure 1. Relative cost contributions of various segments to the CoO for CIGS module production.

Cost-reduction potential: materials

The basic assumptions made here concerning target utilization and transfer coefficients show that during device deposition a significant part of the raw materials does not end up in the device. A better utilization of materials therefore reduces the costs for the coating materials.

"During device deposition a significant part of the raw materials does not end up in the device."

To evaluate the impact on the CoO, the following improvements concerning material utilization are assumed:

- The rotatable target utilization is increased by 10%, to 85%.
- The sputter transfer coefficient is increased by 10%, to 65%.
- The evaporation transfer coefficient is increased by at least 10%.

The successful implementation of these improvements decreases the coating material costs, and consequently the direct CoO, by around €0.02/Wp; coating material costs would then amount to €0.05/Wp. However, while it is very easy to write down these numbers, it takes hard and long-drawn-out work to achieve these improvements. Furthermore, with so few ongoing CIGS activities at the moment, CIGS producers are highly dependent on technology progress induced by other products, rather than improving sputtering and evaporation technologies themselves within a relevant time window. The most significant leap forward with regard to material costs – the change from planar to rotatable targets – has already been implemented. The numbers quoted above are therefore considered a necessary but highly ambitious and long-term goal.

In arriving at these figures no account was taken of the fact that if the material utilization increases, the capacity of a given production line increases as well, which translates into lower capital expenditure. This leads to an even greater reduction in production costs, as will be shown in the next section; to what extent this occurs largely depends on the specific technology of a production line.

Current status – total material costs	30% saving	50% saving
€0.193/Wp	€0.162/Wp	€0.141/Wp

Table 1. Cost-reduction potential for the total material costs as a result of 30% and 50% procurement savings on glass, encapsulation materials and the junction box.

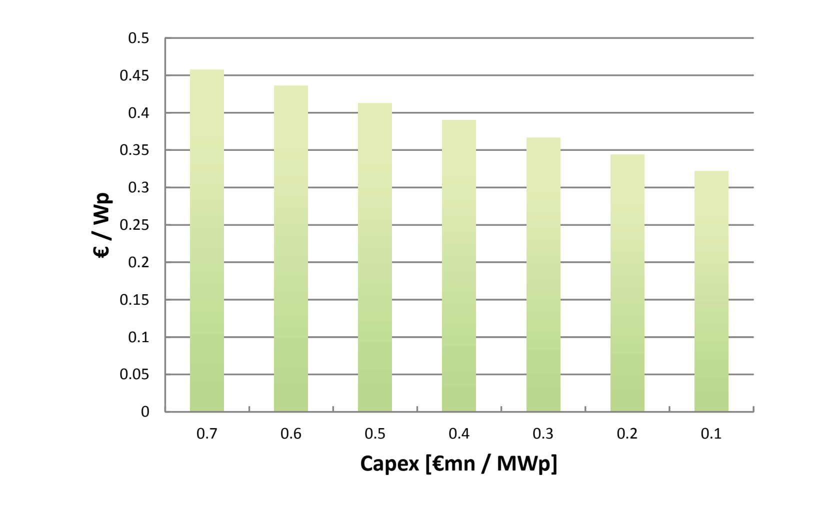

Figure 2. Impact of capital expenditure on direct CoO for CIGS module production.

Another, and much easier, way of reducing material costs is to purchase at lower prices: significant material cost reductions should be achievable by procuring glass, encapsulation materials and the junction box in Asia, and specifically China. The impact of 30% and 50% procurement savings for these items on the total material costs is shown in Table 1: more stringent procurement saves €0.03/Wp, or even €0.05/Wp. The result also impressively reconfirms the truism that "for material-intensive products, procurement is everything". A value of 30% is considered by the author to be feasible with reasonable effort, whereas 50% is (too) ambitious to be achieved within a meaningful time frame.

"CIGS production equipment is more expensive than that for standard c-Si cell and module production."

Cost-reduction potential: equipment depreciation

Although the financial investment required for CIGS has come down significantly in recent years, CIGS production equipment is still more expensive, by at least a factor of six, than that for standard c-Si cell and module production. Fig. 2 indicates the impact of this difference on the direct CoO for CIGS: every €100,000 reduction in capital expenditure diminishes the depreciation and the production costs by approximately €0.022/Wp. A capital expenditure of €0.1m/MWp, equivalent to that for c-Si, would make CIGS more competitive; a value of €0.3m/MWp would be sufficient for CIGS to realize similar direct production costs to c-Si. However, considering the huge progress made in this field during the last few years, and that fairly often large-area and high-vacuum equipment is involved,

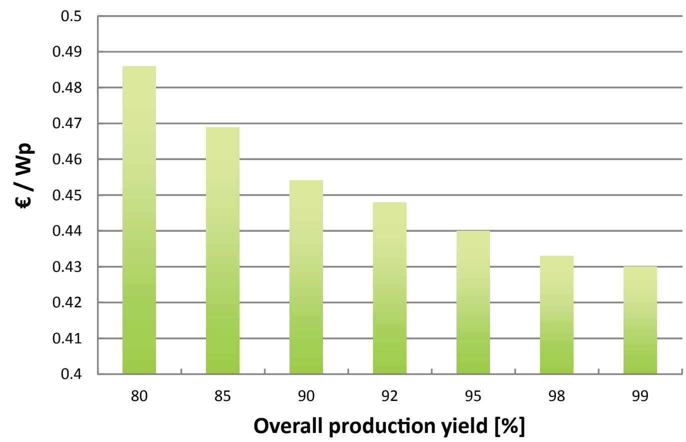

Figure 3. Impact of overall production yield on CoO.

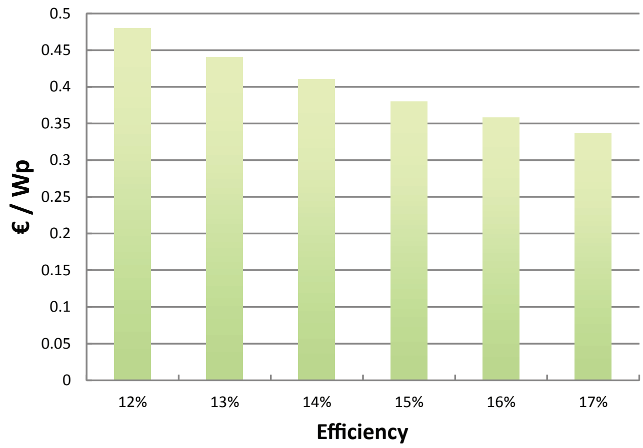

Fig. 4. Impact of module efficiency on CoO.

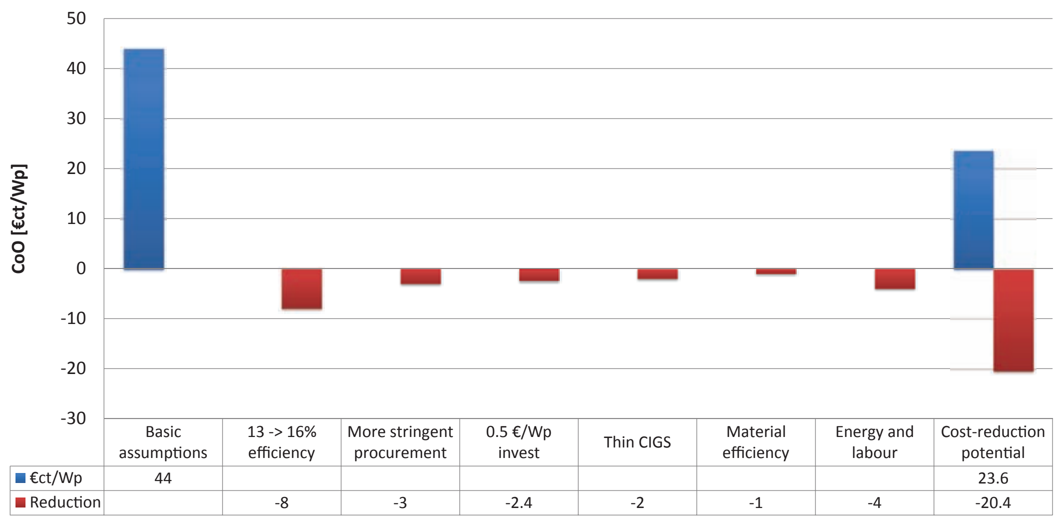

Figure 5. Contributions of the various elements to the cost-reduction potential.

capital expenditures any lower than €0.5m/MWp are not expected to be seen in the near and mid term.

Cost-reduction potential: energy and labour

Two other fairly significant cost factors, with a contribution of around 10% each to CIGS production costs, are energy and labour. If it is assumed that both factors can be reduced by 50%, the savings in terms of direct CoO are a little over €0.02/Wp for cheaper electricity and just under €0.02/Wp for a less costly labour force. A cost reduction in both these factors can be realized by a careful and cost-aware choice of the production site; such a production site is likely to be found outside of Europe and North America.

Cost-reduction potential: production yield

So far, the production yield has only appeared as one of the assumptions for the CoO calculation. A 95% overall yield is estimated, which is mandatory for production in the semiconductor sector but is ambitiously high for thin-film PV production. It is very likely the most optimistic of the assumptions made for this CoO calculation.

Fig. 3 demonstrates how different yields influence the production costs: increasing the yield brings down the CoO in a continuous way. However, an increase in yield from 95% to 98%, which requires significant efforts on the shop floor, only results in less than €0.01/Wp cost savings. There are better opportunities elsewhere that can be exploited to reduce production costs more impressively with fewer struggles once the production has reached this level. Accordingly, no contribution is expected from this segment, and if anything, a downturn is anticipated rather than an upturn.

Cost-reduction potential: efficiency

The negative impact of the low efficiency of CIGS modules compared with c-Si modules has already been discussed in the previous paper [1]. To avoid the disadvantages due to per item costs – such as the junction box – and sealing and area penalties in the PV system, it is absolutely essential to boost the efficiency to at least 16% in order to achieve cost competitiveness for CIGS production.

Fig. 4 shows that 16% efficiency cuts the production costs to a competitive €0.36/Wp. Well, paper does not blush: it took the industry two years to increase efficiency by 1%. Even if it is assumed that this development speeds up, because consolidation turmoil irritations and timely financing procedures are now over, these higher efficiencies are not envisaged anytime soon – in any case, no earlier than four to six years from now. One has to keep in mind that the more a technology matures, the more cumbersome the implementation of the improvements becomes.

> "It is absolutely essential to boost the efficiency to at least 16% in order to achieve cost competitiveness of CIGS production."

The derivation of these figures does not take into consideration the fact that increasing the efficiency also increases the capacity of a given production line, which again translates into lower capital expenditure. As shown in a previous section, this reduces production costs even further; the extent of such reduction is highly dependent on the specific technology of a production line.

Cost-reduction potential: thinner CIGS absorber

An absorber thickness of 1.6μm was assumed for CIGS in the initial

Cost structure	€/Wp Current status		€/Wp Cost reduction potential	
Total material cost	0.193	44%	0.099	43%
Equipment depreciation	0.109	25%	0.057	25%
Facility depreciation	0.018	4%	0.015	6%
Energy cost	0.049	11%	0.022	9%
Maintenance cost	0.016	4%	0.011	5%
Consumables cost	0.016	4%	0.011	5%
Labour cost	0.039	9%	0.016	7%
Total cost	0.440		0.231	

Table 2. Absolute and relative cost contributions of various segments to the current and to the mid- to long-term CoO of CIGS.

calculation, but the absorption coefficient of this material allows even thinner absorbers. From the physical point of view, a homogeneous layer of 1.2μm is sufficient for the proper functioning of the device; the subsequent reduction in material usage translates into a cost reduction of €0.008/Wp. More important than the material savings is the increase in production capacity or the reduction in capital expenditure, since less equipment is required for co-evaporation. If a ballpark figure of a 10% reduction in capital expenditure is assumed, the reduced amount of equipment aspect adds another €0.014/Wp to the cost-reduction potential.

Summary

The analysis presented in this paper regarding the cost-reduction potential of CIGS has revealed numerous segments where cost savings appear to be achievable. Better material utilization, more stringent procurement, lower capital expenditure for the production equipment, selection of low-cost production sites, higher device efficiencies, and thinner absorber layers may add up to a total potential cost saving of €0.204/Wp. Future production costs of €0.236/Wp for CIGS appear reasonable. Fig. 5 summarizes the impact of the various segments on the direct CoO.

> "Future production costs of €0.236/Wp for CIGS appear reasonable."

As regards the various segments and actions within them, it is helpful to differentiate these according to technical feasibility and the corresponding timeline for achieving the cost reduction:

- *Short-term achievability, with low technical complexity.* The only action that features these properties is a more stringent procurement in the materials segment. This action can be taken immediately and is completely within the producer's control. If the time effort for sourcing, testing and recertification is considered, an impact on the cost structure can be expected within one to two years.

- *Medium-term achievability, with low to medium technical complexity*. This category includes energy and labour savings as a consequence of newly identified production sites. The setting up of new production sites will also help new generations of equipment to come online, which will also further reduce the capital expenditure. The impact of these actions is expected to become noticeable in production costs within two to four years. An increase in efficiency to 14–15% for the module in this category is also anticipated.

- *Long-term achievability, with medium to high technical complexity*. This category is where an efficiency increase to 16% and beyond belongs. Of similar technical difficulty to this are the shift to thinner absorber layers and the improvements in material utilization. In the case of the latter, only 50% of its potential was considered in the evaluation of overall cost reduction of CIGS. The impacts on production costs are expected no sooner than five years from now.

The contributions of the various segments to the mid- to long-term CoO of CIGS are listed in Table 2. To obtain these numbers, all changes were simultaneously fed into the computer model. This approach gives rise to slight differences in absolute values for some of the segments and to the even lower production costs. If their relative proportions are compared with the current status analysis, no major changes are observed.

All four major cost drivers contribute to cost-reduction potential, with the cost structure remaining dominated by the material costs. Although equipment depreciation has fallen, it has not come down sufficiently to be of low significance. Energy and labour add their share to the cost-reduction potential, but keep their relative significance. The facility depreciation, maintenance and consumables segments have not been evaluated for their cost-reduction potential separately, because of their low relative shares.

It is appreciated that the calculations to the third decimal place made here suggest more accuracy than can actually be obtained, with so many assumptions on future developments involved. Nonetheless, the accuracy of this evaluation is sufficient for illustrating the impressive cost-reduction potential of CIGS. Production costs of €0.23/Wp would help significantly in making solar electricity highly competitive worldwide; however, the road to realization is expected to be a lengthy and costly one. And one should not ignore the fact that c-Si production costs are a moving target that will continuously challenge the cost competitiveness of CIGS.

Acknowledgement

I would like to thank my colleagues Dr. S. Schuler and Ms. E. Benfares, without whose support this article would not have been written.

References

[1] Luck, I. 2014, "Competitiveness of CIGS technology in the light of recent PV developments – Part 1: The state of the art in CIGS production", *Photovoltaics International*, 24th edn, pp. 69–72.

About the Author

Dr. Ilka Luck founded PICON Solar GmbH in 2008 to provide consultancy services for the PV industry. Prior to that she was managing director of Global Solar Energy Deutschland GmbH and founder and general manager of Sulfurcell Solartechnik GmbH. She has also co-founded several other companies in the renewable energy sector. She holds a doctorate and diploma in solid-state physics and an MBA.

Enquiries

Dr. Ilka Luck
PICON Solar GmbH
Wrangelstraße 100
D-10997 Berlin
Germany

Tel: +49(0)30 8145264-502
Email: luck@picon-solar.de
Website: www.picon-solar.de

PV Modules

News

China wants talks on settlement in US solar trade case

Lawyers representing China's government have asked the US Department of Commerce (DoC) to begin talks on a suspension agreement in the ongoing solar trade dispute between the two countries. According to the DoC, a suspension agreement would put preliminary anti-dumping duties, and the requirement of cash deposits, on hold until an alternative agreement to nullify any unfair trade is agreed. The current filing does not apply to the anti-subsidy case. A document sent on behalf of the Beijing government requested talks, but no firm proposals on the substance of any talks was submitted. Earlier in August, the original petitioner, SolarWorld Americas, and the Solar Energy Industries Association (SEIA) engaged in a public row over proposed agreements.

Many in the industry would like to see a settlement but its unlikely to be an issue for the country's respective leaders in the immediate future.

Source: White House

Anti-Dumping Continues to Rock Module Exports

India rejects solar anti-dumping duties

The Indian government has decided against imposing duties on Chinese, Taiwanese, US and Malaysian solar manufacturers. The ministry of commerce had recommended duties of up to US$0.81/W for Chinese firms, but after consideration, the finance ministry has rejected the duties. A deadline of 22 August had been set but was allowed to pass without the introduction of punitive trade tariffs. Thin-film manufacturer, First Solar would have faced US$0.11/W while US silicon-based panels would have been subject to US$0.48/W duties. Malaysian manufacturers were facing US$0.62/W and Taiwanese firms, US$0.59/W.

Domestic Content to the Fore

Brazil confirms details of PV local content rules

Brazil's national development bank, BNDES, has released details of the new local content requirements that solar projects must fulfil to access finance. The conditions are only for solar developers who win bids in the upcoming reserve (LER) auction's solar-specific category. The conditions are to help create a national production chain for domestic PV manufacturing in Brazil. BNDES said in a statement that the aim of the funding is to "seize the opportunity" presented by the solar auction to kick start a domestic PV supply chain. The LER auction is to be held on 31 October, and is the first time that national energy auctions have allowed solar to have its own section of the auction. Only solar projects that meet the BNDES criteria for domestic content will be funded by the bank. Solar projects must have registered for the BNDES' accreditation of PV equipment prior to bidding to be awarded funding. The register was launched this August.

India tells manufacturers to run at full capacity and expand

The government has promised to support all domestic solar manufacturing and has encouraged plants to run at full capacity and expand. Minister for power, coal, new and renewable energy, Shri Piyush Goyal told developers, manufacturers and stakeholders that the government will provide full support for domestic solar manufacturing, according to the Press Information Bureau for the Government of India's Ministry of New and Renewable Energy (MNRE). The move to support domestic manufacturing follows the recent dismissal of anti-dumping duties (ADD) on foreign imports, after industry experts argued they would decrease overall deployment and hurt the solar industry in India as a whole. This is despite the ministry of commerce ruling that dumping had occurred, recommending US$0.11 to US$0.81 in duties, and domestic manufacturers, such as Tata Power, arguing India's solar manufacturing will be "dead in six months" without ADD. In response, the government is now "open to provide all support", the MNRE statement said.

Financial Results Bring Good News

ReneSola stretches profit margin

PV module manufacturer, ReneSola, reported increased profits and a higher margin in its Q2 2014 results. Revenue was US$387.1 million compared to US$377.4 million in the same period last year. Profit was US$56.9 million, with a margin of 14.7%, up on US$30.4 million and a margin of 8% in Q2 2013. Module shipments were 498.7MW, up on 434.1MW in Q2 last year. The company cited savings from its polysilicon plant resuming 100% operation and the increased use of wafers for internal use as a contributing factor to its results. Guidance for Q3 2014 was announced as 530-550MW and a margin of 15-17%.

Meyer Burger cites beginning of PV equipment recovery as sales increase

Switzerland's Meyer Burger has confirmed the beginnings of a recovery for PV equipment manufacturers after posting encouraging first-half results. Although the company said it continued to be "cautious" about the market for PV equipment, it cited the beginnings of a "certain recovery" following the hammering taken by equipment suppliers in the recent industry downturn. These were reflected in results that showed orders up 90% on the same period last year and a book-to-bill ratio up to 1.21 from 0.9 last year.

SunEdison posts profit as projects business makes gains

SunEdison posted US$0.12 earnings per share (EPS) profit in the second quarter of 2014 as the company's projects business enjoyed strong growth. The company has negotiated a complex financial period of late with the IPO of its semiconductor division, a bond placement and the IPO of its spin-off yield co, TerraForm Power, shortly after the conclusion of Q3. Revenue of US$646.2 million was an improvement of 61% on the same period last year. EPS in the same period last year was a loss of US$0.19. It retained an additional 164MW of projects on its balance sheet, 44MW higher than the upper end of its guidance. Backlog increased 100MW to 1.1GW and the pipeline as a whole added 700MW since the last quarter to 4.3GW.

New Module Certifications

Trina Solar's 72-cell frameless dual glass module gains quality certifications

Major PV manufacturer Trina Solar has received quality certifications, including the IEC61215, IEC 61730 and UL1703 standards from UL and TUV Rheinland for its 'Duo-Max' 72-cell frameless dual glass module. The PEG14 and PDG14 series modules are typically designed for utility-scale PV power plants often located in harsh environments such as deserts. Trina Solar said that its Duo-Max modules also meet UL's Fire Class A safety standards as well as meeting PID testing conditions of 1500V system voltage under relative humidity of 85% and a temperature of 85°C for 192 hours. Both the 60-cell and 72-cell Duo-Max series modules carry a 30-year linear warranty with a maximum annual degradation of 0.5%.

Source: Trina Solar

More certs for Trina's module range.

WINAICO PV module passes stringent IEC 61215 hail impact test

Taiwan-based PV module manufacturer, WINAICO, a division of Win Win Precision Technology, has secured IEC 61215 certification via TÜV Rheinland. IEC 61215 certification includes tests to ensure modules withstand the impact of 35mm diameter hail stones travelling at a speed of 27.2 m/s or over 98 kph. WINAICO said that its WST-250P6 series modules, survived the newer test that involves projectiles with approximately four times the kinetic energy of the standard 25mm stones travelling at 23 m/s (83 kph).

Module Supply Contracts Confirmed

ReneSola to supply 22MW of modules to UK solar projects

Chinese manufacturer, ReneSola, is to supply 22MW of its modules to two solar projects in the UK. ReneSola UK will provide its polycrystalline Virtus I and Virtus II solar modules to two ground-mount solar plants. The first project is the 10.8MW Low Carbon project in Bottom Plain in Dorset. ReneSola's modules will also be supplied to the 15.6MW Cofely GDF Suez project in Bilsham Farm, Arundel. The solar power plant is part of a local initiative to provide clean energy for the grid and will power 3,600 homes. The two solar farms will incorporate two module sizes of 250W and 255W, to increase efficiency.

Yingli continues Japanese PV surge with 30MW supply deal

Manufacturer Yingli Solar's subsidiary, Yingli Green Energy Spain, has agreed to supply 31.6MW of modules to Spanish developer, Gestamp Solar. The 125,000 multicrystalline YGE 60 Cell Series are to be supplied between: October 2014, to February 2015, for a plant to be located in Daigo, Japan, built on a former golf course in the Ibaraki Prefecture. The plant is predicted to generate 33GWh a year. Grid connection is scheduled for April 2015 and electricity will be sold to the Tokyo Electric Power Company (TEPCO). The plant will qualify for government support under Japan's feed-in tariff (FiT) and is the first Gestamp solar project to be built in Japan. Yingli CEO, Liansheng Miao said the company's shipments to Japan increased by 50% in the first quarter of 2014, in comparison to the last quarter of 2013.

Hanwha Solar One supplies Inner Mongolian PV project

Module manufacturer, Hanwha Solar One has signed a 50MW module supply deal for a project in Inner Mongolia. The agreement is with Baotou Shansheng New Energy, a subsidiary of the Inner Mongolia Shanlu Energy Group. The delivery of Hanwha's modules began at the start of August and is to be complete by mid-September. The modules will be installed at two ground-mount projects in the capital of Inner Mongolia, Hohhot, and the largest industrial city of the region, Baotou, northern China. Hanwha Solar One said there had been a surge in business opportunities since the third quarter of 2014, and was is optimistic that market demand in China will continue to be substantial throughout 2014. China has just set a 13GW solar target for 2014 and has installed 3.3GW of solar power capacity in 2014 so far.

Hareon Solar signs multiple PV project deals totalling 3,350MW

China-based PV energy provider, Hareon Solar Technology, has signed a number of project development deals in China and Turkey totalling around 3,350MW. The company has also secured lines of credit with two Chinese banks totalling RMB20 billion (US$3.25 billion). Hareon Solar's overseas project pipeline through 2017 recently stood at around 6.27GW. A key portion of the pipeline was in Turkey at around 3.3GW. The company said in financial filings in China that it had signed a cooperation framework agreement with the Turkish Agricultural Credit Cooperative Central Union (TKKB) and Swiss-based, ILB Helios Energy, to build PV power plant projects in collaboration with TKKB's 11 million farmer members, totalling around 2.5GWp over the next three years. An initial 'pilot' project totalling 300MW was said to be the first phase of the partnership that is expected to complete planning phase in the third or fourth quarter of 2014.

Yingli Green to supply 2MW to Japanese commercial rooftop project

Yingli Green Energy has announced that it will supply modules to a 2MW commercial rooftop project in Japan, which will be built by engineering, procurement and construction (EPC) firm Benex Japan. Through its Japanese subsidiary, Yingli will supply around 8,000 of its monocrystalline PANDA modules to the project, Benex Nagareyama Solar Port, Chiba Prefecture. The shipments are scheduled to be delivered by the end of this month, with the project due to be connected to the grid in October. Yingli claims it will generate around 2,150,000kWh of energy annually. Activity in the Japanese market has been dominated by high-profile, ground-mounted projects and the project remains unusual in scope for the country. Additionally, the project is being hosted on a rented rooftop, making it even rarer. Ground-mount projects continue to be built but land shortages and grid interconnection have meant the sector has stumbled.

Source: Wikimedia

Yingli's Mount Komekura plant.

Benex Japan executive vice president, Yohei Kobayashi said the project was limited by a small roof, making Yingli's high efficiency PANDA modules a good fit.

News

Product Reviews

BenQ Solar

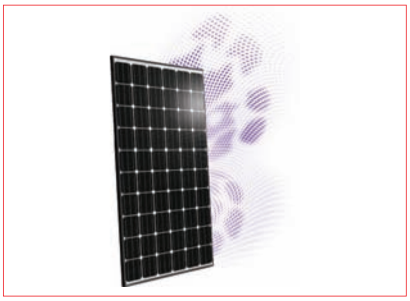

BenQ Solar offers high-performance ultra-light monocrystalline module

Product Outline: BenQ Solar, a division of AU Optronics, has developed an ultra-light monocrystalline module weighing only 10.5kg (5.3kg/m2), with a maximum power output of 285W. The module is designed for low-stress rooftops and was initially supplied to the Japanese residential market.

Problem: With the continued strong demand for high-performance and cost-efficient residential solar solutions across a growing geographical base, lightweight modules are essential for low-stress rooftops and are used in earthquake zones.

Solution: The Aer PM060M01 module is approximately 45% lighter than conventional counterparts, making it one of the world's lightest 60-cell modules. It is safe to be installed on thin metal-sheet roofs, which effectively reduces the risk of collapsing if an earthquake strikes. The module complies with advanced loading tests to meet 5400Pa loading requirements.

Applications: Low-stressed residential and commercial rooftops, including thin metal-sheet roofs.

Platform: BenQ Solar partnered with IRFTS, the French company renowned for building-integrated photovoltaics (BIPV) mounting systems, to deliver the lightweight 'EASY ROOF EVOLUTION' mounting system, weighing only 4.2kg, which is flexible, easy to install and aesthetically pleasing in design. BenQ Solar offers the G-Racking Series for different roof types.

Availability: Currently available. Initially available to the Japanese residential market.

Agfa

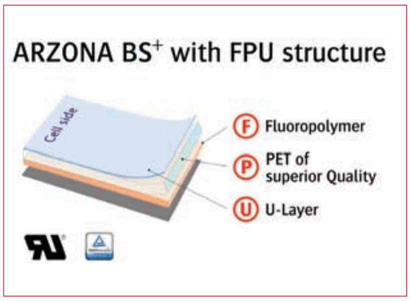

Agfa's 'ARZONA BS+' PV module backsheet provides humidity and UV protection

Product Outline: Agfa's 'ARZONA BS+' is a high-performance backsheet for crystalline silicon PV modules that builds on Agfa's 100+ years of experience in chemical-coating formulation, polyester extrusion and multi-layer coating know-how. ARZONA BS+ is a clear film based on polyethylene terephtalate (PET) with high-quality coated layers on both sides to provide extra protection against humidity and UV.

Problem: The backsheet material is required to withstand long-term environmental impact, providing strong adhesion and protection to the module's solar cells in order to meet a module lifetime expectation of over 25 years.

Solution: ARZONA BS+ uses a unique coated FPU-layer structure, i.e. fluoropolymer/polyester/UV-protection, to provide long-lifetime power output efficiency, durability and safety. On the cell side, the PET core layer is coated with Agfa's U-layer, providing strong adhesion to the encapsulant and protecting the core against UV radiation. On the air side, a fluoropolymer-coated layer offers protection against humidity and UV.

Applications: Backsheets for crystalline silicon PV modules.

Platform: ARZONA BS+ is a backsheet with a PET core, characterized by excellent mechanical properties, and is claimed to have one of the lowest shrinkage levels available on the market.

Availability: Currently available.

Solvay

Solvay develops two high-performance PV film grades for front-sheet applications

Product Outline: Solvay Specialty Polymers has launched two new high-performance film grades of its 'Halar' ethylene chlorotrifluoroethylene (ECTFE) – Halar PV ECTFE and Halar ECTFE UV blocking technology – which have been specifically designed for PV module front-sheet applications.

Problem: Critical film requirements for front sheets include low water vapour permeation and excellent UV resistance, a high degree of visible light transmission, a service life of up to 25 years and, in some cases, increased mechanical impact strength.

Solution: Halar PV ECTFE offers greater fire resistance, higher tensile modulus and lower density than its direct competitors. The new PV film grade is an excellent water vapour barrier (<1g/m2/day) in a wide range of temperatures and offers strong chemical and fire resistance and long-term weatherability, making it suitable for 20+ years of direct exposure to sunlight. Films made of Halar ECTFE exhibit nearly an order of magnitude lower permeation rate than ETFE, as well as better mechanical properties than competitive products, allowing thinner films and a reduction in the cost of front sheets. Offering the same properties as Halar PV, the new Halar UV blocking technology also delivers long-lasting UV blocking performance to meet the solar industry's 25-year PV module performance lifetime.

Applications: Front sheets for PV modules.

Platform: Films are available up to 1.5m wide and 50µm thick.

Availability: Currently available.

Reliability testing of backsheets: Thermal analysis for comparing single and module aged films

Gernot Oreski[1], **Marlene Knausz**[1], **Gabriele Eder**[2], **Yuliya Voronko**[2,3], **Thomas Koch**[3] & **Karl Berger**[4]

[1]Polymer Competence Center Leoben GmbH, Leoben; [2]OFI Austrian Research Institute for Chemistry and Technology, Vienna; [3]Institute of Materials Science and Technology, Vienna University of Technology; [4]Austrian Institute of Technology (AIT), Vienna, Austria

ABSTRACT

The main objective of this study was to evaluate the suitability of thermal analysis for characterizing the stage of hydrolytic degradation of PV backsheets containing polyethylene terephthalate (PET) as a core layer. Additionally, the ageing behaviour of single backsheets was compared with that of backsheets incorporated within PV modules. Test modules using identical components (glass, encapsulant, solar cells, etc.), varying only in the type of backsheet used, were fabricated and artificially aged (damp heat: 85°C / 85% relative humidity storage up to 2000h). The material characteristics of the single backsheets and module-incorporated backsheets before and after artificial ageing were determined by thermal analysis. It was shown that the most significant changes between unaged and aged sheets can be observed in the cooling curve of the differential scanning calorimetry (DSC) runs. For all materials, a significant increase in the crystallization temperature was found. Furthermore, the results revealed no influence of the PV module lamination procedure on the thermal characteristics of the polymeric backsheets. Even after artificial ageing under damp-heat conditions, differences between single and module-incorporated laminated backsheets were negligible. The ageing-induced degradation effects of PET could be detected by DSC for all the aged sheets. It is therefore proposed that the testing of single PET-based backsheets under accelerated ageing conditions may be a practicable way to investigate the applicability of a new backsheet material for use in reliable PV modules.

Introduction

In the PV industry, discussions about reliability testing of materials and modules are still ongoing, with a particular focus on the ageing behaviour of backsheet films and their influence on PV module reliability. Among the reported failures of backsheets are delamination within the multilayer laminate, and embrittlement, leading to cracks, yellowing etc. [1–7]. Yellowing of backsheets, however, is reported to have no effect on the electrical performance of the modules [1]. The worst failures within backsheets are cracks and delaminations, because they allow enhanced water vapour and oxygen ingress into the PV module. Water vapour is known to have a critical impact on various degradation phenomena, such as corrosion of metal cell parts, potential induced degradation (PID) of PV modules, and encapsulant degradation [5–6]. As a consequence, these failure modes can impair the performance of a PV module and shorten its lifetime [4].

To fulfil all requirements, most backsheet films for PV modules are multilayer composites comprising three or more polymer layers. The outer layers have to be resistant to various weathering impact factors (irradiance, humidity, etc.). Fluoropolymers – for example polyvinylfluoride (PVF), polyamide (PA) or specially stabilized polyethylene terephthalate (PET) – are often used as protection layers. The main purposes of the core layer are to offer mechanical stability, act as a barrier against water vapour and oxygen, and provide electrical isolation; the most frequently used polymer for this purpose is PET. In some cases barrier layers – for example aluminium or silicon oxide (SiO_x) – are additionally incorporated between the protection and core layers in order to improve the barrier properties of the backsheet [7].

> “Should the individual components and materials be tested in isolation or when laminated within a PV module?”

Of particular interest is the question: should the individual components and materials be tested in isolation or when laminated within a PV module? On the one hand, individual component testing would simplify sample preparation and reduce costs; moreover, destructive tests methods – such as tensile tests or dynamic mechanical analysis (DMA) – can also be employed, which are very sensitive in detecting chemical and physical ageing processes. On the other hand, there remains the important question of material (in)compatibility and synergistic effects, and thus how the results of single materials and components correlate with those of specimens aged within PV modules. In the case of solar cell encapsulants, the testing of whole modules is preferred, since some interactions (PID, snail tracks, corrosion, yellowing, etc.) cannot be reproduced by ageing of the individual materials. Only the main applicability, the pre-selection or process unit improvements can be determined by the testing of an encapsulant material on its own. Backsheet films, however, when subjected to accelerated ageing and testing, seem to be less critical with respect to the installation situation, as fewer failure/degradation cases occur when they are combined with other PV module components.

Previous studies have shown that hydrolysis is the dominant ageing mechanism of PET, whereas the other materials used within the backsheets, such as fluoropolymers or polyamides, are not affected significantly by exposure to high humidity at elevated temperatures; in most cases the failure of the backsheet was caused by the

failure of the PET core layer [7–9]. Therefore, this paper focuses on the description of the ageing behaviour of the PET core layer of various polymeric multilayer backsheets, as the stability of this layer defines the reliability of the backsheet as a whole. Hydrolysis of PET results in polymer chain scission, leading not only to embrittlement, but also to physical ageing processes, such as post-crystallization or a decrease in free volume. Both embrittlement and physical ageing may result in a significant stiffening accompanied by crack formation in backsheets, and can be detected very well using destructive methods such as tensile testing [10].

Unfortunately, mechanical testing is not applicable to backsheets that have been incorporated into PV modules. Spectroscopic methods – such as Raman spectroscopy, which as a matter of principle allows the non-destructive testing of backsheet films as well as PV modules – can detect hydrolysis and other chemical ageing processes. However, a reliable assessment of the stage of hydrolysis, in other words the stage of embrittlement and crack formation, has not yet been achieved using a spectroscopic characterization of the polymers [7,10].

Although destructive, thermal analysis may be a possible approach to testing single backsheets as well as backsheets laminated within a PV module. The crystallization behaviour in particular may indicate changes in the chemical structure of a material, such as the decrease in molecular mass as a result of polymer chain scission caused by hydrolysis [11–13].

The main aim of this paper, therefore, is to evaluate the use of thermal analysis for characterizing the stage of hydrolytic degradation of PV backsheets containing PET as the core layer. In a second step, the ageing behaviours of PV backsheets with PET core layers after exposure to damp-heat (DH) conditions, both as a single film and when laminated within a PV module, are investigated and compared. The influence of material interactions on the reliability of the PET core layer within the PV module is discussed.

Experimental

In the study reported here, the ageing behaviour of four different types of backsheet, all of which contain PET core layers, from three different producers was investigated. The outer/inner layers of the backsheets were either 1) fluoropolymers (symmetric composition), or 2) stabilized PET on the outer side and ethylene vinyl acetate (EVA)/polyethylene (PE) as a primer on the inner side. Test modules consisting of a glass front sheet (float glass, 2mm), a fast cure EVA encapsulant, six polycrystalline Si cells, and polymeric backsheets were fabricated using a standard lamination process. The composition of all test modules was identical except for the type of backsheet used; a description of the backsheet films investigated is given in Table 1. Single backsheet films and one set of test modules were exposed to DH conditions at 85°C and 85% relative humidity (RH) for 1000h and 2000h. A second set of test modules and backsheets was set aside as original reference samples.

The thermal behaviour was characterized by means of differential scanning calorimetry (DSC) using a Perkin Elmer DSC 4000; the measuring programmes and parameters are listed in Table 2. Samples of the backsheets (~10mg) were cut and placed in 50µl pans with perforated lids. Samples from the modules were taken from the border regions. For each evaluation, an average was taken from at least two sample runs. Melting points, melting enthalpies and crystallization temperatures were evaluated in accordance with ISO 11357-3 [11].

Results and discussion

The results will be described and discussed by considering first the DSC curves of single backsheet films in their original state and then after ageing (DH storage). The description of the results will focus on the ageing behaviour of the PET core layer, which is mainly responsible for the mechanical stability, and thus the reliability, of the backsheets [8,9]. In the following step, single backsheets and sheets incorporated into modules in the original state will be compared. Finally, the ageing-induced (DH storage) changes at the module and component levels will be compared, and the influence of material interactions on the reliability of the PET core layer within the PV module will be discussed.

The results of the DSC runs (first heating, cooling, second heating) for backsheet B1 are shown in Fig. 1. For the first heating curve (in black) the first melting peak, T_m = 194°C, can be attributed to the PVF outer layers.

Abbreviation	Inner layer	Core layer	Outer layer	Thickness [µm]
B1	PVF	PET	PVF	340
B2	PVDF	PET	PVDF	325
B3	EVA/PE	PET | aluminium	PET	390
B4	EVA/PE	PET	PET	370

Table 1. Properties of backsheets used.

	Start	End	Time/ramp
Isothermal segment	20°C		5min
Segment 1	20°C	270°C	10°C/min
Isothermal segment	270°C		5min
Segment 2	270°C	20°C	10°C/min
Isothermal segment	20°C		5min
Segment 3	20°C	270°C	10°C/min

Table 2. Experimental parameters for DSC measurements (nitrogen atmosphere).

The highest melting peak with respect to temperature and area (T_m = 256°C) is attributed to the melting of the main fraction of the PET crystallites. A secondary melting peak of the PET core layer was found at 219°C, which can be attributed to small crystallites formed during exposure to elevated temperatures. This peak was not detected in the second heating run (red curve), which confirms its irreversible, ageing-induced character. Glass transitions or the thermodynamic melting of a polymer are reversible effects and will therefore be seen in each heating run, irrespective of the history of the polymer. The second heating run gives information about material-specific constants and includes only reversible effects; it plays a subordinate role in the analysis of ageing-induced changes. In the second heating run, the PVF melting peak was detected at 192°C and the PET melting peak at 248°C.

The first crystallization peak (T_c) on the cooling curve is attributed to PET (205°C) and the second to PVF (169°C). The information obtainable from the crystallization behaviour (i.e. cooling run) is rarely discussed in standard literature. However, it bears evidence of changes in the chemical structure of a material, such as the decrease in molecular mass because of polymer chain scission, etc. [12–13].

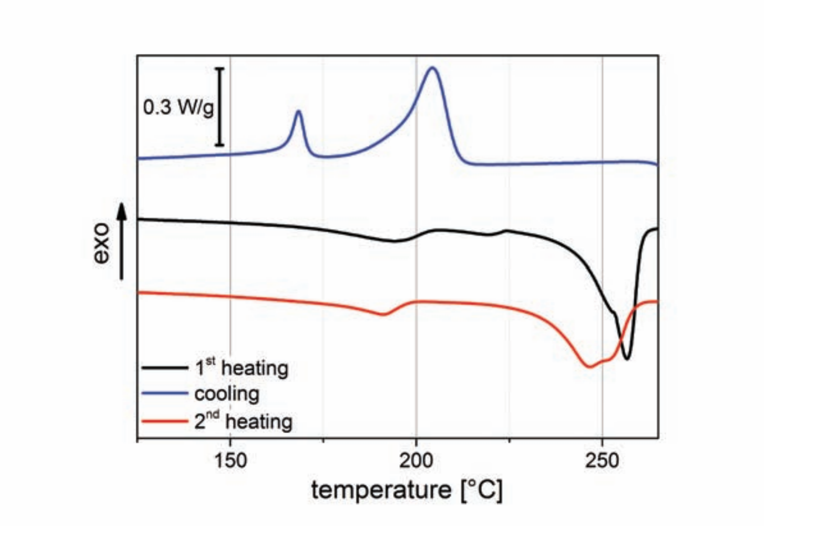

Figure 1. DSC curves for the initial state of single backsheet B1.

Post-crystallization of polymers results in an increase in the melting enthalpy as well as a shift to higher melting temperatures. Hydrolysis induces polymer chain scission, leading to a decrease in molecular mass and to a shift in the crystallization temperature to higher values as well as to an increase in the crystallization enthalpy [12].

For all backsheets the melting region of PET was found to be rather broad (230–270°C), although the maximum of the peak was highly reproducible in a very narrow temperature range, between 256 and 258°C. The maxima of PET on the crystallization curves varied between 204 and 214°C. For backsheets B3 and B4, a double peak of PET on the crystallization curves was seen, which can be attributed to the two PET layers (core and outer layer), which vary in composition. The outer PET layer is claimed to be hydrolysis- and UV-resistant: a different additive formulation, molecular mass distribution and/or crystallinity of the

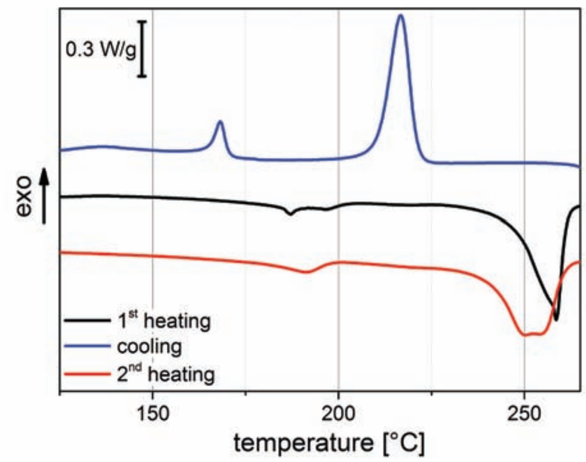

Figure 2. DSC curves after 2000h DH exposure of single backsheet B1.

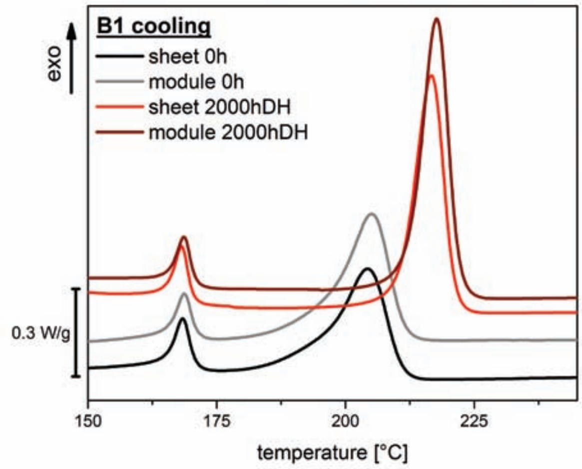

Figure 3. DSC cooling curves for the initial state and aged (2000h DH) samples of backsheet B1.

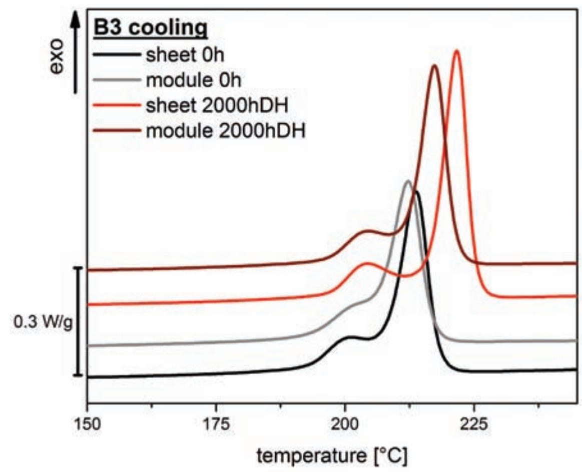

Figure 4. DSC cooling curves for the initial state and aged (2000h DH) samples of backsheet B3.

material is therefore expected.

The DSC runs (first heating, cooling, second heating) of backsheet B1 after 2000h of damp-heat testing are shown in Fig. 2. The maxima of the melting peaks of the PET materials lie between 258 and 259°C, with a standard deviation of less than 0.3°C; in comparison to the initial state samples, this means a small increase of ~1–2°C in the melting temperature. The melting enthalpies, on the other hand, show a significant increase. Both of these factors indicate a post-crystallization, which generally appears as a result of the ageing of PET at elevated temperatures [12]. The mechanism is enhanced because of the exposure of PET over the glass transition temperature (~80°C).

"Compared with the unaged samples, the aged samples exhibited an increase of ~5–13°C in the crystallization temperature."

The most significant differences between unaged and aged sheets can be seen in the cooling curve of the DSC runs. The maxima of the PET crystallization peaks of the various backsheet materials were found between 217 and 222°C, with a standard deviation of less than 0.4°C; compared with the unaged samples, the aged samples exhibited an increase of ~5–13°C in the crystallization temperature. Changes in the DSC cooling curve are related to chemical changes in the polymers. Polycondensation polymers are susceptible to hydrolysis, which in the case of PET is the cleavage of the ester groups in the polymer chain by the addition of water. This reaction therefore leads to chain scission and thus a reduction in average molecular weight. Crystalline parts of the polymer can be regarded as being impermeable to water vapour, so hydrolysis occurs solely in amorphous parts of the polymer or in imperfections in the crystalline zones [14,15]. All terminal groups produced during artificial ageing act as a nucleating agent for new crystals: as a consequence, smaller crystals, but with broader lamellae sizes, are formed, which is known to enhance crystallization temperatures [12,13].

The next step was a comparison between single backsheets and sheets incorporated into modules. In general, the DSC curves for samples taken from single sheets were comparable to those for samples taken from modules, for initial and aged samples. Fig. 3 shows the resulting DSC cooling curves for B1 for the initial stage and aged samples. The increases in the maximum of the crystallization temperature for B1, B2 and B4 are identical for samples taken from the single backsheet and from the module.

"The lamination process of the PV module has no influence on the thermal properties of the backsheets."

Two main conclusions can be drawn from these results. First, the fact that the curves for single backsheets and for sheets laminated into a PV module are almost identical confirms that the lamination process of the PV module (even though enhanced temperatures of up to 150°C are involved) has no influence on the thermal properties of the backsheets. Presumably, the lamination times of a maximum of 30 minutes do not lead to significant physical changes in the PET core layer. Second, the interactions between the materials in a PV module seem to be negligible in relation to the degradation behaviour of backsheets consisting of a PET core layer.

In contrast with the other samples, for backsheet B3 a significant increase in the crystallization temperatures of the PET core layer was observed for the samples taken from the single sheets compared with those taken from the module (see Fig. 4). The likely reason for this effect is the additional aluminium barrier layer, which is the only difference between backsheets B3 and B4. In the module, with the impermeable glass front sheet on one side and the impermeable aluminium layer between the outer and core layers on the other side, the ingress of water vapour into the PET core layer is restricted and thus hydrolysis/degradation is reduced [16]. This observation reaffirms the feasibility of thermal analysis for investigating the stage of hydrolysis of PET, as it demonstrates that the limited availability of water vapour because of a barrier layer leads directly to a smaller increase in crystallization temperature.

The DSC results showed that, for the reliability testing of backsheets for PV modules, generally no significant differences between single and module-incorporated aged sheets can be found. The only exception is backsheet B3, which contains a gas-tight Al barrier layer. The interactions between materials in a PV module are negligible in relation to backsheets.

"Generally no significant differences between single and module-incorporated aged sheets can be found."

As described above, evidence for the reliability and long-term stability of backsheets with PET layers can be deduced from the ageing-related changes derived from the thermal analysis. The DSC results of aged backsheets taken from single and module-incorporated sheets indicated post-crystallization and hydrolysis/degradation of PET. Nevertheless, further research is warranted in order to obtain a comprehensive knowledge of the chemical ageing processes and to support the results presented here.

Summary and conclusions

This paper has presented an evaluation of the suitability of thermal analysis for characterizing the stage of hydrolytic degradation of PV backsheets containing PET as a core layer. The question as to whether meaningful reliability testing of backsheets should be performed on backsheets laminated within a photovoltaic module or on single backsheets was examined. Single and module-incorporated, unaged as well as artificially aged, backsheets were tested.

The most significant differences between unaged and aged sheets were seen in the cooling curves of the DSC runs. For all materials tested, a significant increase in the crystallization temperature was found.

Moreover, the DSC results for the reliability testing of accelerated aged backsheets of PV modules revealed no significant differences between single and module-incorporated aged sheets. In the case of backsheets with a PET core layer, the results indicate that the reliability testing for the ageing characterization of single sheets yields meaningful results which can be directly correlated to the behaviour of the backsheets laminated within a module. The interactions between the materials in a PV module seem to be negligible for the stage of hydrolysis of the PET core layer of the backsheets investigated. It can therefore be concluded that the testing of single PET-based backsheets under accelerated ageing conditions may be a practicable way of investigating the applicability of a new backsheet material for use in PV modules to ensure their reliability and stability in the long term. This would allow simplified sample preparation, reduce costs and offer more testing options for the characterization of ageing-induced changes of the polymeric materials.

A proposed next step of the study would be to correlate the results from DSC with those from additional methods, such as tensile testing, rheology or size exclusion chromatography, which are very sensitive in characterizing the decrease in average molar mass resulting from hydrolytic chain scission.

PV Modules

Acknowledgements

We thank our colleagues A. Rauschenbach (PCCL) and Prof. G. Pinter (University of Leoben) for their support in this project. This research was carried out at the Polymer Competence Center Leoben (PCCL) within the Analysis of PV Aging project (FFG Nr. 825379, 4. Call 'Neue Energien 2020', Klima- und Energiefonds) in cooperation with the Chair of Materials Science and Testing of Plastics at the University of Leoben. The PCCL is funded by the Austrian Government and the State Governments of Styria, Lower Austria and Upper Austria.

References

[1] Köntges, M. et al. 2014, "Review of failures of photovoltaic modules", Report IEA-PVPS T13-01:2014 [available online at http://www.iea-pvps.org/index.php?id=275].

[2] Gambogi, W.J. et al. 2013, "Backsheet and module durability and performance and comparison of accelerated testing to long term fielded modules", *Proc. 28th EU PVSEC*, Paris, France, pp. 2846–2850.

[3] Gambogi, W. 2011, "The role of backsheet in photovoltaic module performance and durability", *Proc. 26th EU PVSEC*, Hamburg, Germany, pp. 3325–3328.

[4] Kim, N. et al. 2014, "Study on the degradation of different types of backsheets used in PV module under accelerated conditions", *Solar Energy Mater. & Solar Cells*, Vol. 120, Part B, pp. 543–548.

[5] Stollwerck, G. et al. 2013, "Polyolefin backsheet protects solar modules for a life time", *Proc. 28th EU PVSEC*, Paris, France, pp. 2842–2845.

[6] Reid, C. et al. 2013, "Contribution of PV encapsulant composition to reduction of potential induced degradation (PID) of crystalline silicon PV cells", *Proc. 28th EU PVSEC*, Paris, France, pp. 3340–3346.

[7] Oreski, G. & Wallner, G.M. 2005, "Aging mechanisms of polymeric films for PV encapsulation", *Solar Energy*, Vol. 79, pp. 612–617.

[8] Ehrenstein, G.W. & Pongratz, S. 2007, *Beständigkeit von Kunststoffen*, 1st edn. Munich: Carl Hanser Verlag.

[9] Oreski, G. 2010, "Accelerated indoor durability testing of polymeric photovoltaic encapsulation materials", *Proc. SPIE*, San Diego, California, USA, pp. 77730D-1–11.

[10] Oreski, G., Wallner, G. & Lang, R. 2009, "Ageing characterization of commercial ethylene copolymer greenhouse films by analytical and mechanical methods", *Biosys. Eng.*, Vol. 103, pp. 489–496.

[11] ISO 11357-3:1999 (1st edn), "Plastics – Differential scanning calorimetry (DSC) – Part 3: Determination of temperature and enthalpy of melting and crystallization".

[12] Ehrenstein, G.W., Riedel, G. & Trawiel, P. 2004, *Thermal Analysis of Plastics: Theory and practice*. Munich: Carl Hanser Verlag.

[13] Badia, J. et al. 2012, "The role of crystalline, mobile amorphous and rigid amorphous fractions in the performance of recycled poly (ethylene terephthalate) (PET)", *Polym. Degrad. Stabil.*, Vol. 97, pp. 98–107.

[14] Menges, G. et al. 2002, *Werkstoffkunde Kunststoffe*, 5th edn. Munich: Carl Hanser Verlag.

[15] Duncan, B., Urquhart, J. & Roberts, S. 2005, "Review of measurement and modelling of permeation and diffusion in polymers", NPL Report DEPC MPR 012.

[16] Koehl, M., Heck, M. & Wiesmeier, S. 2012, "Modelling of conditions for accelerated lifetime testing of humidity impact on PV-modules based on monitoring of climatic data", *Solar Energy Mater. & Solar Cells*, Vol. 99, pp. 282–291.

About the Authors

Dr. Gernot Oreski is a senior researcher at the Polymer Competence Center Leoben (Austria) and heads the photovoltaic group. His main fields of research are polymer science and testing, as well as the long-term reliability and degradation behaviour of polymeric materials and components for PV modules. In addition to his work for the PCCL, Dr. Oreski serves as a lecturer in the Department of Polymer Science and Engineering at the University of Leoben.

Marlene Knauzs studied polymer engineering and science at the University of Leoben and is a researcher at the Polymer Competence Center Leoben. She is currently working on her Ph.D. thesis concerning polymers for solar energy applications at the University of Leoben.

Dr. Gabriele Eder holds a Ph.D. in chemistry from Vienna University of Technology. Since 2005 she has been working at the OFI Austrian Research Institute for Chemistry and Technology, where she is responsible for research in the field of photovoltaics. Her main focus is on the characterization of degradation mechanisms of materials and PV modules and investigating material interactions.

Yulija Voronko studied materials science at the Martin Luther University of Halle-Wittenberg and has worked as a researcher at the OFI Austrian Research Institute for Chemistry and Technology. She is currently writing her Ph.D. thesis at the Vienna University of Technology.

Dr. Thomas Koch studied materials science at the Martin Luther University of Halle-Wittenberg and received his Ph.D. from the Vienna University of Technology, where he is currently working as a senior scientist in the structural polymers working group. His main focus is on polymer characterization and testing.

Karl Berger studied electric energy technology at the Vienna University of Technology. Since 2004 he has been with the Energy Department of the Austrian Institute of Technology (AIT). He has been engaged in projects concerning the reliability of high- and low-voltage electrical components, and dealing mainly with photovoltaic modules and systems since 2008.

Enquiries

Dr. Gernot Oreski
Polymer Competence Center Leoben GmbH
Roseggerstraße 12
A-8700 Leoben, Austria

Tel: +43 3842 42962 51
Email: gernot.oreski@pccl.at

Stress analysis of manufacturing processes for solar modules

Sascha Dietrich, **Matthias Pander**, **Martin Sander**, **Rico Meier** & **Matthias Ebert**, Fraunhofer Center for Silicon Photovoltaics CSP, Halle (Saale), Germany

ABSTRACT
Cracking of solar cells is a serious issue for product safety and module performance. Cracks may result in power loss, hot spots or arcing, and are caused by exceeding the strength limit of silicon. During the last few years, various studies have shown that fracture of encapsulated solar cells can be influenced by the manufacturing processes, which lead to residual stresses in solar cells. The results presented in this paper will give insights into the stresses generated by soldering and lamination. Furthermore, mechanisms of stress generation will be explained. On the basis of these findings, recommendations are made as to how to mitigate stresses, for example by means of alternative soldering processes, different soldering parameters or material optimization of the copper ribbon or the encapsulant.

Introduction
Fracture of solar cells has been identified as one of the most frequent failures in solar modules – it can lead to power loss over time as well as safety issues because of arcing or hot spots [1–3]. Furthermore, cell cracks are related to the presence of snail trails [4], which is an optical blemish on solar modules. Fracture is a mechanical issue related to mechanical stresses, which are caused by temperature changes or mechanical loads, and will occur when a certain stress limit for a material is reached. Therefore, in order to reduce crack initiation in solar cells, it is necessary to study single loads as well as load histories (during both manufacturing and operation) and how they form stresses. By means of such an approach, mechanisms can be understood, critical parameters identified, and measures derived in order to mitigate crack formation. For a deep understanding of the mechanical conditions in a PV module during manufacturing and operation, a combination of finite-element analysis and experiments under well-known conditions were performed.

"To reduce crack initiation in solar cells, it is necessary to study single loads as well as load histories and how they form stresses."

Mechanically induced loads can be static (wind, snow) or dynamic (shock, vibration, wind gusts). Loads from temperature changes occur during manufacturing (soldering, lamination) or operation (seasons, day/night shift). It is known that thermomechanically induced stresses often lead to residual stresses, which may remain in the material; these will add to any additional stresses, such as from mechanical loading. In the case of mechanical loading, the properties of the polymeric encapsulant in the module laminate significantly influence the level of induced stress [5].

Thermomechanically induced stress is caused by a mismatch of the coefficients of thermal expansion (CTE) of materials that are bonded together. Table 1 lists typical properties of materials used in PV modules: it can be clearly seen that there are large differences in CTE as well as stiffness (Young's modulus) between the respective materials. In particular, the CTE mismatches between silicon, copper and the metallization pastes are of great importance. Since in solar module laminates the whole stack is bonded, residual stress can be expected.

Finite-element set-up
Parameterized finite-element models for cells, mini-modules and complete solar modules have recently been developed: these models comprise all material and structural components of a solar module (cells, polymers, interconnectors, frame). Figs. 1 and 2 show a portion of a model for a complete solar module. Specific material behaviour was implemented

Material	CTE at 20°C [10^{-6} K^{-1}]	Young's modulus at 20°C [GPa]
Silicon [6–8]	2.60	130–180
Copper [9]	16.65	86
Solder alloy (Sn94.5Ag4Cu0.5) [10]	22.00	40
Al paste [11–13]	15.90	6
Ag paste [9,12,14]	10.40	7
Glass [15]	8.50	63–70
EVA	300.00	1–100MPa
Backsheet	67.00	2.1

Table 1. Material properties of typical materials used in solar module laminates.

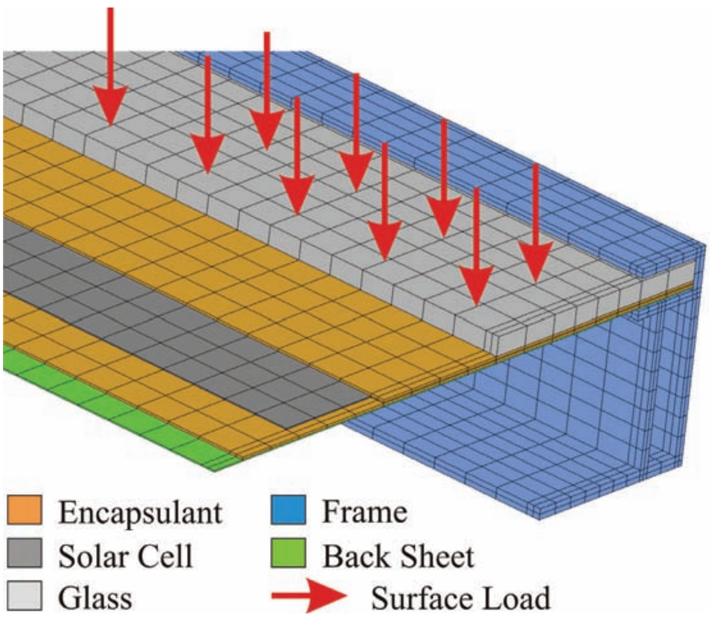

Figure 1. Portion of a finite-element model of a solar module, with a distributed surface load.

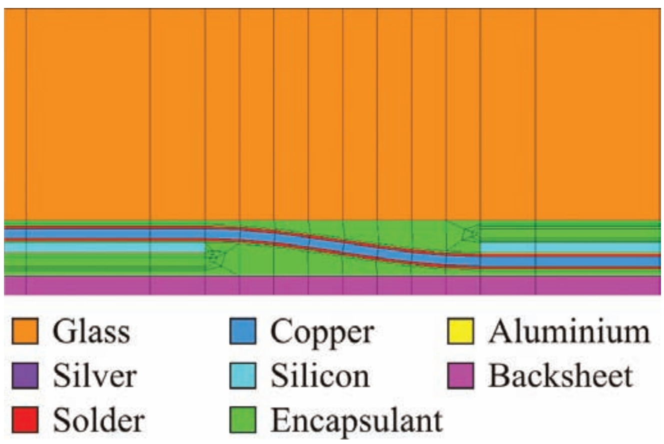

Figure 2. Detail of the finite-element model of a mini-module at the cell gap (cross section).

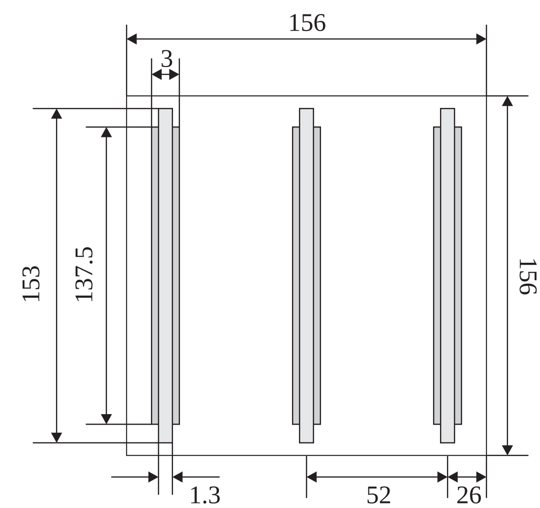

Figure 3. Cell layout used in this investigation.

in the simulation as realistically as possible. Glass and silicon were modelled by means of a linear-elastic-material model. Because polymers demonstrate a distinct time-dependent behaviour, a viscoelastic model represented by Prony series was used in this case. In the case of metallization pastes, aluminium, interconnectors and solder bonds, an elastic-plastic material behaviour was assumed. Furthermore, creep for the solder was taken into account by means of a power law behaviour.

Finite-element modelling allows the simulation of loads arising from temperature changes as well as from mechanical loads, and the calculation of strains or stresses in all components. Fig. 3 shows the layout of the solar cell used in the investigations reported in this paper: it consists of three busbars, with front and back contacts and continuous busbars.

Experiments

Experiments were carried out on representative laminates consisting of 10 solar cells (two strings each with five cells). The test set-up, test procedure and evaluation are presented in Fig. 4. A four-point bending set-up is used, in which the laminate is placed with the cells sunny-side upwards. Load steps of 10N increments are applied to the laminate. For each step, an electroluminescence (EL) image is taken from the cells between the load rollers, which allows the determination of cell cracking with respect to stress direction and finally of the in-laminate strength of solar cells. More details about the experimental approach can be found in Sander et al. [16]. The result of this test is a value for the effective strength of the encapsulated solar cells, where all previous steps from manufacturing (introduced defects through processing, residual stresses) are included. For the evaluation, all cells are assumed to be stress free; this allows influences to be recognized by a change in fracture force or fracture strength.

> "Process parameters during soldering may influence the in-laminate fracture strength of solar cells."

For the experimental studies, cell strings with two different soldering techniques (laser, infrared) and

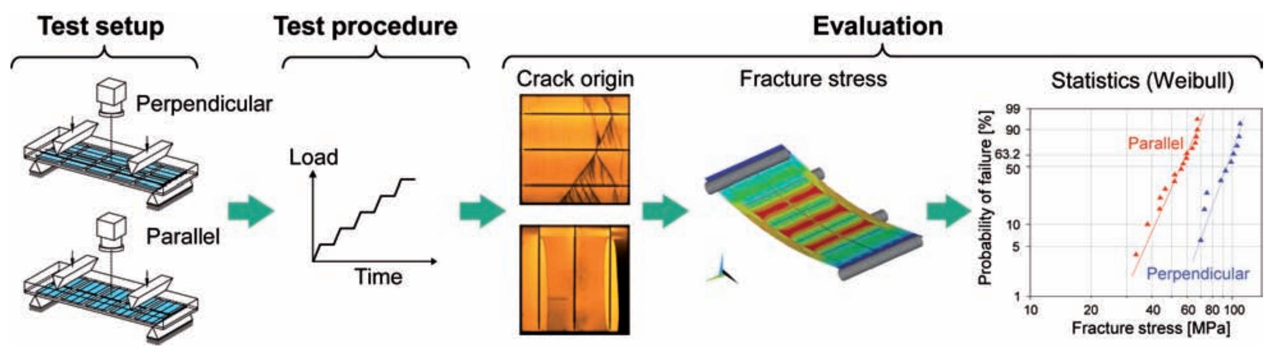

Figure 4. Experimental approach for in-laminate strength testing of solar cells [5].

process parameters were produced and laminated. For each technique and parameter set, laminates were produced with a stiff and a soft EVA encapsulant; they were then subjected to in-laminate strength testing, giving the results shown in Fig. 5. It can be seen that process parameters during soldering may influence the in-laminate fracture strength of solar cells (especially infrared soldering); this correlates with previous results [17]. However, for laser soldering, no major influence of process parameters could be found, which may imply a robust technology with a wider process window. If the two process techniques are compared, a statistically significant difference can be found when lower temperatures are used with a longer duration: the differences, however, are fairly small.

Also included in this investigation was a comparison of two EVA encapsulants having different stiffness properties. Depending on the composition of the EVA, especially the VA content, stiffness can be adjusted by moving the glass transition to higher or lower temperatures. The results show that a soft EVA leads to higher in-laminate strength values, implying that a module would resist higher loads (Fig. 5).

During the experiments it can be asserted that crack initiation often occurs at the busbars (see Fig. 6); this can also be observed on complete modules, where cracks often start at the end of the busbars or along them. In addition, cracks often propagate along the busbars [18]. In order to understand the reason for this, the manufacturing processes need to be considered. The soldering and lamination processes have therefore both been simulated in order to analyse stress distribution in the silicon.

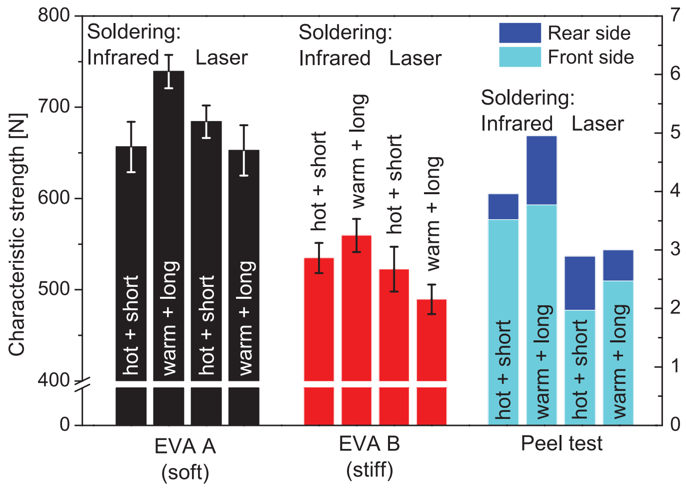

Figure 5. Measured in-laminate fracture strength/force of specimens produced under different manufacturing conditions, and the results of the peel test of the soldered cells for the different soldering conditions [5]. (The error bars are the confidence intervals for a confidence level of 95%.)

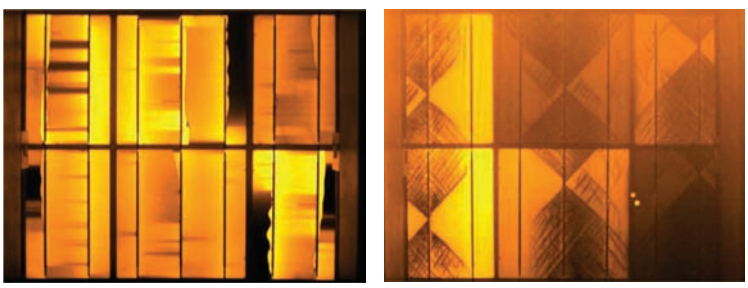

Figure 6. EL image of broken cells after in-laminate strength testing [5].

Stress analysis of soldering processes

The first temperature-driven process during module production is the fabrication of cell strings; temperatures up to 240°C can be reached, depending on the composition of the solder. Besides the metallurgical aspects, the solidus temperature differentiates types of solder. This is of particular interest since, along with material properties, it defines the temperature difference ΔT from room temperature. Typical solidus temperatures are between 180 and 220°C, but some special solders, such as tin/bismuth, have even lower solidus temperatures of around 130°C.

Since materials with different coefficients of thermal expansion

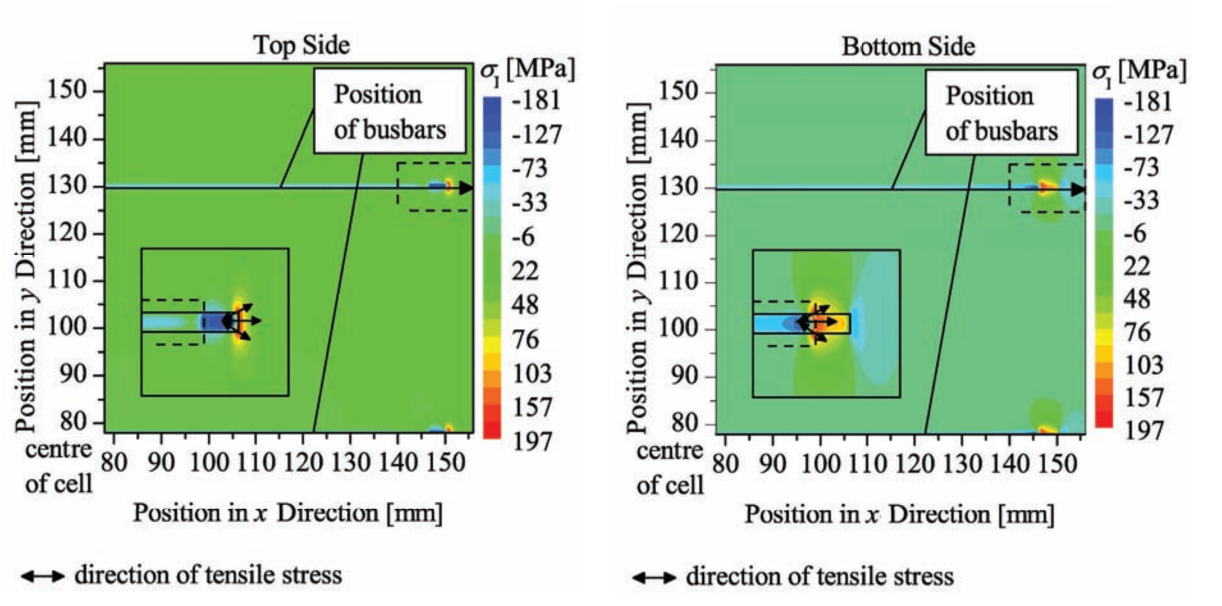

Figure 7. First principal stress in the silicon after soldering (only a quarter of a cell is shown for reasons of symmetry).

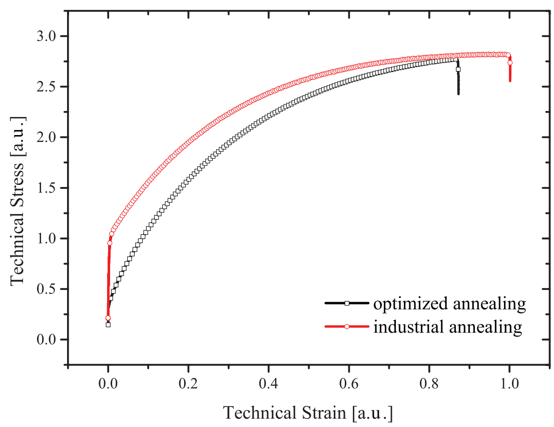

Figure 8. Tensile testing results for a standard industrial interconnector and an optimized interconnector [19].

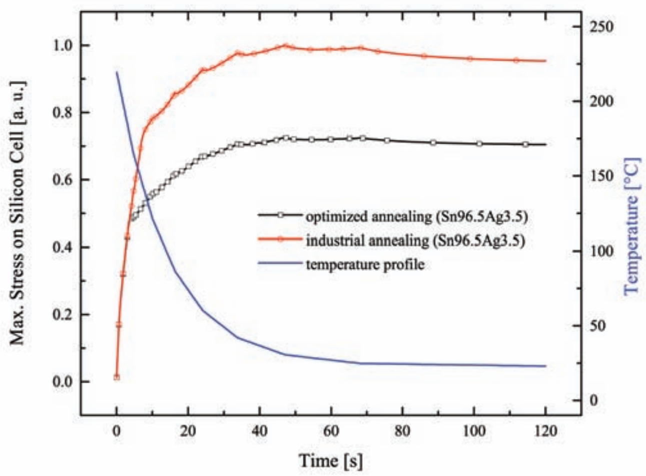

Figure 9. Maximum stress during the cooling phase of the soldering process for a standard industrial interconnector and an optimized interconnector [19].

are bonded together, stresses are developed in each material. In the case of ductile materials – such as solder, copper or the silver pastes – the increase in stress is lower because of plastic deformation and hardening, which is an important aspect that will be discussed later. However, silicon does not have this quality, since it is a linear elastic material within the respective temperature ranges of module manufacturing and operation. Stresses therefore increase with a steady gradient until brittle fracture occurs.

Simulations have been carried out with a solder (SnAg4Cu0.5) that has a solidus temperature of 217°C: this temperature represents the stress-free state in the performed simulation. A single solar cell was cooled to 25°C within 60 sec. Fig. 7 shows the stress distribution on the top and bottom surfaces of the solar cell: the influence at the busbars can be clearly seen. Pressure stresses are developed underneath the busbar, which is in accordance with mechanical principles, since copper and metallization pastes have a higher CTE than silicon. As a consequence, stress peaks can be found at the end of the soldered busbar on both the top and bottom sides. The arrows in Fig. 7 indicate the direction of the first principal stress. It is directed in a perpendicular direction to the perimeter of the soldered area, which is an important fact since any additional stress – for example from lamination or later module bending – has to be oriented in the same direction in order that a constructive or destructive superimposition can take place.

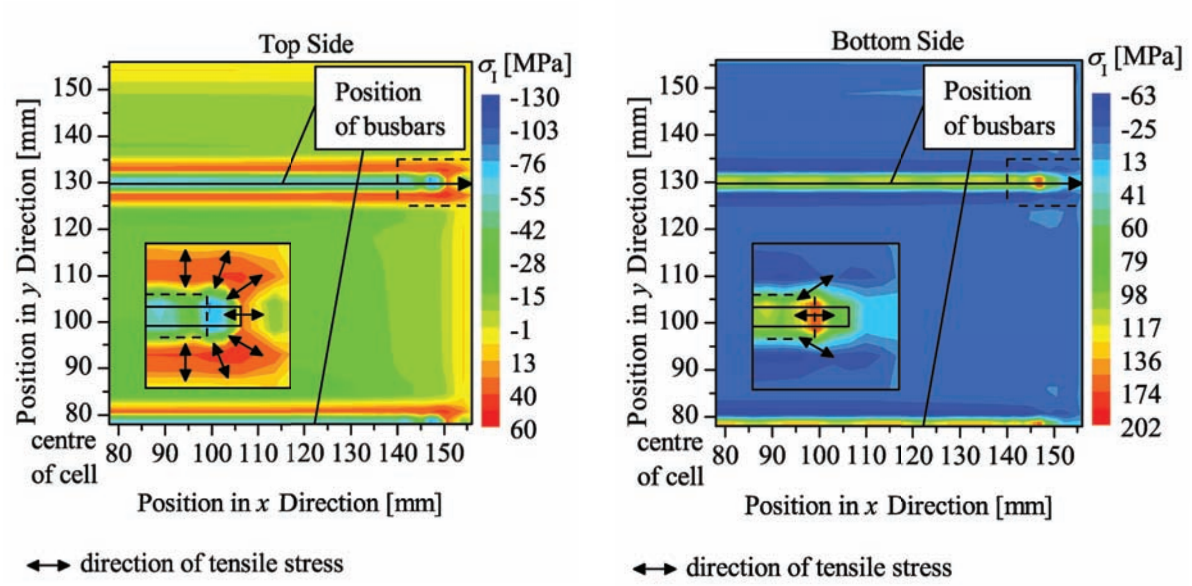

Figure 10. First principal stress in the silicon after lamination (only a quarter of a cell is shown for reasons of symmetry).

Optimized interconnectors for reducing mechanical stresses from soldering

The experimental studies discussed above showed that the soldering technique and process parameters do not necessarily have a large impact on cell reliability. Material properties, however, may have an influence. Interconnectors are produced from copper material in order to achieve a low series resistance at an acceptable cost. As described above (Table 1), the CTE of copper is about six times as large as that of silicon, which is one of the main reasons for stress evolution in solar cells. The magnitude of this stress is mostly limited by the yield strength and the strain hardening properties of the copper; basically, yield strength should be as low as possible. Meier et al. [19] investigated how the yield strength of copper ribbons can be reduced by annealing. In Fig. 8 the yield strength of a standard industrial interconnector was reduced by changes to the annealing process.

"Yield strength should be as low as possible."

An elastic-plastic material model was used in order to transfer the experimental data to the finite-element model. Fig. 9 shows the result for the evolution of the maximum first principal stress in the silicon during cooling: it can be clearly seen that the reduced yield strength leads to a stress reduction in the silicon.

(a) (b) (c)

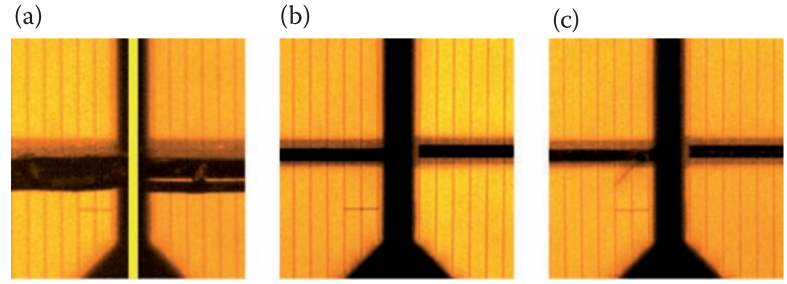

Figure 11. Crack initiation in a solar cell at the end of the soldered region after different manufacturing steps: (a) initial, (b) soldered, and (c) laminated [20].

Stress analysis of the lamination process

After the soldering process, cell strings are placed on a glass pane between two layers of encapsulant. In a first step the laminate stack is heated up to lamination temperature (around 150°C); during this heating, the laminate compound is assumed to be not bonded, so the cells are able to move freely. The heating step is included in the simulation immediately after cooling from the soldering temperature. This is important since copper is deformed plastically during these large temperature changes, which influences the outcome of the stress calculation. After being heated up to lamination temperature, all materials are defined to be bonded, and the laminate is cooled down to room temperature within 50 min (in-house measurements at Fraunhofer CSP).

Fig. 10 illustrates the calculated first principal stress distribution on the surfaces of the silicon after lamination: it is obvious that there are major differences between the top and bottom sides of the cell. On the top side, pressure stress can be found underneath the busbars; in contrast, on the bottom side, tensile stress is created, which exceeds the intrinsic compressive stress from soldering. At the sides of the busbars, the opposite is true: there is tensile stress on the top side, whereas there is pressure stress on the bottom.

A lamination stress peak similar to the one in the case of soldering can be found at the end of the soldered region on the bottom side of the cell. The direction of the stress correlates with that caused by soldering. As a result, stresses from soldering and lamination will superimpose and, in this case, accumulate at this position, leading to a higher probability of fracture.

Qualitatively similar stress results can be found on the top side at the end of the busbar.

> "Stresses from soldering and lamination will superimpose, leading to a higher probability of fracture."

Sander et al. [20] investigated cell fracture for each manufacturing step of small cell strings. Fig. 11 shows EL images in the initial state of two adjacent solar cells, after soldering and lamination. Typically, it was discovered that there is a high likelihood of crack initiation during lamination at the end of the busbar, which usually corresponds to the end of the soldered length. This correlates well with the observations in the stress analysis.

Fig. 12 shows the exaggerated deformed finite-element mesh from a portion of the perpendicular cross section through the busbar. This deformation plot is extracted after cooling down from the lamination temperature to 20°C, and shows that the main mechanism of stress generation is the contraction of the encapsulant during cooling. Since the solar cell is bonded to the glass via the encapsulant, the contraction of the latter pulls it to the glass. The distance between the copper ribbon and the glass is smaller than the distance between the surface of the cell and the glass, since the polymer is squeezed out during lamination. Measurements taken of some samples showed that the distance between the glass and the copper ribbon is 160–170µm, whereas the distance between the cell and the glass is approximately 400µm. Since the relative contraction of the polymer is the same at any point, the absolute contraction is determined by the initial thickness of the polymer. Thus the absolute contraction between the cell and the glass is larger than that between the ribbon and the glass. Contractions of 60µm between the cell and the glass, and 14µm between the ribbon and the glass, were determined from the simulation. Furthermore, pressure stresses were created between the busbars, because the contraction of the glass was larger than that of silicon.

Finite-element simulation on full-scale modules

Finite-element simulation models of complete modules were used for investigations of full-scale modules. A distributed load of 2400Pa, in accordance with the IEC standard for testing against wind loads, was applied to the glass surface of the module, which was defined to be supported along its long perimeter. Fig. 13 shows a contour plot of the first principal stress of the encapsulated solar cells; the stress which is applied by mechanical bending is shown in Fig. 13(a). High stresses, which increase the likelihood of cell breakage, can be expected in the corner cells and in the cells in the centre of the module, with maximum stresses ranging between 40 and 50MPa. However, this stress distribution will change if the position of the support is moved (as shown by Dietrich et al. [21]) or if the load changes.

In Fig. 13(b) the intrinsic stresses from manufacturing are superimposed with stresses from bending. Very localized stress peaks are created along the busbars, increasing the maximum stress to 93MPa. Moreover, the magnitude of the stress between the busbars is reduced because of the pressure stress that is applied during lamination, implying that fracture will more likely start from the busbars.

Summary

Experimental and simulation studies showed that cracks in solar cells are likely to start along the busbars of solar cells.

These cracks may be either initiated during manufacturing (most likely during lamination) or a result of bending caused by a mechanical load (wind or snow) on a solar module. Since several materials with very different material properties, and in particular different coefficients of thermal expansion, are bonded together, they will contract or expand differently during temperature changes, causing stresses in each material component. Because of the brittle characteristic of silicon, fracture occurs suddenly without any previous indication of overload. Numerical studies have shown that high local stress peaks are induced in the silicon around the busbars. As a result of plastic deformation, materials such as metal pastes, solder and copper ribbons can limit the stress. These types of material can therefore also be optimized to limit the stress in the solar cell, which can be achieved, for example, by optimizing yield strength.

"Cracks in solar cells are likely to start along the busbars of solar cells."

Furthermore, lamination turns out to be rather critical as regards the fracture of solar cells: experimental studies have shown that this manufacturing step has the highest probability of initiating cracks, and numerical studies have confirmed these observations. Stresses from soldering and lamination add together on the basis of the same mechanism (temperature change and CTE mismatch). A second mechanism was found to be the bending of the solar cell around the busbar caused by the contraction of the encapsulant. This bending gives rise to high stress peaks in a relatively large area around the busbar. Therefore, alternative polymers (such as a silicone-based material with a lower CTE), a different lamination profile, or a lower stiffness can all reduce those stresses.

Residual stresses generated in the manufacturing chain remain in the silicon. Although viscoelastic effects of the polymers involved and solder may reduce some of those stresses over time (creeping), the effect decreases as the stresses become smaller, so that after a while a non-diminishing stress minimum is reached. Therefore intrinsic stresses from manufacturing are present in a module and will superimpose with stresses from additional mechanical loads or from loads due to temperature changes, which dominate the fracture of an encapsulated solar cell, as numerical studies demonstrate. Simulation results from lamination showed that a region of high tensile stresses is present along the busbar, and these stresses are directed in a perpendicular direction to the busbar. As a consequence, it is likely that cracks will propagate closely along the busbar; this correlates with results from module EL imaging as well as in-laminate strength tests when stress from bending is also perpendicular to the busbars [16].

Finally, it can be stated that systematic experimental studies in combination with sophisticated numerical simulation can contribute to a comprehensive knowledge about fracture mechanisms in solar cells. Interpretations can be made in order to optimize a solar module in terms of mechanical reliability. However, these interpretations are individual, as they are limited by certain constraints (such as the processes that are currently

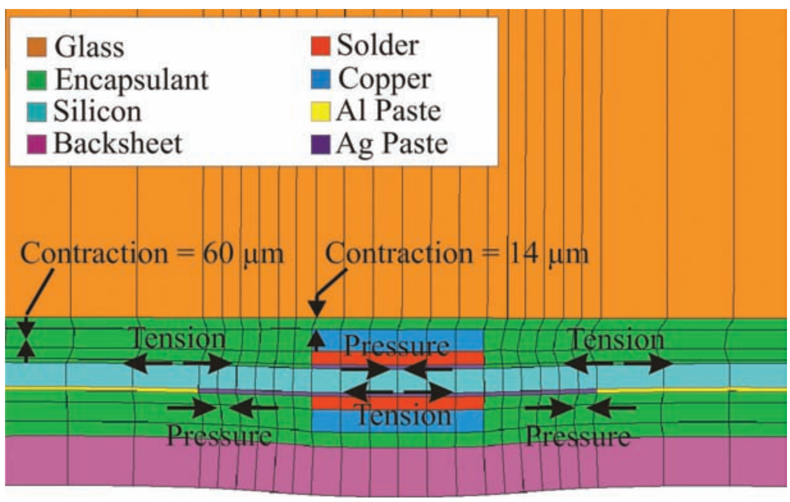

Figure 12. Plot of the deformed finite-element mesh after lamination (perpendicular cross section through the busbar).

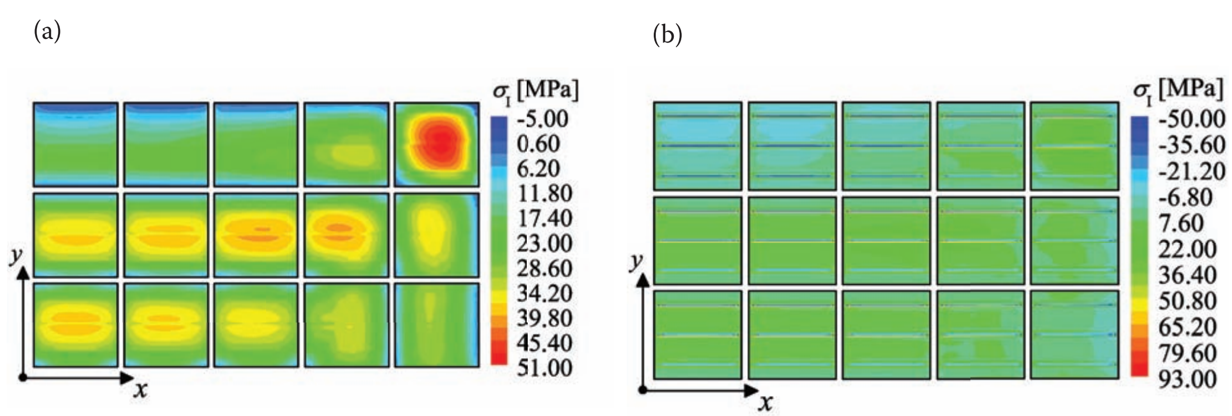

Figure 13. First principal stress plot of encapsulated solar cells at 2400Pa supported along the long perimeter of the module: (a) stress due only to mechanical bending; (b) superimposition of stresses from soldering, lamination and bending.

PV Modules

used for module production) or design restrictions.

References

[1] Koentges, M. et al. 2011, "The risk of power loss in crystalline silicon based photovoltaic modules due to micro-cracks", *Solar Energy Mater. & Solar Cells*, Vol. 95, pp. 1131–1137.

[2] Wohlgemuth, J. et al. 2011, "Reliability testing beyond qualification as a key component in photovoltaic's progress toward grid parity", *Proc. IEEE Intl. Rel. Phys. Symp.*, Monterey, California, USA, pp. 5E.3.1–5E.3.6.

[3] Wohlgemuth, J. et al. 2006, "Long term reliability of PV modules", *Proc. 4th IEEE WCPEC*, Waikoloa, Hawaii, USA, pp. 2050–2053.

[4] Ezquer, M. 2013, "Characterization defects detected on c-Si PV modules after certain period of field exposure", *Proc. 28th EU PVSEC*, Paris, France, pp. 3269–3274

[5] Sander, M. et al. 2013, "Influence of manufacturing processes and subsequent weathering on the occurrence of cell cracks in PV modules", *Proc. 28th EU PVSEC*, Paris, France, pp. 3275–3279.

[6] Hull, R. (Ed.) 1999, *Properties of Crystalline Silicon*. London: INSPEC, The Institution of Electrical Engineers.

[7] Okada, Y. et al. 1984, "Precise determination of lattice parameter and thermal expansion coefficient of silicon between 300 and 1500 K", *J. Appl. Phys.*, Vol. 56, pp. 314–320.

[8] Okaji, M. 1988, "Absolute thermal expansion measurements of single-crystal silicon in the range 300–1300 K with an interferometric dilatometer", *Intl. J. Thermophys.*, Vol. 9, pp. 1101–1109.

[9] Chang, Y.A. et al. 1966, "Temperature dependence of the elastic constants of Cu, Ag, and Au above room temperature", *J. Appl. Phys.*, Vol. 37, pp. 3567–3572.

[10] Wiese, S. et al. 2002, "Characterisation of constitutive behaviour of SnAg, SnAgCu and SnPb solder in flip chip joints", *Sens. and Act. A*, Vol. 99, pp. 188–193.

[11] Brandes, E.A. & Brook, G.B. (Eds.) 1983, *Smithells Metals Reference Book*, 6th edn. Oxford: Butterworth-Heinemann.

[12] Kohn, C. et al. 2007, "Analyses of warpage effects induced by passivation and electrode coatings in solar cells", *Proc. 22nd EU PVSEC*, Milan, Italy.

[13] Tallon, J.L. et al. 1979, "Temperature dependence of the elastic constants of aluminium", *J. Phys. Chem. Solids*, Vol. 40, pp. 831–837.

[14] Smith, D.R. et al. 1995, "Low-temperature properties of silver", *J. Res. Natl. Inst. Stand. Technol.*, Vol. 10, pp. 119–171.

[15] Scholze, H. 1988, *Glas – Natur, Struktur und Eigenschaften* (in German), 3rd edn. Berlin: Springer Verlag.

[16] Sander, M. et al. 2013, "Systematic investigation of cracks in encapsulated solar cells after mechanical loading", *Solar Energy Mater. & Solar Cells*, Vol. 111, pp. 82–89.

[17] Gabor, A.M. et al. 2006, "Soldering induced damage to thin solar cells and detection of cracked cells in modules", *Proc. 21st EU PVSEC*, Dresden, Germany.

[18] Koentges, M. et al. 2011, "Crack statistics of crystalline silicon photovoltaic modules", *Proc. 26th EU PVSEC*, Hamburg, Germany, pp. 3290–3294.

[19] Meier, R. et al. 2011, "Reduction of soldering induced stresses in solar cells by microstructural optimization of copper-ribbons", *Proc. SPIE*, San Diego, USA, pp. 811206-1–811206-13.

[20] Sander, M. et al. 2011, "Investigations on crack development and crack growth in embedded solar cells", *Proc. SPIE*, San Diego, USA, pp. 811209-1–811209-10.

[21] Dietrich, S. et al. 2012, "Interdependency between mechanical failure rate of encapsulated solar cells and module design parameters", *Proc. SPIE*, San Diego, USA, pp. 84720P-1–84720P-9.

About the Authors

Sascha Dietrich studied mechanical engineering at the University of Applied Sciences Leipzig and at the University of Paisley in Scotland. Since 2008 he has been working in the module reliability group at Fraunhofer CSP. Currently he is head of the lifetime and weathering team, which is responsible for lifetime testing of PV modules and components. During this time, he worked on his Ph.D., with a thesis topic involving numerical studies of the mechanical reliability of encapsulated solar cells.

Matthias Pander studied mechanical engineering at the University of Applied Sciences Leipzig. His master's thesis involved the simulation of the thermomechanical stresses in embedded solar cells. Since 2010 he has been working in the module reliability group at the Fraunhofer CSP, focusing on material characterization and finite-element simulations for components of photovoltaic modules.

Martin Sander studied mechanical engineering in Ilmenau, Germany, and received his diploma in 2008. He then worked in the module reliability group at Fraunhofer CSP, where he completed his Ph.D. thesis on the investigation of cracks in encapsulated solar cells during thermal and mechanical loads. He recently joined TOTAL New Energies and works in solar R&D.

Rico Meier studied in the International Physics Studies Program at Leipzig University. In his master's thesis, he addressed the influence of mechanical stress and temperature on the ultrasonic time of flight in solid objects. Since January 2009, he has been working with the module reliability group at Fraunhofer CSP, where he specializes in the ultrasonic characterization of solar cell interconnectors in crystalline PV modules.

Matthias Ebert is head of the module reliability group at Fraunhofer CSP in Halle (Saale), Germany. He studied civil engineering at the Bauhaus University Weimar and received his Ph.D. from the Institute for Structural Mechanics in Weimar. He began working at Fraunhofer Institute for Mechanics of Materials in 2003, and has been at Fraunhofer CSP since 2007.

Enquiries

Sascha Dietrich
Fraunhofer Center for Silicon Photovoltaics CSP
Otto-Eissfeldt-Str. 12
06120 Halle (Saale)
Germany

Tel: +49 (0) 345 5589 5210
Email: sascha.dietrich@csp.fraunhofer.de
Website: www.csp.fraunhofer.de

Module technologies for high-efficiency solar cells: The move away from powerful engines in old-fashioned car bodies

Joris Libal, **Andreas Schneider**, **Andreas Halm** & **Radovan Kopecek**, ISC Konstanz, Konstanz, Germany

ABSTRACT

Why change a product which can be sold in high quantities with a large margin? This is one of the reasons why crystalline silicon modules look the same today as they did 30 years ago. In addition, a module has to last for more than 20 years; to change the technology, or even just the material, many complicated, long-lasting and costly tests are necessary. And even after a series of successful tests there is no guarantee of a long-lasting product. Moreover, during the PV crisis starting in 2009, module manufacturers did not have the manpower and budget for introducing novelties into the module market. All the above are reasons why module architecture and materials did not significantly change with time and did not adapt to the introduction of powerful, highly efficient solar cells. After the crisis, however, many module manufacturers became aware that in order to be able to sell modules on the market with a high margin, their products not only have to be cost effective but also must differentiate themselves from the mass product. Consequently high-power, optically nice, colourful, back-contact, transparent, bifacial, light and highly durable modules are now being developed and are gradually being introduced into today's market. This paper reports on current trends and discusses future developments.

Introduction

As part of continuous efforts in the PV industry to further drive down the total cost of PV-generated electricity (the levelized cost of energy – LCOE), more and more cost-effective high-efficiency cell concepts are in the process of being implemented in the manufacturing lines of various solar cell producers. The following are just a few of these innovations: n-type metal wrap-through (MWT) at Yingli [1]; p-type MWT at JA Solar [2]; p-type passivated emitter rear cell (PERC) at many large solar cell manufacturers; and n-type passivated emitter, rear totally diffused (PERT), or BiSoN, at MegaCell [3]. Because of the new technological features of these cell concepts and their continuously decreasing manufacturing cost, the development and adoption of innovative technologies in the field of module assembly and related materials is essential, and motivates module

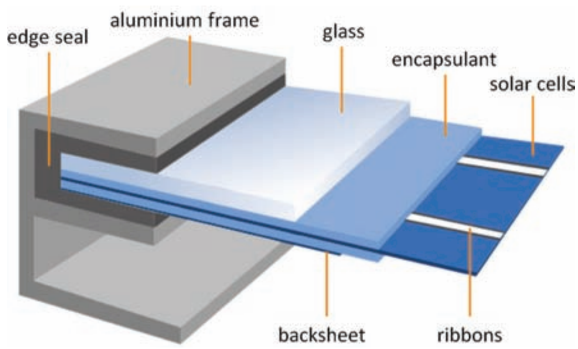

Figure 1. Cross section of a standard module.

	Current status 2014	Expected for 2018
Cell technology		
Average cell thickness [µm]	180	150
Back-contact market share	5%	12%
n-type market share	5%	20%
Module technology		
Average module glass thickness [mm]	3.2	2
Glass–glass module market share	5%	20%
Cell-to-module Pmpp losses multi cells	0–1% loss	1.5% gain
Cell-to-module Pmpp losses mono cells	>3% loss	0%

Table 1. PV industry expectations according to the latest edition of the ITRPV [4].

manufacturers to gradually move away from today's standard module design (see Fig. 1).

These new module technologies must have the following characteristics:

- Transfer a maximum fraction of the cell power to the module (i.e. exhibit low cell-to-module Pmpp losses).
- Guarantee an extended module lifetime and stable performance for 30–40 years.
- Contribute to a further cost reduction of the PV modules in €/Wp and – even more importantly – of the LCOE in €/kWh.

> "The development and adoption of innovative technologies in the field of module assembly and related materials is essential."

In addition, new types of module that feature a significantly reduced weight, a frameless design or even bifacial energy conversion will contribute to a reduction in the PV system cost by significant savings in the balance of system (BOS) cost.

The latest edition of the International Technology Roadmap for PV [4] gives some interesting insights concerning the technological achievements that are expected by the PV industry in the future. Since the focus in this paper is on the near future, Table 1 lists the technological developments that are expected to be implemented by 2018 compared with the current status.

The following sections will give an overview of innovative technologies that are ready to be implemented in industry and that will contribute to fulfilling the expectations listed in Table 1. In this context, new materials – such as conductive adhesives (replacing soldering), alternative encapsulant materials and new backsheets (e.g. conductive backsheets for back-contact cells) – that are in the process of being introduced in industrial PV module manufacturing will be discussed.

Electrically conductive adhesives for thin cells and high durability of modules

Compared with the well-established soldering process, electrically conductive adhesives (ECAs) offer major advantages in solar cell interconnection, including:

- Bow is strongly reduced because of reduced process temperatures.
- Solar cells without front busbars can be contacted by means of adhesive (hence offering huge savings potential as regards Ag paste usage for cell metallization).
- Lead-free ribbons can be used, which is currently rarely the case because of the necessary 50K increase in soldering temperature, leading to increased cell breakage.
- Problems are avoided with the soldering process during cell interconnection of certain high-efficiency cell designs, such as rear-contact solar cells (e.g. the interdigitated back contact – IBC – cell design).

Recently, stringer equipment suppliers released new stringer generations for which the gluing process is adapted and modified (see Osborne [5] and teamtechnik [6], for example). Other suppliers are in the process of developing new stringers or modifications for existing equipment to adapt it to the glue application (dispensing or printing) and curing process.

Particularly because the entry into the market of new, highly efficient cell designs – such as IBC cells – is on the increase, the conductive adhesive technique promises significant advantages compared with soldering. This development coincides with a substantial reduction in the price of conductive adhesives, because of recent product developments, generally with fewer silver particles or alternative conductive materials in the adhesive. Conductive adhesive suppliers have recently developed new products which demonstrate increased conductivity and bonding strength to the solar cells, thereby eliminating two of the major disadvantages associated with conductive adhesives: their low bonding strength in the range of 0.5–1.5N and significantly higher cell-to-module losses than for cells interconnected by soldering.

With the new adhesives and stringer systems, a real alternative to the soldering process for interconnection now exists, providing potential customers with quality and reliability which are comparable – or even superior – to what they received from systems based on soldering. Fig. 2 shows the excellent performance of modules where gluing of Cu ribbons has been used for the interconnection of two-side contacted cells: when combined with a suitable encapsulant (EVA for example), the tested modules exhibited less than 1% Pmpp loss after 3000h of damp-heat testing [7]. In addition, it has been shown that this type of module configuration also resists very well thermal-cycling tests with up to 600 cycles [8].

Cell encapsulation

The cell encapsulation material – such as EVA, which for decades has been the main material used in industry – is one of the key materials in solar module

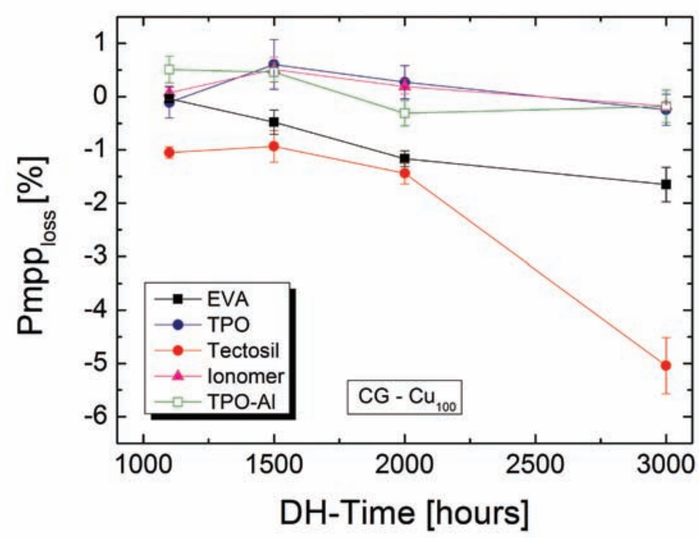

Figure 2. Pmpp loss after climate chamber testing for modules with (two-side contacted) standard cells interconnected using copper ribbons that have been glued with conductive adhesive. Choosing a suitable encapsulant enables very good reliability to be achieved, even after 3000h of damp-heat testing [7].

processing. On the one hand, it has to be highly transparent to allow as much incident sunlight as possible to reach the cell surface, thus keeping the cell-to-module losses low. On the other hand, the material has to demonstrate strong adhesive bonding to the solar cells, glass and backsheet in order to resist UV irradiation, environmental factors (such as acid rain and ammonia gases) and permanent temperature cycles with large peaks at lower and higher temperatures.

The first key performance indicator (KPI) is typically established by measuring the cell-to-module losses, whereas the second is determined during thorough climatic tests and exposure to UV light. Only recently, the encapsulation material was found to be one of the key materials in preventing potential-induced degradation (PID) [9], hence leading to a strong push towards the development of encapsulation materials with very small water diffusion and storage and high volume resistance. Another crucial aspect is the development of highly efficient solar cell technologies that demonstrate a strong spectral response in the blue wavelength. Such a characteristic requires encapsulation materials which exhibit sufficient transparency at lower light wavelengths but, at the same time, do not jeopardize either the bonding strength to other materials or the long-term stability, both of which are subject to degradation by UV radiation.

Besides NICE module technology by Apollon (requiring no encapsulant at all – see the discussion later in this paper), all high-efficiency solar cell concepts – in particular those based on n-type wafers – have two important requirements with respect to the encapsulant. First, the encapsulant has to be chemically compatible with the metal pastes used for cell fabrication as well as with the conductive adhesive. Second, many advanced cell concepts, especially IBC cells, feature an excellent spectral response in the short-wavelength range (300–400nm). In order to transfer this efficiency increase to the final module, highly UV-transparent encapsulants are necessary. Promising candidates for meeting these requirements are ionomers, polyolefines, liquid silicone and recent newly developed EVA products. Moreover, certain polyolefines have demonstrated a resistance to PID, for example when used in modules incorporating Zebra cells [10]. When considering back-contact cells, the front-side encapsulant can in any case be thinner than that for standard modules, leading to an increase in light transmission and hence significantly reducing the costs.

Very thin module glass for low-weight glass–glass modules

The standard thickness of solar glass used in the PV industry for the construction of PV modules has gone down steadily over the last few years. In 2008 the industry switched from a 4mm-thick glass to 3.2mm, and we are now looking at another thickness reduction in the near future from 3.2mm to 2mm, or even 1.5mm.

> "Glass–glass PV modules have significant advantages in terms of mounting, since no metal frame is required."

Because of its considerably reduced weight, glass of 2mm and below offers the important advantage of the production of glass–glass modules with the superior characteristics of such glass. In general, glass–glass PV modules have significant advantages in terms of mounting, since no metal frame is required. The heavy weight of glass–glass modules using 4mm or 3.2mm glass was the main factor that prevented industry from supplying this extraordinary product to the market. The thickness reduction is accompanied by an improved light transmission, hence reducing the cell-to-module Pmpp losses. Another advantage is the increased durability, since, in contrast to foil backsheets, no water at all can penetrate the solar module interior (except for a small fraction at the edge region of a module, which applies to any module technique).

Thin glass significantly increases the flexibility of glass–glass PV modules. The strong mechanical resistance and flexibility of tempered thin glass allows the processing of extremely lightweight glass–glass PV modules. With a thickness of both the front- and back-side glass of 2mm and below, glass–glass modules are remarkably efficient and diffusion-proof. This is true not only for water but also for ammonia gases, which are fully blocked by the glass and cannot damage the module interior. Furthermore, this module technology does not require any metal frames, which saves on materials and weight. The reduced weight of thin glass–glass modules opens up new markets, such as building-integrated photovoltaics (BIPV) products or bifacial solar modules. The excellent flexibility of glass–glass modules makes this product mechanically very robust, even under large loads. One advantage here is that the solar cells are placed in the neutral zone of the module, thus reducing the effective mechanical stress imposed on the solar cell to a minimum when a mechanical load is applied to the module.

In short, by taking the glass–glass module approach, it is possible to solve many of the problems typically observed with standard backsheet PV modules, such as low light transmission (hence high cell-to-module losses), poor flexibility and unsatisfactory durability.

Liquid silicone

Because of its excellent and stable optical properties, as well as its chemical stability, silicone was a common encapsulant material for c-Si PV modules in the 1970s and early 1980s. Since at this time silicone was rather costly, and the related processing technology was not compatible with high-volume production of PV modules, it was rapidly forced out of the market by EVA.

In recent years, new silicone formulations – specially adapted to the requirements of PV – have been developed, along with process technologies that enable low-cost and high-volume production of PV modules (e.g. Dow Corning/Reis and Momentive/Kuka). Compared with EVA, from the point of view of processing, liquid silicone encapsulants enable short cycle times and reduced process temperatures (curing within several minutes at around 80°C). With the optimum silicone formulation, this type of liquid encapsulant features a number of advantages, such as high light transmission in the wavelength range of 300 to 400nm [11] and the capability of suppressing PID effects considerably [12].

Being much more resistant to yellowing after UV exposure than EVA, as well as retaining much less humidity, silicone encapsulants promise very low degradation rates for PV modules; these encapsulants will therefore contribute to achieving module lifetimes of more than 30 years, particularly if they are integrated in a glass–glass module design, in which the traditional backsheet materials are replaced by a thin glass sheet.

All the characteristics mentioned above are gaining more importance with the increased demand for the installation of modules in regions with harsh climatic conditions, such as deserts in, for example, the MENA region and South America (see also

Source: Meyer Burger.

Figure 3. Schematic representation of SmartWire technology, showing the metal fingers of a single cell contacted with smart wires.

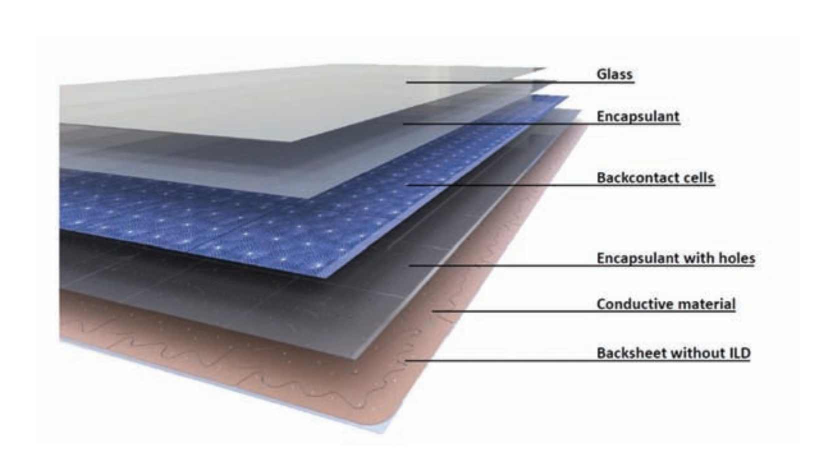

Source: Eurotron.

Figure 4. Cross section of an MWT module constructed with conductive backsheet technology.

the 'Development of desert modules' section later in this paper).

SmartWire approach

SmartWire Connection Technology (SWCT) (see Söderström et al. [13], for example) – formerly called *Day4Energy Electrode* – is a novel module technology which has been further developed and distributed by Meyer Burger. This technology is based on an electrode in which metal wires are retained in an adhesive film, and replaces the conventional solar ribbon (see Fig. 3). In contrast with soldering, SWCT involves a low-temperature process, resulting in a significant improvement in efficiency and reducing the negative effects of micro-crack generation by thermomechanical stress typically seen with soldering at high temperatures.

The wire matrix generates more than 2000 contact points between the solar cell and the wires: the solar cell therefore exhibits a significantly higher efficiency and reliability in terms of electrical contact. Meyer Burger states that in comparison with conventional three-busbar technology, SWCT results in a reduction in Pmpp losses by 3% for solar cells after encapsulation in the module. Because of the reflections from the wires in the SWCT design, the effective shading on the solar cells is only 70% of the wire diameter. The large number of contact points leads to excellent performance, as observed in extended climatic tests. A broken metal finger or chipped or cracked solar cell usually means a loss in electrical connection, resulting in significant electrical losses. In the case of SWCT, each finger is electrically contacted to the matrix of wires, which serves as a backup for the electrical contact: therefore even cells with micro-cracks or broken cells exhibit little or no loss in performance, yielding a 1% increase in production, according to Meyer Burger.

Another noteworthy advantage of SWCT technology is the price reduction realized in the solar cell process, since this technology does not require busbars, and significant economies are made on the amount of silver paste used during the cell process. It is also worthy of mention that SWCT technology facilitates the interconnection of high-efficiency cell designs for which currently no, or only non-optimized, interconnection technologies exist. For example, heterojunction solar cells combined with SWCT can be interconnected in a reliable way, yielding the lowest cell-to-module Pmpp losses.

Back-contact modules based on a conductive backsheet

One new approach used in module assembly which breaks away completely from the tabbing-stringing technology is the conductive backsheet (CBS) technique. This method was adopted from printed-circuit board production and is only suited to back-contact cells. It was developed by TTA and ECN for p-type MWT solar cells and was introduced to the market in 2009 by Eurotron, a daughter company of TTA. Other providers of technology and equipment for module assembly based on CBS are the Finnish company Cencorp and the Italian company Formula E.

The typical module sandwich including CBS (see Fig. 4) is composed of glass, front encapsulant, back-contact cells, rear encapsulant with local openings to contact the cells, and the conductive backsheet, including a polyethylene terephthalate (PET) and Tedlar or similar layer on the rear. The metal layer, which is the basis of each type of CBS, is around 35µm thick (depending on the supplier), making its total mass on the area of a solar cell more than twice the mass of ribbon (2 × 0.2mm) needed to interconnect a three-busbar cell. This results in very low series-resistance-related Pmpp cell-to-module losses.

The CBS is mostly made from copper or aluminium coated with a thin layer of copper to aid contacting (e.g. Hanita Coatings' DuraShield). The metal covers nearly the whole module area and is only interrupted by small isolating trenches, which define conduction paths for both polarities.

Initially, structuring of the metal layer was solely realized by wet chemical processes; nowadays, cheaper and simpler structuring tools based on laser or mechanical milling are gaining popularity. The copper layer is finished with, for example, ZnCr (e.g. Krempel's AKACON BCF) or treated with an organic surface protectant (OSP) on the side (e.g. Isovoltaic's Icosolar TPC 3480) facing the solar cells to avoid corrosion. For most CBS concepts the rear encapsulant provides electrical isolation between the CBS and the cell. The encapsulant is locally opened by mechanical punching or laser.

These types of backsheet also include a stack of PET and Tedlar (or similar material) on the rear side to protect against environmental influences. Other concepts, such as 'contacfoil-connect' by Eppstein Technologies, use a polyvinyl butyral (PVB) layer on top of the Cu for electrical isolation. This PVB layer is locally ablated by laser to allow contacting. In module assembly, the rear encapsulant is placed behind the CBS, followed by a standard backsheet or Eppstein's 'contacfoil-back'. The EBfoil BYS developed by EBfoil and produced by Coveme is a stack system consisting of an encapsulant with a dielectric interlayer combined with a conductive backsheet composed of PET layers, a copper or aluminium conductive layer and a primer layer. After structuring the two components according to the desired module circuit design, both sheets are pre-tagged by dedicated Formula E equipment and can be handled within the module assembly line by Formula E as one single sheet combining the CBS and the rear-side encapsulant.

The interconnection of a back-contacted solar cell using a CBS is accomplished by ECAs, solder paste or laser soldering. Laser soldering is performed after module lamination, whereas ECAs and solder paste are applied locally onto the CBS by stencil printing or dispensing during module assembly. The printing image matches the openings in the isolation layer to allow contact formation. Back-contact cells are precisely placed on top of the rear module stack using a pick-and-place unit, which subjects the cell to very low mechanical stresses compared with soldering. Usually, after cell placing the finished sandwich is flipped before lamination. During lamination, ECA or solder paste is cured and establishes the contact between the cell and the CBS while they are enclosed by the insulating layer; this is the reason why no electroluminescence (EL) inspection of modules prior to lamination is possible.

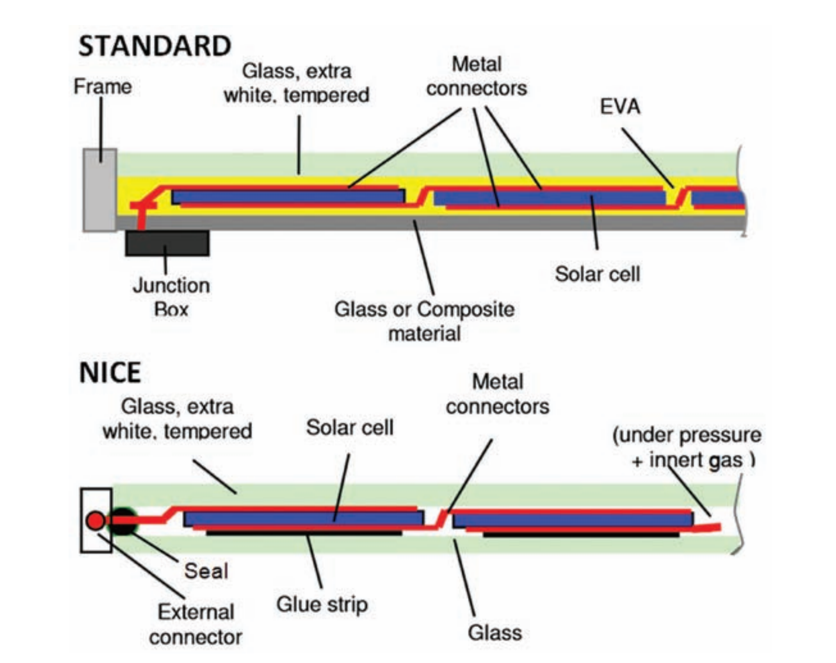

Figure 5. Standard module technology (top) compared with NICE technology (bottom) (image from Dupuis [14]).

Back-contact module assembly by tabbing–stringing

The traditional way of assembling back-contact modules is the single-sided tabbing–stringing procedure. Dedicated equipment for 6" cells with several (up to eight) rear busbars is offered on the market by different companies (e.g. Komax Solar, teamtechnik and Meyer Burger) and is already in use for the production of MWT modules. The contact between the cell and the ribbon can be realized by soldering or ECA gluing. For MWT, only point contacts between the cell and the ribbon are possible; an isolation layer has to be introduced locally to separate the ribbon and the cell. This isolation is not needed for IBC cells, such as the Zebra cell, featuring a floating busbar structure on the rear, and soldering on the full length of the busbar can be achieved. Single-sided ribbon interconnection imposes high mechanical stresses on the solar cell, impacting only from one plane, which is why either structured or super-soft ribbon is used to minimize bowing.

"Single-sided ribbon interconnection imposes high mechanical stresses on the solar cell."

An important advantage of a ribbon interconnection compared with a CBS is the possibility of constructing a bifacial module by either using a transparent backsheet or assembling a glass–glass module. In this case the bifaciality of rear-contacted cells, like the Zebra cell, can also be exploited at the module level, leading to a significantly increased energy yield (kWh/kWp(front)) and hence a reduced LCOE (€/kWh).

NICE module technology

Apollon Solar has developed a novel industrial PV module technology under the acronym NICE, standing for 'new industrial cells encapsulation' [14]. The key elements of this module technology (Fig. 5) are:

- The electrical series connection between the solar cell contacts and the metal interconnectors is soldering free. Contact is obtained by creating and maintaining a lower pressure inside the module, which establishes a pressure contact between the solar cell contact terminals and the metal interconnectors.
- The NICE module is sealed by a polyisobutylene (PIB) edge seal that also provides the mechanical contact between the module front glass and rear glass, as well as acting as a barrier to moisture and air ingress. The inner volume of a NICE module is filled with a neutral gas to protect the module components from oxidation.
- The absence of lamination and soldering for the cell interconnection in NICE module technology for

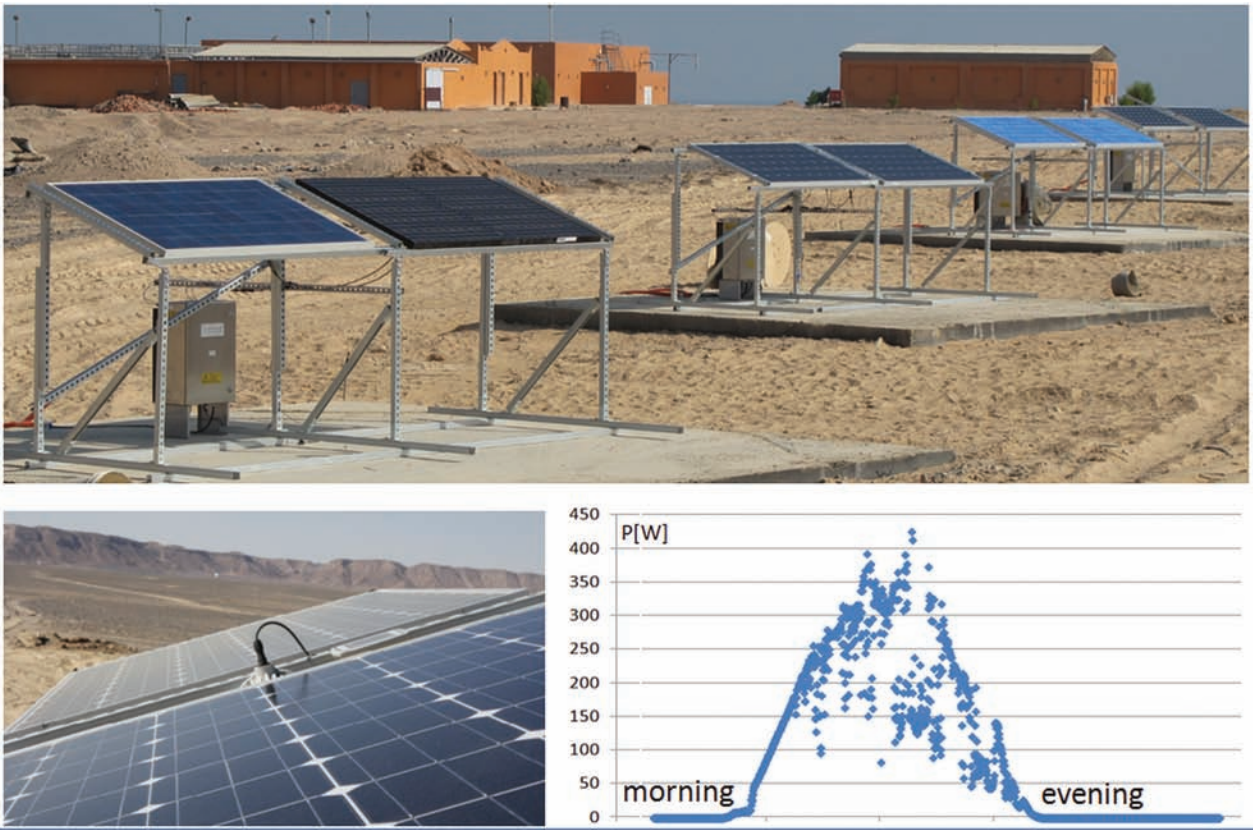

Figure 6. Measurement set-ups for standard and bifacial modules under desert conditions in el Gouna, Egypt. A peak power of around 450W was measured for the non-optimized bifacial BOSCH module (see graph).

solar cell encapsulation simplifies the recycling of modules, because they can be easily disassembled and separated into their different components: glass, copper interconnectors and cells.

As NICE is a glass–glass technology it can be used for bifacial applications. Production of 40MW NICE modules is already in operation in Tunisia and is currently set up in Algeria.

Development of desert modules

In the past, the modules have been developed for the European market, as this technology was cost effective only with feed-in tariff schemes: all the properties and testing, therefore, were adapted to conditions in Europe. The modules have to withstand, for example, strong hailstorms and heavy wind and snow loads. However, now that the technology is so cost effective even without any subsidies, it can be deployed with grid parity in many regions, such as desert areas. Consequently other testing conditions and module properties are crucial in order to ensure that modules will withstand a harsh desert environment. In addition, all deserts are not the same and conditions in, for example, the Atacama region are different from those in the Sahara, different properties for the modules are essential. In the Atacama Desert high UV irradiation and powder-like sand are present, while in the Sahara very high temperatures and powerful sandstorms attack module stability. The material used must therefore be inert to abrasion and withstand high temperatures. In addition the module efficiency must remain high, even at high temperatures, which makes the use of solar cells with a low temperature coefficient necessary. Such cells require high voltage, for example PERC cells using solar-grade (SoG) mc-Si wafers [15] in the case of multicrystalline cells, or n-type solar cells in the case of Cz cells. Since development is leaning towards glass–glass modules anyway, and high reflectivity is present in desert areas, it makes sense to use bifacial modules. To summarize, a module for desert conditions will have the following properties:

- glass–glass module
- glass with coatings that protect against, for example, soiling and abrasion
- solar cells with high voltage
- bifacial solar cells
- half cells for improved fill factor (*FF*), enabling the use of standard bypass diodes

Fig. 6 shows a test field in el Gouna (Egypt), where such modules with different architectures are deployed. For an n-type BOSCH module with a front power of 300Wp, a record 'effective power' (We) of close to 450Wp has been achieved.

> **"The future of desert systems belongs to bifacial glass–glass modules."**

With a real system, of course, there will be more shadowing than with an almost free-standing module. However, compared with monofacial systems, yearly increased electricity productions of 10–25% (depending on albedo, module technology, system set-up and the ratio of diffuse irradiation to direct irradiation) have already been reported from bifacial systems. The authors are sure that the future of desert systems belongs to bifacial glass–glass modules, which yield a longer system lifetime as well as greater electricity production, thus reducing the cost per kWh. Bifaciality in general will gain in importance, as can be witnessed, for instance, in the set-up of the bifacial solar cell factories of MegaCell in Italy and Mission Solar Energy in the USA.

(A follow-up article dealing with the topic of bifaciality is planned for a future issue of *PV International*.)

Summary and outlook

This paper has summarized (without claiming to be comprehensive) future module technologies, which will be introduced to the PV market at an increasing rate. The authors believe that the PV market will develop similarly to the car industry, where adapted versions of the standard product will be used for different regions and different 'occasions', even if the functions of a module remain the same, namely to live long, to produce plenty of electricity (low cost per kWh) during that lifetime, and, in some cases, to also look good.

In addition, the electric car and PV industries currently have one more thing in common: in order to reach the full potential of both technologies, better and more cost-effective batteries need to be developed.

References

[1] Colthorpe, A. 2014, "Trial production of Yingli Green's metal-wrap-through modules has begun", News Report (22 May) [http://www.pv-tech.org/news/trial_production_of_yingli_greens_metal_wrap_through_modules_has_begun].

[2] Osborne, M. 2013, "JA Solar starts production of MWT solar cell technology from ECN", News Report (24 April) [http://www.pv-tech.org/news/ja_solar_starts_production_of_mwt_solar_cell_technology_from_ecn].

[3] Meza, E. 2014, "Italy: MegaCell to invest EUR 10 million in former Helios cell fab", News Report (21 July) [http://www.pv-magazine.com/news/details/beitrag/italy--megacell-to-invest-eur-10-million-in-former-helios-cell-fab-_100015793/#axzz38lt4xHvE].

[4] SEMI PV Group Europe 2014, "International technology roadmap for photovoltaic (ITRVP): Results 2013", 5th edn (March) [http://www.itrpv.net/Reports/Downloads/].

[5] Osborne, M. 2012, "Komax Solar offers new stringer for 6-inch back contact solar cells", News Report (3 September) [http://www.pv-tech.org/product_reviews/komax_solar_offers_new_stringer_for_6_inch_back_contact_solar_cells].

[6] teamtechnik 2013, "The STRINGER TT1200 HS single-track system from teamtechnik now strings BC, MWT, 5-busbar and half-cells", Press Release [http://www.pes.eu.com/wind/teamtechnik-group-presents-the-stringer-tt1200-hs-which-now-strings-bc-mwt-5-busbar-and-half-cells/4226/].

[7] Schneider, A. et al. 2014, "Comprehensive study of material dependency for silver based conductive glues", *Energy Procedia* [in press].

[8] Schneider, A. et al. 2013, "Progress in interconnection of busbar-less solar cells by means of conductive gluing", *Energy Procedia*, Vol. 38.

[9] Reid, C.G. et al. 2013, "Contribution of PV encapsulant composition to reduction of potential induced degradation (PID) of crystalline silicon PV cells", *Proc. 28th EU PVSEC*, Paris, France.

[10] Halm, A. et al. 2013, "Reducing cell to module losses for n-type IBC solar cells with state of the art consumables and production equipment", 3rd nPV Worksh., Chambery, France.

[11] McIntosh, K.R. et al. 2009, "An optical comparison of silicone and EVA encapsulant for conventional silicon PV modules: A ray-tracing study", *Proc. 34th IEEE PVSC*, Philadelphia, Pennsylvania, USA, pp. 544–549.

[12] Thompson, J. et al. 2014, "Silicone encapsulation enhances durability, efficiency, and enables new PV cell and modules technologies", NREL PV Mod. Rel. Worksh., Golden, Colorado, USA.

[13] Söderström, T. et al. 2013, "Smart Wire Connection Technology", *Proc. 28th EU PVSEC*, Paris, France.

[14] Dupuis, J. 2012, "NICE module technology – from the concept to mass production: A 10 years review", *Proc. 38th IEEE PVSC*, Austin, Texas, USA.

[15] Tayyibet, M. et al. 2013, "Effect of temperature and sun intensity on multicrystalline silicon solar cells", *Proc. 28th EU PVSEC*, Paris, France.

About the Authors

Dr. Joris Libal works at ISC Konstanz as a research engineer, focusing on business development and technology transfer in the areas of high-efficiency n-type solar cells and innovative module technology. He received a diploma in physics from the University of Tübingen and a Ph.D. in the field of n-type crystalline silicon solar cells from the University of Konstanz. Dr. Libal has been involved in R&D along the entire value chain of crystalline silicon PV for more than 10 years, having held various positions at the University of Konstanz, at the University of Milano-Bicocca and, more recently, as the R&D manager at the Italian PV module manufacturer Silfab SpA.

Dr. Andreas Schneider received his diploma in physics from the University of Freiburg in 1999 and his Ph.D., with a thesis topic concerning crystalline silicon solar cells, from the University of Konstanz in 2004. He then worked at the University of Konstanz, where he was responsible for the development of crystalline silicon solar cells. From 2005 to 2011, he was employed at Day4Energy, first as the head of R&D and then as the director of the company's quality management department. At the beginning of 2011, Dr. Schneider worked for a short while at Jabil, before joining ISC Konstanz as the head of the module development department.

Andreas Halm studied physics at the University of Konstanz and completed his diploma, with a thesis topic of nanomechanics and nano-optics. Since June 2008 he has been working as a project manager at ISC Konstanz, specializing in solar cells made of SoG silicon. He has also been heavily involved in the development of high-efficiency back-contacted n-type silicon solar cells since the beginning of 2010.

Dr. Radovan Kopecek, one of the founders of ISC Konstanz, has been working at the institute as a full-time manager and researcher since January 2007, and is currently the head of the Advanced Solar Cells Department. Dr. Kopecek has also been teaching the basics of PV at the DHBW in Friedrichshafen since 2012. He received his master's degree from Portland State University (Oregon, USA) in 1995, and then obtained his diploma in physics at the University of Stuttgart in 1998. He completed his Ph.D. in 2002 in Konstanz, with a dissertation topic of thin-film silicon solar cells.

Enquiries

ISC Konstanz
Rudolf-Diesel-Straße 15
78467 Konstanz
Germany

Tel: +49-7531-36 18 3-22
Email: Joris.Libal@isc-konstanz.de
Website: www.isc-konstanz.de

Power Generation

India rooftop solar subsidy finally released, but industry says better off without

India's Ministry of New and Renewable Energy (MNRE) has finally received funds to pay a 30% subsidy promised to rooftop solar installations. The 30% subsidy is to help reduce the cost of a total of 25MW of rooftop installations on government buildings of 3-100kW in size. Despite the development some installers look set to shun the scheme in the future, owing to the uncertainty. The announcement on 12 August had been eagerly awaited following previous payment deferrals creating a backlog of projects viable for funding and delaying new projects. The 30% subsidy also previously applied to installations up to 500kW in size, but budgetary constraints lowered the upper limit to 100kW. No residential solar is included in the 25MW subsidy's budget allocation. To be eligible for the subsidy, projects must have completed installation (meeting the MNRE criteria); payments have no bearings on other JNNSM solar missions projects.

Boost for Rooftop Generation

Hawaii to triple rooftop solar by 2030

Hawaii's electric companies declared in August that they would triple rooftop solar by 2030. As part of a goal to achieve a minimum of 65% renewable energy generation, and lowering electric bills by 20%, also by 2030, the electric companies, Hawaiian Electric, Maui Electric and Hawaii Electric Light, collectively known as HECO, released plans to upgrade the grid and boost rooftop solar. Utilities and grid firms will publish an annual limit for solar installs to ensure the grid can cope with demand. The new plans are for the Oahu, Maui County, and Hawaii Island electricity systems, and are intended to help the Oceania state use more renewable energy and less fossil fuels.

Bayern Munich training ground now features 29.2kWp rooftop PV

Work to install a 29.2kWp rooftop PV system has been completed at German football club Bayern Munich's training facility, installed by Chinese company Yingli Green. Yingli was one of the sponsors at the recent football World Cup in Brazil, making it the first solar company to do so and the first Chinese company in history to sponsor the event. It has been an official sponsor or "premium partner" to Bayern Munich since 2011. The newly completed system will produce more than 31,000kWh of clean energy a year at Sabener Strasse training facility. Yingli claims it will save the equivalent of 21,000kg of carbon dioxide emissions annually. The PV plant will eventually be connected to an LCD display that shows readouts of generation data at Sabener Strasse's visitor centre.

Source: Yingli Solar

Yingli revised down its shipment guidance for the year.

Ups and Downs of Solar Demand in South America and China

Suntech eyes solar potential in Brazil, Mexico and Chile

Suntech is targeting the South American markets and expects Brazil and Mexico to follow Chile's lead on utility-scale solar. The company exhibited at Intersolar South America in late August. The company is continuing its expansion, geographically and sectorally, following its acquisition by Shunfeng.

Yingli Green lowers 2014 shipment guidance on weaker China, US demand

The PV industry's largest manufacturer, Yingli Green Energy revised down full-year module shipment guidance due to weaker than expected demand in China and the US as it cut third-party cell and module purchasing to keep in-house production at high utilization rates. The company reported second quarter module shipments of 887.9MW, up 40.8% from 630.8MW in the first quarter. Module shipments included 71.8MW for its own downstream PV power plants business in China. Total net revenues were US$549.5 million, up from US$432.2 million in the previous quarter but remained below the US$613.0 million generated in the fourth quarter of 2013.

New Frontiers for Commercal and Residential Solar Leasing

SunPower pilots solar leases in Australia

SunPower is to trial a residential leasing scheme in Melbourne, Australia. The SunPower Choice programme will offer solar power at a pre-determined rate for 25 years with no upfront payment. The company has included a money-back guarantee should the system under-perform. SunPower will also be responsible for monitoring the systems.

Suniva to offer commercial-scale solar leases

Cell and module manufacturer, Suniva has signed a customer finance agreement with Technology Credit Corporation (TCC). The agreement will allow Suniva to offer its customers leases and power purchase agreements (PPAs). TCC has already backed 300 commercial-scale PV systems in the US.

Governments Get Creative With Solar Incentives

Governor of New York consolidates solar incentives under NY-Sun banner

The governor of New York, Andrew Cuomo, has announced the NY-Sun Initiative, will consolidate all the state's existing solar incentive programmes into a single support scheme, aimed at adding 3GW of solar generation capacity by 2023. Cuomo announced in August that current multiple incentive schemes will be incorporated into the US$1 billion NY-Sun Initiative. Cuomo added that the NY-Sun Initiative would "stimulate development of solar projects across this state, and sends a clear message that New York is a leader in solar energy innovation". Cuomo said the plan was intended to foster a self-sustaining solar industry for New York. Financial support will be provided for projects by public funds and is intended to "drive the industry to scale and reduce burdens on ratepayers".

Japan to subsidise solar projects on landfill sites

Japan's environment ministry is looking to boost the deployment of ground-mounted solar farms by offering extra support to projects being built on landfill sites that have reached full capacity, according to reports in the Japanese press. According to newspaper Asahi Shimbun and other sources, a study commissioned by the ministry in 2013 and recently concluded, found that the total area spanned by landfill sites could accommodate around 7.4GW of extra solar generation capacity if utilised effectively.

Energy Storage News

TÜV SÜD to issue certified standards for renewable energy storage systems

TÜV SÜD has developed a certificate for renewable energy storage systems, which the testing house claims will "provide reliable information on the safety, performance and service life of stationary energy storage systems". Industry figures, academics and even politicians have called for standardisation across energy storage markets with increasing frequency. At a UK event in April, Nicola Cosciani of Italian battery maker FIAMM, which has added grid storage to its range of products, said that companies would find developing global strategies for tackling the energy storage market difficult without being able to adapt to the local needs of each of the regions companies wish to be active in.

Sheikh Mohammed Bin Rashid Al Maktoum at the World Economic Forum.

Sunpower CEO: Ide of grid independence is naive

Sunpower CEO Tom Werner has said that the idea of solar power users combining their systems with battery storage to become fully independent of the grid is "naïve", echoing the views of one of SolarCity's founders. SolarCity chief technology officer Peter Rive, who started the company with his brother Lyndon, wrote in April that while mass defections from the grid were technically possible, SolarCity had "no interest in this scenario". Asked if Sunpower agreed with Rive's assertion and whether Sunpower was also uninterested in a grid-independent approach using energy storage, Werner said: "I'd go further and say that grid independence is naïve. That's not going to happen in the foreseeable future."

Mega Solar Project News

Rajasthan could cancel 4GW World Bank solar project

The Indian state of Rajasthan's 4GW mega solar power project could be cancelled. The chief minister of Rajasthan, Vasundhara Raje, has written a letter to the Ministry of New and Renewable energy (MNRE) to oppose the World Bank-backed project. The state government has raised the objection based on the 4GW solar site being developed on ecologically and environmentally sensitive land, according to local reports. The proposed solar project site spans 23,000 acres of land owned by the government-run salt source manager, Sambhar Salts Limited. However, Raje has contested that due to migratory birds that could be affected, such as flamingos, the project is unviable, and is also part of an intergovernmental treaty to protect wetland areas, the 1971 Ramsar Convention. But it is suspected that political reasons are the actual cause of the objection.

Dubai shortlists developers for second phase of 1GW Dubai solar project

Dubai Electricity and Water has shortlisted developers for the tender of the 100MW second phase of Mohammed Bin Rashid Al Maktoum Solar Park. The tender is to be awarded to independent power producers (IPP). The qualification process for applicants began in May, with 24 developers shortlisted, out of 49 applicants who qualified from the open request for proposals by the government. Numerous bids so far have been from international developers. The deadline for bids is 23 October 2014.

Product Reviews

HiQ Solar

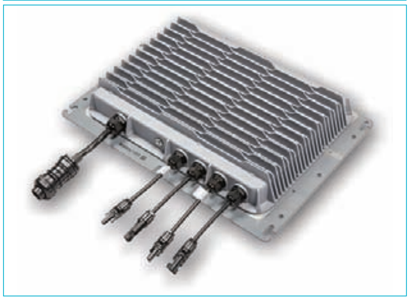

HiQ Solar offers compact rugged commercial rooftop string inverter

Product Outline: HiQ Solar has introduced its new 'Liberty' 480V 3-phase, 1000Vdc inverter into the US market. The 8kW-rated string inverter is incorporated into a NEMA6 enclosure and weighs 24 lbs (11kg).

Problem: Installers and project developers require lower BOS costs and reduced O&M risk in commercial projects. Simplified installations, low weight and compact design of string inverters in a microinverter format could also provide long cycle lifetimes with improved safety margins.

Solution: The Liberty 480V 3-phase inverter handles two 4kW single strings individually, providing separate monitoring, MPPT and arc detection for each, compared with conventional string inverters that parallel several strings together. The system is suitable for use in ungrounded systems, with reduced labour costs, while offering greater protection from ground faults and increased personnel safety. The system provides an ideal level of management and monitoring for commercial-sized installations, with enough granularity to see issues as they arise without being swamped by data.

Applications: Commercial rooftops and carports, including desert and coastal installations, and hostile environments with sand, heat, salt or high elevations.

Platform: The Liberty inverter is fully sealed, waterproof and silent, and is particularly suitable for hostile environments, such as desert, coastal and high-altitude locations. It has a peak efficiency above 98.5%, conforms to UL1741, and has a power density of 0.72kW/kg – twice that of large string inverters.

Availability: Currently available.

Ampt

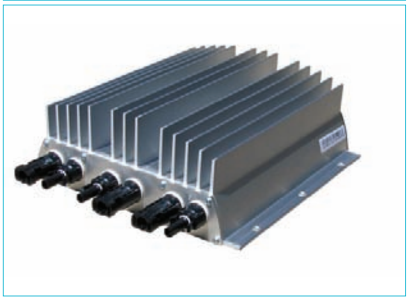

Ampt's string optimizer for large-scale systems reduces costs and increases performance

Product Outline: Ampt has introduced a new string optimizer – a DC power converter with multiple maximum power point tracking (MPPT), and output voltage and current limits for optimizing system design and maximizing performance of large-scale PV systems.

Problem: In an effort to lower the cost of electrical components, large-scale PV developers and EPCs are looking to next-generation system designs. A string optimizer allows PV power plants to be deployed with the cost-saving benefits of a 2000V system using only 1000V components and meeting all 1000V code requirements.

Solution: Ampt string optimizers can be used in large-scale PV systems to reduce costs and increase performance. The optimized system has twice as many modules per string as conventional systems and also higher-resolution MPPT. More modules per string decreases the number of combiners by 50% and reduces the amount of cabling, which results in significant electrical BOS savings. Putting MPPT on each string increases lifetime system production.

Applications: PV power plants.

Platform: Ampt-optimized systems use inverters configured to operate in Ampt Mode, thus yielding a higher rated output power than the same inverters operating in standard mode. Delivering more power per inverter reduces the overall cost per watt. Compatible with any inverter, the optimized system has a high (99.1%/99.0% CEC/€) efficiency.

Availability: Currently available.

Locus Energy

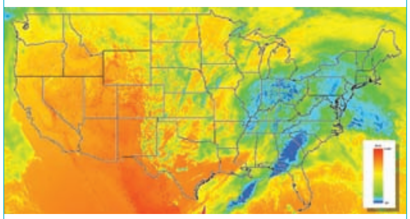

Locus Energy's virtual irradiance modelling tool lowers O&M PV fleet costs

Product Outline: Locus Energy has launched an advanced irradiance modelling tool, 'Virtual Irradiance (VI)', which provides solar fleet operators with data on the amount of sunlight striking the ground, enabling a highly accurate assessment of PV system performance.

Problem: There is a greater need to optimize PV system performance because of lower incentives and the switch to self-consumption. PV fleet managers require accurate data to understand performance and effectively handle O&M issues.

Solution: VI allows fleet managers to determine if a system is performing to expectations given the amount of sunlight that is available at a particular time and location. The tool uses data from weather stations and satellite imagery to provide highly accurate, ground-level irradiance data for any location in the continental USA. For small- to medium-sized systems, VI eliminates the need for an on-site sensor, which may be prohibitively expensive. For larger systems in which an on-site sensor may have already been installed, VI can fill gaps in, and validate, sensor data, which can become skewed because of miscalibration etc.

Applications: Solar irradiance analytics for problem solving and O&M operations.

Platform: VI may be used with existing system software or as an add-on to Locus Energy's SolarNOC (Network Operations Center) software. The filters of SolarNOC's customized dashboard provide an unprecedented level of control over how performance data is aggregated and displayed.

Availability: Currently available.

Fab & Facilities

Materials

Cell Processing

Thin Film

PV Modules

Power Generation

Reliable methods for PV power plant performance testing

Evan S. Riley, Black & Veatch , San Francisco, California, USA

ABSTRACT

Using a prescribed test protocol to compare the measured performance of a solar PV power plant relative to its expected performance is often a means by which the value of the facility is determined. Performance testing is used contractually to determine matters such as the fee paid to a constructor, the price paid to a seller, and the cost of capital from a lender or investor. To ensure that performance testing produces consistent and independently verifiable results, it is essential that accurate and repeatable test methods be used. This paper outlines critical deficiencies in older solar PV performance testing protocols, and how the methods prescribed in ASTM E2848 and E2939 eliminate these deficiencies and enable test practitioners to produce consistent, verifiable results with a high degree of confidence.

Introduction

In the past five years, the renewable power generation market in much of the USA and Europe has undergone a fundamental shift. Driven by rapid declines in equipment prices and installation costs, improved performance, and strong policy support, market participants have deployed an unprecedented amount of renewable wind and solar generating capacity. Once viewed as niche resources, renewable generating facilities are now changing the electric power industry and expanding participation in the electricity supply market.

One of the most striking differences between fossil fuel-based and renewable power generating facilities is the way in which the projects are financed. Both require a significant amount of up-front capital to develop and construct. However, unlike fossil fuel power plants, renewable energy power plants typically have minimal operating costs. As a result, the up-front cost of a renewable energy facility is a significantly greater fraction of its overall lifetime cost than that of a fossil fuel facility.

"It is critical to have reliable performance models and accurate performance-testing protocols for renewable generating facilities."

The cost of capital for long-term project financing is directly related to project risk. For fossil fuel power generating facilities, which have well-understood performance characteristics and operating costs, the primary risk is the uncertainty in the future price of fuel. In contrast, because renewable generation does not operate in a fuel price risk environment, the primary financial risk is the accuracy and uncertainty of the performance model used to estimate the expected production from the renewable energy facility. It is therefore critical to have reliable performance models and accurate performance-testing protocols for renewable generating facilities. Reliable performance models reduce uncertainty and risk, and accurate performance testing provides a means of demonstrating that a constructed facility will meet the expectations upon which the financial model of the project is based.

Performance modelling and testing of solar PV generating facilities

To determine the pro forma bankability of a potential future solar PV generating asset, a project developer typically begins by forecasting the expected energy production from the proposed facility by inputting historically typical solar resource and weather data (i.e. metrology or 'met' data) into a performance model that simulates the facility's efficiency in converting sunlight into electricity. For solar PV projects, a bankable performance model may include upwards of 50 parameters which specify a wide variety of important factors, including the characteristics of the solar resource, the PV module performance, the inverter performance, the DC and AC electrical losses, and other performance factors.

The combination of the large number of performance modelling parameters and the uncertainty in each produces an aggregate modelling uncertainty in an energy production estimate for a facility that can range from 1 to 10% based on the skill of the modeller, the capabilities of the performance modelling software used, and the quality of information provided to the modeller. This in turn directly determines the uncertainty in the expected revenue for the solar PV project from the sale of electricity it produces.

In addition to performance modelling uncertainty risk, project developers and financiers must also have a means of addressing construction quality risk. The construction quality of a solar PV facility can directly impact its performance and the revenue it will produce. Construction quality factors that can impact performance include:

- The types of PV modules, inverters, electrical cables and components used.
- The quality of the PV modules and other equipment.
- The correctness, quality and completeness of electrical connections.
- The correct programming of inverters and other equipment.

In order to mitigate the risk that a solar PV project will not perform as expected because of modelling and/or construction errors, the industry has begun to utilize comprehensive system-level performance testing in order to evaluate how completed projects perform, on a resource-adjusted basis, to the expectations established by their production estimate. Consequently, to reduce project financing risk and the associated cost of capital, both the modelled production estimates and the results of performance testing need to be valid. A valid performance testing protocol satisfies the following criteria:

- It is well defined, unambiguous and reproducible, such that two independent analysts will always arrive at the same result when analysing the same test data.
- It is effective at testing the ability of the project to convert the available solar resource into electricity, as modelled.

- It specifies a performance target in a manner that is consistent with how measured performance is determined.

- It specifies reference operating conditions, under which measured performance is compared with expected performance, that are within the operating conditions of the project.

- It produces a result that is not influenced (biased) by factors outside the control of the project, including variations in the solar resource, ambient temperature, wind speed and soiling of the PV modules by dust and dirt.

To achieve these goals, performance tests commonly used in the industry are being improved and evolving into trusted standards through the efforts of a wide range of industry participants who are working together to create more-comprehensive testing methodologies.

> "To reduce project financing risk and the associated cost of capital, both the modelled production estimates and the results of performance testing need to be valid."

The PVUSA performance test specification

The first well-documented performance test specification for solar PV generating facilities was developed by the Bechtel Corporation in 1995 and published by the United States Department of Energy in the "PVUSA model technical specification for a turnkey photovoltaic power system" [1]. This specification included a performance test which was intended to help ensure that the completed facility met the requirements set forth in the project specification, but did not necessarily reach a specific energy production target.

The PVUSA test specification defines the test target for a facility by applying a series of derating factors to its DC capacity (kWp), which is defined as the sum of module nameplate ratings (Wp) specified at PVUSA test conditions (PTC), i.e. 1000W/m^2 irradiance, 20°C ambient temperature and 1m/s wind speed. The idea is that each derate can be contractually stipulated in the technical specification of a construction contract, and that the expected energy production of the facility can be forecast using those contractual derates. In this *indirect* way, the test could be used to demonstrate to a potential project owner that the project was built as specified and is capable of performing as expected. The diagram shown in Fig. 1 illustrates the process flow of the PVUSA performance test method.

Shortcomings of the PVUSA test method

As discussed above, the most important aspect of modelling the performance of a solar PV facility from a project financing perspective is the *expected energy production* (MWh), which determines expected future revenue flows as a pro forma baseline. An assessment of the actual performance of a facility once it has been constructed is then performed by comparing its *measured energy production*, in a consistent way, with the baseline expectation. The goal is to provide a reliable basis for confidence in how the project will perform over its useful operating life, compared with expectations.

As shown in Fig. 1, the primary deficiency in the PVUSA test method is that the *target capacity* of the facility is determined solely by the project specification without referencing the expected energy production. This can, and often does, create inconsistencies which bias the performance test results.

Overall, there are five critical shortcomings of the PVUSA test method:

1. It does not specify what test equipment should be used to take the measurements, or how the instruments should be calibrated.

2. It does not specify how to filter the measured data, nor does it specify important data requirements, such as the minimum number of data points to be analysed and the time interval between them (over which measured data within each interval are averaged).

3. It requires a detailed and comprehensive project specification that is consistently applied in building the project and modelling its energy production; a weak or incomplete project specification may give a project constructor an opportunity to knowingly or unknowingly create a mismatch between the target capacity specified and what has actually been built.

4. It does not address the fact that the measured capacity of a PV power plant varies seasonally, often testing low in the summer and high in the winter.

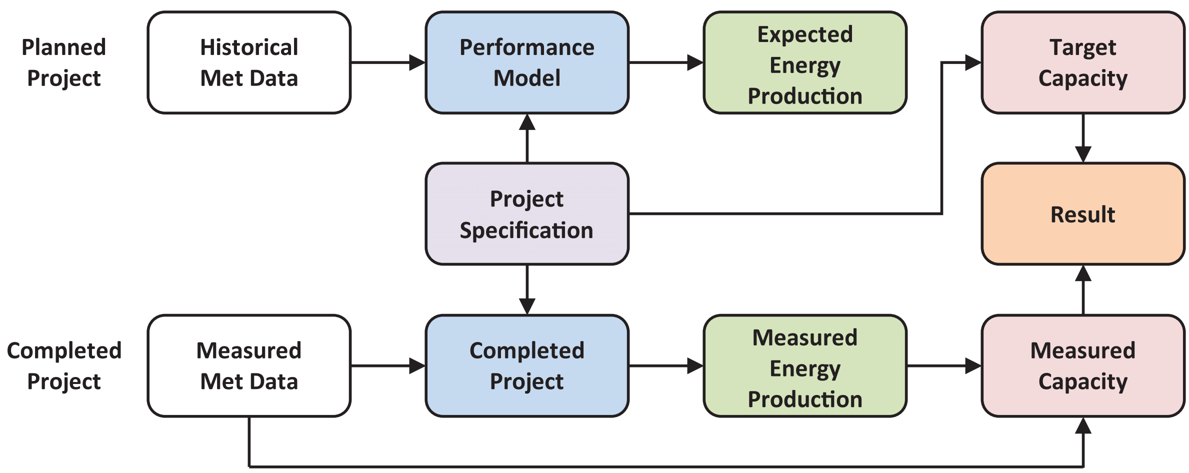

Figure 1. PVUSA performance test process flow.

5. It suggests, but does not mandate, how best to determine the test reporting conditions; this is problematic when a plant is operating far from the reporting conditions, because the test results would then need to be extrapolated far outside the measured performance dataset.

ASTM standards that address the shortcomings of the PVUSA test method

ASTM International, formerly known as the American Society for Testing and Materials, is a globally recognized leader in the development of international voluntary standards [2]. From 2009 to 2013, teams throughout the solar PV performance community worked with ASTM to develop two new standards:

- ASTM E2848 – Standard test method for reporting photovoltaic non-concentrator system performance [3].
- ASTM E2939 – Standard practice for determining reporting conditions and expected capacity for photovoltaic non-concentrator systems [4].

ASTM E2848 and ASTM E2939 address the shortcomings of the PVUSA test method: the E2848 standard addresses the first and second, and E2939 addresses the third, fourth and fifth.

> "ASTM E2848 and ASTM E2939 address the shortcomings of the PVUSA test method."

ASTM E2848

ASTM E2848 was developed as a first step in advancing the testing of solar PV facility performance from a rough guideline published in the PVUSA technical specification to a comprehensive suite of industry standards [3]. This ASTM standard does many things, including specifically:

- defining the scope of the test;
- defining terminology;
- defining measurement equipment and calibration;
- providing criteria for filtering data;
- specifying minimum data requirements.

One of the most important improvements provided by ASTM E2848 is to define the scope of the test as "useful for acceptance testing and performance monitoring of a solar PV power plant, but not for testing single modules or comparing different projects in different locations or of different technologies". For example, because of the complex nature of the performance of solar PV facilities, two co-located solar PV facilities with identical DC capacities but using different technologies, and/or with differences in row spacing or module tilt, can have significantly different capacity factors, generation profiles and measured capacity values under ASTM E2848.

To reduce measurement uncertainty, ASTM E2848 also specifies the requirements for the types, accuracy and calibration of the instrumentation used to collect measurement data during a performance test. It further specifies minimum data requirements and establishes data filtering criteria to remove ambiguities about how data should be aggregated, parsed and filtered. This reduces analysis uncertainty and allows test results to be repeatable. This is an essential feature of the specification because it enables different project stakeholders to independently calculate the test results in a consistent manner and arrive at the same result, which helps ensure the test's validity.

While ASTM E2848 establishes a foundation for a comprehensive capacity test protocol, by itself it does not address all the shortcomings of the PVUSA test method.

ASTM E2939

ASTM E2939 was specifically developed to create consistency in determining the *expected capacity* and *measured capacity* of a solar PV facility by recognizing seasonal variability and by specifying a better method for determining reporting conditions [4]. However, to do this required a restructuring of the process by which the test was carried out. The goal of this restructuring was to ensure consistency by directly tying the expected capacity to the performance model used in financing the project. This was done by applying the same regression curve to both the performance model used to determine the expected capacity, and the measured data used to determine the measured capacity. This was something that was not feasible when the PVUSA technical specification was issued, because sufficiently accurate solar PV performance modelling software did not exist at that time. The diagram

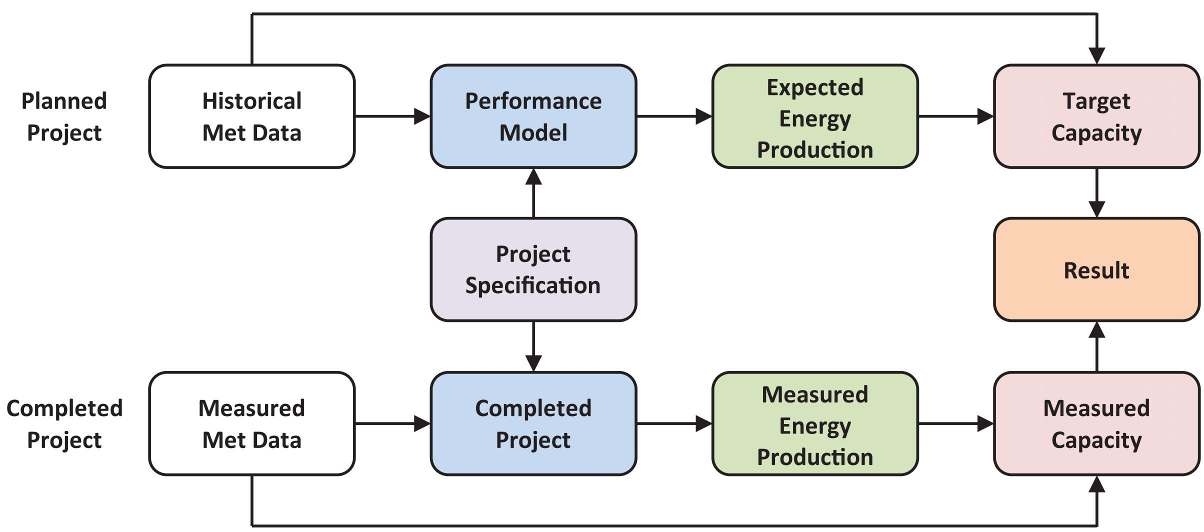

Figure 2. ASTM E2848–E2939 performance test process flow.

shown in Fig. 2 illustrates the restructured process flow specified in the ASTM performance test standard.

Calculating the expected capacity according to the ASTM standards has three advantages over using the PVUSA test method:

1. The expected capacity of a facility is directly tied to its performance model.

2. Seasonal biases are minimized, because the performance targets display the same seasonality as the measured performance.

3. How performance targets and measured values are determined is specified in a consistent way.

Power Generation

The logic of the ASTM performance test protocol is based on ensuring symmetry, and therefore consistency, in the methods used to determine the expected capacity and those used to measure capacity. Another important advantage of this protocol is that the process of making consistent financial decisions based on a test result becomes straightforward for individuals who are not necessarily technically versed in photovoltaic performance.

"The legacy PVUSA test method has been transformed into a comprehensive, bankable and trusted standard that can be used consistently by technical and financial practitioners across the industry."

Conclusions and the future of performance testing for PV power plants

ASTM E2848 and E2939 constitute the first published suite of comprehensive performance testing standards for flat plate (non-concentrator) solar PV facilities. Through the work of the ASTM committee, the legacy PVUSA test method has been transformed into a comprehensive, bankable and trusted standard that can be used consistently by both technical and financial practitioners across the industry. Black & Veatch has extensive experience with applying these protocols to performance acceptance test specifications and procedures on solar PV projects ranging from 2 to 50MW.

Although the performance testing for PV power plants has improved significantly since the time when the PVUSA model technical specification was developed, there is still more work to be done. Black & Veatch champions the idea of collaborative innovation and improvement, and actively contributes to these efforts by participating in industry working groups and publishing technical papers in the field of PV performance testing [5,6].

References

[1] Dows, R.N. & Gough, E.J. 1995, "PVUSA model technical specification for a turnkey photovoltaic power system", Report No. DOE/AL/82993-27, Pacific Gas and Electric Co., R&D Dept., San Ramon, California, USA.

[2] ASTM International [details online at http://www.astm.org].

[3] ASTM E2848:2011, "Standard test method for reporting photovoltaic non-concentrator system performance", DOI: 10.1520/E2848-11.

[4] ASTM E2939:2013, "Standard practice for determining reporting conditions and expected capacity for photovoltaic non-concentrator systems", DOI: 10.1520/E2939.

[5] Dierauf, T. et al. 2013, "Weather-corrected performance ratio", DOI:10.2172/1078057 [http://www.osti.gov/scitech/servlets/purl/1078057].

[6] Kurtz, S. et al. 2013, "Analysis of photovoltaic system energy performance evaluation method", DOI:10.2172/1111193 [http://www.osti.gov/scitech/servlets/purl/1111193].

About the Author

Evan Riley is a renewable energy consultant specializing in PV and other renewable energy technologies in the Renewable Energy Group of Black & Veatch's global energy business. In this role his work includes independent engineering, PV production estimation, technical and economic project evaluation, contract review, and preliminary design assignments for MW-scale PV projects. Evan has been involved in over 4000MW of PV capacity in late-stage development, construction or operation globally.

Enquiries

Evan Riley
Black & Veatch
353 Sacramento St #1900
San Francisco, CA 94111
USA
Tel: +1 415 292-3556
Email: RileyE@bv.com

Advertisers & Web Index

To advertise within Photovoltaics International, please contact the sales department: Tel +44 (0) 20 7871 0122

Who can take advantage of the US anti-dumping decision?

Although the dust has yet to truly settle on the second US anti-dumping investigation and the preliminary findings, mainstream media and financial analysts are already undertaking a post mortem and trying to pick the winners and losers.

Judging by the response from various trade associations and some Chinese PV manufacturers, in general there are no winners.

That hasn't stopped the speculation, which has initially pointed to US PV manufacturers benefiting the most from the decision, although a negotiated settlement remains on the table between the US, China and Taiwan.

Source: Hanwha Q CELLS

Hanwha QCELLS is among the potential beneficiaries of the latest US duties, but clear winners are hard to identify

Winners touted

Two US companies, SunPower and First Solar have been extensively quoted as key beneficiaries of the AD ruling, while by association with the case, SolarWorld is inferred to also benefit.

The problem with this top-down analysis and simple assumptions is the lack of evidence provided to suggest this would be the case.

Reports have failed to highlight that both SunPower and First Solar simply do not have the manufacturing capacity to fill the potential supply void should many Chinese producers decide to look elsewhere for business.

Little thought has been given to the fact that when both companies sell just modules, margins are low and both have spent years developing their business models into PV energy providers, where margins are higher and offer a controlled and better protected business. Both companies have limited availability of modules for sale outside their own PV power plant businesses regardless of being cost-competitive or not with Chinese rivals.

With regards to SolarWorld the scenario is less clear. Having lost market share in the US for several years and continuing to do so after the first AD case in 2012, SolarWorld has a mountain to climb to restore its market position.

SolarWorld's near financial collapse may have been averted via a major restructuring but the company also lacks meaningful capacity in the US to fill the void. New capacity expansions would seem a few years out as it rebuilds its balance sheet.

Small domestic producers such as Suniva, which recently announced a 200MW expansion would benefit but their business model has not been dependent on protectionism, rather they have slowly built a high-performance module market that is also not dependent on the US market alone.

Any small manufacturer in the US could possibly benefit in a small way from the AD decision but other factors such as technology, capital and expertise dictate the benefits, though calling them winners would be over optimistic.

Real winners?

Analysts from the financial community seem to agree in one key area and that is the likelihood that major Chinese producers that continue to see the US as a strategic market would more than likely decide to undertake all manufacturing steps in China, stop using Taiwanese solar cells and pay the already imposed duties under the 2012 ruling, which targeted cells made in China. This would raise module prices in the US but would be the lowest cost approach.

However, looking back at the different duties companies were given in the 2012 ruling highlights that some players are better positioned from an overall penalty cost base than others.

That was spotted by ROTH Capital Partners equity analyst, Philip Shen, who noted that Trina Solar was a likely beneficiary as it had the 2012 combined (AD and CVD) duties of 23%, compared to the average of its peers of 30.7%.

Shen also pointed out ReneSola as another beneficiary, due to its 1.1GW of OEM outsourced capacity at multiple locations around the world.

However, other beneficiaries could be REC Solar and Hanwha Q CELLS with production in Singapore and Malaysia. Korean firms could also be added to the list of potential beneficiaries but these companies all have one thing in common and that is the lack of capacity to meet demand now and through 2015 if they don't start building new gigawatt fabs this year.

This would also be true for Chinese producers wanting to continue to benefit from the US market. Trina Solar, Yingli Green and JinkoSolar fit that profile and potentially could meet increased demand in the short term from China and take a duty hit but would subsequently be looking at locating cell and module production elsewhere to avoid US duties in the longer term.

Companies that look set to be hit hard by the AD ruling could move production to places like Mexico and Malaysia at low cost should they shift existing tool sets as well and some like Taiwan-based Neo Solar Power have already noted that relocation was an option. However, these types of companies are leaning more towards the losers' end than the winners' end of the ruling.

Finally, there is a company with module manufacturing closer than many to the US – Canadian Solar. To truly benefit from the ruling, Canadian Solar would need to fabricate solar cells at its 500MW capacity module assembly plant in Ontario and boost overall capacity to the gigawatt level and more.

The company has issued a statement on the AD ruling noting that it would continue to serve its US-based customers.

It would seem likely that some of the major China-based producers that look upon the US market as strategic could be the real winners from the AD ruling, while US touted players would have to adapt business models and add capacity to take advantage.

However, none of the above is certain and when taking into account the EU anti-dumping settlement, some suppliers both large and small simply walked away from the EU market.

Should module ASPs rise significantly and fail to track lower over time then the US market has no winners as the market will decline and fade away.

Mark Osborne is Senior News Editor of Solar Media, publisher of Photovoltaics International


efficiency